Emission line diagnostics of the progenitors of type Ia supernovae

Tyrone E. Woods

München 2015

Emission line diagnostics of the progenitors of type Ia supernovae

Tyrone E. Woods

Dissertation
an der Physik
der Ludwig–Maximilians–Universität
München

vorgelegt von
Tyrone E. Woods
aus Edmonton, Alberta, Canada

München, den 10.03.2015

Erstgutachter: Prof. Dr. Rashid Sunyaev
Zweitgutachter: Prof. Dr. Gerhard Börner
Tag der mündlichen Prüfung: 13.04.2015

Contents

List of Figures

List of Tables

Summary

In this dissertation, we consider the origin of thermonuclear supernovae, known by their observational classification as type Ia (hereafter SNe Ia). In particular, we develop an entirely new means to test the "single-degenerate" hypothesis, in which the progenitors of these tremendous explosions are suggested to be hot and luminous accreting white dwarfs. We then strongly constrain the role of any such "hot-mode" SN Ia progenitor channel using both a population-based argument and an individual case study, before concluding with some more general considerations of nebulae ionized by accreting white dwarfs.

Type Ia supernovae have now been the subject of intensive study for decades, particularly in light of their role as standard(-izable) candles in measuring cosmological distances. However, there remains no consensus model for the evolutionary channel(s) by which they originate. In the so-called "double-degenerate" scenario, a binary pair of white dwarfs shed angular momentum through gravitational-wave radiation, until they inspiral and merge, triggering an explosion. Alternatively, in the classic picture of the single-degenerate scenario, a white dwarf accretes hydrogen-rich material from some main sequence or red giant companion, and grows through nuclear burning of this material at its surface until reaching sufficient mass to trigger an explosion. This suggests that single-degenerate progenitors should be extremely luminous sources in the EUV and soft X-ray bands during the accretion phase (lasting $\sim 10^5$–10^6 years). For this reason, such objects are generally associated with observed "supersoft X-ray sources" (SSSs). Previous efforts to detect or constrain the role of any such channel have focused on detecting these objects directly in the soft X-ray band (photon energies in the range $0.3 - 0.7$ keV), either on an individual basis or as the combined emission of a diffuse population. Such an approach has yielded important constraints, but only if white dwarfs accrete principally at very high temperatures (T $\sim 5 \times 10^5$K). However, observed SSSs are understood to lie in a broad range of temperatures, with a possible range of at least 2×10^5–10^6K, and some theoretical models suggest even lower temperatures are possible. This necessitates the development of an alternative, complimentary test which can constrain the luminosity of accreting white dwarfs across a wider range of photospheric temperatures.

In this work, we demonstrate that if the single-degenerate model is correct, then accreting, nuclear-burning white dwarfs should provide the dominant source of ionizing radiation in passively-evolving galaxies, roughly 40% of which are known to host extended low-ionization emission-line regions (so-called "retired" galaxies, i.e. emission-line galaxies without either a central AGN or significant ongoing star formation). Therefore, one can

search for the presence of any high-temperature single-degenerate progenitor population in these galaxies by looking for emission lines characteristic of ionization by very high-temperature (10^5 K – 10^6 K) sources. In particular, we find that recombination lines of He II, and forbidden lines of [N I] and [O I], provide the most sensitive diagnostics in retired galaxies to assess the role of accreting white dwarfs as SN Ia progenitors in any "**hot**-mode" (T $\gtrsim 1.2 \times 10^5$K) accretion regime.

Following this, we limit the contribution of any high-temperature single-degenerate channel to the SN Ia rate at relatively early delay-times (1 Gyr $\leq$ t $\leq$ 4 Gyr) to < 5–10% (for T$\gtrsim 1.2 \times 10^5$K) using He II 4686Å and [O I] 6300Å measurements from a stacked sample (provided by Dr Jonas Johansson) of several thousand retired galaxies in the Sloan Digital Sky Survey. We also discuss how these constraints, as well as the observed soft X-ray emission of several nearby galaxies, reveal fundamental problems in our present understanding of the population synthesis of SSSs and other accreting white dwarf binaries.

We then revise the standard picture for the observational appearance of nebulae ionized by individual accreting white dwarfs, accounting for a more realistic assessment of the typical ISM densities in which such objects are likely embedded. We then provide the first formal justification for why so few SSS nebulae have been detected thus far, and demonstrate that a complete survey is within the means of modern large-aperture telescopes (such as ESO's Very Large Telescope). We then show how this approach can be extended to individual SNe Ia, by searching for fossil nebulae in the vicinity of nearby events. In particular, we use an archival pre-explosion narrow-band Hα + [N II] image of the vicinity of SN2014J to place constraints on the luminosity of any putative high-temperature progenitor for SN2014J (such as an accreting white dwarf).

Zusammenfassung

Diese Dissertation beschäftigt sich mit der Frage der Entstehung thermonuklearer Supernovae, welche die beobachtende Astronomie als Typ Ia Supernovae (im folgenden „SNe Ia") klassifiziert. Insbesondere wird in dieser Arbeit eine völlig neue Methode beschrieben, mit deren Hilfe sich die sogenannte „einfach entartete" Hypothese überprüfen lässt. Nach dieser Hypothese entsteht eine SN Ia aus einem heißen und sehr leuchtkräftig, akkretierenden Weißen Zwerg. Anschließend kann die Bedeutung dieser Art der „hot-mode"-SN Ia, sowohl durch ein Populationsargument als auch anhand eines Einzelbeispiels, stark eingeschränkt werden. Abschließend werden generelle Effekte der ionisierenden Wirkung akkretierender Weißer Zwerge auf Nebel erörtert.

Typ Ia Supernovae sind seit Jahrzehnten Gegenstand intensiver Forschung, besonders aufgrund ihrer Eignung als „Standardkerzen" zur Messung kosmologischer Distanzen. Nichtsdestotrotz gibt es keinen Konsens bezüglich der Entwicklungspfade, die zu solchen Sternexplosionen führen. Das sogenannte „zweifach entartete Szenario" beschreibt den Drehimpulsverlust zweier Weißer Zwerge in einem Binärsystem durch die Abstrahlung von Gravitationswellen. Infolgedessen kommt es zur spiralförmigen Annäherung beider Weißer Zwerge, bis diese verschmelzen und damit die eigentliche Explosion auslösen. Im Gegensatz hierzu wird im klassischen „einfach entartete Szenario" einem Weißen Zwerg, der wasserstoffreiches Gas von einem Hauptreihenstern oder einem Roten Riesen akkretiert, durch nukleares Brennen dieses Materials an der Oberfläche des Weißen Zwerges, Masse zugeführt, bis dessen Masse einen kritischen Wert übersteigt, um die Explosion zu zünden. Als Konsequenz sollten diese Objekte während der Akkretionsphase ($10^5 - 10^6$ Jahre) im extremen Ultraviolett- (EUV) und weichen Röntgenspektralbereich äußerst leuchtkräftig sein. Solche Objekte werden im Allgemeinen mit beobachteten „superweichen Röntgenquellen" (SSSs) assoziiert. Bisherige Anstrengungen die Relevanz dieses Entwicklungspfades zu messen oder einzuschränken, konzentrierten sich immer auf die direkte Beobachtung dieser Objekte im weichen Röntgenspektralbereich (Photonenergien im Bereich von 0.3 - 0.7 keV), entweder durch Beobachtung einzelner Objekte oder der kombinierten Emission einer diffusen Population von Quellen. Dieser Ansatz liefert Einschränkungen, aber nur unter der Annahme, dass Weiße Zwerge Materie bei sehr hohen Temperaturen (T $\sim 5 \times 10^5$K) akkretieren. Jedoch füllen beobachtete SSSs einen weiten Temperaturbereich von $2 \times 10^5 K$ bis 10^6K aus, und zudem lassen einige theoretische Modelle noch niedrigere Temperaturen zu. Deshalb ist die Entwicklung eines alternativen, komplementären Tests, mit dem man die Leuchtkraft akkretierender Weißer Zwerge in einem breiteren Spektralbereich photosphärischer

Temperaturen eingrenzen kann, notwendig.

Diese Arbeit demonstriert, unter Annahme des „einfach entarteten" Modells, dass akkretierende, thermonuklear-brennende Weiße Zwerge den dominanten Anteil ionisierender Strahlungsquellen in „passively-evolving" Galaxien darstellen. Von etwa 40% dieser Galaxien ist bekannt, dass sie „low-ionization emission-line regions" beherbergen (auch als „retired" bezeichnet, d. h. „emission-line galaxies" entweder ohne aktiven Galaxienkern (AGN) oder ohne signifikante Sternentstehungsrate). Folglich können solche Galaxien auf eine heiße „einfach entartete" Sternpopulation untersucht werden, indem nach Emissionslinien gesucht wird, die charakteristisch für die Ionisation durch Objekte mit hohen Temperturen (10^5K - 10^6K) sind. Insbesondere zeigt sich, dass die Rekombinationslinien von He II und die verbotene Übergänge von [N I] und [O I], die genauesten diagnostischen Größen in diesen „retired" Galaxien darstellen, um die Rolle der, im „hot-mode" ($T \gtrsim 1.2 \times 10^5$K) akkretierenden Weißen Zwerge, als Vorläufer von Typ Ia SNe zu beurteilen.

Diesem Ansatz folgend, kann der Anteil des hochtemperatur-„einfach entarteten"-Entwicklungspfades an der Supernovarate vom Typ Ia zu relativ frühen „delay-times" (1Gyr $\leq$ t $\leq$ 4Gyr) auf $< \sim 5$– 10% (für T $\gtrsim 1.2 \times 10^5$K) beschränkt werden, unter Verwendung von He II 4686Å- und [OI] 6300Å-Messungen in einem kombinierten Satz von einigen tausend „retired" Galaxien aus dem Sloan Digital Sky Survey (zur Verfügung gestellt von Dr. Jonas Johansson). Außerdem diskutiert diese Arbeit, wie die gefundenen Obergrenzen und die beobachtete weiche Röntgenemission einiger naher Galaxien fundamentale Probleme im Verständnis der Populationssynthese von SSSs und anderen akkretierenden Binärsystemen mit Weißen Zwergen aufzeigen.

Im Weiteren wird die gängige Theorie eines durch einen akkretierenden Weißen Zwerg ionisierten Nebels verfeinert, wobei eine realistischere Abschätzung typischer ISM-Dichten, in denen das Objekt mit großer Wahrscheinlichkeit eingebettet ist, verwendet wird. Damit kann zum ersten Mal rigoros gezeigt werden, weshalb so wenige SSS-Nebel beobachtet wurden und dass eine allumfassende Studie mit heutigen, modernen Teleskopen (beispielsweise das „Very Large Telescope" der ESO) möglich ist. Es zeigt sich außerdem, dass dieser Ansatz auf einzelne SN Ia erweitert werden kann, indem nach fossilen Nebeln in der Umgebung eines nahen Ereignisses gesucht wird. Insbesondere wurden schmalbandige Hα+[N II]-Archivaufnahmen der Umgebung von SN2014J verwendet, um die Leuchtkraft eines potentielle Hochtemperatur-Vorläufersterns einzuschränken.

Chapter 1

Introduction

1.1 Thermonuclear (type Ia) supernovae

1.1.1 Observed characteristics

In recent years, an incredible effort has been undertaken to understand the nature of so-called type Ia supernovae (hereafter SNe Ia, and recently reviewed in Hillebrandt et al., 2013; Maoz et al., 2014). These tremendous explosions are seen to briefly outshine their host galaxies, with inferred total energies on the order of 10^{51}ergs. In the last two decades, they have come under particular scrutiny for their use as standard candles in measuring cosmological distances (Phillips, 1993), which first revealed the accelerating expansion of the Universe (Riess et al., 1998; Perlmutter et al., 1999). However, in reality the study of these fascinating events traces back as far as the very beginnings of modern science.

"Guest stars" had been reported by Chinese and Arab astronomers for millenia, with the brightest (now identified with supernovae) having been observed at least as far back as 185, 1006, and 1054 AD. The first stellar explosion to ignite tremendous interest in the western world was that discovered by Tycho in 1572 AD. In the modern era, the "remnant" of this explosion, i.e. the expanding shock front, continues to produce considerable X-ray and optical-line emission (see e.g. fig. 1.1), and has been the subject of intensive study. Analysis of the "light echo"[1] of this event (Krause et al., 2008) revealed its spectra to be typical of the majority of SNe Ia. This classification system delineates type I supernovae as being those whose spectra are without absorption lines of Hydrogen, as opposed to supernovae of "type II" (Minkowski, 1941), with the "a" denoting the presence of strong emission lines of neutral and singly-ionized Silicon. Within the type I classification, this distinguishes SNe Ia from Ib and Ic supernovae, which together with those of type II are now understood to originate via the "core-collapse" mechanism. For these supernovae, the explosion is ultimately powered by the gravitational collapse of the iron cores of massive evolved stars (for thorough reviews, see Bethe, 1990; Woosley et al., 2002) upon their

---

[1]Wherein light from an earlier event is scattered by dust, allowing it to be observed by present Earth-based telescopes even when emission from the source traveling along the line of sight reached the Earth long ago.

reaching the Chandrasekhar limit (Chandrasekhar, 1931). Conversely, the total energy release of a SN Ia is approximately the binding energy of a carbon-oxygen white dwarf, and its observed spectrum is clearly dominated by emission lines of elements which are the products of thermonuclear burning of such a star (as well as unburnt carbon and oxygen); in particular, reprocessing of high-energy photons produced in the electron-capture decay of ^{56}Ni to ^{56}Co and finally ^{56}Fe primarily powers the optical emission. In short, it appears that SNe Ia are the thermonuclear explosions of white dwarfs comprised of ^{12}C and ^{16}O.

This raises a critical question: how does a carbon-oxygen white dwarf, a largely inert object held-up by degeneracy pressure, achieve the conditions necessary to undergo a thermonuclear explosion? For a non-rotating sphere composed of ^{12}C and ^{16}O, the maximum mass for which electron degeneracy pressure may balance against gravitational collapse is $\approx 1.4 M_\odot$ (Chandrasekhar, 1931). Yet detailed stellar-evolutionary calculations suggest that the normal evolution of an isolated star may produce a carbon-oxygen white dwarf no more massive than $\approx 1.07 M_\odot$ (Umeda et al., 1999). The natural conclusion then is that there must be some outside influence upon the course of the white dwarf's evolution prior to its explosion as a SN Ia. Indeed, it has been known since the 19$^{\text{th}}$ century that many stars do no exist in true isolation, but share an orbit with some stellar mass companion. The ubiquity of such "binary stars" has been thoroughly demonstrated in the modern era, with roughly half of all stars in the vicinity of the Sun understood to have binary companions (Abt, 1983). However, the nature of these companions, and how they bring about the disruption of their white dwarf companion, remains a matter of heated debate, and must satisfy a very stringent set of observational requirements.

1.1.2   Possible progenitor pathways

Nearly all plausible progenitor pathways for the production of type Ia supernovae involve the accumulation of matter on a carbon-oxygen white dwarf from some binary companion (with a few notable, though perhaps improbable, alternatives, e.g. Chiosi et al., 2014; Di Stefano et al., 2015). Any of these may be broadly grouped into one of two categories, based on the nature of the donor star. In the "single-degenerate" scenario, as presented by Whelan & Iben (1973), a single carbon-oxygen white dwarf accretes hydrogen-rich material from some main sequence or red giant companion, and grows through nuclear-burning of this material at its surface until reaching the Chandrasekhar mass, triggering an explosion. Alternatively, in the "double-degenerate" scenario introduced by Webbink (1984), the mass-donor is itself a white dwarf, which falls to an ever shorter orbit with the white dwarf primary by shedding angular momentum through gravitational wave radiation. This eventually leads the two white dwarfs to merge, leading perhaps to an explosion.

For many years, the mechanism of the explosion itself has presented one of the greatest challenges. The merger of two white dwarfs had long been thought to almost unavoidably lead to an accretion-induced collapse before any point in the merged spheroid reached the conditions necessary for an explosion (e.g. Saio & Nomoto, 1985). For the steadily-accreting case, this is true only for the most massive white dwarfs, comprised of oxygen, neon, and magnesium, which one can also rule out as SNe Ia progenitors on nucleosynthetic grounds.
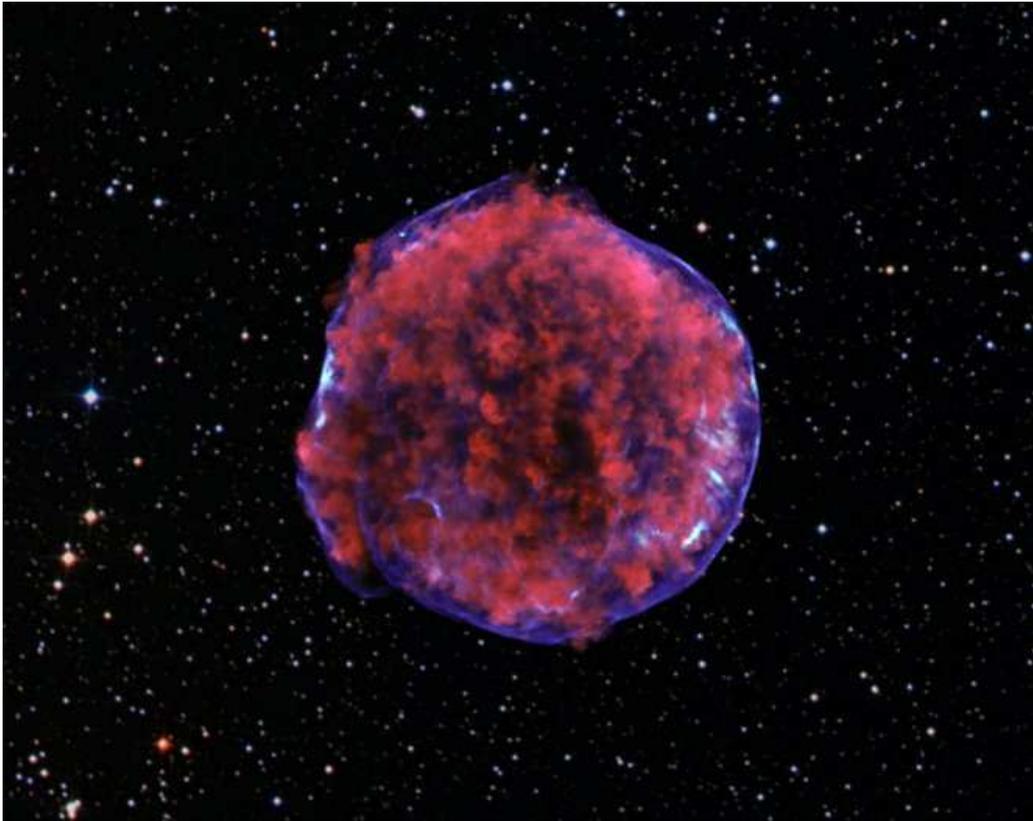
Figure 1.1: Chandra X-ray telescope image of the remnant of Tycho's supernova (SN 1572), a SN Ia in our Galaxy. Red denotes soft band X-ray flux, while blue denotes higher energy emission. The optical emission from the background stars are from the Digitized Sky Survey (DSS).

Figure 1.2: *Left*: Schematic representation of a possible single-degenerate SN Ia progenitor; a white dwarf accreting hydrogen-rich material from a non-degenerate companion star. Image credit: David A. Hardy (www.astroart.org). *Right*: Similar depiction of a double-degenerate SN Ia progenitor; a binary pair of white dwarfs which are shedding angular momentum through gravitational wave radiation, gradually shrinking their orbit. Image credit: NASA/Tod Strohmayer (GSFC)/Dana Berry (CXC)

This lent further credence to the single-degenerate scenario, which had already been the long-favoured candidate due to the natural explanation it provides for the uniformity of these events; in all cases, a white dwarf of approximately the same composition explodes at the same mass. There remained the difficulty in explaining the absence of Hydrogen lines in SN Ia spectra, but solutions have been proposed (e.g. Justham, 2011).

However, recently several developments have come forth which suggest that the explosion of a double white dwarf merger remnant is quite feasible (Pakmor et al., 2010, 2012), and observationally, the inferred merger rate of **all** double white dwarfs in the Milky Way has been found to approximately match the SN Ia rate (Badenes & Maoz, 2012, note however that this would require relaxing the requirement of strictly Chandrasekhar-mass explosions).

Meanwhile, the single-degenerate channel has met several challenges, most particularly in its confrontation with observations, in that any viable single-degenerate scenario predicts that an incredible number of accreting white dwarfs must exist in any population at a given time. The canonical picture for the observational appearance of accreting, steadily-nuclear burning white dwarfs is that of van den Heuvel et al. (1992), in which accreted hydrogen is processed though nuclear-burning at the surface of the white dwarf, yielding luminosities of order 10^{38}erg/s. Their spectra are found to be reasonably well-approximated by blackbodies with photospheric temperatures of $\sim 10^6$K. This means much of any steadily nuclear-burning white dwarf's emission should be detectable in the "soft X-ray" band (≈ 0.3

- 0.7 keV) of space-based telescopes such as Chandra[2] and XMM-Newton[3].

In practice, such steady accretion is only possible for a somewhat narrow range in accretion rates, the so-called "stable-burning strip" (with a range which varies slowly as a function of mass, see fig. 1.3). Within this range, any perturbation in the temperature of the nuclear-burning layer modifies the cooling rate faster than the nuclear-burning rate, and the perturbation is damped out (see e.g. Shen & Bildsten, 2007). Therefore, accreted hydrogen can be processed through steady nuclear-burning at the surface of the white dwarf at the same rate at which it is accreted, yielding a luminosity:

$$L = \epsilon \chi \dot{M} \tag{1.1}$$

for a given accretion rate $\dot{M}$, where $\epsilon \approx 6.4 \times 10^{18}$erg/g is the energy released from nuclear-burning and χ is the fraction of the accreted material which is Hydrogen (≈ 0.72 assuming approximately solar composition).

For accretion rates below this, the onset of nuclear-burning occurs after material has accumulated on the surface, but the corresponding increase in temperature increases the rate of energy generation (through nuclear-burning) faster than the increase in the cooling rate, leading to a runaway in a matter analagous to the classic "thin-shell" instability (see, e.g. Prialnik, 2000). This is the origin of classical and recurrent novae. The upper boundary of the stable-burning strip roughly coincides with the accretion rate at which the luminosity of the white dwarf equals that of a giant-branch star with the equivalent core mass; in effect, the white dwarf is "resuscitated."

The further evolution of the accreting white dwarf at such high accretion rates ($\gtrsim 10^{-6} M_\odot$/yr) is highly uncertain. On the one hand, one may presume that the star would then return to the asymptotic giant branch, with the extent of its photosphere swelling to a thermal equilibrium radius of order 100 solar radii (Nomoto et al., 1979). This would likely engulf the donor star, leading to the onset of a common envelope phase and the end of accretion, and excluding the binary from any role as a single-degenerate SN Ia progenitor (Cassisi et al., 1998). Alternatively, some dynamical process may be able to modulate mass transfer before this can happen, as has been proposed by Hachisu, Kato & Nomoto (1999). In their scenario, a peak in the opacity of material of solar composition at $\approx 10^{5.2}$K (from the OPAL project, e.g. Iglesias & Rogers, 1993) results in a local violation of the Eddington limit within the photosphere of the white dwarf. This expels the excess accreted material in a fast ($\approx 10^4$ km/s) wind, and expands the photospheric radius by up to an order of magnitude. Unfortunately, without any clearly identifiable observational counterpart, the outcome of very rapid accretion onto white dwarfs remains unclear.

With the above observational descriptions (and uncertainties) in mind, we may now turn to evaluating the possible role of any such objects playing a role as the progenitors of SNe Ia. There are a number of criteria which any candidate SN Ia progenitor population must satisfy in order to remain plausible. In particular, any putative model for the progenitor system(s) must be able to account for not only the observed average cosmological rate of

---

[2]http://www.nasa.gov/mission_pages/chandra/main/
[3]http://xmm.esac.esa.int/
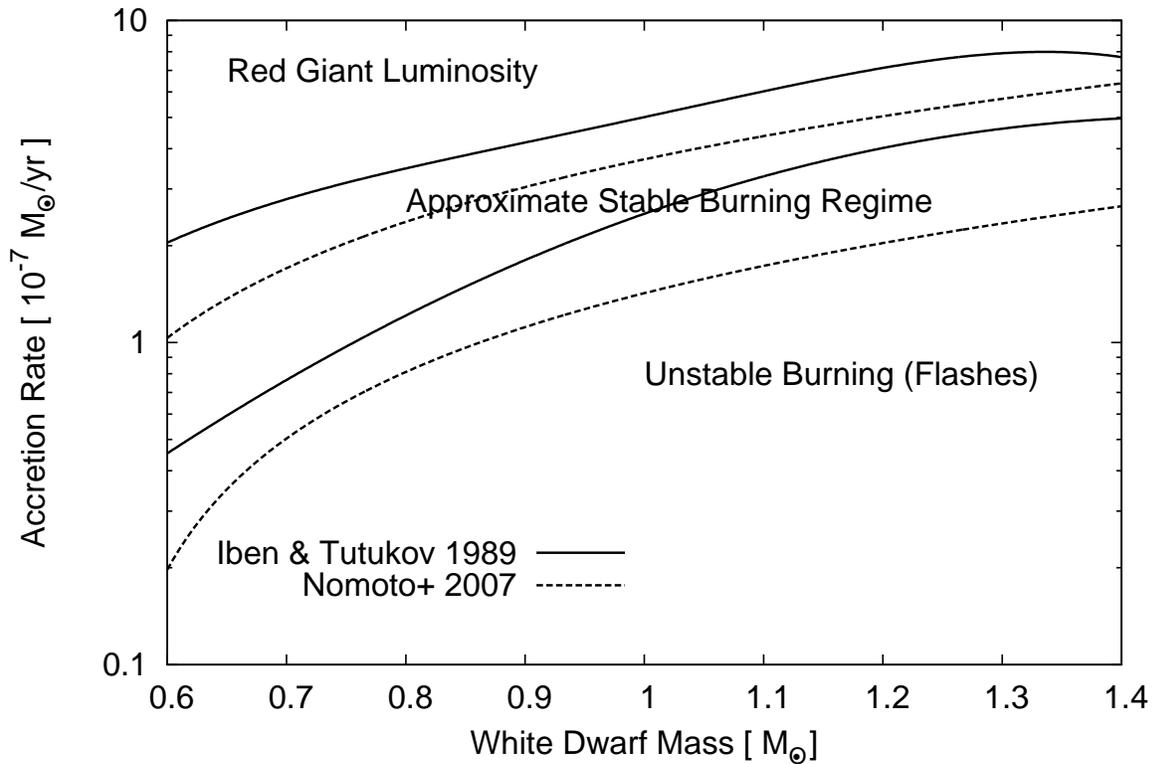
Figure 1.3: Accretion regimes as a function of white dwarf mass. Solid lines denote the results of Iben & Tutukov (1989), while dashed lines denote the more recent results of Nomoto et al. (2007). In each case, the region bounded by these lines marks the range in accretion rates for which steady nuclear-burning is possible (that is, all accreted Hydrogen may be processed through stable nuclear-burning). For accretion rates below the lower boundary of this region, nuclear-burning is only possible in unstable flashes, giving rise to novae. At the upper boundary of this range, the accreting white dwarf has the same luminosity as would be expected on the core-mass – luminosity relationship for giants. In this upper regime, the observational appearance and ultimately the long-term behaviour of the white dwarf photosphere is uncertain.

SNe Ia (e.g. the rate per cubic megaparsec), but also the variation in the observed rate in differing stellar populations. Careful deconstruction of the star-formation histories of entire galaxies and resolved stellar populations have now demonstrated that this variation arises primarily from a dependence of the SN Ia rate in a given population on the age of its constituent stars. This is most conveniently expressed as a "delay-time distribution," or a function describing the rate of SNe Ia in a single-aged stellar population as a function of time. The efforts over the last decade to determine this function are well-summarized in Maoz et al. (2014), with the result being that the SN Ia rate in a given generation of stars goes roughly inversely with their age ($\propto t^{-1.1}$), with an abrupt turn-on at ≈ 100 million years.

For the single-degenerate channel, we can estimate (at least in an average sense) the total luminosity of accreting white dwarfs implied by the observed SN Ia rate in a given stellar population as a function of the "typical" mass accreted per white dwarf (ΔM_{Ia}) prior to explosion (Gilfanov & Bogdán, 2010). With this in mind, Gilfanov & Bogdán (2010) demonstrated that whatever the progenitors of SNe Ia may be, they cannot radiate as classical supersoft sources (with $T \sim 10^6 K$) for a significant fraction of their evolution without grossly exceeding the observed soft X-ray luminosity of several nearby early-type galaxies (with relatively old stellar populations). A similar argument excludes any single-degenerate channel from accreting significant material in the low-$\dot{M}$ regime without producing a far higher classical nova rate than presently observed in nearby stellar populations, such as the Andromeda galaxy (see Gilfanov & Bogdán, 2011; Soraisam & Gilfanov, 2014).

However, the soft X-ray constraints published in Gilfanov & Bogdán (2010) are not constraining for temperatures typical of many observed supersoft sources in the Magellanic clouds (often $\lesssim 5 \times 10^5 K$), nor does it provide any insight if single-degenerate progenitors accrete primarily at very high $\dot{M}$ with extended photospheres (in the "rapidly-accreting regime" of Hachisu, Kato & Nomoto, 1999, discussed above). Indeed, if significantly sub-Chandrasekhar mass explosions are possible ($\approx 1 M_{\odot}$, see e.g. Hillebrandt et al., 2013, and references therein), then $T \lesssim 10^5 K$ may be the norm for expected photospheric temperatures for single-degenerate progenitors. Furthermore, if the prior evolution of the accreting white dwarf substantially pollutes the surrounding circumstellar medium, the excess column density could limit the efficacy of (easily-absorbed) soft X-ray emission as a means of detecting accreting, steadily nuclear-burning white dwarfs. Ideally, one would like to devise a new test which could account for all such possibilities, and broadly constrain any possible single-degenerate progenitor. In the following chapters, we develop and thoroughly explore the implications of just such a test, capable of revealing the presence of any high-temperature ("hot-mode," $T > 10^5 K$) single-degenerate SN Ia progenitor, by studying the impact of accreting, nuclear-burning white dwarfs on their surrounding interstellar medium (ISM). With this in mind, we will now turn to a brief summary of the present understanding of the ISM of differing environments, and the numerical tools employed in its study.
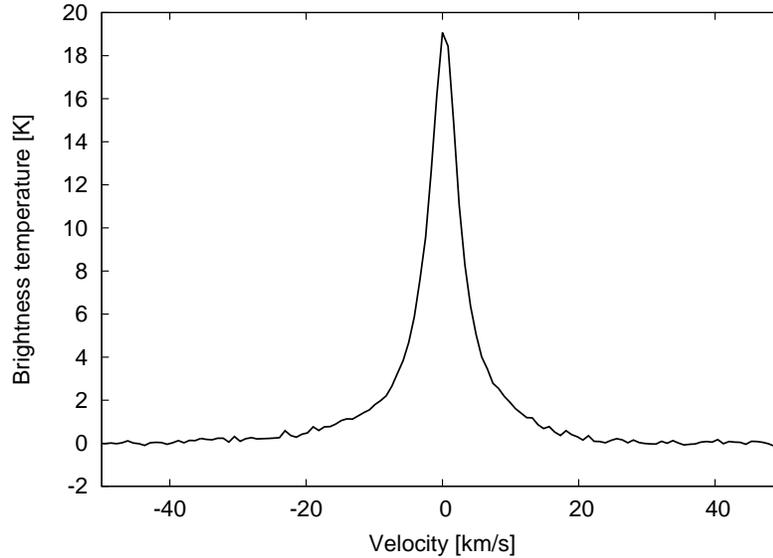
Figure 1.4: H I 21cm emission from neutral gas in our Galaxy, the Milky Way, along an arbitrary line of sight (McClure-Griffiths et al., 2009; Kalberla et al., 2010).

1.2 Photoionized nebulae

1.2.1 Fundamentals

Looking up at the night sky, we see the seemingly innumerable number of stars which make up the stellar population of our Galaxy in the vicinity of the Sun. However, the vast distances between these stars are not truly empty; although not readily apparent to the naked eye, our Galaxy is permeated with a low-density interstellar medium (ISM). The evidence for this gas[4] and the relevant physics are summarized in Dyson & Williams (1980) and Osterbrock & Ferland (2006). In brief, radio observations reveal the presence of neutral Hydrogen from the 21-cm fine structure line (see fig. 1.4). This medium is heated by the diffuse light of the stars and, in the presence of high-temperature sources, is ionized, producing beautiful nebulae which radiate from the infrared to the UV (e.g. fig. 1.5). Observations of many other galaxies reveal extended regions of ionized Hydrogen (fig. 1.6).

In actively star-forming galaxies, the most luminous ionized nebulae frequently arise as follows: dense clouds of interstellar gas condense and, through a still-uncertain process, form stars. The most massive of these are the so-called "O" stars, with are both very luminous and very hot, with temperatures on the order of several 10^4K. This makes them prodigious sources of high-energy photons (E>13.6eV), which ionize the gas in their im-

---

[4]Note that here and throughout I will adopt the inaccurate but standard convention in ISM studies of using the words "gas" and "plasma" somewhat interchangeably. This is primarily for the sake of simplicity, as one will often speak of differing ionization states in the same breath.

Figure 1.5: Composite image using Spitzer (infrared) and Hubble Space Telescope (ultra-violet and optical) colours of the Orion nebula. Image credit: NASA.
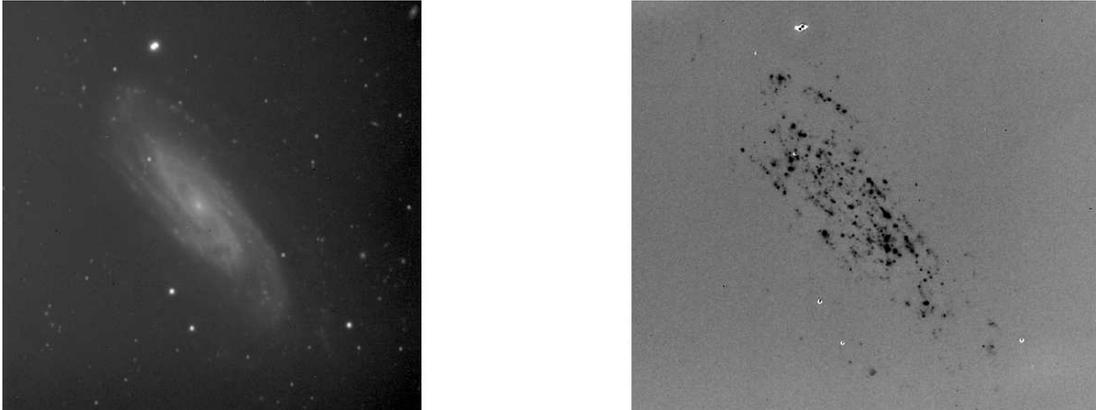
Figure 1.6: Images of NGC 3198 provided in the ancillary data from the Spitzer Infrared Nearby Galaxies Survey (SINGS, Kennicutt et al., 2003). NGC 3198 is a barred spiral galaxy (SBc), not unlike our own Galaxy, the Milky Way. To the left is a (logscale) image taken in the broad R band (tracing the light produced by the stellar population), while to the right, we see (in linear scale and inverted color for ease of viewing) the continuum-subtracted image of the Hα produced by diffuse ionized gas in the galaxy.

mediate vicinity. The excess energy in any ionization event (photon energy - ionization energy) is imparted to the electron as thermal energy (with the distribution of electron energies quickly equilibrating with a Maxwellian distribution), which may be re-radiated through interactions with atoms of Hydrogen, Helium, or the various metals. Similar processes govern all nebulae, regardless of the ionizing source (e.g. a post-AGB/pre-white dwarf star, active galactic nucleus, etc.).

In ionization equilibrium, the rate of photoionizations is precisely balanced by the rate of recombinations of electrons and atoms at any point in the cloud. For the Hydrogen-only case, this may be written as:

$$\dot{N_{\mathrm{I}}} = n_{\mathrm{H}} \int_{\nu}^{\infty} \frac{4\pi J_{\nu}}{h\nu} \sigma_{\nu}(H^0) d\nu = n_{\mathrm{e}} n_{\mathrm{p}} \alpha(H^0, T_{\mathrm{gas}}) = \dot{N_{\mathrm{R}}} \tag{1.2}$$

where J_{ν} is the mean intensity of radiation (in erg/cm^2/s/steradian/Hz), and σ_{ν} is the ionization cross-section of, in this case, Hydrogen (Osterbrock & Ferland, 2006). The densities of neutral Hydrogen, ionized Hydrogen (protons), and electrons are n_{H}, n_{p}, and n_{e} respectively, while $\alpha(H^0, T_{\mathrm{gas}})$ denotes the recombination rate of Hydrogen as a function of the gas temperature.

We will now introduce two approximations in order to make a simple estimate of the total recombination rate in an ionized gas. The first is the nebular approximation, which states that at sufficiently low densities, the rate of transitions of electrons in excited states to lower energy levels is orders of magnitude faster than the rate of collisions or photoionizations (see Osterbrock & Ferland, 2006, for a general discussion). We may assume that a recombination to any energy level of the Hydrogen atom in an ionized gas quickly cascades

through all downward transitions to the ground state. This allows us to compute the total recombination rate as the sum of all recombinations to all levels:

$$\alpha_{\mathrm{A}} = \sum_{\mathrm{n}} \alpha_{\mathrm{n}}(H^0, T_{\mathrm{gas}}) \tag{1.3}$$

$$\alpha_{\mathrm{B}}(T_{\mathrm{e}}) \approx 2 \times 10^{-10} T_{\mathrm{e}}^{-3/4} \mathrm{cm}^3 \mathrm{s}^{-1} \tag{1.4}$$

After Hydrogen, the next most abundant element in the typical composition of interstellar gas is Helium, with roughly ten Hydrogen atoms for every Helium atom. In treating ionization and recombination balance, much of the same formalism applies, albeit with a few notable differences, in particular the presence of a second electron in the neutral state. We will deal with the intricacies of Helium ionization and recombination in great detail in the following chapter.

The next most abundant elements, Oxygen and Carbon, are roughly ten thousand times less abundant than Hydrogen in the interstellar medium. The ionization and recombination of these and other "metals" do not contribute significantly to the ionization and thermal balance of nebulae. However, they do still contribute critically to the thermal balance of many ionized regions, by emission following collisional excitation through so-called "forbidden" transitions. This name comes from the fact that such transitions cannot occur through electric dipole interactions, leaving any atom excited to such a state meta-stable until a much less likely transition can occur. For most atomic transitions, at densities greater than $\sim 10^3$–$10^4 \mathrm{cm}^{-3}$ the likelihood of a further encounter resulting in collisional de-excitation is much greater than a spontaneous transition to a lower state (with the emission of a photon). However, at the low densities typical of the interstellar medium, it becomes much more likely that the emission of a photon will occur first, allowing this to become an important mechanism for cooling in many nebulae.

Dalgarno & McCray (1972) famously tabulated the so-called "cooling function": the volumetric cooling rate (per unit density of Hydrogen) of a gas with typical cosmic abundances as a function of the gas electron temperature. This is reproduced in fig. 1.7, showing the total cooling rate for differing fractional ionization fractions. Different elements provide the dominant cooling mechanism at different temperatures, with each species becoming important at electron temperatures where a sufficient number of electrons have sufficient energy to excite the relevant transition. At the lowest temperatures (T < 100K), characteristic of the coldest atomic clouds, the primary cooling mechanism is that of the fine structure transition of ionized Carbon ($^2\mathrm{P}_{3/2} \to {}^2\mathrm{P}_{1/2}$), giving way to fine structure transitions of ionized Silicon and Iron at temperatures of a few hundred to a thousand K. As the gas temperature approaches 10^4K, the thermal energies of many electrons reach the point where they can excite strong transitions of neutral Hydrogen. Even for highly-ionized gases, forbidden transitions of doubly and singly ionized Oxygen and singly ionized Nitrogen remain among many important coolants which suppress further heating in this temperature regime. Given the great abundance of Hydrogen, this presents a formidable barrier to further heating (see fig. 1.7). As a result, nebulae ionized by stellar sources observed in nature are rarely if ever hotter than $\approx 2 \times 10^4$K, with shock heating from
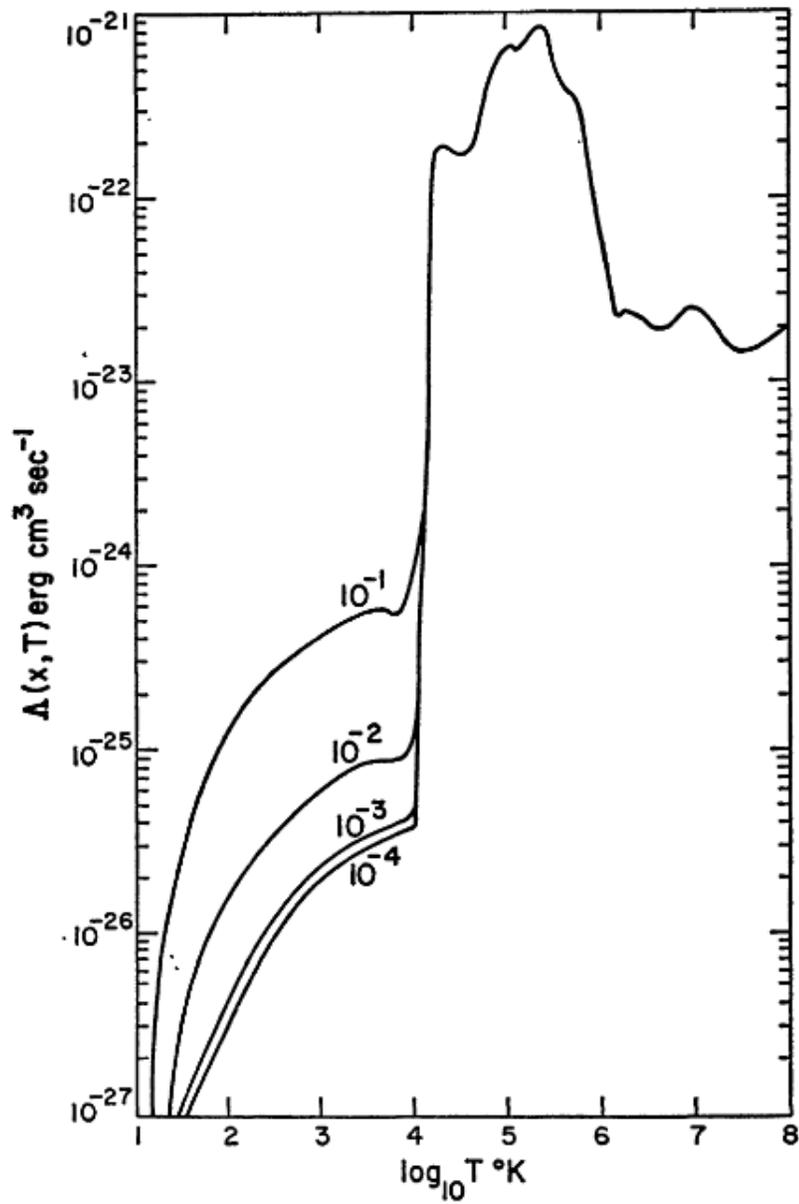
Figure 1.7: Total volumetric cooling rate (per unit hydrogen density) as a function of gas temperature, computed as the sum of contributions from the differing emission mechanisms which dominate at any given temperature. Each curve corresponds to a different fraction ionization (as labeled). From Dalgarno & McCray (1972).

supernovae or other such highly energetic mechanisms required to produce the very high ($\approx 10^6$K) temperatures seen in the hottest, most rarefied ISM.

A quantitative physical picture of ionized nebulae has been sought after from nearly the moment quantum mechanics was born (Zanstra, 1927). However, in practice the incredible number of electronic transitions which must be accounted for in computing the evolution of even a steady-state ionized nebula has defied any straightforward solution by hand for anything but the most simplified of circumstances. Over the past several decades, considerable progress has been made in developing numerical tools to compute the density, temperature, and ionization state of an astrophysical gas, given some ionizing source and other suitable initial conditions. We turn now to a brief summary of one such code in particular (MAPPINGS III), which we will refer to in the course of the following work.

1.2.2 Numerical methods

The history of numerical treatments of modeling photoionized nebulae is well-covered in the review of Ferland (2003), as well as the documentation[5] of the MAPPINGS III code (see below). In brief, early efforts made progress without considering radiative transfer or the detailed structure of ionized nebulae by assuming "Case B" recombination (see above), in which the "on-the-spot" approximation is exact (e.g. Baker & Menzel, 1938; Strömgren, 1939; Zanstra, 1951). Eventually, however, Rubin (1968) and others demonstrated that such a simplified treatment leads to substantial problems in the predicted emission-line fluxes and the temperatures of ionized nebulae, necessitating a more thorough treatment of radiative transfer within nebulae. This sparked an ever growing number of papers devoted to increasingly detailed numerical models of ionized media under differing conditions, and the emergence of several codes which remain in use to this day. Three notable examples are Prof. T. Kallman's Xstar (Kallman & McCray, 1982), Prof. G. Ferland's Cloudy (Ferland et al., 1998, 2013), and MAPPINGS III (e.g. Dopita, 1976; Kewley et al., 2001; Groves et al., 2004), maintained by members of the Australian National University and collaborators at the University of Hawaii and the Max Planck Institute for Astronomy. In this thesis, we will make use of the latter two, and in particular MAPPINGS III, therefore we will briefly review some of their salient features.

Modeling and Prediction in PhotoIonized Nebulae and Gasdynamical Shocks, or "MAPPINGS" began as an effort to develop a new code for numerical modeling of ionized regions which could include shocks (Dopita, 1976). This early work was expanded by Prof. M. Dopita and his then-student, (now Prof.) Luc Binette, into the first iteration of the multi-purpose photoionization and shock simulation code now known as MAPPINGS (e.g. Binette et al., 1982; Dopita et al., 1982; Evans & Dopita, 1985). Considerable improvements were introduced in the 1990s by Prof. Ralph Sutherland (e.g. Sutherland & Dopita, 1993) and Dr. Brent Groves in the 2000s (Groves et al., 2004), with an online version hosted by Prof. Lisa Kewley at the University of Hawaii from the late 2000s on (http://www.ifa.hawaii.edu/ kewley/Mappings/index.html).

---

[5]See http://www.mpia.de/~brent/mapiii_download.html for more information.

In the present version (MAPPINGS III.0.0q), one may specify a model by providing a "geometry," an incident ionizing spectrum, its normalization, the metallicity and filling factor[6] of the gas, and either the gas' density structure or pressure. As MAPPINGS III is a 1-dimensional code, only two geometries are available: either the spherically-symmetric case, or plane parallel. The code may also take a few optional parameters, such as including some model for the distribution and composition of dust, and the initial ionization state of the gas. The user must also specify some initial radius, which by convention is typically chosen to be 10% of the initial estimate of the Strömgren radius. This defines the full extent of an ionized volume for a given ionizing photon luminosity $\dot{N}_{\mathrm{ph}}$ and density of the gaseous medium n:

$$R_S = \left(\frac{3\dot{N}_{\mathrm{ph}}}{4\pi n^2 \alpha_2} \right)^{1/3} \tag{1.5}$$

(for the spherically-symmetric case, see e.g. Strömgren, 1939; Dyson & Williams, 1980), where we have assumed that in a wholly ionized medium (largely) composed of Hydrogen $n_{\mathrm{e}} \approx n_{\mathrm{p}} \approx n$.

The code then computes the thermal and ionization state of the nebula in a series of thin "shells" computed outward from the initial ionized surface until some specified termination condition, usually a threshold ionization fraction of Hydrogen (typically set to stop at $n_{H+}/n_H \approx 1\%$). At each step, the spectrum is attenuated by absorption and geometric dilution (depending on the chosen geometry), and the "diffuse field" (emission arising from the given point in the nebula) is computed and added, including photons generated from recombination, free-free emission, two-photon emission, and emission lines (see http://www.mpia.de/ brent/mapiii/photoionization.pdf for details). This spectrum is divided into roughly 1800 bins from 10^{-3}eV to 10keV, with the intensity within each bin represented by a power-law fit. Edges of many bins are fixed to coincide with the ionization thresholds of the most cosmically abundant atomic elements. Cooling is calculated including collisionally excited lines from the 16 most abundant elements, treating each as multi-level atoms. Cooling from resonance lines is included, however collisional de-excitation of resonance lines is neglected, yielding an upper bound on the densities for which MAPPINGS III produces meaningful predictions of $\approx 10^{10}$cm^{-3}. Cooling from collisional excitation of Hydrogen and Helium is included, with collisional excitation rates of the seven lowest levels of Hydrogen determined using the rates of Johnson (1972). Heating is computed from summing the contributions of each atomic species, with additional heating from secondary ionizations and excitations (by ejected photoelectrons) computed using the calculations of Shull (1979).

As mentioned above, MAPPINGS III is far from the only publicly-available code for numerical simulation of emission-line regions. In this thesis, we also make some small use of the code Cloudy (Ferland et al., 1998, 2013) in chapters 5 & 6. Cloudy requires similar input, with an architecture which focuses on computing as much as possible from first

---

[6]I.e. how much of a unit volume of "nebula" is occupied by the gas.

principles (as opposed to the numerous approximate schemes referred to above). This is admirable, but makes for a considerably slower code, rendering Cloudy much more useful for small experiments using fewer total computed tracks (or when available computing time is not a problem!). Past benchmarking efforts (Péquignot et al., 2001) have demonstrated that the results of Cloudy and MAPPINGS III agree remarkably well under most circumstances.

With the tools and physical understanding surveyed above, we are now ready to investigate in great detail the physics of interstellar media and, in particular, the sources of stellar (and non-stellar) light which influence its evolution. In particular, this will allow us to investigate in detail the emission-line fluxes of nebulae ionized by high-temperature sources, such as accreting white dwarfs. Although this often presents one with difficult, occasionally intractable inverse problems, much can be learned about sources of ionizing radiation from planetary nebulae to active galactic nuclei (Stasińska, 2007). Careful choice of emission lines sensitive to parameters of interest can allow us to construct diagnostics to investigate the ionizing background in galaxies near and far (e.g. Baldwin et al., 1981; Cid Fernandes et al., 2011). In the following section, we review our present understanding of the ISM of galaxies like our own (in which stars are still actively forming), and "red and dead" galaxies (without actively accreting supermassive black holes), in which old stars appear to provide to predominant source of ionizing radiation.

1.3 The interstellar medium of galaxies young and old

1.3.1 A brief overview of the ISM of galaxies

The interstellar medium of our Galaxy is, in a word, complex. Far from uniform, along most sight lines one finds incredible structures exists from subparsec to kiloparsec scales (Dickey & Lockman, 1990; Cox, 2005). Temperatures range from tens to ten million kelvin, though in practice most structure lie in one of the three regimes of the cooling curve discussed in the previous section (recall fig. 1.7). This led Field et al. (1969) to propose their two-phase model of the ISM: a "cold" neutral phase heated by cosmic rays, with cooling dominated by forbidden lines of [C II] and other "impurities" (in their terminology) and temperatures less than 300K, and a "warm" phase with temperatures which range from a few to ten thousand Kelvin, gas may be either neutral or ionized, and in which the predominant cooling mechanisms are collisional excitation of H and He, as well as forbidden line transitions of Oxygen and Nitrogen. In their original paper, Field et al. (1969) attributed heating of this phase to cosmic rays as well, but we now know that the dominant contribution is from stellar light (though there may be a need for an additional component, see Reynolds et al., 1999). This model was expanded by McKee & Ostriker (1977) to include a third phase, the "hot" ISM, heated by the explosion of supernovae, and with temperatures on the order of 10^6K. The three phases exist in approximate pressure equilibrium (with an additional pressure contribution from interstellar magnetic fields), with turbulent mixing powered by supernovae driving continued evolution, as well as new

star formation arising in the coldest, densest regions.

In external galaxies, we observe emission-line nebulae which appear to arise through a variety of means. Although star formation in the Universe peaked at a redshift z∼1.9 (Madau & Dickinson, 2014, ≈3.5Gyrs after the Big Bang), many galaxies in the local volume continue to produce stars at a rapid pace. In these objects, we see that their spectra are dominated by emission lines in ratios typical of H II regions, but on the scale of whole galaxies. In other galaxies, the available ionizing photon budget is dominated by the emission of a powerful central source: an accreting, supermassive black hole. Depending on the mode and rate of accretion, this may manifest itself in one of two ways: the high equivalent widths and highly-ionized emission lines of Seyfert-like galaxies, and the low-equivalent widths and emission lines of low-ionized or neutral species characteristic of Low-Ionized Emission-Line Regions (or LINERs). A number of diagnostic tools have been devised in order to classify the emission-line spectra of galaxies, and for each case identify the dominant source(s) of ionizing radiation, notably that of Baldwin et al. (1981), or the "BPT" diagram. A more modern version of this is presented in fig. 1.8, the "WHAN" diagram of Cid Fernandes et al. (2010) and Cid Fernandes et al. (2011). This uses two measures to delineate differing ionizing backgrounds: first, the equivalent width of the strongest optical line of Hydrogen at 6563Å, which provides a rough measure of the ionizing photon luminosity (per unit stellar mass, and ignoring the fraction of ionizing photons which may escape), and second, the ratio of the forbidden line doublet [N II] 6548Å+6584Å to the very nearby Hα. This allows for a remarkably effective separation of differing sources of ionizing radiation using only three emission lines across a very narrow range in wavelengths, minimizing the effect of reddening.

1.3.2   The extended emission-line regions of retired galaxies

There exists an additional class of emission-line galaxies with LINER-like emission line ratios (e.g. low [O III] 5007Å/Hβ, modestly high [N II] (6548Å+6584Å)/Hβ), but with even lower equivalent widths of Hα ($\lesssim$3Å). These galaxies are all red, evolved stellar populations with little or no ongoing star formation, and no discernible accreting compact central source (Cid Fernandes et al., 2011). Instead, the source of ionizing radiation in these galaxies is now understood to arise from the old stellar population (Sarzi, Shields & Schawinski, 2010), with the most likely candidate on a variety of grounds being so-called post-AGB stars (these are stars which have just completed the last of the thermal pulsations at the end of the AGB, and are evolving toward the white dwarf cooling track). In brief, these appear to be able to satisfactorily reproduce the observed emission-line ratios (Binette et al., 1994; Stasińska et al., 2008), the line luminosity and equivalent width of Hα (Sarzi, Shields & Schawinski, 2010; Eracleous et al., 2010), and the radial variation of the observed intensities of nebular lines (Sarzi, Shields & Schawinski, 2010; Yan & Blanton, 2012; Singh et al., 2013). Accompanying this ionized gas are extended distributions of neutral H I (Serra et al., 2012), with the most common morphology being a disky configuration. Both the neutral and ionized gas extend out to kiloparsec scales, giving rise to the name "LIERs" (Sarzi, Shields & Schawinski, 2010, as the emission-line region is not principally confined to
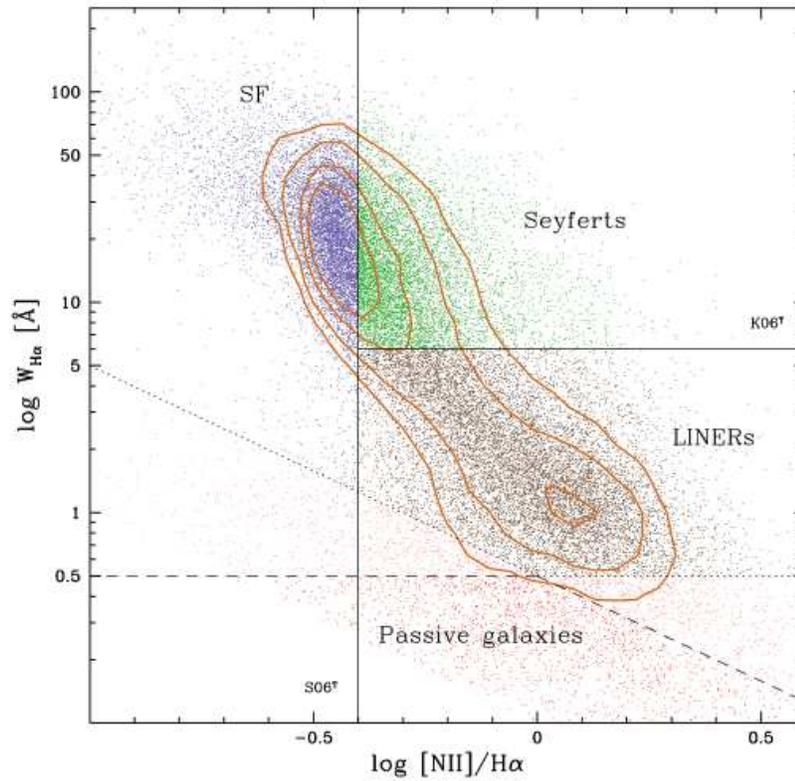
Figure 1.8: The WHAN (equivalent Width of H Alpha and Nitrogen II to h alpha ratio) diagnostic diagram of Cid Fernandes et al. (2010, 2011). On the horizontal axis, the ratio of [N II] 6548Å+6584Å to Hα serves as a measure of the hardness of the ionizing continuum in a given galaxy, while on the vertical axis, the equivalent width of Hα serves as a rough proxy of the total ionizing photon rate (for some assumptions about the covering fraction of the gas).

the nucleus), although "passive" or "passively-evolving" galaxies have also been commonly used (Cid Fernandes et al., 2011).

Although post-AGB stars appear to provide the primary contribution to the ionizing background of these galaxies, other components of the old stellar population may provide additional important contributions. In particular, both extreme-horizontal branch stars and low-mass X-ray binaries certainly exist in some number in any such population; indeed, Sarzi, Shields & Schawinski (2010) found they contribute up to perhaps 10% of the total ionizing background each. Notably, accreting, steadily nuclear-burning white dwarfs had **not** been actively considered in the past.

1.4   Outline of this work

In this thesis, we outline a new means to discover or, as we will see, strongly constrain the progenitors of SNe Ia, which accounts for the broad range of temperatures both observed and predicted for accreting, nuclear-burning white dwarfs. This relies on identifying such sources as the incredibly strong sources of ionizing radiation that they are, and developing diagnostic tools to search for their impact on interstellar matter at all scales.

In Chapter 2, we demonstrate that in the single-degenerate scenario, accreting, nuclear-burning white dwarfs will dominate the ionizing background in early-type galaxies, and demonstrate the utility of recombination lines of ionized Helium as a diagnostic for evaluating the true contribution of such sources. This work is published in *Monthly Notices of the Royal Astronomical Society* (Woods & Gilfanov, 2013). We then expand on this in Chapter 3 with additional diagnostics better suited to the highest temperature sources (paradoxically relying on low-ionized species, in particular forbidden emission lines of neutral Oxygen and Nitrogen and singly-ionized Carbon). This work is published in *Monthly Notices of the Royal Astronomical Society* (Woods & Gilfanov, 2014). We then briefly review the first applications of these diagnostics in Chapter 4, with an emphasis on the contributions of the author. In particular, we demonstrate that the first measurement of the He II recombination line at 4686Å in the extended emission-line regions of passively-evolving galaxies limits the contribution of any "hot-mode" (≈ 1.2–6×10^5K) SN Ia progenitor channel from accounting for more than ≈ 1–5% of the total SN Ia rate at delay times of 1–4Gyrs (published in *Monthly Notices of the Royal Astronomical Society*, Johansson et al., 2014). This emission-line constraint can be extended to source temperatures $\gtrsim 10^6$K with the use of our [O I] 6300Å diagnostic (Johansson et al, to be submitted). We then demonstrate how this can be used to inform our understanding of population synthesis (Chen et al., 2014, , Chen et al (2015), submitted to *Monthly Notices of the Royal Astronomical Society*). We then turn in Chapter 5 to the consideration of individual sources, and address the question of why nebulae are so rarely detected in the vicinity of known accreting, nuclear-burning white dwarfs (to date, only one such nebula is confirmed, that of Cal 83 in the Large Magellanic Cloud). This has been submitted for publication in *Monthly Notices of the Royal Astronomical Society* (Woods & Gilfanov, 2015). Finally, in Chapter 6 we publish our first constraints on the ionizing luminosity of the progenitor of SN2014J, the

nearest supernova in four decades, using a pre-supernova narrow-band Hα image of its host galaxy, M82. This work will be submitted for publication following the reduction (after the submission of this thesis) of some additional narrow-band observations made by the Russian-Turkish 1.5m telescope. We then close with some concluding remarks in Chapter 8.

Bibliography

Abt, H. A. 1983, ARA&A, 21, 343

Badenes, C., & Maoz, D. 2012 ApJ, 749, LL11

Baker, J. G., & Menzel, D. H. 1938, ApJ, 88, 52

Baldwin, J. A., Phillips, M. M., & Terlevich, R. 1981, PASP, 93, 5

Bethe, H. A. 1990, Reviews of Modern Physics, 62, 801

Binette, L., Dopita, M. A., Dodorico, S., & Benvenuti, P. 1982, A&A, 115, 315

Cassisi S., Iben, Jr. I., Tornambe A., 1998, The Astrophysical Journal, 496, 376

Chandrasekhar, S. 1931, ApJ, 74, 81

Chen, H.-L., Woods, T. E., Yungelson, L. R., Gilfanov, M., & Han, Z. 2014, MNRAS, 445, 1912

Chiosi, E., Chiosi, C., Trevisan, P., Piovan, L., & Orio, M. 2014, arXiv:1409.1104

Cid Fernandes, R., Stasińska, G., Schlickmann, M. S., et al. 2010, MNRAS, 403, 1036

Cid Fernandes, R., Stasińska, G., Mateus, A., & Vale Asari, N. 2011, MNRAS, 413, 1687

Cox, D. P. 2005, ARA&A, 43, 337

Dalgarno, A., & McCray, R. A. 1972, ARA&A, 10, 375

Dickey, J. M., & Lockman, F. J. 1990, ARA&A, 28, 215

Dopita, M. A. 1976, ApJ, 209, 395

Dopita, M. A., Binette, L., & Schwartz, R. D. 1982, ApJ, 261, 183

Dyson, J. E., & Williams, D.   1980, New York, Halsted Press, 1980. 204 p.,

Di Stefano, R., Fisher, R., Guillochon, J., & Steiner, J. F. 2015, arXiv:1501.07837

Evans, I. N., & Dopita, M. A. 1985, ApJS, 58, 125

Ferland, G. J., Korista, K. T., Verner, D. A., et al. 1998, PASP, 110, 761

Ferland, G. J. 2003, ARA&A, 41, 517

Ferland, G. J., Porter, R. L., van Hoof, P. A. M., et al. 2013, Rev. Mexicana Astron. Astrofis., 49, 137

Field, G. B., Goldsmith, D. W., & Habing, H. J. 1969, ApJ, 155, L149

Gilfanov M., Bogdán Á., 2010, Nature, 463, 924

Gilfanov, M., & Bogdán,Á. 2011, American Institute of Physics Conference Series, 1379, 17

Groves B. A., Dopita M. A., Sutherland R. S., 2004, The Astrophysical Journal Supplement Series, 153, 9

Hachisu I., Kato M., Nomoto K., 1999, The Astrophysical Journal, 522, 487

Hillebrandt, W., Kromer, M., Röpke, F. K., & Ruiter, A. J. 2013, Frontiers of Physics, 8, 116

Iben, I., Jr., & Tutukov, A. V 1989, ApJ, 342, 430

Iglesias, C. A., & Rogers, F. J. 1993,ApJ, 412, 752

Johansson, J., Woods, T. E., Gilfanov, M., et al. 2014, MNRAS, 442, 1079

Johnson, L. C. 1972, ApJ, 174, 227

Justham, S. 2011, ApJ, 730, LL34

Kallman, T. R., & McCray, R. 1982 ApJS, 50, 263

Kewley L. J., Dopita M. A., Sutherland R. S., Heisler C. A., Trevena J., 2001, The Astrophysical Journal, 556, 121

Krause, O., Tanaka, M., Usuda, T., et al. 2008, Nature, 456, 617

Madau, P., & Dickinson, M. 2014, ARA&A, 52, 415

Maoz, D., Mannucci, F., & Nelemans, G. 2014, ARA&A, 52, 107

McKee, C. F., & Ostriker, J. P. 1977, ApJ, 218, 148

Minkowski, R. 1941, PASP, 53, 224

Nomoto, K., Nariai, K., & Sugimoto, D. 1979, PASJ, 31, 287

Nomoto K., Saio H., Kato M., Hachisu I., 2007, The Astrophysical Journal, 663, 1269

Osterbrock, D. E., & Ferland, G. J. 2006, Astrophysics of gaseous nebulae and active galactic nuclei, 2nd. ed. by D.E. Osterbrock and G.J. Ferland. Sausalito, CA: University Science Books, 2006,

Pakmor, R., Kromer, M., Röpke, F. K., et al. 2010, Nature, 463, 61

Pakmor, R., Kromer, M., Taubenberger, S., et al. 2012, ApJ, 747, LL10

Péquignot, D., Ferland, G., Netzer, H., et al. 2001, Spectroscopic Challenges of Photoionized Plasmas, 247, 533

Perlmutter S. et al., 1999, The Astrophysical Journal, 517, 565

Phillips, M. M. 1993, ApJ, 413, L105

Prialnik, D. 2000, "An Introduction to the Theory of Stellar Structure and Evolution, by D. Prialnik.∼ISBN 052165937X., UK: Cambridge University Press, 2000.",

Reynolds, R. J., Haffner, L. M., & Tufte, S. L. 1999, ApJ, 525, L21, 646

Riess A. G. et al., 1998, The Astronomical Journal, 116, 1009

Rubin, R. H. 1968, ApJ, 153, 761

Saio, H., & Nomoto, K. 1985 A&A, 150, L21

Shen, K. J., & Bildsten, L. 2007, ApJ, 660, 1444

Shull, J. M. 1979, ApJ, 234, 761

Soraisam, M., & Gilfanov, M. 2014, arXiv:1401.6148

Stasińska, G. 2007, arXiv:0704.0348

Strömgren, B. 1939, ApJ, 89, 526

Sutherland, R. S., & Dopita, M. A. 1993, ApJS, 88, 253

van den Heuvel E. P. J., Bhattacharya D., Nomoto K., Rappaport S. A., 1992, Astronomy and Astrophysics, 262, 97

Webbink R. F., 1984, Astrophysical Journal, 277, 355

Whelan J., Iben, Jr. I., 1973, The Astrophysical Journal, 186, 1007

Woods, T. E., & Gilfanov, M. 2013, MNRAS, 432, 1640

Woods, T. E., & Gilfanov, M. 2014, MNRAS, 439, 2351

Woods, T. E., & Gilfanov, M. 2015, *submitted*

Woosley, S. E., Heger, A., & Weaver, T. A. 2002, Reviews of Modern Physics, 74, 1015

Zanstra, H. 1927, ApJ, 65, 50

Zanstra, H. 1951, Bull. Astron. Inst. Netherlands, 11, 341

Chapter 2

He II recombination lines as a test of the nature of SN Ia progenitors in elliptical galaxies

2.1   Abstract

To date, the question of which progenitor channel can reproduce the observed rate of Type Ia supernovae (SNe Ia) remains unresolved, with the single and double degenerate scenarios remaining the leading contenders. The former implies a large population of hot accreting white dwarfs with photospheric temperatures of $T \sim 10^5 - 10^6$ K during some part of their accretion history. We show that in early-type galaxies, a population of accreting white dwarfs large enough to reproduce the SN Ia rate would contribute significantly to the ionizing UV radiation expected from the stellar population. For mean stellar ages $\lesssim 5$ Gyr, single degenerate progenitors would dominate the ionizing background produced by stars, increasing the continuum beyond the He II-ionizing limit more than ten-fold. This opens a new avenue for constraining the progenitors of SNe Ia, through consideration of the spatially extended low-ionization emission-line regions now found in many early-type galaxies. Modeling the expected emission, we show that one can constrain the contribution of the single degenerate channel to the SN Ia rate in E/S0 galaxies from upper limits on the luminosity of He II recombination lines in the optical and FUV. We discuss future directions, as well as possible implications for the evolution of SNe Ia in old stellar populations.

2.2   Introduction

Type Ia supernovae (SNe Ia) remain without a definitive model for their origin, despite their great importance in the measurement of cosmic distances (Riess et al., 1998; Perlmutter et al., 1999) and their vital role in the chemical evolution of the Universe (see e.g. Matteucci & Greggio, 1986). The two leading models are the single degenerate scenario (Whelan & Iben, 1973), in which a single white dwarf (WD) reaches the Chandrasekhar mass (M_{Ch}) through accretion from a red giant or main sequence companion; and the double degenerate scenario (Webbink, 1984; Iben & Tutukov, 1984), in which a SN Ia results from the inspiral and merger of a binary pair of white dwarfs. Unfortunately, unlike the progenitors of Type II supernovae, SN Ia progenitors are too faint to be detectable (to date, e.g. Li et al., 2011; Nielsen, Voss & Nelemans, 2012) in archival images retrieved after the explosion. Therefore, indirect arguments must be introduced in order to place limits on the likely progenitors.

The single degenerate channel implies the existence of a large population of steadily accreting WDs. If steady nuclear burning occurs near the surface, each of these should spend some fraction of its accretion history as a strong supersoft X-ray source (SSSs, van den Heuvel et al., 1992; Kahabka & van den Heuvel, 1997). Recently however, the total soft X-ray emission of elliptical galaxies was found to be far too low (Gilfanov & Bogdán, 2010), and the number of observed SSSs in nearby galaxies too few (Di Stefano, 2010), for the SD scenario to hold in its standard form. Population synthesis calculations have also demonstrated the great difficulty of producing a sufficient number of high-mass, accreting WDs to account for a significant fraction of the SN Ia rate (see e.g. Ruiter, Belczynski & Fryer, 2009, and for an extreme example Yungelson (2010)), at least given our current understanding of binary evolution.

As a possible resolution to the deficit of observed supersoft sources, Hachisu, Kato & Nomoto (2010) suggested that a WD's photosphere is inflated in a so-called accretion wind state for much of its accretion phase. This shifts the peak of its emission from soft X-rays to the (extreme) UV, where it can not be directly observed due to absorption. However, for mass transfer rates $\lesssim$ a few $10^{-6} M_{\odot}$/yr, relevant to this scenario, the accreting WD should remain an incredibly powerful ionizing source with photospheric temperatures on the order of $\gtrsim 10^5 K$ (Hachisu, Kato & Nomoto, 1999), possibly resembling a Wolf-Rayet star (Lepo & van Kerkwijk, 2013).

At least $\sim 40\%$ of nearby early type galaxies outside the Virgo cluster are known to contain a detectable mass of neutral hydrogen ($M(HI) \sim 10^8 - 10^9\ M_{\odot}$, Serra et al., 2012). The morphology of this gas ranges from irregularly distributed clouds scattered throughout the galaxy to regular disks or rings, the latter constituting the majority of H I detections. The H I disks may be confined within the stellar body of the galaxy, or extend to tens of kpc far beyond the stellar light, and have typical H I column densities on the order of $N_H \sim 10^{20}$ cm^{-2} (Serra et al., 2012).

In addition to the neutral matter are *extended* (well beyond the nucleus) regions of

LINER[1]-like line emission (see e.g. Sarzi, Shields & Schawinski, 2010), indicating the presence of warm (T $\approx 10^4$ K) ionized gas. This appears to be primarily powered by a diffuse galactic background, rather than being the summation of many overlapping H II regions. Post asymptotic giant branch stars (pAGBs) may provide the dominant contribution to the needed diffuse ionizing background (Sarzi, Shields & Schawinski, 2010; Eracleous et al., 2010). The ionizing spectra of pAGBs also produce reasonable agreement with the observed optical line ratios (Binette et al., 1994; Stasińska et al., 2008), and appear to adequately predict the radial dependence of the inferred ionizing flux (Yan & Blanton, 2012).

A population of accreting white dwarfs implied by the SD scenario, with temperatures $> 10^5$ K would, however, introduce a substantially harder component to the ionizing background, in particular beyond the He II photoionizing limit. The presence of such a component would dramatically change the ionization structure of the H II gas and the line content of its emission. The greater flux of high energy ionizing photons will have a pronounced effect on several characteristic line ratios (Rappaport et al., 1994). Most importantly, the total luminosity reprocessed into recombination lines of He II should be greatly enhanced. These lines are characteristic of the youngest starbursts (the result of ionization by WR stars), and are not normally observed in old stellar populations outside the innermost nuclear regions. The strongest He II recombination line which is not capable of ionizing hydrogen, and therefore is not heavily absorbed in the ISM, is the $n = 3 \to 2$ transition at ≈ 1640Å. In the optical band, the strongest line is the $n = 4 \to 3$ transition at ≈ 4686Å. The strength of these lines (or their absence) in the optical and UV spectra of early type galaxies can be used to limit the total population of such purported SN Ia progenitors, direct emission from which is unobservable, due to interstellar absorption. Furthermore, contrary to upper limits from X-ray observations, such a method should in principle be strengthened if emission is primarily absorbed near the source, given the higher covering fraction and ionization parameter.

With this in mind, we explore the consequences of introducing a population of SD SN Ia progenitors, which spend some fraction of their accretion history at varying temperatures typical of nuclear-burning WDs. We proceed as follows: in §2.3, we estimate the ionizing background expected from the passively evolving (SFR ≈ 0) stellar population in early-type galaxies, and its modification due to the contribution of a putative population of accreting white dwarfs envisaged by the SD SN Ia scenario. In §2.4 we consider the ionization balance in the photo-ionized gas and model the emitted spectra of these extended nebulae. In particular, we investigate how the total expected luminosity of H and He II recombination lines should vary with age of the underlying stellar population. We demonstrate how one can then constrain the maximum luminosity which may be radiated by a population of SD progenitors at a given temperature using the predicted and observed He II 4686Å flux (or for the latter, upper limits). Finally, we discuss observational prospects and what implications our results have for the possible role of the SD SN Ia channel, as well as whether there may be any caveats to the limits given here.

---

[1]Low-Ionization Nuclear Emission-Line Regions (Osterbrock, 1989).

2.3 The ionizing background in early-type galaxies

2.3.1 Post asymptotic giant branch stars

In order to model the ionizing background from the underlying stellar population, we make use of the spectral evolution calculations of Bruzual & Charlot (2003). For simplicity we model all passively evolving galaxies as having stellar populations born in a single burst of star formation, with initial masses distributed following Chabrier (2003). Though certainly an oversimplification, focusing on such simple populations allows us to emphasize the importance of any age-dependence for the ionizing background. In practice, it is then straightforward to construct more complex star-formation histories.

In this work, we take $Z = 0.05$ ($\approx 2.5Z_\odot$) as the typical metallicity of stellar populations in early-type galaxies, consistent with the value assumed in the "baseline" measurement of the SN Ia rate in Totani et al. (2008). Such a metallicity is well in line with observations of old stellar populations. Although this gives a higher K-band luminosity per unit mass at any given age (increasing the predicted number of SN Ia progenitors), the ionizing continuum from a simple stellar population (SSP) is also generally higher for higher metallicities, minimizing the importance of the stellar population's metallicity (with the continuum varying by only $\approx 10-20\%$, except at the earliest ages). At 1Gyr, the ionizing continuum is roughly the same for $2.5Z_\odot$ as for $Z_\odot$, but the SN Ia rate would be $\sim 40\%$ higher for $2.5Z_\odot$.

2.3.2 Single degenerate progenitors

We can also make an estimate of the expected emission from SD SN Ia progenitors. In the standard SD scenario, the total mass of the WD must reach $M_{\rm ch} \approx 1.4 M_\odot$ through accretion from either a main sequence or red giant companion. In order to avoid an accretion-induced collapse, the accretor must be a carbon-oxygen (CO) WD. The maximum mass with which a CO WD can be born is presently estimated to be approximately $\sim 1.1 M_\odot$ (Umeda et al., 1999), therefore a SN Ia progenitor must accrete *at least* $\Delta M \sim 0.3 M_\odot$ before reaching $M_{\rm Ch}$. Note however that the distribution of WD initial masses falls steeply with greater mass, from a peak around $M_{\rm WD} \approx 0.6 M_\odot$, therefore the mean accreted mass per one type Ia supernova can be expected to typically greatly exceed the value quoted above.

The luminosity of an accreting WD is dominated by the energy release from nuclear burning of accreted matter so long as the mass transfer rate exceeds the minimum limit:

$$\dot{M}_{\rm steady,min} \gtrsim 3.1 \cdot 10^{-7} (M_{\rm WD}/M_\odot - 0.54) M_\odot/{\rm yr} \tag{2.1}$$

(Nomoto et al., 2007). Below this, nuclear burning occurs only in unsteady bursts, giving rise to novae. The retention fraction of matter in this case remains highly uncertain; even optimistic binary evolution models suggest $\Delta m_{\rm WD} \lesssim 0.1 M_\odot$ may be accreted in this low-$\dot{M}$ regime (see e.g. Hachisu, Kato & Nomoto, 2010). In such a case, SN Ia progenitors would necessarily undergo many recurrent novae, in conflict with the observed rate of novae in nearby galaxies (Gilfanov & Bogdán, 2011).

Assuming the steady burning condition is met, the luminosity of the accreting WD is then:

$$L_{nuc} = \epsilon_{\mathrm{H}} \chi \dot{M} \tag{2.2}$$

where ϵ_{H} is the energy release per unit mass of hydrogen ($\sim 6 \cdot 10^{18}$ erg/g), and χ is the mass fraction of hydrogen (~ 0.72). Helium burning is significantly less efficient and contributes to the luminosity only on the order of $\sim 10\%$.

For any given WD mass, there is also a maximum accretion rate for steady burning; when the luminosity approaches that of a red giant the burning luminosity in eq. 2.2 is limited by (Nomoto et al., 2007)

$$\dot{M}_{\mathrm{RG}} \approx 6.7 \cdot 10^{-7} (M_{\mathrm{WD}}/M_{\odot} - 0.45) M_{\odot}/\mathrm{yr} \tag{2.3}$$

Above this limit, it is not immediately apparent what becomes of the excess matter. It is possible that a thick envelope will form around the accreting WD, effectively returning it to a red giant state. However, if this is the case, it is also unlikely that the WD will be able to accrete and retain sufficient matter to produce a SN Ia (e.g. Cassisi et al., 1998). Another possibility is that for any mass transfer rate greater than this, the excess matter is lost in a fast wind driven from within the WD's now significantly expanded photosphere (Hachisu, Kato & Nomoto, 1999). The possible accretion states are then:

- $\dot{M} > \dot{M}_{\mathrm{RG}}$ Envelope or wind

- $\dot{M}_{\mathrm{steady,min}} < \dot{M} < \dot{M}_{\mathrm{RG}}$ Steady burning

- $\dot{M} < \dot{M}_{\mathrm{steady,min}}$ Unstable, nova flashes

In the SD scenario, the total number of SN Ia progenitors within a galaxy with instantaneous SN Ia rate $\dot{N}_{\mathrm{Ia}}$ is given by (Gilfanov & Bogdán, 2011)

$$N_{\mathrm{progenitors}} \approx \dot{N}_{\mathrm{Ia}} \cdot \Delta M / \dot{M} \tag{2.4}$$

We compute the specific SN Ia rate per unit K-band luminosity from the delay-time distribution found by Totani et al. (2008) in galaxies with old stellar populations

$$\dot{N}_{\mathrm{Ia}} = 0.57 (t/\mathrm{Gyr})^{-1.11} \mathrm{Sne/century}/10^{10} \mathrm{L_{K,\odot}} \tag{2.5}$$

Here we use their fit obtained for $Z = 2.5 Z_{\odot}$ and a Chabrier IMF. Note that in the study of Totani et al. (2008), they take the rate per unit K-band luminosity found by Mannucci et al. (2005) for E/S0 galaxies as the value at $t = 11$ Gyr.

If we assume that throughout the growth of the accreting WD, the mass transfer rate lies somewhere in the range 10^{-7} $M_{\odot}/\mathrm{yr} \lesssim \dot{M} \lesssim 10^{-6}$ $M_{\odot}/\mathrm{yr}$, then the number of (either steadily or unsteadily) nuclear burning WDs in a 10 Gyr-old elliptical with a K-band luminosity 10^{11} $L_{\mathrm{K,\odot}}$ is accordingly $10^3 \lesssim N_{\mathrm{progenitors}} \lesssim 10^4$.

While their total number may be difficult to pinpoint due to the uncertain (yet certainly varying) accretion rate, there is far less freedom in the total bolometric luminosity emitted by a population of SD progenitors. We can estimate this luminosity as

$$L_{\text{tot,SNIa}} \approx N_{progenitors} \cdot L_{nuc} = \epsilon_{\text{H}} \chi \Delta M_{\text{Ia}} \dot{N}_{\text{SNIa}} \tag{2.6}$$

Note that the mass transfer rate cancels out in this estimation; whether a few nuclear-burning WDs accrete very quickly until reaching M_{Ch}, or many WDs accrete very slowly, a certain amount of mass must be processed in the SD scenario at any instant, fixed by the SN Ia rate. If, for a given SD progenitor scenario, the accreting component is X-ray or UV-luminous only for some subset of its entire accretion history, we can compute the total luminosity from eq.(2.6), replacing the total ΔM with the amount of mass Δm_{i} accreted during that phase.

Choosing a particular model for the spectra of SN Ia progenitors, we can then estimate the energy output per unit wavelength of their entire population in any galaxy, from the latter's age and K-band luminosity:

$$L_{\lambda,\text{net}} = \dot{N}_{\text{Ia}} \int_{\text{M}_{\text{i}}}^{\text{M}_{\text{Ch}}} \frac{L_\lambda(M, \dot{M})}{\dot{M}} \text{dM} \tag{2.7}$$

The mass transfer rate $\dot{M}$ varies over the course of the WD's accretion phase, and the emission spectrum $L_\lambda(M, \dot{M})$ generally depends on the white dwarf mass and the accretion rate.

The case of supersoft sources (steady nuclear burning WDs) was studied extensively by Rauch & Werner (2010). It has been shown that, despite a number of strong atmospheric absorption lines from various elements, the overall shape of their ionizing continuum does not deviate too strongly from that of a blackbody whose temperature is close to the effective SSS temperature. The latter is given by

$$T_{\text{eff}} = \left(\frac{L_{nuc}}{4\pi R_{WD}^2 \sigma_{SB}} \right)^{\frac{1}{4}} \approx 5.3 \cdot 10^5 \; \dot{M}_{-7}^{1/4} \; R_{-2}^{-1/2} \; K \tag{2.8}$$

where $\dot{M}_{-7}$ is the mass accretion rate in units of $10^{-7} \; M_\odot/\text{yr}$ and R_{-2} is the white dwarf radius in units of $10^{-2} \; R_\odot$. Thus, typical SSS temperatures lie in the range $\sim 2 - 7 \cdot 10^5 K$ (van den Heuvel et al., 1992).

For the optically-thick wind case however ($\dot{M} > \dot{M}_{\text{RG}}$), the expected observable appearance is less certain. For expected mass transfer rates ($\sim 10^{-6} M_\odot/\text{yr}$) the effective temperature should be $\sim 2 \cdot 10^5 K$ for WDs of mass $\gtrsim 0.9 M_\odot$ (Hachisu, Kato & Nomoto, 1999). One can demonstrate that for these parameters, the nuclear-burning WD should be able to fully ionize hydrogen and helium beyond the wind's photosphere (see appendix A); therefore in the energy range of interest the spectrum should be at least roughly represented by a black body. In particular, no photoabsorption cutoff at the He II 54.4eV edge should be expected (cf Rauch, 2003). Therefore in the following calculations we assume blackbodies of fixed temperatures to represent the emission spectra of SD SN Ia
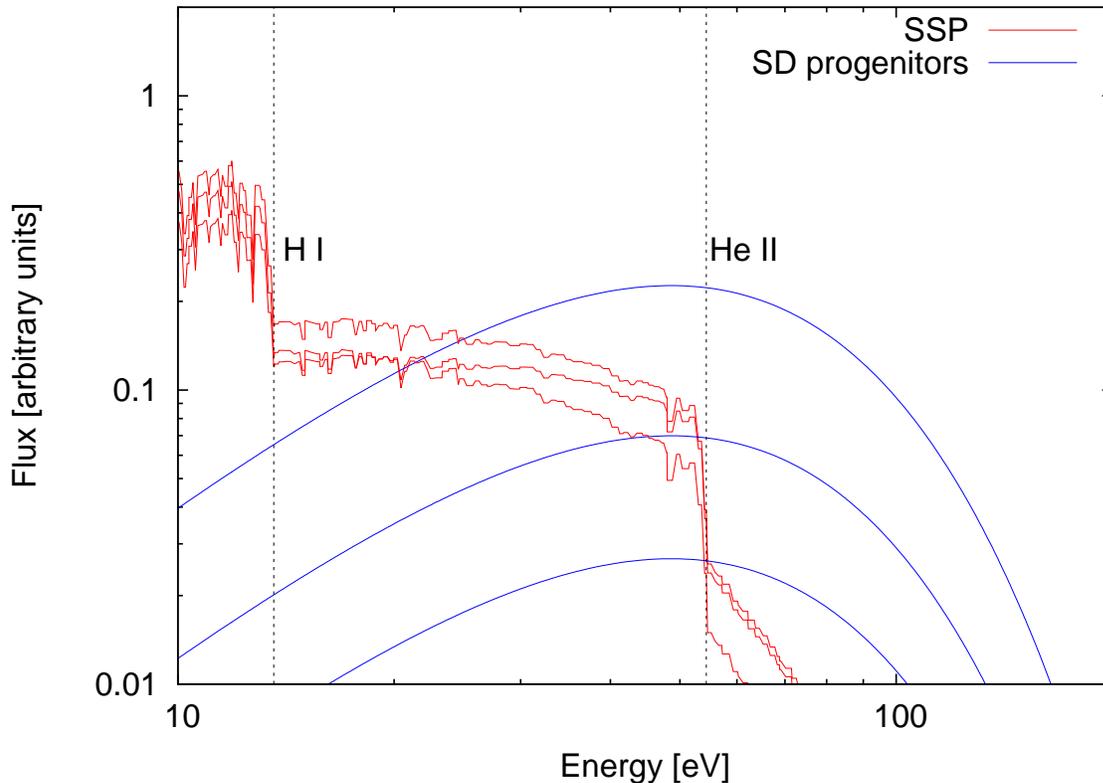
Figure 2.1: Comparison of the emitted spectrum at 3, 6, and 10 Gyr (upper to lower lines) from the normally-evolving stellar population (red) and from a population of SD SN Ia progenitors (blue) assuming that $\Delta M = 0.3 M_\odot$ of material is accreted with an effective temperature of $T = 2 \cdot 10^5$ K, as described in §2.3.

progenitors. One can then test any SN Ia progenitor channel through superposition of the appropriate results, for differing L_{Ia} and T_{eff}.

2.3.3   The ionizing radiation field in ellipticals

We can now compare the anticipated ionizing emission from normally-evolving SSPs with that from a putative SD progenitor population. Shown in Fig. 2.1 is the emitted spectrum predicted for 3, 6, and 10 Gyr-old populations, overlayed with that from a hypothetical SD channel which processes $\Delta M = 0.3 M_\odot$ at an effective temperature of $\approx 2 \cdot 10^5 K$ (near the lower bound for observed temperatures in symbiotic SSSs, and consistent with what would be expected during the wind phase). Above the He II-photoionizing limit, we see that the contribution from SD progenitors dramatically hardens the spectrum, and begins to dominate even the H-ionizing continuum for young, passively-evolving stellar populations.

This is further illustrated in Fig.2 where we plot the integrated total H- and He II-
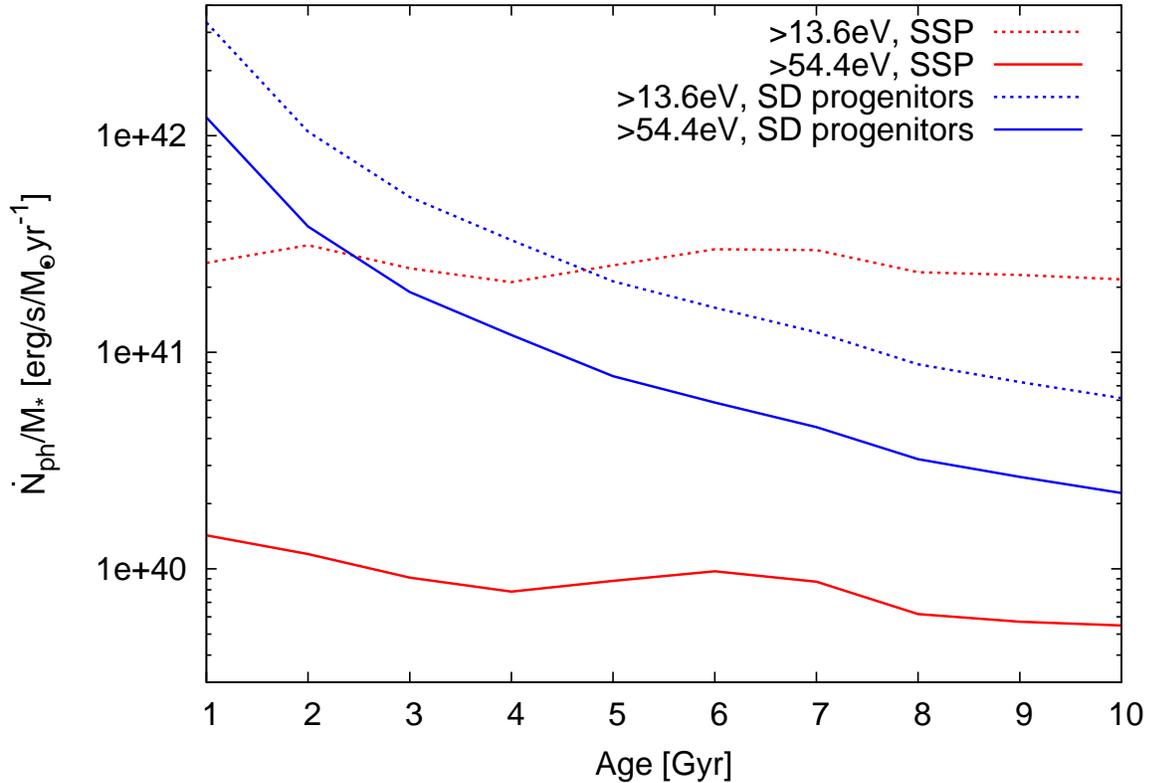
Figure 2.2: Comparison of the H I (dotted lines) and He II (solid lines) ionizing photon luminosity per unit mass from pAGB stars (red lines) with that from a population of SD progenitors (blue lines) as a function of stellar age (from initial starburst). The latter was computed assuming that $\Delta M = 0.3 M_\odot$ of material is accreted with an effective temperature of $T = 2 \cdot 10^5$ K.

ionizing photon emission for two cases: photoionization by a SSP, and by an example SD progenitor population. The He II-ionizing luminosity is increased by a factor of ~ 5 at $\sim$ 10 Gyr, rising to roughly two orders of magnitude for the youngest populations. There is an accompanying, less significant boost in the H-ionizing luminosity, though this rises to an order of magnitude at the youngest ages. Clearly, this will have a strong impact on the observed emission lines in any nebulae ionized by the diffuse background produced by such a population. In particular, this suggests that a population of accreting WDs sufficient to match the SN Ia rate should make their presence clear through the observation of He II recombination lines in the spectra of low-ionization emission line regions in passively-evolving galaxies. In order to quantify this, we turn now to modeling these nebulae.
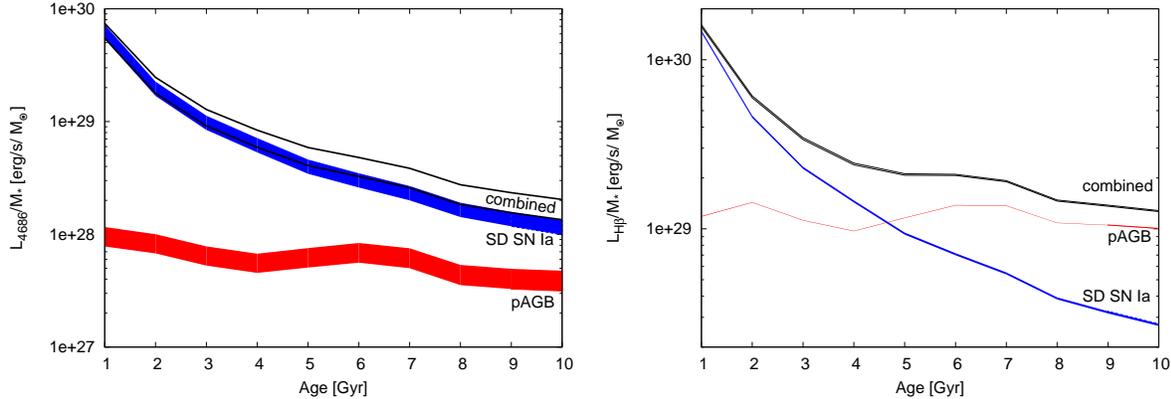
Figure 2.3: He II 4686Å (*left*) and Hβ (*right*) luminosity per unit mass assuming ionization by pAGB stars alone (red), ionization by a population of SD SN Ia progenitors (blue), and ionization by their combined luminosity (outlined in black), as a function of stellar age (from initial starburst). Here we use the same example parameters for the SD channel as before. In this and all further figures, the thickness of lines shows the effect of the uncertainty in ionization parameter (Section 2.4.1). This is negligible for the Hβ line.

2.4 Constraining the characteristics of SN Ia progenitors

2.4.1 Modeling low-ionization emission-line regions

Typically, the luminosity in any recombination line can be estimated analytically based on the total ionization rate and branching ratios for recombination (e.g. Osterbrock, 1989). However, the extended emission-line regions of early-type galaxies are observed to be in a very low state of ionization (Binette et al., 1994), such that this is not sufficient in computing the luminosity of He II recombination lines (see appendix B). Therefore, to determine the effect on the nebular emission of introducing a previously unaccounted-for ionizing stellar sub-population, we make use of the photoionization code MAPPINGS III (e.g. Kewley et al., 2001; Groves et al., 2004).

The code allows us to model the emission lines resulting from an incident ionizing background within a 1-D cloud (where we assume plane-parallel geometry). The incident flux is prescribed by an input spectral shape, normalized by the ionization parameter $U = \dot{Q}_{\mathrm{ph}}/(n_{\mathrm{H}}c)$ (where $\dot{Q}_{\mathrm{ph}}$ is the ionizing photon flux and n_{H} is the hydrogen density at the outer face of the slab). Previous studies (Binette et al., 1994; Stasińska et al., 2008; Yan & Blanton, 2012) have found that one requires $-4 \lesssim \log(U) \lesssim -3.5$ given photoionization by stellar sources, in order to produce the observed LINER-like emission-line ratios.

We assume a fixed hydrogen density of $n_{\mathrm{H}} = 100 \mathrm{~cm}^{-3}$, consistent with the measured ratio of S II 6717Å/6731Å in these nebulae (e.g. Yan & Blanton, 2012). Metallicities
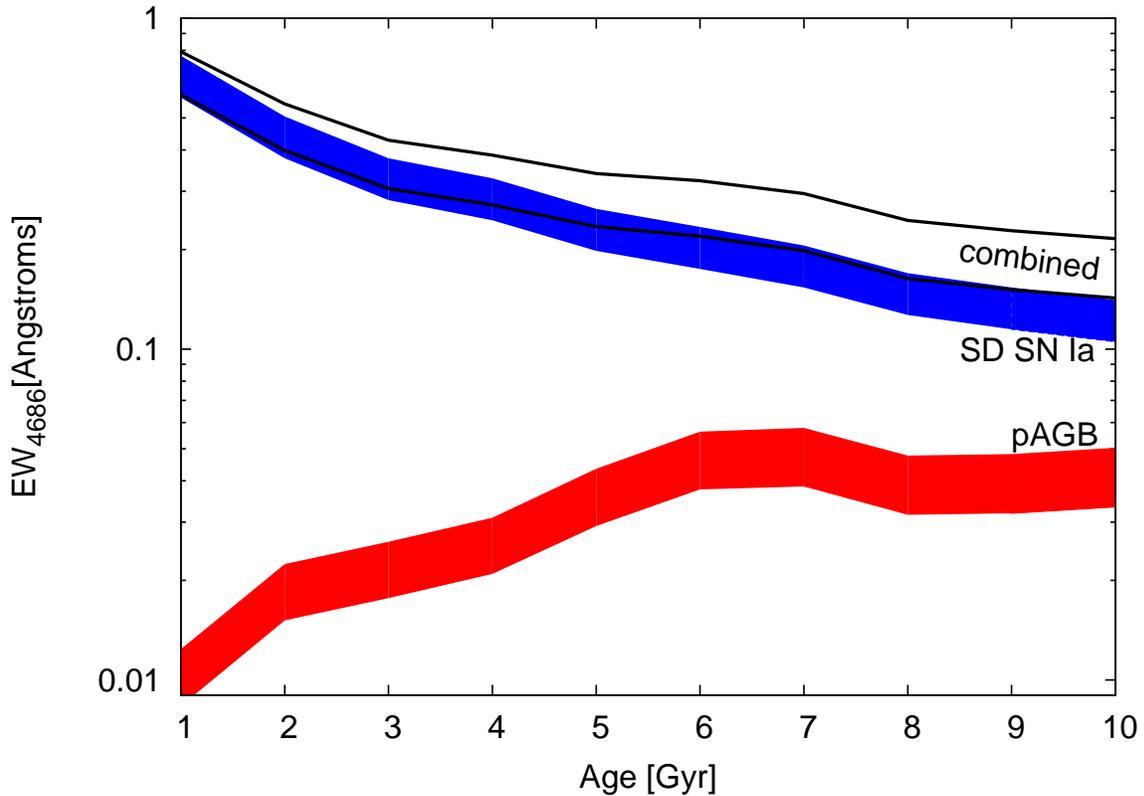
Figure 2.4: Equivalent width of He II 4686Å assuming SSPs as computed by Bruzual & Charlot (2003). Red denotes the case for ionization by pAGBs only, blue by our standard case SD progenitors, and outlined in black is the EW(4686Å) assuming ionization by both populations. Here we assume again our standard SD case ($\Delta M = 0.3 M_\odot$ of material is accreted with $T_{\text{eff}}=2\cdot10^5$ K).

of the warm ISM in passively-evolving galaxies have been estimated from the Oxygen abundance, with Athey & Bregman (2009) finding a mean value of $Z_{\text{Oxygen}} \approx Z_{\text{Oxygen},\odot}$ in the 7 galaxies in their sample. Therefore, in this work we assume solar metallicity (Anders & Grevesse, 1989) for the warm phase ISM in our calculations. Annibali et al. (2010) found a broader range of $0.25Z_\odot < Z < 2Z_\odot$, using a much larger sample of galaxies. However, since we focus on recombination lines of He II, the metallicity of the gas has only a relatively small effect (Binette et al., 1994). For similar reasons, we ignore dust in our calculations, although it has been found to accompany the warm and neutral gas in elliptical galaxies (Sarzi, Shields & Schawinski, 2010). The inclusion of dust in our models however introduces only very minimal reddening (Binette et al., 1994), principally effecting forbidden lines through depletion of the gas phase metallicity.

The gas temperature is computed self-consistently, determined primarily by the spectrum of ionizing radiation for a given density and composition of the nebula. Along the
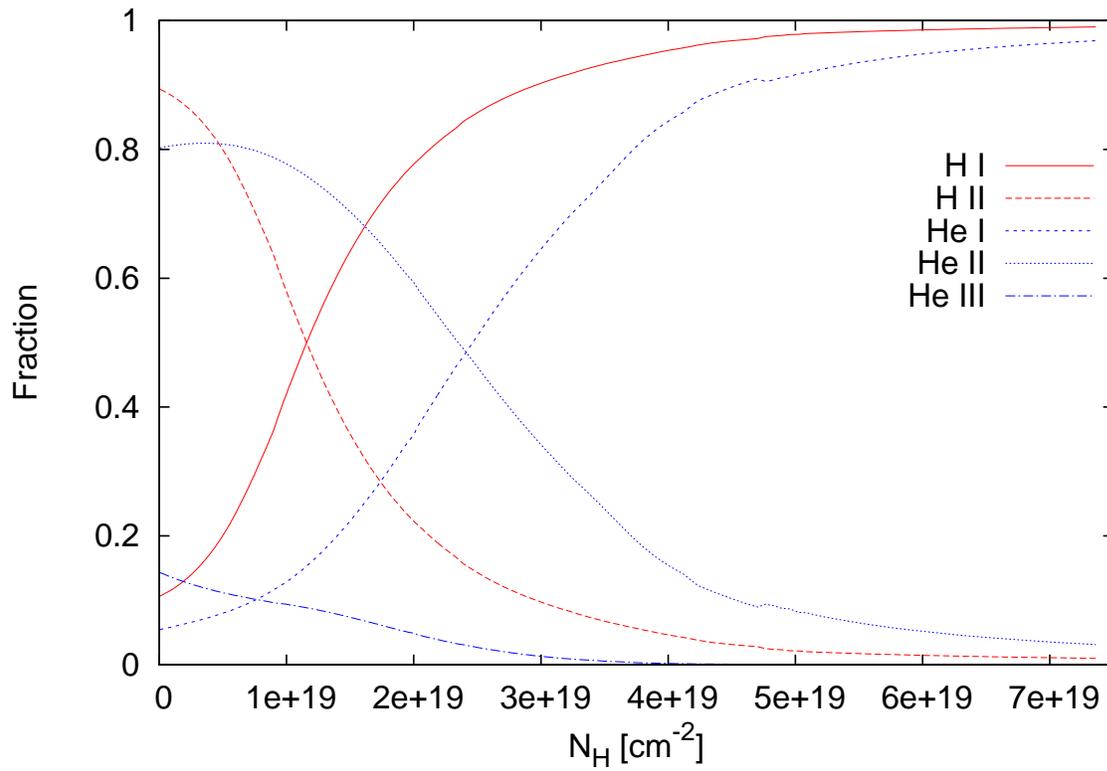
Figure 2.5: Ionization structure for a model nebula assuming plane-parallel geometry, log(U) = –4, and photoionization by a 5 Gyr-old SSP with the contribution of the example SD progenitor population from the text.

spatial coordinate, calculations are run until the hydrogen ionization fraction drops below 10^{-2}. For the parameter range considered here this typically occurs at the depth corresponding to $N_{\rm H} \sim 10^{20}$ cm^{-2}. The typical ionization structure for hydrogen and helium obtained in one of the runs is shown in Fig. 2.5. The typical column density of the neutral gas observed in the 21 cm line is of roughly the same order (Serra et al., 2012). Therefore the standard assumption that nebulae in low-ionization emission-line galaxies are ionization-bounded remains justified, though Strömgren boundaries may overlap for relatively high ionization parameter. Note that in Fig. 2.5 it is clear all He II recombination emission must principally originate from a relatively thin outer layer.

Finally, note that unless otherwise stated, we assume a covering fraction (f_c) of unity in computing the luminosity of any line. This can be scaled as appropriate given the inferred geometry of the gas; for the case of a smoothly distributed disk (see § 2.3), we would expect the covering fraction to be $\approx 1/2$.

2.4.2 Recombination lines of He II

In the context of this study, the two most important recombination lines of He II are:

1. the $n = 4 \to 3$ transition at ≈ 4686Å – the strongest He II line in the optical band

2. the $n = 3 \to 2$ transition at ≈ 1640Å – the strongest He II line longward of 912Å which is not capable of ionizing hydrogen in the ground state, and therefore is not heavily absorbed by the ISM.

In the case of photoionization by the "normally-evolving" stellar population, the He II ionization rate and luminosity in any recombination line of He II will remain small (Fig. 2.1) due to the strong cutoff in pAGB spectra shortward of 228Å (Rauch, 2003). As the total ionizing luminosity remains relatively constant for SSPs older than ~ 1 Gyr (Fig. 2.2), the recombination line luminosities do not exhibit any strong trend with age. In particular, the luminosity of any He II recombination line falls slowly by a factor of ≈ 2 from $1 - 10$ Gyr (see Fig. 2.3 *left* for the case of 4686Å emission).

With the introduction of a SD progenitor population (as given in §2.3), the He II ionization rate and the luminosity of its recombination lines is greatly enhanced over the SSP-only case. Due to the $\sim t^{-1}$ dependence of the SN Ia rate, the recombination line luminosity rises steeply with decreasing mean stellar age, from a factor of ~ 3 increase over the SSP-only case at 10 Gyr to ~ 60 for 1 Gyr old populations. We also plot in Fig. 2.3 the expected He II 4686Å luminosity given ionization by SD progenitors alone, showing that the contribution of the SSP does not significantly affect the He II line luminosities. If there are far fewer pAGB stars then presently predicted by population synthesis (Brown et al., 2008), SD progenitors alone would still remain an important ionizing source and our predictions hold nearly unchanged (recall Fig. 2.2 above).

We can also eliminate any dependence on the total stellar mass by instead considering the He II 4686Å equivalent width (EW(4686Å)), shown in fig. 2.4 for $f_c = 1$ (again, the EW scales linearly with f_c and can be adjusted accordingly).

Note that there is a range in the predicted He II 4686Å luminosity for all ages. This is a direct result of the range in plausible values of the ionization parameter; for low-ionization nebulae the flux of He II recombination lines has a direct dependence on U (see appendix B).

We find similar results for a range in photospheric temperatures spanning that expected for (steadily) nuclear-burning WDs. Plotted in Fig. 2.6 is the predicted luminosity of the He II 4686Å line per unit mass for varying source temperature, assuming a 3 Gyr-old stellar population. With the inclusion of a SD progenitor population, the expected He II 4686Å line luminosity is enhanced by a factor of 4 (3) for $T_{\text{eff}} \approx 10^5 K$ ($10^6 K$). This boost is much greater for all intervening temperatures, with a maximum factor of ≈ 20 at $T_{\text{eff}} \approx 2.5 \cdot 10^5 K$.

For low-density photoionized gases (with $T_{\text{gas}} \approx 10^4 K$), the luminosity of the 1640Å line is roughly 6.15 times greater than that in 4686Å emission (Osterbrock, 1989). Given that the FUV continuum in elliptical galaxies is nearly 2 orders of magnitude lower than in the optical, the line should also be quite conspicuously prominent. This suggests that FUV spectra available from GALEX may also be quite useful in constraining the hardness of the ionizing spectrum in low-ionization emission-line regions. Unfortunately, there remains a dearth of such galaxies with available FUV spectra (Gil de Paz et al., 2007). We leave further discussion of constraints from the 1640Å line to a future work.

2.4.3   Hβ and diagnostic line ratios

As with He II, in the case of pAGB-ionization only, the total luminosity of any recombination line of hydrogen (per unit stellar mass) should remain roughly constant at $\gtrsim 1$ Gyr. This is illustrated in the right panel in Fig. 2.3 for the case of Hβ. However, in the same figure we see that with the addition of a SD progenitor population, the situation is much different. In this case, we expect an enhancement by up to an order of magnitude in the flux of Hβ line emission per unit stellar mass for starburst ages of $\lesssim 4$ Gyrs.

In principle one can avoid any dependence on the covering fraction if we normalize the He II 4686Å flux to any recombination line of Hydrogen, such as Hβ. Though not the strongest optical recombination line of Hydrogen (Hα/H$\beta \approx 3$), Hβ is not too faint to be detectable in moderately nearby galaxies. At the same time, it is not too greatly separated from the 4686Å line, minimizing the importance of extinction in computing their ratio. The predicted He II 4686Å/Hβ ratio as a function of age is given in Fig. 2.7. As one can see, the He II 4686Å/Hβ ratio changes from ~ 0.05 to $\sim 0.4 - 0.5$ between the SSP-only and SD-only limits.

However, there are a few difficulties with using the He II 4686Å/Hβ ratio to constrain the population of SD progenitors. Firstly, SD progenitors will also contribute to the ionization of hydrogen, and thus to Hβ emission (Fig. 2.3). Of course, this is accounted for self-consistently in calculations presented in Fig. 2.7, but it requires precise knowledge of the spectral shape of the SD progenitors down to to the hydrogen ionization limit of 13.6 eV. The curves in Fig. 2.7 were computed assuming a black body spectrum, which may be only approximately true for rapidly-accreting WDs (see appendix A). Secondly, the line
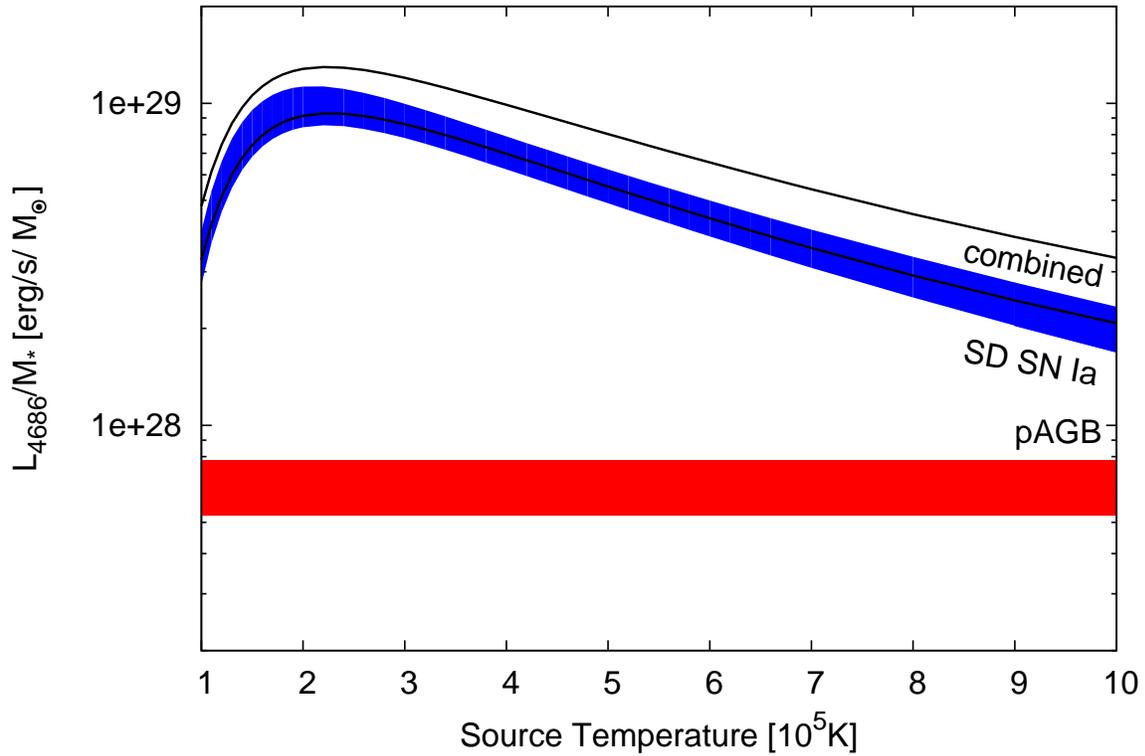
Figure 2.6: Dependence of He II 4686Å specific luminosity on the assumed WD photospheric temperature, for $\Delta M = 0.3 M_\odot$ and an age of 3 Gyr. Blue denotes ionization by SD progenitors alone, and outlined in black is the luminosity assuming ionization by SD progenitors combined with a SSP at 3 Gyr. Also shown is the predicted He II 4686Å flux without the influence of any possible SD SN Ia progenitors (red).
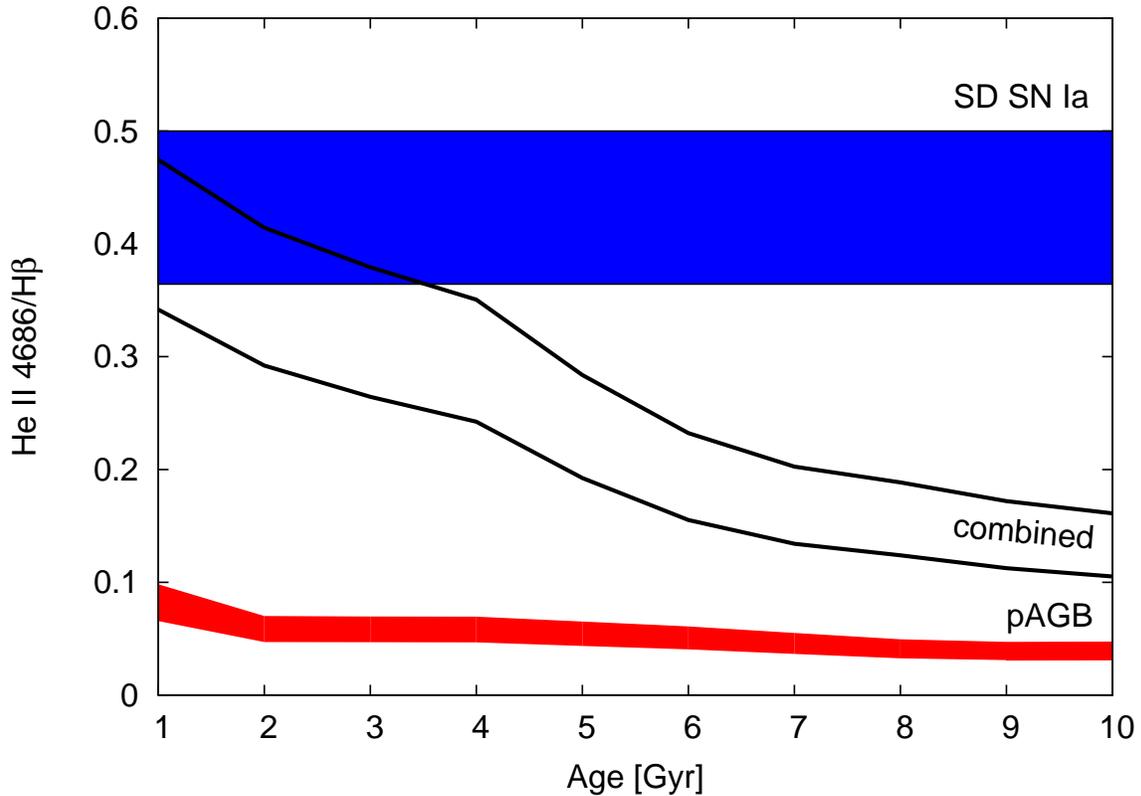
Figure 2.7: The ratio He II 4686Å/Hβ as a function of stellar age (from initial starburst) for ionization by pAGBs only (red), a population of SD progenitors only (blue), and their combined luminosity (outlined in black). Here we use the same example parameters for the SD channel (assuming $\Delta m = 0.3 M_\odot$, T $= 2 \cdot 10^5 K$).

ratio is quite sensitive to ionization parameter for such low values (for the same reasons as discussed in appendix B). This, however, can be estimated from the nearby [O III] 5007Å line; specifically, its ratio to Hβ (which increases monotonically with U for the range in U considered, see e.g. Binette et al., 1994). Finally, there may be Hβ "contamination" from other ionizing sources, such as low-luminosity AGN (LLAGN). Such objects likely provide the dominant ionizing source in the nuclear regions of many low-ionization emission line galaxies (Eracleous et al., 2010; Annibali et al., 2010). Therefore, it is important that one isolate "retired" galaxies (Cid Fernandes et al., 2011), in which the aging stellar population plays the dominant role in photoionizing emission-line regions. Significant contamination can occur with the inclusion of galaxies hosting LLAGN (Annibali et al., 2010), or regions with strong shocks (Sarzi, Shields & Schawinski, 2010). Such galaxies can however be excluded with strict selection criteria, as outlined by Cid Fernandes et al. (2011).

2.5   Observational prospects

2.5.1   Optical and UV observations

Spectroscopic surveys suggest that between $\sim 50\% - 75\%$ (varying from those in the field to clusters) of E/S0 galaxies contain extended emission-line regions. Despite extensive study, no detection of the He II 4686Å line has yet been reported. Moreover, its presumed intrinsic weakness in passively evolving stellar populations rendered this line uninteresting in spectroscopic studies of these galaxies. It is therefore unsurprising that no attempt to find weak 4686Å line emission in early type galaxies has been undertaken and, consequently, no upper limits have been reported. However, as we discuss below, detection of the He II recombination line emission in the optical and far-UV bands should certainly be feasible in the SD scenario. Conversely, upper limits on such emission can be used to constrain the collective nuclear burning rate of the population of accreting white dwarfs in a galaxy, and thus gauge the importance of the SD scenario.

For an early-type galaxy hosting $M(t)$ solar masses in stars of age t Gyrs, our calculations predict that in the SD scenario the luminosity of the He II 4686Å line is (in the absence of any other ionizing source) roughly:

$$L_{4686} \approx 1.4 \cdot 10^{40} \; t_{Gyrs}^{-1.7} \; T_5^{-1} \; f_{\rm c} \; \frac{\Delta M}{0.3 M_\odot} \frac{M(t)}{10^{10} M_\odot} \;\; {\rm erg/s} \qquad (2.9)$$

where $f_{\rm c}$ is the covering fraction, and ΔM is the mass accreted by a typical white dwarf with photospheric temperature $T = T_5 \times 10^5$ K. This formula approximates the numerical results presented in Figs. 2.3 & 2.6 and is valid for $T \gtrsim 2 \cdot 10^5$ K. In order to obtain the equivalent width, one can divide the specific luminosity by the specific continuum emission at ≈ 4686Å, given approximately by $L_{\rm SSP,4686} = 5.7 \cdot 10^{29} t^{-1.1} {\rm erg/s/Å}/M_\odot$. We then find the EW(4686Å) from SD progenitors should follow:

$$\text{EW}(4686\text{Å}) \approx 2.5 \; \text{t}_{\rm Gyrs}^{-0.6} \; \text{T}_5^{-1} \; \text{f}_{\rm c} \; \frac{\Delta \text{M}}{0.3 \text{M}_\odot} \text{Å} \qquad (2.10)$$

For an early type galaxy hosting a 3 Gyr-old $10^{10} M_\odot$ stellar population, with an accompanying SD progenitor population (our standard case from above) and $f_{\rm c} = 1/2$, our calculations predict a He II 4686Å line-luminosity of $\sim 3 - 5 \cdot 10^{38}$ erg/s (for $-4 \leq \log(\text{U}) \leq -3.5$). In the absence of any SD progenitors, the predicted line luminosity will be at most $\sim 4 \cdot 10^{37}$ erg/s (assuming ionization by pAGB stars only, Fig.2.3), i.e. ≈ 10 times smaller. At a distance of 100 Mpc, the expected line flux in the He II 4686Å line is $\approx 4 \cdot 10^{-16}$ erg/s/cm^2 for the SSP+SD case. As a conservative estimate, we can assume here a limit for a confident line detection of $\sim 10^{-16}$ erg/s/cm^2. Thus, our example galaxy above should be detectable out to ~ 200 Mpc (or z ~ 0.05). Ongoing integral field spectroscopic surveys, such as CALIFA (Sánchez et al., 2012), should easily achieve comparable or better sensitivity, and therefore will find it well within their grasp to either detect He II 4686Å emission or derive useful upper limits.

Note however that for SDSS galaxies, such an assumption is overly optimistic, as detection is limited by the S/N in the spectra (typically S/N $\approx$ 10 – 15 per pixel). On the positive side, however, this is not dominated by systematic errors (e.g. in stellar continuum models; Jonas Johansson, private communication). Therefore, as noted above, stacking spectra may allow for a confident detection of 4686Å emission for much smaller ΔM or larger distances. Given EW(4686Å), we can estimate the signal-to-noise ratio needed in order to barely detect the line:

$$\frac{S}{N} = \frac{A/N\sqrt{2\pi}\sigma}{EW(4686\text{Å})} \tag{2.11}$$

as given in Sarzi et al. (2006). Here we assume an intrinsic broadening $\sigma_\text{gas} \sim 150$km/s ($\approx$ 2.3Åat 4686Å) typical of the gas in the central regions of early-type galaxies hosting extended emission-line regions. Assuming a threshold A/N $\approx$ 4 is needed for detection, one would then require S/N $\approx$ 500 in order to detect an EW(4686Å) $\approx$ 0.05Å. This would allow for a nominal detection of He II 4686Å from pAGBs for relatively old stellar populations, and enable a strong detection of (or robust upper limit on) any SD progenitor population. In the SDSS sample, such a target S/N should be possible with stacking of $\sim$ 2000 galaxies.

Fig. 2.8 illustrates how an upper limit on the He II 4686Å line can be used to constrain the SD scenario. It shows the upper limit which can be placed on the mass ΔM accreted by each successful SN Ia progenitor at the given photospheric temperature in the SD scenario, assuming a null detection of the He II 4686Å line with an upper limit of 10^{-16} erg/s/cm^2. For illustrative purposes, we assume a $5 \cdot 10^{10} M_\odot$ stellar population of varying ages at a distance of 100 Mpc^2, and ionization by a SD SN Ia population only. The plot demonstrates that even a rather moderate upper limit on the He II 4686Å line emission can constrain the mass accreted by each SN Ia progenitor down to $\sim$ few $\times 10^{-3} - 10^{-1}$ M$_\odot$. Alternatively, this can also be used to constrain the fraction of SNe Ia produced via the SD channel. Indeed, if we assume some value of ΔM and T, the upper limit on the SD fraction is given by $\Delta M_\text{max}/\Delta M$.

In their survey of nearby LINERs, the Palomar survey did not detect He II 4686Å line emission, but found upper limits of He II 4686Å/H$\beta \lesssim$ 10% (Ho, 2008). Unfortunately, this number can not be directly used for our purpose, as it applies only to the nuclear regions of mostly old galaxies, where we also expect a central source to play a strong role in the available ionization budget (section 2.4.3). However, it does characterize the sensitivity to the He II 4686Å/Hβ line ratio which can be routinely achieved. The upper limit of $\sim$ 0.1 on the He II 4686Å/Hβ line ratio is large enough not to be in conflict with the pAGB-photoionization model for low-ionization emission-line regions. However, in the absence of contamination by ionizing sources other than pAGB stars and SD progenitors, we should expect to see $0.1 \lesssim$ He II 4686Å/H$\beta \lesssim 0.5$. Therefore, an upper limit on this ratio of $\sim$ 0.1 in extended low-ionization emission line regions will also place meaningful constraints on the SD scenario, as illustrated by Fig. 2.9.

---

[2]Note that this is much too great a mass to be enclosed in an SDSS fiber at this distance, but would be possible with e.g. long-slit or integral field spectroscopy.
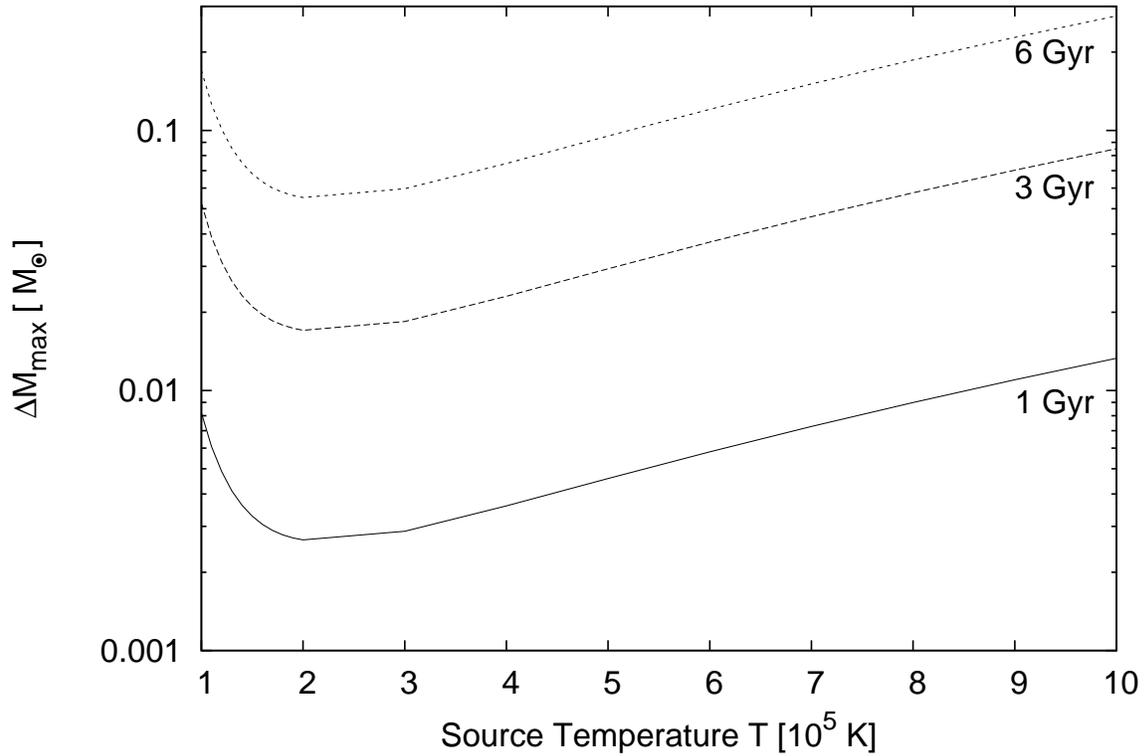
Figure 2.8: Maximum mass which may be accreted by the typical WD in the SD scenario for a given photospheric temperature, given a null detection of the He II 4686Å line with an upper limit of 10^{-16} erg/s/cm^2. Here we assume a $5 \cdot 10^{10} M_\odot$ stellar population aged 1, 3, and 6 Gyrs, a distance of 100 Mpc, with a gas covering fraction of 1/2, and log(U) = -4.
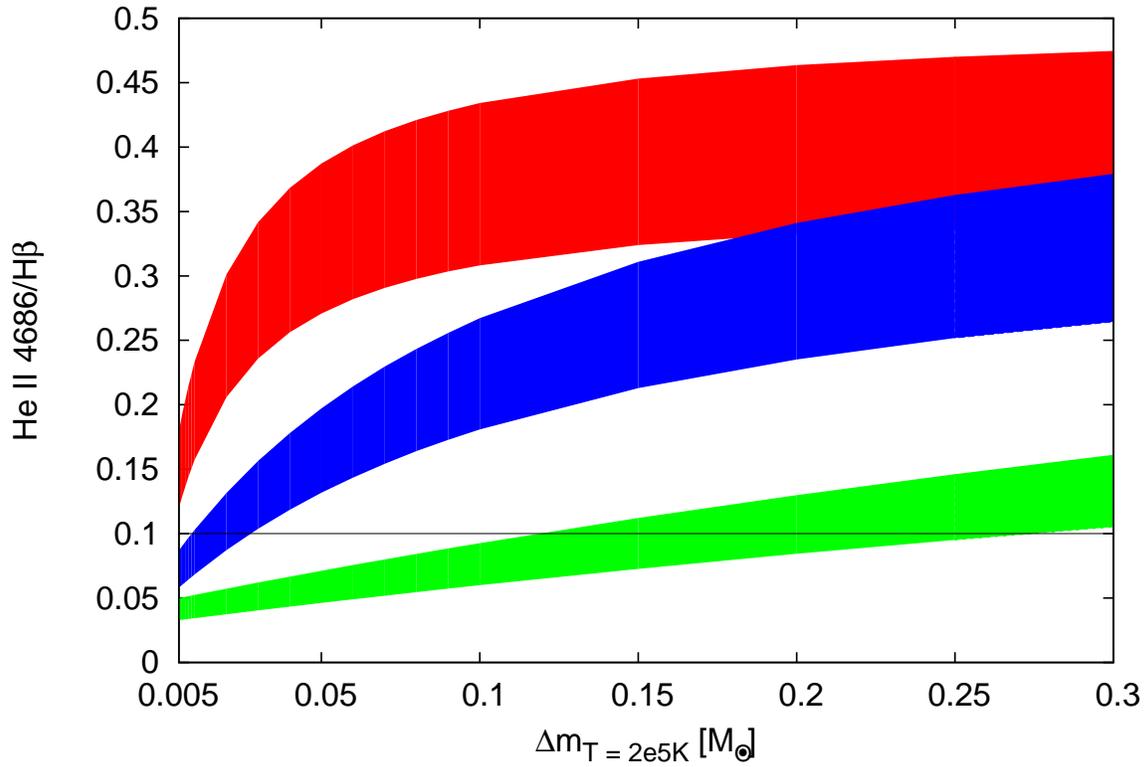
Figure 2.9:   An example of the He II 4686Å/Hβ line ratio diagnostics. The predicted line ratio for a (1 Gyr – red, 3 Gyr – blue, 10 Gyr – green) SSP+SD population with varying assumed ΔM – the mass accreted by WDs at the photospheric temperature of T ≈ 2 · $10^5 K$. Black line shows the line ratio level of 0.1, which should be routinely achievable in spectroscopic observations.

In the FUV, detection of (or robust upper limits on) the He II 1640Å line is even more promising. The nearby early-type galaxy NGC 3607 ($d \approx 21$ Mpc) has a mean stellar age of $\approx 3 - 4$ Gyr (Annibali et al., 2007), and is known to host an extended low-ionization emission-line region. We can compute the expected 1640Å line flux from the K-band luminosity ($\approx 3 \cdot 10^{10} L_{K,\odot}$ within 14"x14" from the 2MASS survey, Jarrett et al., 2003), and the appropriate M/L_K from Bruzual & Charlot (2003). Assuming $f_c = 1/2$, and our prototypical case for the SD channel, the total luminosity reprocessed into He II 1640 Å emission is $\approx 3 \cdot 10^{39}$ erg/s. Using the GALEX Exposure Time Calculator (ETC)[3], we find that this should be detectable with S/N ≈ 5 given a ≈ 3 ksec observation[4].

2.5.2   Possible outcomes

With the observations described above, there are 3 possible outcomes, all of great interest:

• He II 4686Å/H$\beta \lesssim$ few % ($L_{4686}/M_* \lesssim$ few $\times 10^{27}$ erg/s/M$_\odot$) at high confidence: Along with placing tight constrains on the SD scenario, this may pose a problem for our understanding of ionization by pAGB stars, in particular, their spectra beyond the He II-ionization limit.

• He II 4686Å/Hβ is detected at $\approx$ few % ($L_{4686}/M_* \sim 10^{28}$ erg/s/M$_\odot$) for all $t_{gal} \gtrsim 1$ Gyr: This would provide strong evidence against a high-temperature SN Ia progenitor population. At the same time it would strongly suggest that pAGB-ionization is the correct model for retired galaxies, especially if there is no strong trend in $L_{H\beta}/M_*$ with age (cf. Fig. 2.3).

• The He II 4686Å line is detected, with He II 4686Å/H$\beta > 10\%$ ($L_{4686}/M_* \gtrsim$ few $\times 10^{28}$ erg/s/M$_\odot$). This would suggest an alternative to pAGB-only ionization. A significant boost found in He II 4686Å emission for younger stellar populations would conform comfortably with the SD SN Ia scenario.

2.5.3   Post-starburst galaxies

Also of interest are the so-called post-starburst galaxies: early-type galaxies with regions of relatively young mean stellar age and extended nebular emission, wherein a burst of star formation has only recently ceased ($\Delta t \lesssim 1$Gyr). Sarzi, Shields & Schawinski (2010) find such galaxies account for roughly 10% of their sample of nearby E/S0 galaxies. Especially puzzling, were the SD scenario to hold, is the existence of the rare class of E+A galaxies (Dressler & Gunn, 1983; Yagi & Goto, 2006; Kaviraj et al., 2007). These show evidence of a very young population, yet are without strong emission lines. Sarzi, Shields & Schawinski (2010) suggest that these galaxies are within a (possibly very) brief epoch shortly after a sudden burst of star formation has ceased. In this phase, OB stars have left the main sequence ($t > 10^8$ years), however there are insufficient pAGB stars to strongly ionize the ISM ($t <$ a few 10^8years). Yet SNe Ia at the shortest delay times can already be expected

---

[3]http://sherpa.caltech.edu/gips/tools/expcalc.html

[4]Note that here we report 3 times the value given by the ETC, as recommended in the GALEX Spectroscopy Primer. www.galex.caltech.edu/researcher/gr1_docs/grism/primer.html

to detonate in this age range, suggesting that given the SD channel, a large population of accreting WDs would need to be present at this time. These galaxies are understood not to be devoid of gas (Buyle et al., 2006), therefore the lack of emission-lines characteristic of ionization by hot accreting WDs is certainly conspicuous.

2.6   Conclusions

We have demonstrated that, for temperatures characteristic of WDs accreting above the steady nuclear burning limit, the SD SN Ia channel implies nuclear-burning WDs should provide a substantial contribution to the He II-ionizing continuum in non-star-forming stellar populations. Their contribution rises dramatically at earlier delay-times, with the enhancement of the He II-ionizing continuum growing to nearly 2 orders of magnitude over that of a SSP alone at ~ 1 Gyr. This provides a unique opportunity to test for the presence of any such population through the detection (or lack thereof) of He II recombination lines. In particular, the luminosities predicted in He II 1640Å and He II 4686Å suggest interesting upper limits should already be possible with GALEX and in the SDSS. Ongoing IFU spectroscopic surveys, such as CALIFA, should also be able to improve upon this further, being capable of isolating emission-line regions with no evidence for any contribution from shocks or a central source.

In the absence of any ionizing sources other than the stellar population, an upper limit on the He II 4686Å line flux of $\lesssim 10\%$ that of Hβ (or $L_{4686}/M_* \lesssim$ few $\times 10^{27}$ erg/s/M$_\odot$) in the low-ionization emission-line regions of many ellipticals should tightly constrain the possible luminosity of any population of hot nuclear-burning WDs. This may also provide a crucial test of models of ionization by pAGB stars in galaxies hosting extended low-ionization emission-line regions, wherein one may expect He II 4686Å/H$\beta \approx$ a few %. A non-detection of the He II 4686Å line in a galaxy located within 100 Mpc from the Sun with a rather moderate upper limit of 10^{-16} erg/s/cm^2 will place an upper limit of $\sim$ few $\times 10^{-3} - 10^{-1}$ M$_\odot$ on the total mass accreted by each successful SN Ia progenitor at photospheric temperatures in the range $\sim 10^5 - 10^6$ K.

In the preceeding analysis, we have primarily considered the case wherein SD progenitors account for all SNe Ia. However, one may see from eq. 2.6 that a limit on the total luminosity of any SD SN Ia progenitor population may also be interpreted as a limit on the fraction of the total SN Ia rate which SD progenitors account for. This is in keeping with recent suggestions (e.g. Maoz & Mannucci, 2012) that there may be evidence for multiple progenitor channels.

Acknowledgements

hd.mpg.de/~brent/mapiii.html.

Bibliography

Anders E., Grevesse N., 1989, Geochimica et Cosmochimica Acta, 53, 197

Annibali F., Bressan A., Rampazzo R., Zeilinger W. W., Danese L., 2007, Astronomy and Astrophysics, 463, 455

Annibali F., Bressan A., Rampazzo R., Zeilinger W. W., Vega O., Panuzzo P., 2010, Astronomy and Astrophysics, 519, A40

Athey A. E., Bregman J. N., 2009, The Astrophysical Journal, 696, 681

Binette L., Magris C. G., Stasińska G., Bruzual A. G., 1994, Astronomy and Astrophysics, 292, 13

Brown T. M., Smith E., Ferguson H. C., Sweigart A. V., Kimble R. A., Bowers C. W., 2008, The Astrophysical Journal, 682, 319

Bruzual G., Charlot S., 2003, Monthly Notices of The Royal Astronomical Society, 344, 1000

Buyle P., Michielsen D., De Rijcke S., Pisano D. J., Dejonghe H., Freeman K., 2006, The Astrophysical Journal, 649, 163

Cassisi S., Iben, Jr. I., Tornambe A., 1998, The Astrophysical Journal, 496, 376

Chabrier G., 2003, Publications of the Astronomical Society of the Pacific, 115, 763

Cid Fernandes R., Stasińska G., Mateus A., Vale Asari N., 2011, Monthly Notices of the Royal Astronomical Society, 413, 1687

Cumming R. J., Lundqvist P., Smith L. J., Pettini M., King D. L., 1996, Monthly Notices of the Royal Astronomical Society, 283, 1355

Di Stefano R., 2010, Astrophysical Journal, 712, 728

Dressler A., Gunn J. E., 1983, The Astrophysical Journal, 270, 7

Eracleous M., Hwang J. A., Flohic H. M. L. G., 2010, Astrophysical Journal, 711, 796

Gil de Paz A. et al., 2007, The Astrophysical Journal Supplement Series, 173, 185

Gilfanov M., Bogdán Á., 2010, Nature, 463, 924

Gilfanov M., Bogdán Á., 2011, ASTROPHYSICS OF NEUTRON STARS 2010: A Conference in Honor of M. Ali Alpar. AIP Conference Proceedings, Volume 1379, pp. 17-22 (2011)., 1379, 17

Groves B. A., Dopita M. A., Sutherland R. S., 2004, The Astrophysical Journal Supplement Series, 153, 9

Hachisu I., Kato M., Nomoto K., 1999, The Astrophysical Journal, 522, 487

Hachisu I., Kato M., Nomoto K., 2010, The Astrophysical Journal Letters, 724, L212

Ho L. C., 2008, Annual Reviews of Astronomy and Astrophysics, 46, 475

Iben, Jr. I., Tutukov A. V., 1984, The Astrophysical Journals, 54, 335

Jarrett T. H., Chester T., Cutri R., Schneider S. E., Huchra J. P., 2003, The Astronomical Journal, 125, 525

Kahabka P., van den Heuvel E. P. J., 1997, Annual Review of Astronomy and Astrophysics, 35, 69

Kaviraj S., Kirkby L. A., Silk J., Sarzi M., 2007, Monthly Notices of the Royal Astronomical Society, 382, 960

Kewley L. J., Dopita M. A., Sutherland R. S., Heisler C. A., Trevena J., 2001, The Astrophysical Journal, 556, 121

Lepo K., van Kerkwijk M., 2011, ArXiv e-prints

Li W. et al., 2011, Nature, 480, 348

Maggi P., 2011, Master's thesis, Université de Strasbourg, Observatoire Astronomique, 11, rue de l'Université, 67000 Strasbourg

Mannucci F., Della Valle M., Panagia N., Cappellaro E., Cresci G., Maiolino R., Petrosian A., Turatto M., 2005, Astronomy and Astrophysics, 433, 807

Maoz D., Mannucci F., 2012, Publications of the Astronomical Society of Australia, 29, 447

Matteucci F., Greggio L., 1986, Astronomy and Astrophysics, 154, 279

Nielsen M. T. B., Voss R., Nelemans G., 2012, Monthly Notices of the Royal Astronomical Society, 426, 2668

Nomoto K., Saio H., Kato M., Hachisu I., 2007, The Astrophysical Journal, 663, 1269

Osterbrock D. E., 1989, Astrophysics of gaseous nebulae and active galactic nuclei

Perlmutter S. et al., 1999, The Astrophysical Journal, 517, 565

Raiter A., Schaerer D., Fosbury R. A. E., 2010, Astronomy and Astrophysics, 523, A64

Rappaport S., Chiang E., Kallman T., Malina R., 1994, The Astrophysical Journal, 431, 237

Rauch T., 2003, Astronomy and Astrophysics, 403, 709

Rauch T., Werner K., 2010, Astronomische Nachrichten, 331, 146

Riess A. G. et al., 1998, The Astronomical Journal, 116, 1009

Ruiter A. J., Belczynski K., Fryer C., 2009, Astrophysical Journal, 699, 2026

Sánchez S. F. et al., 2012, Astronomy and Astrophysics, 538, A8

Sarzi M., Shields J. C., Schawinski K. e. a., 2010, Monthly Notices of the Royal Astronomical Society, 402, 2187

Sarzi, M., Falcón-Barroso, J., Davies, R. L., et al. 2006, Monthly Notices of the Royal Astronomical Society, 366, 1151

Serra P., Oosterloo T., Morganti R., Alatalo K., Blitz L., Bois M. e. a., 2012, Monthly Notices of the Royal Astronomical Society, 422, 1835

Stasińska G., Tylenda R., 1986, Astronomy and Astrophysics, 155, 137

Stasińska G. et al., 2008, Monthly Notices of the Royal Astronomical Society, 391, L29

Totani T., Morokuma T., Oda T., Doi M., Yasuda N., 2008, Publications of the Astronomical Society of Japan, 60, 1327

Umeda H., Nomoto K., Yamaoka H., Wanajo S., 1999, The Astrophysical Journal, 513, 861

van den Heuvel E. P. J., Bhattacharya D., Nomoto K., Rappaport S. A., 1992, Astronomy and Astrophysics, 262, 97

Webbink R. F., 1984, Astrophysical Journal, 277, 355

Whelan J., Iben, Jr. I., 1973, The Astrophysical Journal, 186, 1007

Yagi M., Goto T., 2006, The Astronomical Journal, 131, 2050

Yan R., Blanton M. R., 2012, The Astrophysical Journal, 747, 61

Yungelson L. R., 2010, Astronomy Letters, 36, 780

Chapter 3

Emission line diagnostics to constrain high temperature populations in early-type galaxies

3.1   Abstract

Once thought to be devoid of warm and cold interstellar matter, elliptical galaxies are now commonly observed to host extended regions of neutral and ionized gas. Outside of the innermost nuclear regions of these galaxies, the favoured candidate ionizing source remains some component of the stellar population, with mounting evidence suggesting post-asymptotic-giant-branch stars (pAGBs). In a recent paper, we demonstrated that observations of recombination lines of He II (or upper limits thereof) may provide a strong constraint on the presence of any other, higher temperature ionizing sources, in particular nuclear-burning white dwarfs in the context of the single degenerate (SD) scenario for type Ia supernovae. The sensitivity of the HeII test is greatest for WD effective temperatures $\sim 2 \cdot 10^5 K$. Here we extend our analysis to include predictions for all of the "classical" strong optical lines, as well as UV, optical, and infra-red lines of neutral Oxygen, Nitrogen, and singly-ionized Carbon. This allows us to extend the temperature range over which we can meaningfully constrain the collective luminosity of nuclear-burning WDs to $10^5 K \lesssim$ T $\lesssim 10^6 K$. We then demonstrate how observations of nearby early-type and post-starburst galaxies can place strong limits on the origin of type Ia supernovae.

3.2 Introduction

It is now well-established that early-type galaxies possess substantial ISM, with neutral hydrogen masses on the order of $\sim 10^6 - 10^9 M_\odot$ (Serra et al., 2012). Accompanying this neutral gas are emission-line regions extending out to several kiloparsecs, with line ratios characteristic of gas in a relatively low state of ionization. They appear to be powered by the diffuse galactic background, rather than being a superposition of individual H II regions around bright compact sources. In the past, much effort has been devoted to understanding the sources of ionizing radiation powering these nebulae. In passively-evolving (non-star-forming) galaxies, it is the old stellar population itself which appears likely to provide the dominant contribution to the local extreme-UV background (e.g Yan & Blanton, 2012), at least outside of their innermost nuclei. There, low-luminosity AGN had until recently been thought to provide at least a significant contribution, at least in many cases (e.g. Annibali et al., 2010). However, increasing evidence suggests that the old stellar population may still provide a significant, or even dominant role in powering LINER emission (e.g. Kehrig et al., 2012). Within the stellar population, post-asymptotic giant branch stars (pAGBs) remain the favoured candidate for powering the observed emission lines. In particular, pAGB stars are expected to provide sufficient ionizing photons in order to account for the observed Hβ flux (Sarzi, Shields & Schawinski, 2010), and the radial surface brightness profiles of the observed emission lines are consistent with ionization by a diffuse population, rather than a central source (e.g. Singh et al., 2013; Papaderos et al., 2013).

At the same time, similar arguments have proven capable of ruling out other possible ionizing sources. Recently, Woods & Gilfanov (2013) proposed that understanding the mechanism powering the diffuse line-emission in passively-evolving galaxies may shed light on the origin of type Ia supernovae (SNe Ia). There exist two families of models for how these tremendous explosions come about: in the double-degenerate scenario (Webbink, 1984), these events result from the merger of a binary pair of white dwarfs (WDs). In the standard model of the single-degenerate channel (Whelan & Iben, 1973), a carbon-oxygen WD accretes matter from a main sequence or red giant companion until triggering a thermonuclear explosion. If the latter is correct, then accreting, nuclear-burning WDs should be an extremely luminous component of any stellar population. With temperatures on the order of $10^5 - 10^6 K$, they should provide the dominant ionizing background in relatively young ($\lesssim$ 4Gyr) passively-evolving stellar populations. If this is the case, it should be readily apparent from spectroscopic observations of those ellipticals which host low-ionization emission-line regions (Woods & Gilfanov, 2013). This provides a unique opportunity to constrain plausible progenitor models for SNe Ia.

In particular, the observed line flux in recombination lines of ionized Helium can provide an excellent test for the presence of relatively high temperature sources ($\approx 2 - 6 \cdot 10^5 K$), and their total ionizing luminosity. This covers much of the temperature range we expect from accreting, nuclear-burning white dwarfs, such as supersoft sources (SSSs), or in particular, the so-called 'ultra-soft sources' (those accreting white dwarfs with greatly inflated photospheres, see Hachisu, Kato & Nomoto, 1999). However, we expect higher temperatures (up to $\sim 10^6 K$) for the most massive ($\gtrsim 1.0\ M_\odot$) nuclear-burning white

dwarfs. In the past, any possible population of such objects has been severely constrained based on the observed paucity of soft X-ray emission in early type galaxies, and the lack of individual soft X-ray sources (e.g. Gilfanov & Bogdán, 2010; Di Stefano, 2010). However, independent diagnostic tools remain extremely important.

Here we extend the work of Woods & Gilfanov (2013) to include a number of emission-line diagnostic tests for the presence of a population of very hot sources ($T_{\mathrm{eff}} \gtrsim 5 \cdot 10^5 K$), as well as those too cool to strongly ionize He II ($T_{\mathrm{eff}} \approx 10^5 K$). In § 3.3, we review our model assumptions for the ISM in early-type galaxies, as well as the possible sources of ionizing radiation in passively-evolving stellar populations. In § 3.4, we discuss those lines which are most sensitive to ionization by high temperature sources, in particular those of [O I], [N I], and [C II]. Together with observations of recombination lines of He II, this extends the range over which emission lines can meaningfully constrain the hardness of the ionizing background in passively-evolving galaxies to cover all temperatures expected from steadily nuclear-burning white dwarfs, including those with inflated photospheres ($1.5 \cdot 10^5 K \leq T_{\mathrm{eff}} \leq 10^6 K$). In § 3.5, we outline the even more pronounced effect of any putative SD progenitor population (with $T_{\mathrm{eff}} \gtrsim 10^5 K$) in young (t $\lesssim$ 1Gyr), post-starburst populations (such as E+A galaxies). In this case the ionizing luminosity provided by SD progenitors would exceed that available from any other stellar source by up to two orders of magnitude, indicating the specific luminosity in any of the classical strong optical lines (Hα, [O II] 3727Å, etc.) should be similarly enhanced. We follow this in § 3.6 with estimates of the observational prospects for producing limits using a number of instruments and surveys, as well as how the presence of a significant population of accreting WDs may compromise measures of the SFR in galaxies. Finally, we discuss implications for the evolution of binary stellar populations and the progenitors of type Ia supernovae.

3.3   Modeling low-ionization emission line regions

3.3.1   Density, metallicity, and ionization parameter

We model the emission-line regions in early-type galaxies using the 1-D photoionization code MAPPINGS III (see e.g. Groves et al., 2004). Our procedure follows closely that of Woods & Gilfanov (2013); here for convenience we summarize some of the essential ingredients.

Unless otherwise stated, we assume a solar (Anders & Grevesse, 1989) metallicity for the gas phase, and 2.5 solar for the stellar population. The former is consistent with the mean Oxygen abundance measured in the warm ISM of nearby retired galaxies (Athey & Bregman, 2009; Annibali et al., 2010). For the ionizing continuum from the 'normally-evolving' (single star) stellar population, we use the population synthesis calculations of Bruzual & Charlot (2003).

The most common morphology of the cold ISM in such galaxies is a disky distribution extending from the nucleus out to several tens of kpc (Serra et al., 2012), with emission-line nebulae typically ionized by the diffuse background of the stellar population rather than

nearby individual sources. Therefore, we assume plane parallel geometry throughout. For our standard case, we assume a constant hydrogen number density of 100cm^{-3}, consistent with the observed [S II] 6717Å/6731Å ratio observed in stacked passively-evolving galaxies from the SDSS (Yan & Blanton, 2012), although this may only be an approximate upper bound (Osterbrock & Ferland, 2006). In principle, the majority of the optical emission lines considered in this work are relatively insensitive to variations in the density.

In our photoionization calculations, we assume that the modeled nebulae are ionization-bounded (see Woods & Gilfanov, 2013, and references therein), and terminate our calculations when the ionized Hydrogen fraction falls below 1%. The ionization parameter (U $= \dot{N}_{\text{ph}}/4\pi r^2 c n_{\text{H}}$) is similarly well constrained by the observed ratio of [O III] 5007Å/Hβ, generally lying in the range -4 $\lesssim$ log(U) $\lesssim$ -3.5 (e.g. Binette et al., 1994; Yan & Blanton, 2012).

Where appropriate, we normalize the line flux per unit stellar mass of the host population, and assume a covering fraction of unity. This can of course be scaled as needed, since the line luminosity is directly proportional to the stellar ionizing luminosity absorbed by the ISM in ellipticals. In practice, it is often more convenient to provide line predictions normalized to the nearest recombination line of Hydrogen, in order to minimize the importance of reddening in comparison with observed values. This has the added benefit of removing any dependence on the covering fraction of the gas, therefore we also provide predictions for each optical line luminosity relative to the nearest Hydrogen recombination line.

3.3.2   Available ionizing sources

In early-type galaxies, pAGBs remain favoured to be the predominant ionizing source (at least within the stellar population). Empirically, this has been strongly supported by energetic considerations (e.g. Sarzi, Shields & Schawinski, 2010), as well as more detailed emission-line studies (Binette et al., 1994). The spectral emission from these sources has been studied in detail by Rauch (2003), whose models are included in the spectral synthesis calculations of Bruzual & Charlot (2003) used here. Despite mounting evidence (e.g. Binette et al., 1994; Sarzi, Shields & Schawinski, 2010; Yan & Blanton, 2012), some doubt remains about the longevity of post-AGB stars, and therefore their expected numbers and contribution to the ionizing background (Brown et al., 2008). Therefore, where appropriate, we will consider in our calculations the ionizing background with and without the contribution normally expected from pAGBs.

Non-stellar sources, such as low-luminosity AGN, likely also play a role in many galaxies (Annibali et al., 2010), at least in their central regions. Fast shocks have been thought to play a role in some cases, as well as ionization by the hot, X-ray emitting diffuse ISM (Sarzi, Shields & Schawinski, 2010). However, such contaminating cases can be excluded with the careful use of line diagnostics (e.g Cid Fernandes et al., 2011), allowing one to confine their attention to so-called 'retired' galaxies where the old stellar population is the principle source of ionizing emission.

Other stellar sources, such as low-mass X-ray binaries, have been suggested, but do
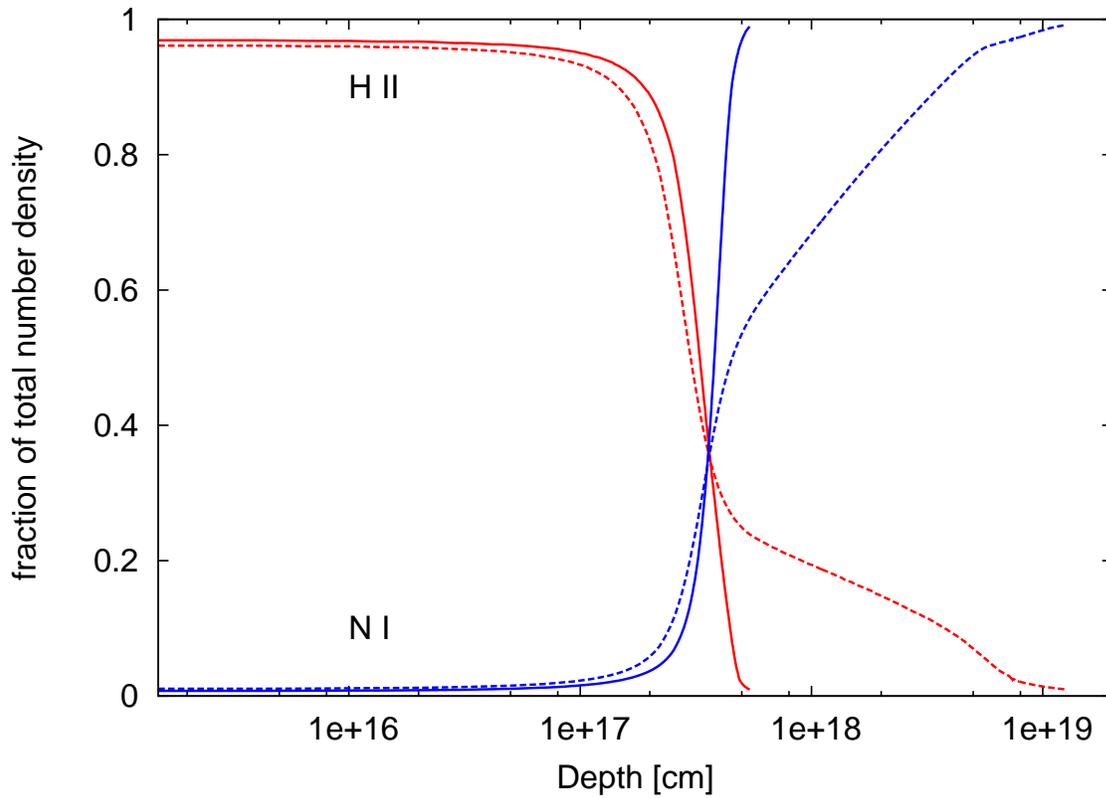
Figure 3.1: Ionization structure of a model nebula, given photoionization by a 3 Gyr-old stellar population (solid lines), and with the addition of our standard example SD SN Ia progenitor population (dashed lines). Red lines indicate the ionized hydrogen fraction, while blue lines follow the neutral fraction of the total Oxygen number density. We assume in both cases log(U) = -3.5. Note that we stop our model calculations when the Hydrogen ionization fraction reaches 1%.

not appear to be significant in this regard (Sarzi, Shields & Schawinski, 2010). Accreting, nuclear-burning WDs have, however, been found to likely provide a significant contribution, and would be expected to dominate the ionizing contribution for relatively young, passively-evolving stellar populations, at least if they exist in sufficient numbers to account for the observed SN Ia rate (Woods & Gilfanov, 2013). Even if they are not the primary evolutionary channel for SNe Ia, accreting WDs may still account for a substantial contribution to the ionizing background (see Chen et al. in prep).

The number of nuclear-burning WDs expected in any stellar population, assuming the SD channel accounts for all SNe Ia, can be estimated from the SN Ia rate, the mass accretion rate, and the characteristic mass accreted per SN Ia (as in Gilfanov & Bogdán, 2010; Di Stefano, 2010):

$$N_{\mathrm{SD}} = \frac{\Delta m_{\mathrm{Ia}}}{\dot{M}} \dot{N}_{\mathrm{Ia}} \tag{3.1}$$

where $\dot{N}_{\mathrm{SNIa}}$ is SN Ia rate of the galaxy, and Δm_{Ia} is the total mass accreted prior to explosion ($\approx 0.3 - 0.7 M_{\odot}$). This depends sensitively on our assumptions regarding the typical accretion rate, which in turn depends on as-yet poorly understood details of binary evolution. Fortunately, we can remove any dependence on the accretion rate if we consider instead the total bolometric luminosity of all accreting, nuclear-burning WDs, $L_{\mathrm{tot,SNIa}} = L_{\mathrm{WD}} \cdot N_{\mathrm{SD}}$. The luminosity of any individual source is simply $L_{\mathrm{WD}} = \epsilon \chi \dot{M}$, with $\epsilon = 6 \cdot 10^{18}$erg/s the energy release from nuclear-burning of hydrogen, and $\chi = 0.72$ the hydrogen fraction of solar metallicity gas. Therefore, the total luminosity of any putative SD progenitor population can easily be estimated as:

$$L_{\mathrm{tot,SD}} = \epsilon_{\mathrm{H}} \chi \Delta m_{\mathrm{Ia}} \dot{N}_{\mathrm{SNIa}} \tag{3.2}$$

independent of the assumed accretion rate (Gilfanov & Bogdán, 2010). For the SNIa rate we will use the delay time distribution derived for passively evolving galaxies by Totani et al. (2008): $\dot{N}_{\mathrm{SNIa}} = 0.57(t/1\mathrm{Gyr})^{-1.11}$SNIa/century/$10^{10} L_{\mathrm{K},\odot}$ (assuming a Chabrier IMF and Z = 0.05).

The spectral shape of the ionizing background in ellipticals can then be found from the sum of two terms:

$$L_{\nu}(t) = L_{\nu}^{\mathrm{SSP}}(t) + S_{\nu}^{WD} \cdot \Delta \mathrm{m}_{\mathrm{Ia}} \cdot \dot{\mathrm{N}}_{\mathrm{Ia}}(t) \tag{3.3}$$

where $L_{\nu}^{\mathrm{SSP}}(t)$ is the specific ionizing luminosity of the SSP (principally arising from pAGBs), and S_{ν}^{WD} is the spectrum of radiation emitted by the population of nuclear burning white dwarfs per unit accreted mass. S_{ν}^{WD} describes the spectral energy distribution of radiation emitted by the population of SN Ia progenitors, whose bolometric luminosity is defined by eq.(3.2). It is a superposition of spectra of individual nuclear-burning white dwarfs, each having approximately blackbody shape (Rauch & Werner, 2010) with the effective temperature determined by the mass accretion rate and the white dwarf mass. Therefore, the precise shape of S_{ν}^{WD} depends on the (poorly known) distribution of these parameters in the population of SN Ia progenitors. For the purposes of the present study,

Line	λ	SSP only	SSP+SD channel	relative enhancement
Ultraviolet				
[C II]	1335.3Å	2.0e27	5.6e28	26
Optical				
[N I]	5200.17Å	4.9e27	2.3e29	45
[N I]	5197.82Å	3.6e27	1.6e29	43
[O I]	6363.67Å	1.3e28	3.0e29	20
[O I]	6300.2Å	4.0e28	9e29	20
Infra-red				
[O I]	146μm	2.0e28	5.8e29	28
[O I]	63μm	1.1e29	3.1e30	28
[C II]	158μm	3.9e28	9.1e29	22

Table 3.1: Predicted specific line luminosities (in units of erg/s/$M_\odot$) for those lines most strongly effected by the introduction of a high temperature source population. We assume ionization by a 3 Gyr-old 'normal' stellar population only (column 3), and with the addition of a $T_{\text{eff}} = 10^6 K$ SD SN Ia progenitor population (column 4). In both cases, we take log(U) = -3.5.

we will simply assume that S_ν^{WD} has a blackbody shape and can be characterized by a single photospheric temperature. In practice, any more realistic model can be constructed out of a superposition of such templates. We will then investigate how the ionization state of the ISM and the luminosity of the emission lines of interest depend on the assumed value of T_{eff}. Comparison of these results with observations can be used to constrain the maximum amount of material $\Delta m_{Ia}(T_{\text{eff}})$ which can be accreted on average by a white dwarf at various photospheric temperatures.

Unless otherwise stated, we will consider in our calculations a superposition of emission from a SSP and a high temperature SD progenitor population as a source of ionizing radiation and, when appropriate, compare obtained results with the SSP-only case. For our standard example of a high-temperature SD progenitor population, we will assume that for each SN Ia $\Delta m_{Ia} = 0.3 M_\odot$ of matter is accreted with a WD effective temperature of $T_{\text{eff}} = 10^6 K$. In those cases where we investigate the dependence of line luminosities on the WD effective temperature, we will typically consider the $10^5 - 10^6$ K temperature range. As discussed in Woods & Gilfanov (2013), §2.2, this covers the temperatures expected of steadily nuclear-burning WDs in the standard picture of SSSs ($2 \cdot 10^5 - 10^6 K$, van den Heuvel et al., 1992), as well as the so-called "accretion-wind" binaries with somewhat inflated photospheres (Hachisu, Kato & Nomoto, 1999). For the present study, we do not consider any explicit dependence of either the temperatures of accreting WDs or the accreted mass Δm_{Ia} on the age or metallicity of the stellar population. Unless otherwise stated, we will take a 3Gyr-old SSP as representative of the relatively young passively-
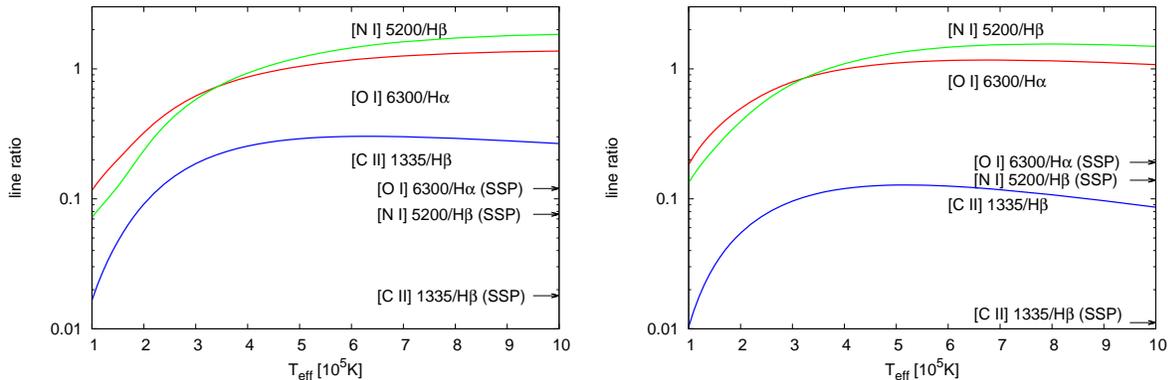
Figure 3.2: Predicted strength of the [C II] 1335Å/Hβ, [N I] 5200Å/Hβ, and [O I] 6300Å/Hα ratios as a function of the effective temperature of nuclear burning WDs in the SD scenario, given ionization by both SD progenitors and pAGB stars. We assume a 3Gyr-old SSP, and a typical ionization parameter log(U) = -3.5 (*left*) and -4 (*right*), roughly spanning the expected range inferred from prior observations of early-type galaxies. Values for each ratio given ionization by the SSP alone (without the inclusion of any SD progenitor population) are labelled on each figure.

evolving galaxies in which we are interested, and a 500Myr SSP in our discussion of post-starburst populations.

3.4 Emission-line diagnostics for high-temperature source populations

In the standard picture of photoionized plasmas, the nebula exhibits a very sharp transition at the interface between the ionized and neutral regions (Osterbrock & Ferland, 2006). However, this picture can be expected to change for ionization by very high temperature sources (e.g. blackbody temperatures of $\sim$ few $10^5 K$ and higher). In this case, soft X-ray photons penetrate much deeper into the illuminated cloud, substantially broadening the transition region (see fig. 3.1). As noted by e.g. Rappaport et al. (1994), this leads to the paradoxical conclusion that a strong enhancement in the luminosity of forbidden lines of neutral or low-ionized atoms **(i.e. tracers of the Strömgren boundary)** may be indicative of ionization by the hottest sources.

The emission lines whose luminosities are most strongly enhanced (relative to the case for low-temperature ionizing sources) are those originating from neutral Nitrogen and Oxygen, and singly-ionized Carbon. For Nitrogen and Oxygen, the first ionization energies of these relatively abundant elements ($\approx$ 14.5 eV for Nitrogen, and $\approx$ 13.6 eV for Oxygen, respectively) are very close to that of Hydrogen ($\approx$ 13.6 eV). Thus, emission from the
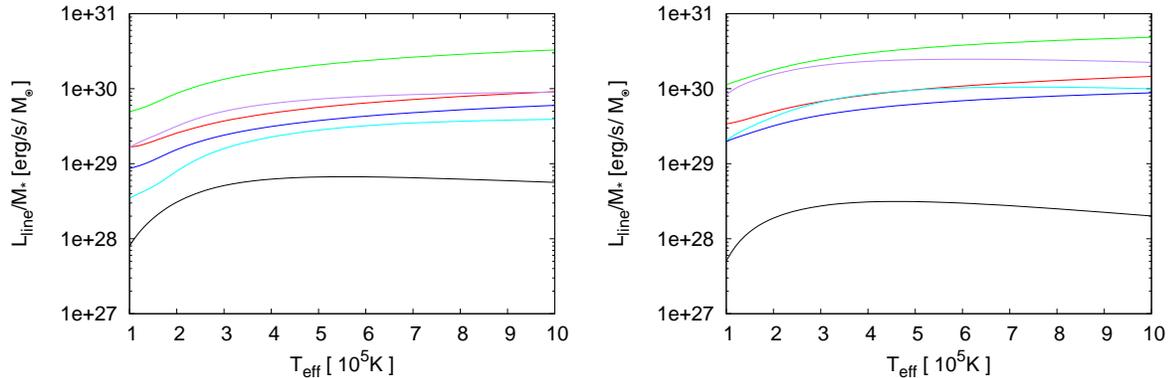
Figure 3.3: Predicted specific luminosities of the [C II] 157μm (red), [O I] 147μm (blue), [O I] 63μm (green), [O I] 6300Å (purple), [N I] 5200Å (cyan), and [C II] 1335Å (black) emission lines (per unit stellar mass, for a covering fraction of unity) as a function of effective temperature of nuclear burning WDs for our example accreting WD population, given ionization by both SD progenitors and pAGB stars. We assume an ionization parameter of log(U) = -3.5 (*left*) and -4 (*right*), for a 3Gyr-old stellar population. For clarity, we omit the line luminosities for ionization by the SSP alone from the plots. For log(U) = -3.5, and ionization by the SSP only, the line luminosities are: $L_{\text{[CII]1335Å}} = 2.0 \cdot 10^{27}$erg/s/M$_\odot$, $L_{\text{[NI]5200Å}} = 8.5 \cdot 10^{27}$erg/s/M$_\odot$, $L_{\text{[OI]6300Å}} = 4.0 \cdot 10^{28}$erg/s/M$_\odot$, $L_{\text{[OI]63}\mu\text{m}} = 1.2 \cdot 10^{29}$erg/s/M$_\odot$, $L_{\text{[OI]146}\mu\text{m}} = 2.0 \cdot 10^{28}$erg/s/M$_\odot$, $L_{\text{[CII]157}\mu\text{m}} = 3.9 \cdot 10^{28}$erg/s/M$_\odot$.

forbidden transitions of [O I] and [N I] closely trace the interface of the neutral and ionized regions of nebulae. Similarly, [C II] lines are well-known for their importance in the heating balance of largely neutral ISM (Osterbrock & Ferland, 2006), given the relatively high abundance of Carbon and the low ionization potential of its valence electron. For example, the fine structure transition $^2P_{1/2} \rightarrow^2 P_{3/2}$ is easily excited by collisions with neutral hydrogen for low gas temperatures and very low fractional ionizations (Dalgarno & McCray, 1972).

The above can easily be confirmed in a systematic manner with detailed photoionization modeling. In our calculations, we include predictions for the 50 strongest emission lines, typically extending down to line fluxes $\sim 10^{-6}L_{H\beta}$. As we are chiefly interested in the possible presence of very high-temperature sources within passively-evolving stellar populations, we compare ionization by the "normally-evolving" stellar population alone, to the same with the inclusion of our example high temperature SD progenitor population. Considering both observational errors, as well as the uncertainties inherent in the modelling of photoionized nebulae, we selected only those lines whose ratio to the nearest Hydrogen recombination line is enhanced by an order of magnitude or more. This will allow one to meaningfully constrain the spectral hardness of the ionizing radiation in retired galaxies,

allowing for the clearest distinction between ionization by pAGBs and accreting WDs.

Selected lines are listed in table 3.1. We have considered also intermediate temperatures of $T_{\mathrm{eff}} \sim 5 \cdot 10^5 K$. While the ordering of the lines is rearranged somewhat from table 3.1, we find that at such values for T_{eff} the principally interesting lines remain the same (with the [N I] 5200Å doublet in particular remaining quite impressive). For still lower temperatures, the most interesting lines are those of He II, as discussed in Woods & Gilfanov (2013). Note that, while we assume a fixed density n = 100cm^{-3}, the optical lines quoted in table 3.1 vary only by $\sim 10 - 20\%$ for densities 1cm$^{-3} <$ n < 1000cm^{-3}. However, the [C II] 1335Å line in the UV, and particularly the IR and FIR lines of Carbon, Oxygen, and Nitrogen, are more sensitive to the density of the ionized gas (with [C II] 146μm varying by almost an order of magnitude, and the others by a factor of ~ 2 over the above range in density). Therefore, our results should be used with caution outside of the density range considered here.

By far the most strongly enhanced transition is the doublet [N I] 5197.82Å/5200.17Å (hereafter we refer to their combined emission as simply [N I] 5200Å). In fig. 3.2, we plot the [N I] 5200Å luminosity normalized to that of Hβ, as a function of the effective temperature for our standard case SD progenitor population. We see that for source temperatures on the order of $10^6 K$, we expect a factor of ≈ 25 increase in the predicted emission-line ratio over the SSP-only case. Similarly, for [O I] 6300Å/Hα, we see the predicted line ratio rise by a factor of ≈ 10 for the same conditions [1]. Though less impressive, the [O I] 6300Å line is intrinsically much more luminous than [N I] 5200Å, and therefore more easily (and commonly, e.g. Annibali et al., 2010) detected in ellipticals. However, the [N I] 5200Å doublet is also frequently detected in the SAURON spectroscopic survey of low-ionization emission-line regions in early-type galaxies (e.g. Sarzi et al., 2006; Sarzi, Shields & Schawinski, 2010). We reserve further discussion of observational prospects for § 5.

In fig. 3.2, we also plot the luminosity predicted in the [C II] 1335Å line. Note that here we normalize our predictions to the Hβ line, rather than the luminosity in the strong, nearby Lyα transition. This is because modeling of the total emitted luminosity of the resonant Lyman-α line of Hydrogen would require a careful treatment of the 3 dimensional geometry of the emitting region, in order to account for the real Lyα escape fraction. However, for reference, we plot an example of the Lyα luminosities output from MAPPINGS III in the following section (see fig. 3.5). Although the [C II] 1335Å line is quite faint compared to the strong H and He II recombination lines in the UV, it may be an attractive target for future UV missions, such as the WSO (see § 3.6.2).

As can be seen from figs. 3.2, 3.3, above $T_{\mathrm{eff}} \sim 3 - 4 \cdot 10^5 K$, all three of these lines are relatively insenstive to ionizing source temperature, being more or less uniformly enhanced at these temperatures. This makes them an ideal complement to the He II diagnostic (Woods & Gilfanov, 2013). The [N I] 5200Å and [O I] 6300Å lines have the added benefit of being relatively insensitive to the ionization parameter over the range relevant to retired galaxies.

---

[1]Note that, for clarity, we omit from our plots the [O I] 6363Å/Hα line ratio, as it follows that of the [O I] 6300Å but reduced by a factor of ≈ 3

We can also quantify the effect of introducing a luminous SN Ia progenitor population in terms of the resulting absolute specific luminosities of the nebular emission lines expected in ellipticals. In fig. 3.3, we plot the specific luminosity in each of the optical and UV lines discussed above, as well as the three IR lines predicted to be the most enhanced in the SD scenario.

Note that the contribution of SD progenitors to the predicted ionizing continuum is proportional to the accreted mass Δm_{Ia}. In principle then, an observational constraint on the luminosity of any of the above lines can be understood as an upper limit on the mass Δm_{Ia} which each SD progenitor accretes on average, for a given effective temperature (more on this in the §§ 4,5).

3.5 Calorimetry of stellar ionizing sources using strong emission lines

While the most temperature-sensitive lines may provide an obvious means to test the hardness of the available ionizing spectrum, in practice the Oxygen, Nitrogen, and Carbon forbidden lines discussed above are relatively weak compared to the dominant cooling lines in photoionized nebulae. The "classical" strong emission lines in the optical include Hα (≈ 3Hβ), [N II] 6583Å, the [O II] 3726.03Å+3728.73Å doublet (hereafter, we refer to their combined emission as [O II] 3727Å), and [O III] 5007Å. In the UV, the strongest line is easily the Lyα transition of Hydrogen. As mentioned in the previous section, the majority of these lines are relatively insensitive to the temperature of the ionizing continuum (Osterbrock & Ferland, 2006), and therefore cannot constrain the precise temperature of any SD progenitor population. However their brightness makes them an easily measurable proxy for the absolute intensity of the ionizing radiation field in the galaxy, thus these lines can be used for the calorimetry of the incident flux of ionizing photons.

Such lines are particularly useful in constraining the population of hot nuclear burning white dwarfs in very young post-starburst galaxies. This is because, for delay times less than ~ 1 Gyr, we expect the total ionizing emission from SD progenitors to exceed that from the stellar population by more than an order of magnitude (see fig. 3.4). Therefore, the observed total emission line luminosity per unit stellar mass for **any** strong line can become a useful measure of the total ionizing luminosity in young stellar populations. These lines also have the advantage of being relatively insesnsitive to the density of the ionized gas.

Given a diffuse ionizing luminosity $L_\nu(t, T_{\mathrm{eff}}, \Delta m_{\mathrm{Ia}})$ produced by the stellar population (cf. eq. 3.3), we can parametrize the luminosity in any emission line in the simple form:

$$L_{\mathrm{line}} = f_{\mathrm{c}} \cdot f_{\mathrm{line}}(n_{\mathrm{gas}}, T_{\mathrm{eff}}, U) \cdot \int_{13.6\mathrm{eV}}^{\infty} \frac{L_\nu(t, T_{\mathrm{eff}}, \Delta m_{\mathrm{Ia}})}{h\nu} d\nu \qquad (3.4)$$

where f_{c} is the covering fraction of the ionized gas, and T_{eff} is again the effective temperature of the SD source population. Note that we scale the absolute normalization of any line

to the total ionizing photon luminosity of the stellar population. The coefficient f_{line} (with dimensions of ergs per incident ionizing photon) is in principle a function of the gas density, ionizing source temperature, and ionization parameter. In this way, we encapsulate the physics relevant to any line luminosity within a simple fit to the output of our model calculations (see below). We emphasize, however, that the above parameterization is an artificial construction; for collisionally excited lines, the line luminosity is not linearly proportional to the incident ionizing photon flux, and the ionization parameter, gas density, and total ionizing photon flux are not independent quantities. Rather, this parameterization simply makes for convenient use given the input parameters of our calculations, and should not be seen as applicable outside of our treatment (ionization by blackbody sources with fixed ionization parameter and gas density).

For any recombination line, f_{line} is to first approximation a trivial function of the total recombination rate and the relevant effective recombination rate for the given electronic transition. For example, the total luminosity of the Hα line of hydrogen can be found from eq. 3.4 with

$$f_{\text{H}\alpha} = h\nu_{\text{H}\alpha} \frac{\alpha^{\text{eff}}_{3 \to 2}(\text{T}_{\text{gas}})}{\alpha_{\text{B}}} \sim 10^{-12} \text{erg/photon} \tag{3.5}$$

where $\alpha^{\text{eff}}_{3 \to 2}(T_{\text{gas}})$ is the effective rate of recombinations leading to the $3 \to 2$ transition of hydrogen, and α_{B} is the total recombination rate to the 1st excited state (Osterbrock & Ferland, 2006). For the approximate relation above, we assume $\text{T}_{\text{gas}} \approx 10^4 K$. Of course in practice, the gas temperature will deviate from this value. As well, the simple dependence on the relevant recombination coefficients alone breaks down for the Lyman-α transition of Hydrogen (Lyα) for high-temperature ionizing sources. Here again, the difference comes about as a result of the dramatically broadened Strömgren boundary, with ionization fraction $0 < n_{H^+}/n_H < 1$. For very hot source temperatures, high-energy photons impart significant kinetic energy to ionized electrons, which then induce secondary collisional excitations in neutral hydrogen atoms. The Lyα luminosity is then increasingly dominated by collisional excitations, greatly enhancing its flux over that expected from recombinations alone (Shull & van Steenberg, 1985).

For collisionally excited lines, the coefficient f_{line} is a non-trivial function of the gas temperature, the free electron density, and the elemental abundances. For this reason, we turn again to our detailed photoionization calculations using MAPPINGS III as above. For ionization **by SD progenitors alone**, in table 3.2 we provide polynomial fits to the predicted line luminosities of the form:

$$f_{\text{line}}(T_{\text{eff}}) = (10^{-12} \text{erg/photon}) \cdot \sum_{\text{n}} \text{a}_{\text{n}}(\text{T}_{\text{eff}}/10^5 \text{K})^{\text{n}} \tag{3.6}$$

where T_{eff} is the accreting WD photospheric temperature. This function is valid in the absence of any contribution from the normally-evolving stellar population, or in the limit that their contribution is negligible compared to the total luminosity of SD progenitors (which is the case, for example, for t $<$ 1Gyr and $\Delta m_{\text{Ia}} \sim 0.3 M_\odot$). Any dependence
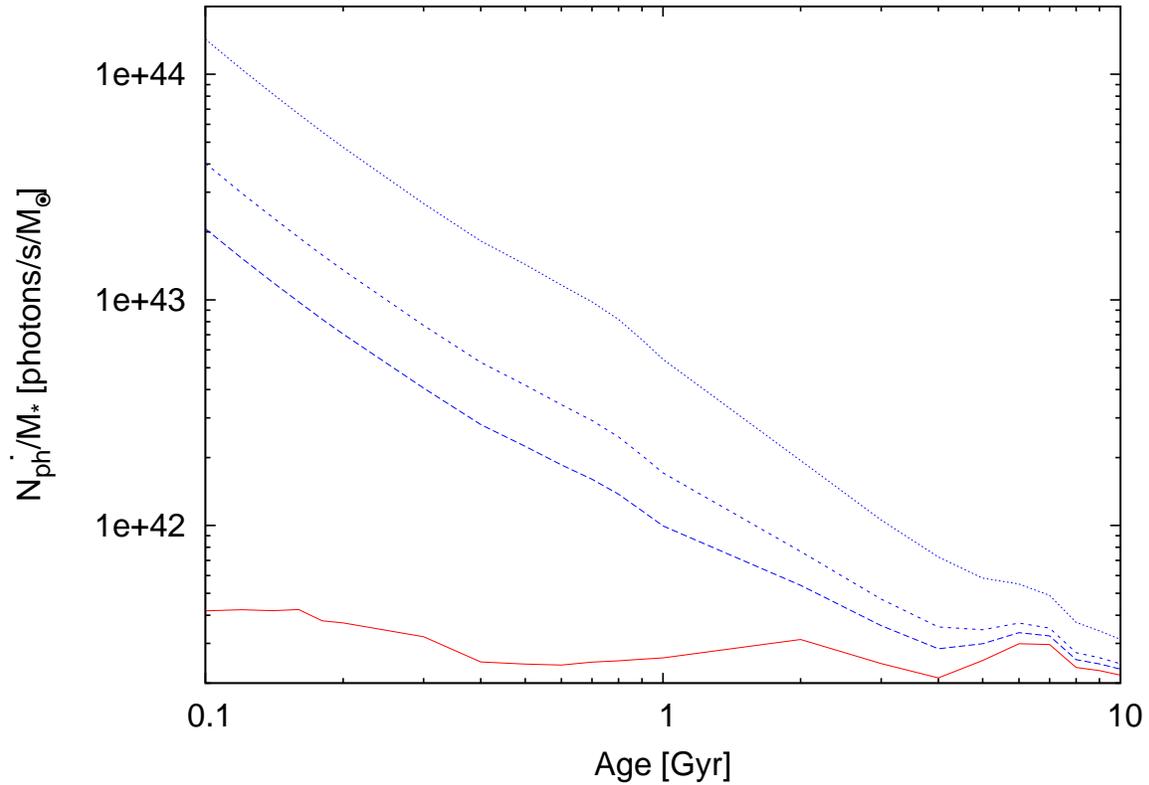
Figure 3.4: H-ionizing photon luminosity for simple stellar populations, given ionization by pAGB stars alone (red), as well as the combined emission of both pAGB stars and SD progenitors (blue lines). Here, we assume the latter accrete $\Delta m_{\mathrm{Ia}} = 0.3 M_\odot$ with effective temperatures of $10^5 K$ (upper blue line), $5 \cdot 10^5 K$ (middle blue line), and $10^6 K$ (lower blue line).

of L_{line} on the age of the stellar population will then come only from the total photon luminosity of the SD progenitor population.

It is therefore convenient to provide fits to the integrated ionizing photon luminosity in eq. 3.4, and to treat the contributions from pAGBs ($\dot{N}^{SSP}_{>13.6eV}$) and SD progenitors ($\dot{N}^{WD}_{>13.6eV}$) seperately:

$$\dot{N}_{>13.6eV}(t) = \int \frac{L^{SSP}_\nu(t)}{h\nu}d\nu + \int \frac{S^{WD}_\nu(T_{\text{eff}})}{h\nu}d\nu \cdot \Delta m_{\text{Ia}} \dot{N}_{\text{Ia}}(t) \qquad (3.7)$$

For nuclear-burning WDs, this can be found directly as a function of the delay time using the observed SN Ia rate, together with eq. 3.2 and assuming blackbody spectra. This gives us a specific ionizing photon luminosity (photons/s/$M_\odot$) of:

$$\dot{N}^{WD}_{>13.6eV} \approx 10^{54.2} \left(\frac{t}{\text{yr}}\right)^{-1.37} \left(\frac{T_{\text{eff}}}{10^6 K}\right)^{-1} \left(\frac{\Delta M}{0.3 M_\odot}\right) \qquad (3.8)$$

for $T_{\text{eff}} \gtrsim 2 \cdot 10^5 K$. Note that the power-law index for the time-dependence differs slightly from the delay-time distribution; this is due to the evolution of the mass to K-band light ratio with age of the stellar population.

The ionizing emission from the normally-evolving stellar population (found from Bruzual & Charlot, 2003), can be approximated with the polynomials:

$$\dot{N}^{SSP}_{>13.6eV} \approx \begin{cases} 6.5 \cdot 10^{41} x^2 - 8.6 \cdot 10^{41} x + 5.2 \cdot 10^{41}, \\ \qquad\qquad\qquad\qquad 0.1 \leq \text{x} < 1.0 \\ \\ -4.3 \cdot 10^{39} x + 2.8 \cdot 10^{41}, \\ \qquad\qquad\qquad\qquad 1.0 \leq \text{x} \leq 10. \end{cases} \qquad (3.9)$$

(for x = (t/1 Gyr) $\lesssim$ 10) where all coefficients are in units of photons/s/$M_\odot$. Note that the sum $\dot{N}^{SSP}_{>13.6eV} + \dot{N}^{WD}_{>13.6eV}$ cannot be used with the fits in table 2, as the latter were computed assuming ionization by SD progenitors alone. In practice, one would need to conduct additional calculations to include the contribution of the SSP population. However, if necessary one can find a useful estimate for the Hα luminosity using eq. 3.5 and eqs. 3.8 and 3.9. Finally, in table 3.2, we also provide power law fits for the spectral intensity of the continuum:

$$\text{L}^{\text{cont}}_\lambda = 10^{\text{b}_0}(\text{t}/1\text{Gyr})^{\text{b}_1}\text{erg/s/\AA}/10^{10}\text{M}_\odot \qquad (3.10)$$

This fit gives the spectral luminosity of the SSP continuum at the wavelength of each optical line, for ease in computing their equivalent widths (EW). Note that, in the case of the fit to the continuum beneath Hα, we include the Balmer absorption feature in stellar atmospheres, as given in Bruzual & Charlot (2003).

Equations 3.4 – 3.9 provide a useful approximation for the predicted luminosity in any of the classical strong lines. For convenience, we also list in table 2 the respective coefficients for the temperature sensitive lines discussed in the previous section.

Table 3.2: Fit coefficients to the line luminosity and continuum flux at each relevant wavelength. For the former, we assume ionization by SD Progenitors alone. Valid for $10^5 K \leq T_{\mathrm{eff}} \leq 10^6 K$. Values a_{n} provide the polynomial coefficients for eq. 3.6, which describe the respective line luminosities, while b_{n} provide the coefficients for eq. 3.10 at the location of the corresponding optical lines. Note that the fits given in eqs. 3.6, 3.10 are valid only for $0.1 \mathrm{Gyr} \lesssim t_{\mathrm{gal}} \lesssim 1$ Gyr.

Emission Line	a_4	a_3	a_2	a_1	a_0	b_1	b_0
Lyα 1216Å	0	-0.13	2.42	-0.37	7.41	/	/
[O II] 3727Å	0	0.036	-0.72	5.04	-1.16	-1.14	39.67
[O III] 5007Å	6.2e-2	-0.64	1.91	-0.28	-1.7e-4	-0.801	39.95
Hα 6563Å	0	-2.5e-3	5.3e-2	-0.15	1.41	-0.524	39.74
[N II] 6583Å	0	8.6e-3	-0.16	1.36	0.14	-0.542	39.93
[C II] 1335Å	0	0	0	0.07	-0.06	/	/
[N I] 5200Å	0	0	0	0.33	-0.58	-0.720	40.0
[O I] 6300Å	0	0	0	0.85	-1.20	-0.574	39.94
[O I] 63μm	0	0	0	2.00	-3.15	/	/
[O I] 146μm	0	0	0	0.37	-0.58	/	/
[C II] 158μm	0	0	0	0.41	-0.53	/	/

In figure 3.5, we plot the total luminosity in Lyα, Hα, [N II] 6583Å, [O III] 5007Å and the [O II] 3727Å doublet, as a function of source temperature for ionization by SD progenitors alone. Note that the predicted Lyα line luminosity should be only be considered an indicative estimate, as discussed in § 3. We take a 500 Myr-old SSP as our example of a post-starburst stellar population and assume our standard characteristic accreted mass $\Delta m_{\mathrm{Ia}} = 0.3 \mathrm{M}_\odot$. From fig.5 one can see that the presence of a high-temperature SD progenitor population leads to an enhancement for all lines by well over an order of magnitude (except for the [O III] 5007Å line for high source temperatures). The [N II] 6583Å line luminosity exceeds that expected in the case of photoionization by the "normally-evolving" stellar population ($\approx 3.6 \cdot 10^{29}$ erg/s/M$_\odot$ for f$_{\mathrm{c}} = 1$) by a factor of $\approx$ 30 − 60 across the considered temperature range. The most luminous of the considered lines is the [O II] 3727Å doublet, which lies in the near-UV on the boundary of the wavelength range typically considered the "optical". However, a number of ground-based surveys have already been carried out specifically investigating this line (typically as a proxy for the SFR, see § 3.6.2).

The total luminosity in any line is determined by the incident ionizing flux, which in the SD scenario is proportional to the accreted (and nuclear-processed) mass (recall eq. 3.2). Therefore any measurement (or upper limit) on their luminosities associated with a given stellar population will constrain the total ionizing luminosity of any putative SD progenitors. This is particularly useful in the lower range of temperatures predicted for nuclear-burning WDs ($T_{\mathrm{eff}} \sim 10^5 K$), where both the He II diagnostic and tracers of the
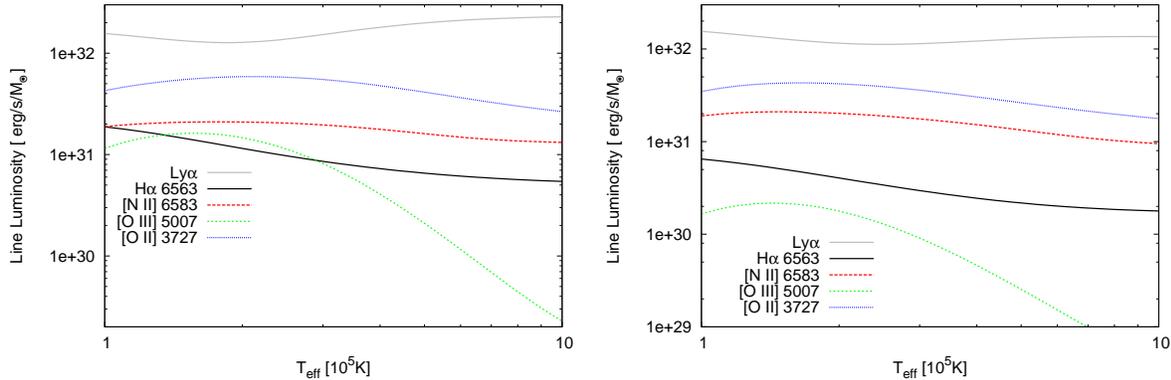
Figure 3.5: Absolute luminosities of the strong optical emission lines Hα, [O III] 5007Å, [O II] 3727Å, and [N II] 6583Å, as a function of the photospheric temperature assumed for accreting, nuclear-burning WDs. Line fluxes are given assuming ionization by SD progenitors alone, for a stellar population of age 500Myr. We assumed $f_c = 1$ and an ionization parameter of $\log(U) = -3.5$ (*left*) and -4 (*right*). For clarity, we omit the line luminosities for ionization by the SSP alone from the plots. For $\log(U) = -3.5$, the luminosities given ionization by the SSP alone are $L_{H\alpha} = 3.2 \cdot 10^{29}$ erg/s/$M_\odot$, $L_{NII6583} = 3.6 \cdot 10^{29}$ erg/s/$M_\odot$, $L_{OIII5007} = 2.4 \cdot 10^{29}$ erg/s/$M_\odot$, $L_{OII3727} = 8.5 \cdot 10^{29}$ erg/s/$M_\odot$, and $L_{Ly\alpha} = 2.7 \cdot 10^{30}$ erg/s/$M_\odot$.

Strömgren boundary fail. The significant enhancement in the line luminosity expected given photoionization by SD progenitors should allow the total mass processed by nuclear-burning accreting WDs to be constrained to $\lesssim 0.01 - 0.001$ M$_\odot$/SN Ia (for example, using the [O II] 3727Å line, see fig. 3.6), should line fluxes be found to be consistent with ionization by pAGBs alone.

3.6   Discussion

3.6.1   Constraints on the steady nuclear-burning WD population from optical emission-line ratios

A number of optical spectroscopic surveys of extended low-ionization emission line regions in early-type galaxies have already been conducted (e.g. Sarzi et al., 2006; Annibali et al., 2010), or are presently ongoing (Sánchez et al., 2012). Therefore, a large sample of such galaxies already exists which can be compared with our predictions. In estimating the feasibility of constraining the SD channel using optical forbidden lines, the most useful quantity is not the absolute luminosity per se, but rather the EW, as it characterizes the observability of the line. In fig. 3.7, we show for a 3 Gyr-old SSP the EW of [N I] 5200Å, [O
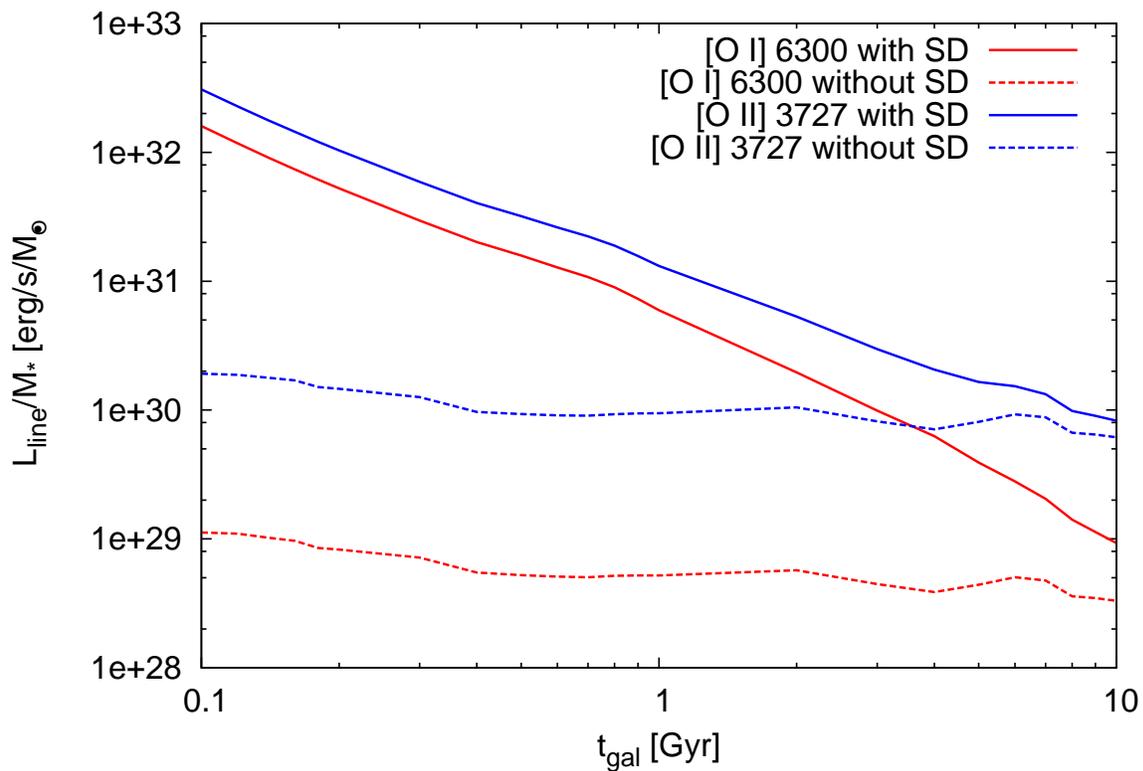
Figure 3.6: Absolute luminosity of the O I 6300Å line and the [O II] 3727Å doublet as a function of stellar population age. We assume $f_c = 1$ and an ionization parameter of log(U) = -3.5, with line fluxes given ionization by the "normally-evolving" stellar population only (red, solid), and with the inclusion of our example SD progenitor population (blue, dashed).
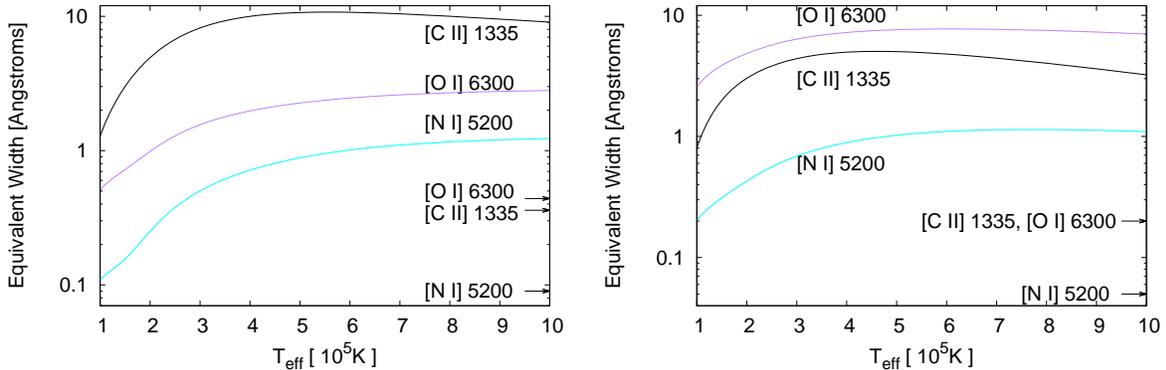
Figure 3.7: Equivalent widths of the [C II] 1335Å, [N I] 5200Å, and [O I] 6300Å emission lines in the SD scenario. We assume $f_c = 1$ and an ionization parameter of log(U) = -3.5 (*left*) and -4 (*right*), for a 3-Gyr-old stellar population. For log(U) = -3.5, the EWs given ionization by the SSP alone are 0.15Å, 0.004Å, and 0.026Å for [C II] 1335Å, [N I] 5200Å, and [O I] 6300Å respectively.

I] 6300Å, and [C II] 1335Å), taking the continuum emission as predicted from Bruzual & Charlot (2003). For significantly older stellar populations (> 5Gyr) our diagnostics become significantly less discriminating, at least for the presence of SD SN Ia progenitors, given their much lower expected luminosity at late times (recall figs. 3.4, 3.6). With the EW of the line and its broadening σ, we can estimate a minimum S/N of the spectrum needed to detect any line at a desired amplitude-to-noise ratio A/N using the formula given by Sarzi et al. (2006):

$$\frac{S}{N} = \frac{A/N \sqrt{2\pi}\sigma}{EW} \tag{3.11}$$

where we will take their characteristic broadening and minimum A/N ($\sigma = 120$km/s, A/N = 4). For SD source temperatures above $\sim 4 \cdot 10^5 K$, we predict for the [O I] line an EW of ~ 1Å for the realistic case $f_c = 0.5$ (see fig. 3.7). Therefore, in order to barely detect [O I] 6300Å emission, we would require a spectrum with S/N ≈ 25. Such a S/N is only just out of reach of typical SDSS spectra (S/N $\sim 10 - 15$), and a very robust detection should easily be possible with stacking. Note that the [O I] line is also frequently detected in individual galaxies in the sample of Annibali et al. (2010). Given the similar continuum level at 6563Å and the much greater intrinsic strength of the Hα line (see fig. 3.5), the latter should similarly be quite easily detectable.

As discussed in § 3.4, normalizing our predictions for the flux in any line to that of the nearest hydrogen recombination line has the advantage of removing any dependence on the covering fraction or total mass of the stellar population. In fig. 3.8, we plot the predicted [O I] 6300Å/Hα ratio as a function of the total mass accreted by SD progenitors
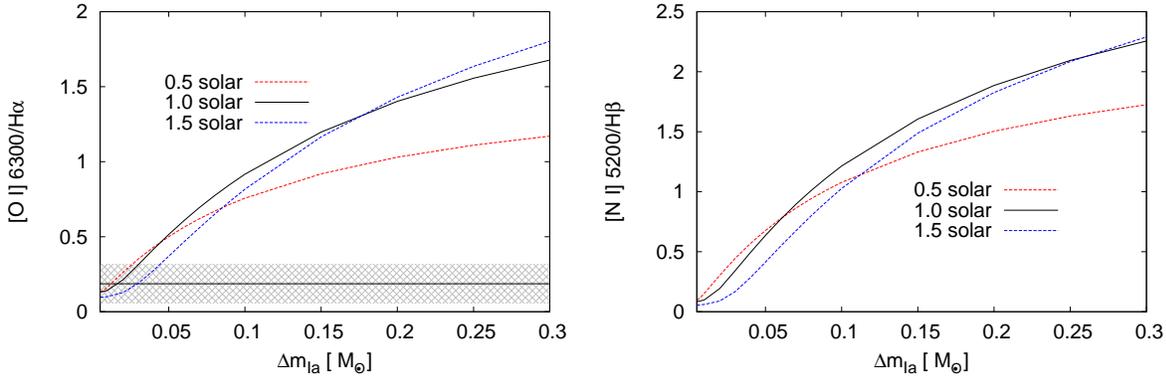
Figure 3.8: Predicted [O I] 6300/Hα (*left*), and [N I] 5200/Hβ (*right*) as a function of mass accreted by a typical WD in the SD scenario, given ionization by both SD progenitors and pAGB stars. In both figures, log(U) = -3.5, the time since initial starburst is 2 Gyr, and we assume SD progenitors with an effective temperature T $= 10^6 K$. In both figures, each of the three lines corresponds to the line luminosity assuming a different metallicity of the ionized gas, but keeping the metallicity of the stellar population fixed. For the [O I] diagram, we overplot the [O I] 6300Å/Hα ratio (solid black line) with 1 sigma error bars (shaded region) for the nucleus of NGC 3489 (Annibali et al., 2010). The [N I] 5200Å doublet was not detected in the same survey.

at an effective temperature of $10^6 K$. Note that, whereas we would expect a linear relation for the total line flux as a function of Δm_{Ia}, this is not the case for diagnostic line ratios. This is primarily due to the contribution of the ionizing luminosity from SD progenitors to the ionization of hydrogen.

As an illustrative example, we can compare our models with the observed [O I] 6300Å/Hα ratio in the nucleus of the post-starburst galaxy NGC 3489 (Annibali et al., 2010; Sarzi, Shields & Schawinski, 2010). As a conservative estimate (see e.g. Annibali et al., 2007), we assume a 2 Gyr-old SSP, with the available photoionizing continuum originating from both pAGBs and SD progenitors. We see that, for a wide range of gas phase metallicities $(0.5Z_\odot \leq Z \leq 1.5Z_\odot)^2$, the [O I] 6300Å/Hα diagnostic can in practice distinguish (at $\approx$ 1σ confidence) between ionization by pAGBs alone and the inclusion of a SD progenitor population which accretes more than $\approx 0.04 M_\odot$ per SN Ia at $T_{eff} = 10^6 K$.

A similar case can be made for the [N I] 5200Å/Hβ line diagnostic (see fig. 3.8). Though the [N I] 5200Å line strength is always weaker than [O I] 6300Å (and, unfortunately, not detected in the sample of Annibali et al., 2010), it is still observed with confidence in a number of LIERs (e.g. Sarzi et al., 2006). In fig. 3.7, we see that for SD source temperatures $\gtrsim 7 \cdot 10^5 K$, the [N I] 5200Å EW is roughly ~ 0.5Å (for $f_c = 0.5$ and log(U)=-

---

[2]Roughly spanning the range expected in the ISM of early-type galaxies (Annibali et al., 2010).
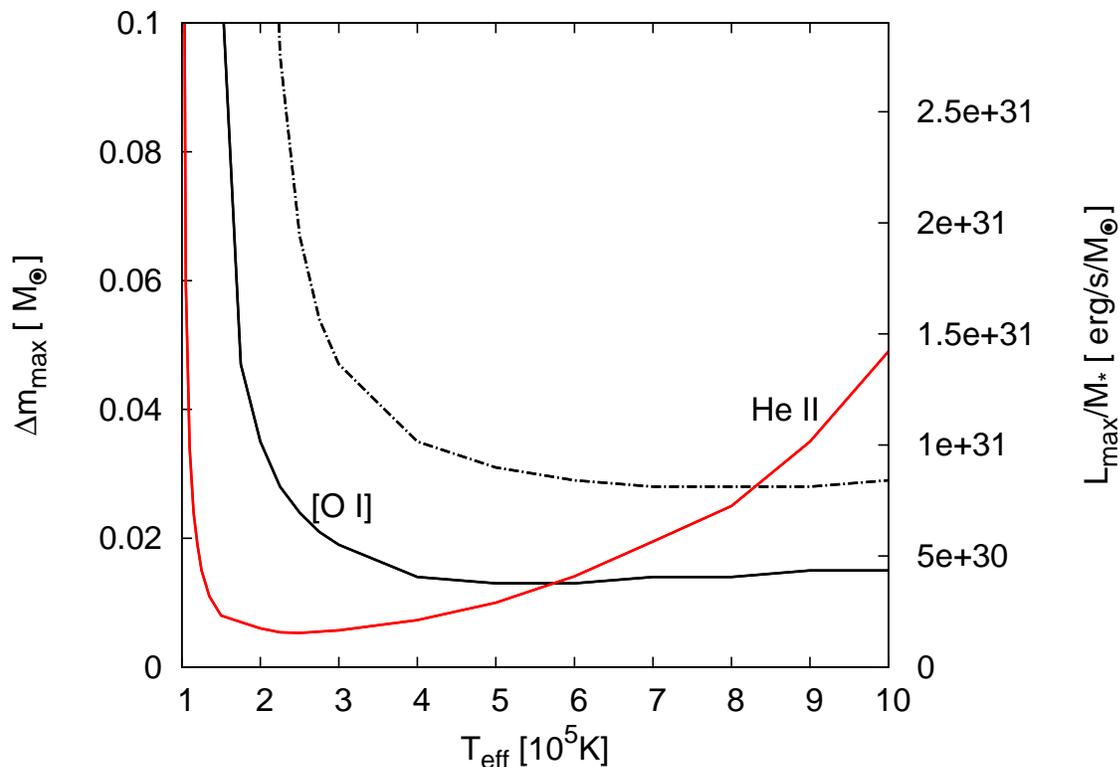
Figure 3.9: Upper limits on the average mass Δm_{Ia} which may be accreted by the typical WD in the SD scenario at a given photospheric temperature. Upper limits are obtained assuming an upper limit of 10% on the He II 4686Å/Hβ ratio (red line), and for the measured [O I] 6300Å/Hα ratio in the nucleus of NGC 3489 (Annibali et al., 2010) (black, solid). For the latter, we also show 1σ upper limit (black, dashed line). Note that any upper limit on the accreted mass is equivalent to an upper limit on the total luminosity of the population of high temperature sources (right y-axis). We assume 2 Gyr-old stellar population, $\log(U) = -3.5$, and solar metallicity for the gas phase.

3.5). Using eq. 3.11 above, we find that this line could then be detected in a 3 Gyr-old stellar population in spectra with S/N ≈ 40. This is well within what is typically achieved in individual SAURON spectra; with stacking, very robust detections (or upper limits) should be feasible. Stacking of SDSS spectra should allow for a confident detection with only ~ 20 galaxies. From fig 3.8, we see that similar to the [O I] line, a detection or upper limit on the [N I] 5200Å/Hβ ratio of $\approx 10\%$ would constrain the average mass processed by nuclear-burning WDs in the SD channel to a few $10^{-2} M_\odot$ per supernova.

Turning again to the [O I] 6300Å/Hα ratio in NGC 3489, we can extend the exercise in fig. 3.8 to investigate its dependence on WD temperature. In fig. 3.9, we plot the maximum mass which can be accreted by nuclear-burning WDs in the SD scenario for effective temperatures $10^5 \lesssim T_{\text{eff}} \lesssim 10^6 K$, should our models[3] remain consistent with the observed ratio [O I] 6300Å/Hα. Note that the upper limit for any temperature in fig, 3.9 excludes any matter accreted at any other temperature. For example, accretion of $\sim 0.02 M_\odot$ of matter at $T_{\text{eff}} = 7 \cdot 10^5$ K will produce an [O I] line luminosity equal to the observed value, therefore no more material at any other temperature could additionally be accreted without conflicting with observations. In practice, any realistic SD scenario would imply a population of WDs in varying accretion states, with a range in temperatures. Therefore any detailed SD scenario may be constrained considering the integrated luminosity and the spectrum of the ionizing radiation produced by the population of SD progenitors.

For NGC 3489, given the observed value of the [O I] 6300Å/Hα ratio, no more than $\approx 0.015 M_\odot$ per supernova can be accreted and nuclear-processed by WDs with photospheric temperatures $T_{\text{eff}} \gtrsim 4 \cdot 10^5 K$. Taking into account the [O I] line flux error, this translates to an upper limit of $\approx 0.04 M_\odot$ at 1σ. Note that the flux errors in Annibali et al. (2010) are not dominated by systematics, and in principle dedicated observations should be able to reduce the uncertainty considerably. If we compare this figure with the sensitivity of the He II diagnostic in Woods & Gilfanov (2013) (see their fig. 8, or the red curve in our fig. 3.9), we see that the two complement each other remarkably well; upper limits on the He II line luminosity (here we assume He II 4686Å/H$\beta < 10\%$) reach their peak effectiveness at $\approx 2.5 \cdot 10^5 K$, just as the [O I] 6300Å/Hα diagnostic becomes ineffective.

An important point to consider is that, while we typically quote limits here in terms of the average mass accreted by nuclear-burning WDs (Δm_{Ia}), in principle it is rather the total luminosity of any high-temperature sources which we constrain (see right y-axis in fig. 3.9). Even if SD progenitors are not primarily responsible for the SN Ia rate, accreting WDs may still provide a significant contribution to the ionizing background in passively-evolving galaxies. Therefore, their consideration would be of vital importance in any exercise in understanding the role of pAGBs in low-ionization emission line regions, or their relative importance with respect to LLAGN (as in, e.g. Eracleous et al., 2010). Therefore, careful modeling of the evolution of WD binaries and any phases of stable mass transfer are essential (see Chen et al, in prep).

Finally, we note that in the presence of a hot SD progenitor population, the higher

---

[3]Note that here, as in fig. 3.8, we include the expected contribution from pAGBs to the ionizing background.
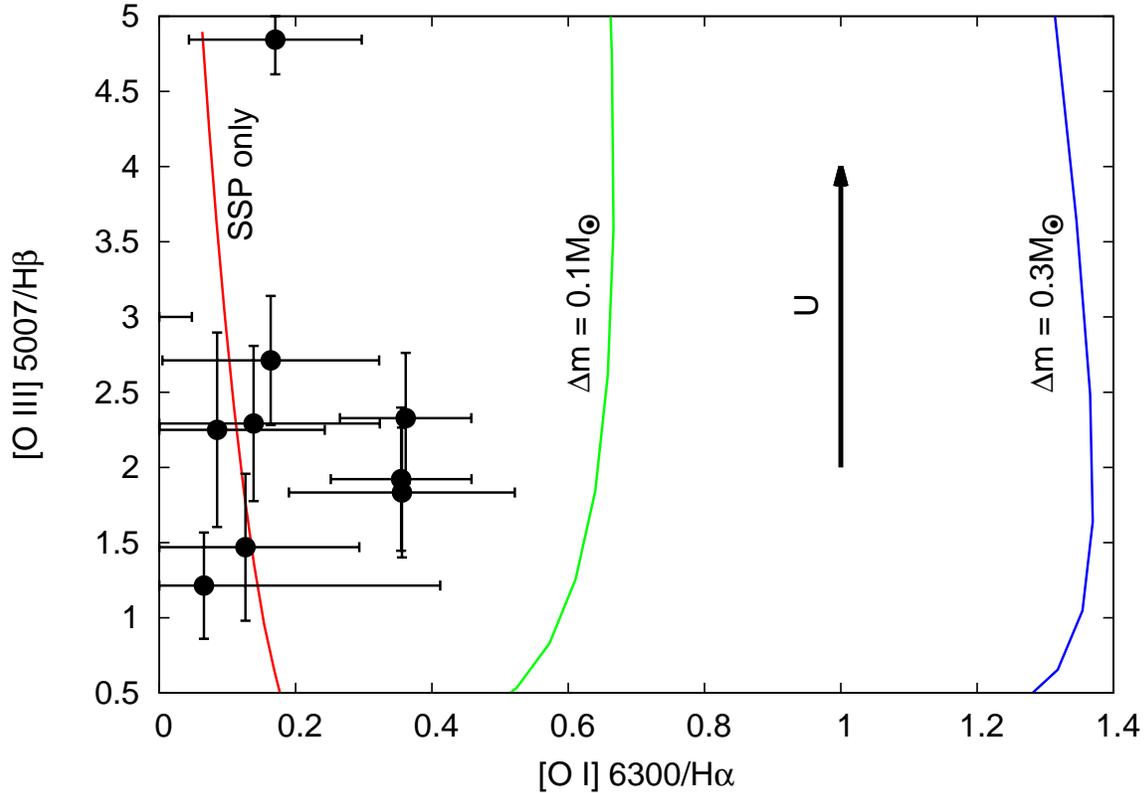
Figure 3.10: Predicted strength of the ratios [O III] 5007Å/Hβ and [O I] 6300Å/Hα for varying ionization parameter, assuming ionization by a 3 Gyr-old SSP alone (red), and with the include of a SD progenitor population which accretes $\Delta m_{\mathrm{Ia}} = 0.1 M_\odot$ (green) and $\Delta m_{\mathrm{Ia}} = 0.3 M_\odot$ (blue) with an effective temperature $T_{\mathrm{eff}} = 10^6 K$. The ionization parameter increases along these lines from $\log(U) \approx$ -4.5 to -3, in the direction indicated by the black arrow. Shown in black are a subset of the results from Annibali et al. (2010).
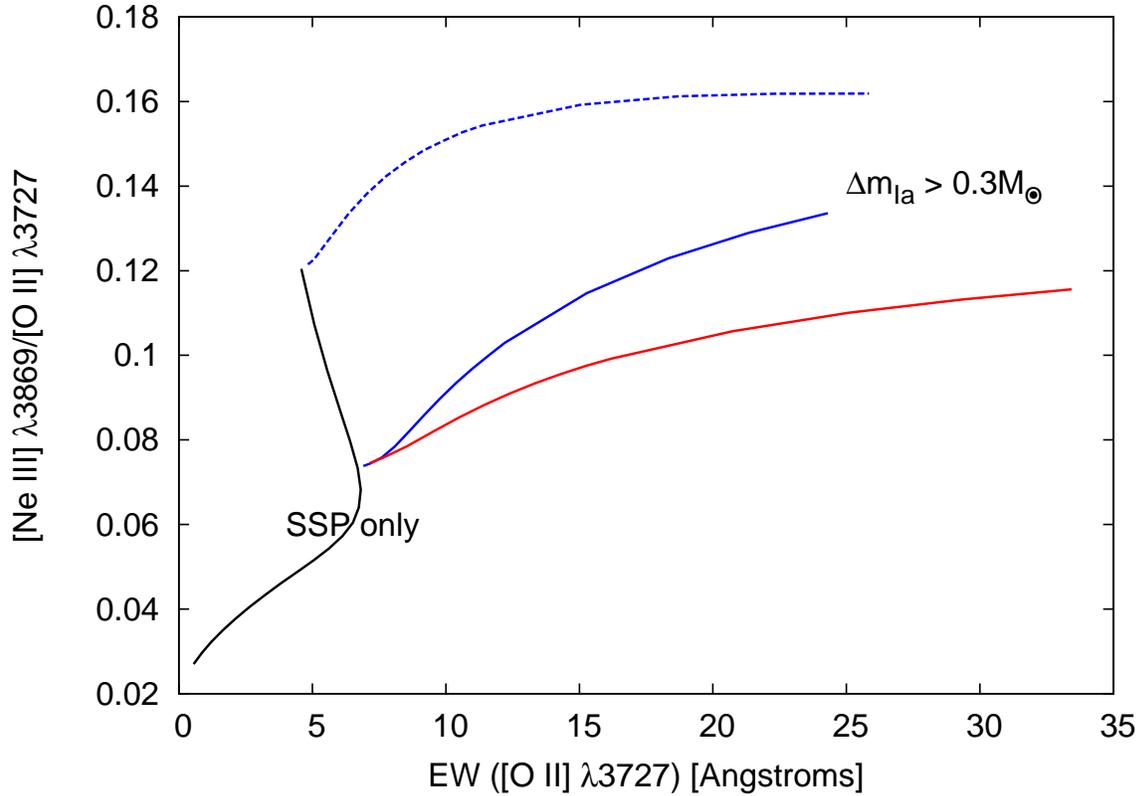
Figure 3.11: Predicted strength of the ratio [Ne III] 3869Å/[O II] 3727Åand the EW of [O II] 3727Å/H for varying ionization parameter, assuming ionization by a 3 Gyr-old SSP alone (black), and with the inclusion of a SD progenitor population which accretes varying Δm_{Ia} with photospheric temperature $T_{\mathrm{eff}} = 5 \cdot 10^5 K$ and log(U) = -3.5 (red, solid) and T_{eff} = $10^6 K$ with log(U) = -3.5 (blue, solid) and log(U) = -3.0 (blue, dashed). For the tracks which include SD progenitors, Δm_{Ia} increases from 0 to $0.3 M_\odot$ from left to right in the figure.

values of [O I] 6300Å/Hα and [N I] 5200Å/Hβ would place most passively-evolving galaxies in the region of the BPT diagram associated strictly with shock ionization (-0.5$\leq$ log([O III] 5007Å/Hβ) $\leq$ 0.5, and log([O I] 6300Å/Hα) > -0.5). However, this has not been observed (e.g. Sarzi, Shields & Schawinski, 2010; Annibali et al., 2010). In fig. 3.10, we plot the predicted values of the [O III] 5007Å/Hβ and [O I] 6300Å/Hα ratios with varying ionization parameter assuming ionization by a 3Gyr-old SSP alone, and with the inclusion of our standard SD progenitor population. We also include a subsample of the results from Annibali et al. (2010); namely, those galaxies with stellar population ages < 4 Gyr (from Annibali et al., 2007), with EW(Hα) < 1.5Å (Cid Fernandes et al., 2011). This restricts us to relatively young early-type galaxies for which the "normally-evolving" stellar population may plausibly power the observed nebular emission. The observed sample in fig. 3.10 appears to be largely reproduceable with ionization by the SSP alone, although any interpretation is complicated by the considerable uncertainty in the majority of the emission line measurements.

For a number of reasons, emission-line diagnostics in the near-UV provides an attractive alternative. As discussed in the previous section, the [O II] 3727Å doublet provides a much higher luminosity than Hα, in a waveband where the continuum is intrinsically lower. The very nearby [Ne III] 3869Å line is also available as a gauge of the ionization parameter (through the [Ne III] 3869Å/[O II] 3727Å ratio, e.g. Levesque & Richardson, 2013). This allows one to construct a BPT-style diagnostic diagram using a remarkably narrow wavelength range (as shown in fig. 3.11), using the EW of the [O II] doublet to measure the specific ionizing luminosity of the observed stellar population, and [Ne III] 3869Å/[O II] 3727Å to fix the ionization parameter. In fig, 3.11, we see that the SSP-only and SD progenitor ionizing populations occupy clearly distinct regions at t = 3Gyr. For a young, post-starburst galaxy (t $\approx$ 500Myr), the EW of [O II] 3727Å would be enhanced by a further order of magnitude for the same ionization parameter (see previous section). The nearby 5$\rightarrow$3 transition of He II (3203Å)[4]. would also allow one to constrain the hardness of the ionizing source population. Together, this presents an excellent opportunity for near-UV spectroscopy to constrain the progenitors of SNe Ia.

3.6.2 Constraints on the SD progenitor populations at early delay-times.

The prospect of calorimetry of the ionizing background in post-starburst galaxies offers a highly promising avenue for constraining the SD channel at the earliest delay-times. In fig. 3.12, we plot the EW of the strongest optical lines for a 500 Myr-old starburst. As discussed in § 3.5, the most intuitive (and least model-dependent) line for this purpose may be the Hα recombination line. In fig. 3.12, we see that in our standard SD case, we predict an Hα EW ranging from $\approx$ 3.5Å at $T_{\rm eff} = 10^6 K$ to $\approx$ 12Å at $T_{\rm eff} = 10^5 K$, assuming $f_{\rm c}$ =

---

[4]Although $\sim$ 3 times weaker than the 4 $\rightarrow$3 transition at 4686Å, the continuum is predicted to be $\sim$4 times weaker at $\approx$3200Å. Therefore the observability and utility of this transition is comparable (see eq. 3.11)

0.5. This may be compared with an Hα EW of ≈ 0.2Å expected from the SSP alone, giving a factor of $\approx 20 - 60$ enhancement. Thus, if observations of post-starburst galaxies gave Hα line intensities consistent with SSP-only case, the contribution of the SD channel could be strongly constrained to a few per cent level, or, equivalently, to $\Delta m_{\mathrm{Ia}} \lesssim 10^{-2} - 10^{-3} M_\odot$ per supernova.

The [N II] 6583Å line can provide a similar constraint (see fig. 3.12). However, the Nitrogen abundance in the ISM of external galaxies is known to be rather uncertain (Groves et al., 2004). Therefore, there is little benefit in focusing on this line for calorimetry, unless it is unresolved from the Hα line. The [O III] 5007Å specific line luminosity drops off dramatically at the highest SD temperatures; this is because with harder spectra, Oxygen is increasingly ionized to O^{3+} near the illuminated face of the gas, reducing the emitting volume for [O III]. At the same time, high-energy photons penetrate deeper into the nebula, preferentially ionizing neutral Oxygen. Note, however, that this itself may pose a problem for any high-temperature SD channel, as the ISM in post-starburst ellipticals are observed to have relatively high values of the [O III] 5007Å/Hβ ratio (Sarzi, Shields & Schawinski, 2010).

The [O II] 3727Å cooling line, originating in the more low-ionized regions of nebulae (the interior, in the geometry discussed here), is expected to have an EW $\gtrsim 15$Å (for $10^5 K \lesssim T_{\mathrm{eff}} \lesssim 10^6 K$). This is a ≈ 40-fold increase over that expected from the SSP alone (≈ 0.41Å, detectable with a minimum S/N ≈ 40). The [O II] 3727Å line (as well as Hα) has been invoked as a proxy for the star-formation rate (more on this in the following section), and already the volumetric [O II] 3727Å luminosity function has been mapped at least to z ≤ 5.4 (see Gallego et al., 2002, and references therein). Individual nearby galaxies which have undergone recent, possibly quenched starbursts would make ideal targets for follow-up studies. As an example, NGC 3156 is a nearby (≈ 22Mpc) early-type galaxy which the SAURON survey found to host a post-starburst subpopulation (with an estimated mass of $\approx 10^9 M_\odot$). The proposed CUBES[5] NUV spectrograph would be able to detect the [O II] 3727Å line (given our standard SD case from above, and assuming $f_c = 0.5$) with a S/N $\approx$ 10 arcsec^{-2} in just 1800 seconds.[6]

Although its specific luminosity is greatly enhanced with the presence of a high temperature source population (see fig. 3.7), the [C II] 1335Å line remains intrinsically weak relative to the strong UV recombination lines (e.g. Lyα, He II 1640Å). The difficulty in detecting this line can best be illustrated with an example. At a distance of ~ 21 Mpc, NGC 3607 is a nearby, relatively young (mean stellar age ~ 3Gyr, e.g. Annibali et al., 2007) elliptical galaxy which hosts an extended low-ionization emission-line region. Assuming our standard SD population from above and a covering fraction of $f_c \sim 1/2$, we can expect a total integrated [C II] 1335Å line flux of $\sim 4.5 \cdot 10^{-16}$ erg/s/cm^2, using the K-band luminosity to estimate the mass as in Woods & Gilfanov (2013). The GALEX FUV spectrograph (now no longer operational) would have required a prohibitive ~ 51

---

[5]For the Phase A Science report, see http://www.eso.org/sci/meetings/2013/UVAstro2013/rationale.html
[6]Found using the CUBES Exposure Time Calculator: http://www.eso.org/observing/
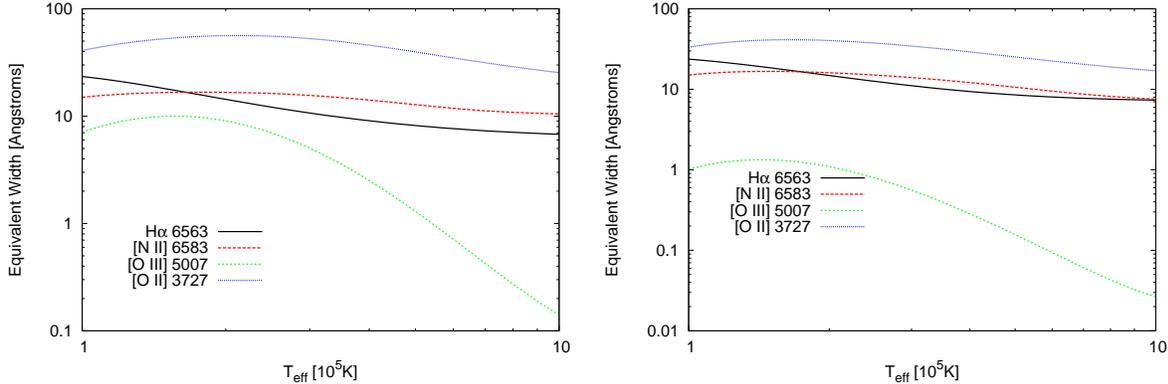
Figure 3.12: Equivalent widths of the strongest optical emission lines given ionization by a high temperature SD channel, assuming a 500 Myr-old stellar population. Here we assumed $f_c = 1$ and an ionization parameter of $\log(U) = -3.5$ (*left*) and -4 (*right*). For $\log(U) = -3.5$, the EWs given ionization by the SSP alone are 0.4Å, 0.29Å, 0.15Å, and 0.8Å for Hα, [N II] 6583Å, [O III] 5007Å, and [O II] 3727Å respectively.

ksec in order to reach S/N ~ 5,[7] with 1335Å lying outside the optimal response of the instrument. However, this remains a promising target for future UV missions, such as the planned WSO. Until such time, the aforementioned He II 1640Å line remains an extremely promising target for observations (see Woods & Gilfanov, 2013), as does the Lyα transition of Hydrogen at 1216Å, the latter being easily detected in any emission-line elliptical galaxy. In the limit where SD progenitors provide the only contribution to the ionizing continuum, the total luminosity expected in Lyα exceeds that of the He II 1640Å line by $1 - 2$ orders of magnitude for SD source temperatures $T_{\text{eff}} \approx 10^5 K - 10^6 K$.

3.6.3 A possible bias in SFR measures?

In young stellar populations, the presence of strong emission lines indicates ongoing star formation (in particular, for low values of N II 6583Å/Hα, e.g. Osterbrock & Ferland, 2006), where interstellar matter is ionized by highly luminous O stars. In this case, the total luminosity in any given line may be used as a tracer of the total ionizing photon flux, and therefore a measure of the number of O stars, indirectly providing the SFR (for an assumed IMF). In practice, the Hα and [O II] 3727Å fluxes are the most practical in the optical, with the standard calibrations being (Kennicutt, 1998):

$$\text{SFR}(M_\odot/\text{yr}) = 8 \times 10^{-42} L_{\text{H}\alpha}[\text{erg/s}] \tag{3.12}$$

---

[7]Found using the GALEX Exposure Time Calculator (http://sherpa.caltech.edu/gips/tools/expcalc.html). In fact, this is only a minimum, as the GALEX Spectroscopy Primer recommends three times the integration time given by the ETC.

$$\mathrm{SFR(M_\odot/yr)} = (1.4 \pm 0.4) \times 10^{-41} \mathrm{L_{[OII]}[erg/s]} \tag{3.13}$$

However, this does not account for the possibility of an additional ionizing source within the stellar population, such as possible SD progenitors of SNe Ia. This would produce an offset in the calibration of any such SFR indicator, which would be dependent on age and mass of the stellar population. For example, for $10^5 \leq T_{\mathrm{eff}} \leq 10^6 K$ SD progenitor population, a 3 Gyr-old $10^{10} M_\odot$ SSP would still appear to have an ongoing star-formation rate of $\gtrsim \mathrm{f_c} \cdot 4 M_\odot/\mathrm{yr}$ from the [O II] 3727Å indicator. Similarly, for a $T_{\mathrm{eff}} = 10^5 K$ SD progenitor population, a 3 Gyr-old $10^{10} M_\odot$ SSP would still appear to have an ongoing star-formation rate of $\approx \mathrm{f_c} \cdot 1 M_\odot/\mathrm{yr}$ from the Hα indicator.

Because of their insensitivity to interstellar reddening, IR lines and the IR continuum itself are extremely useful SFR indicators. As an important coolant in the neutral ISM, the [C II] 157μm line has been proposed as a useful SFR indicator, with the present best calibration given by (de Looze et al., 2011)

$$\mathrm{SFR(M_\odot/yr)} = \frac{(\mathrm{L_{[CII]}[erg/s]})^{0.983}}{1.028 \times 10^{40}} \tag{3.14}$$

Yet there remains considerable scatter in the observed relation. If there is indeed a significant contribution from populations of accreting, nuclear-burning WDs, this should also provide an age-dependent offset. For example, for our standard case SD scenario, a 3 Gyr-old $10^{10} M_\odot$ SSP would still appear to have an ongoing star-formation rate of $\approx \mathrm{f_c} \cdot 1 M_\odot/\mathrm{yr}$.

The [O I] 63μm and 146μm IR lines would provide only a small contribution to any SFR-indicator based on the continuum flux. However, as individual lines, both may in principle be a useful measure of the population of accreting WDs in galaxies, in particular the 63μm line, which is ~ 5 times stronger than the [C II] 157μm line for SD progenitor effective temperatures of $10^5 \leq T_{\mathrm{eff}} \leq 10^6 K$. With the end of the Herschel Space Observatory's operational lifespan, there is at present no instrument which could provide new observations in this waveband, however ample archival data is available. The Field-Imaging Far-Infrared Line Spectrometer (FIFI-LS)[8], will also soon be available, observing in the 42-210 micron band.

As a final word of caution, we recall that our results for the IR and FIR forbidden lines discussed above are sensitive to the assumed density of the gas, which is observed to vary radially (e.g. Yan & Blanton, 2012). Therefore, any quantitative assessment of the contribution of a possible SD channel to the emission of these lines should consider carefully the environment under study. Furthermore, these lines do not originate solely from photoionized regions, but arise also in the neutral medium (Meijerink & Spaans, 2005; Meijerink et al., 2007).

---

[8]www.sofia.usra.edu/Science/instruments/instruments_fifils.html

3.6.4 Mixed-age stellar populations

So far, we have considered only single-age stellar populations, and assumed the same metallicity throughout. Although we have previously demonstrated that varying the metallicity of the stellar population will not significantly alter the ionizing continuum expected from SD progenitors (Woods & Gilfanov, 2013), we have not tested the effect of varying star-formation histories. In a real galaxy, a much more complex superposition of populations of differing ages should be expected. This is particularly concerning, should the presence of a significantly older subpopulation be able to strongly dilute the observed EW in a galaxy with an otherwise young mean stellar age. This could in turn significantly reduce the detectability of our diagnostic lines.

In order to evaluate this possibility, we perform the following experiment. We mix spectra of varying fractions of 1 Gyr-old, $Z = 2.5Z_\odot$ and 10 Gyr-old, $Z = Z_\odot$ stellar populations from Bruzual & Charlot (2003). Using the method of Johansson et al. (2012) based on the Lick indices (Worthey et al., 1994), we find the luminosity-weighted age depending on the relative fractions of young and old populations (Johansson, private communication, see also Johansson et al in prep). At the same time, we compute the expected flux in any of emission lines discussed above for the composite stellar population, using the combined spectra in our photoionization calculations. Here we assume the same gas density $n = 100\text{cm}^{-3}$ with a gas phase metallicity of $Z = Z_\odot$, as above, and with ionization parameter $\log(U) = -3.5$.

The result of this experiment is shown in fig. 3.13, where we plot the EW of the [O I] 6300Å emission line for such composite stellar populations, shown as a function of the derived "mean age." For comparison, we also plot the [O I] EW for a single-aged SSP with $Z = 0.05$. Note that the two tracks do not agree at 10 Gyrs because of the different assumptions for the metallicity of the stellar population. As can be clearly seen, the EW is not significantly affected in the case of composite stellar populations.

3.7 Conclusions

We have demonstrated how observations of forbidden lines of the most abundant metals, as well as recombination lines of Hydrogen and ionized Helium, can be used to constrain any population of sources with effective temperatures $T_{\text{eff}} \gtrsim 10^5 K$ in early-type galaxies. These sources may not be directly detectable due to local interstellar absorption, as well as along the line of sight in the Milky Way, but may be revealed from the dramatic effect on the emission line fluxes predicted for their host galaxies.

A confident detection, or upper limits on, any recombination line of He II in the extended, low-ionization emission line regions of passively-evolving galaxies can constrain the total luminosity of SD progenitors with effective temperatures in the range $1.5 \cdot 10^5 K \lesssim T_{\text{eff}} \lesssim 6 \cdot 10^5 K$. While this comfortably covers the range expected for symbiotics, many super-soft sources, and the so-called ultrasoft sources, other diagnostics must be invoked in order to constrain all possible SD progenitors. We have demonstrated that, in relatively young
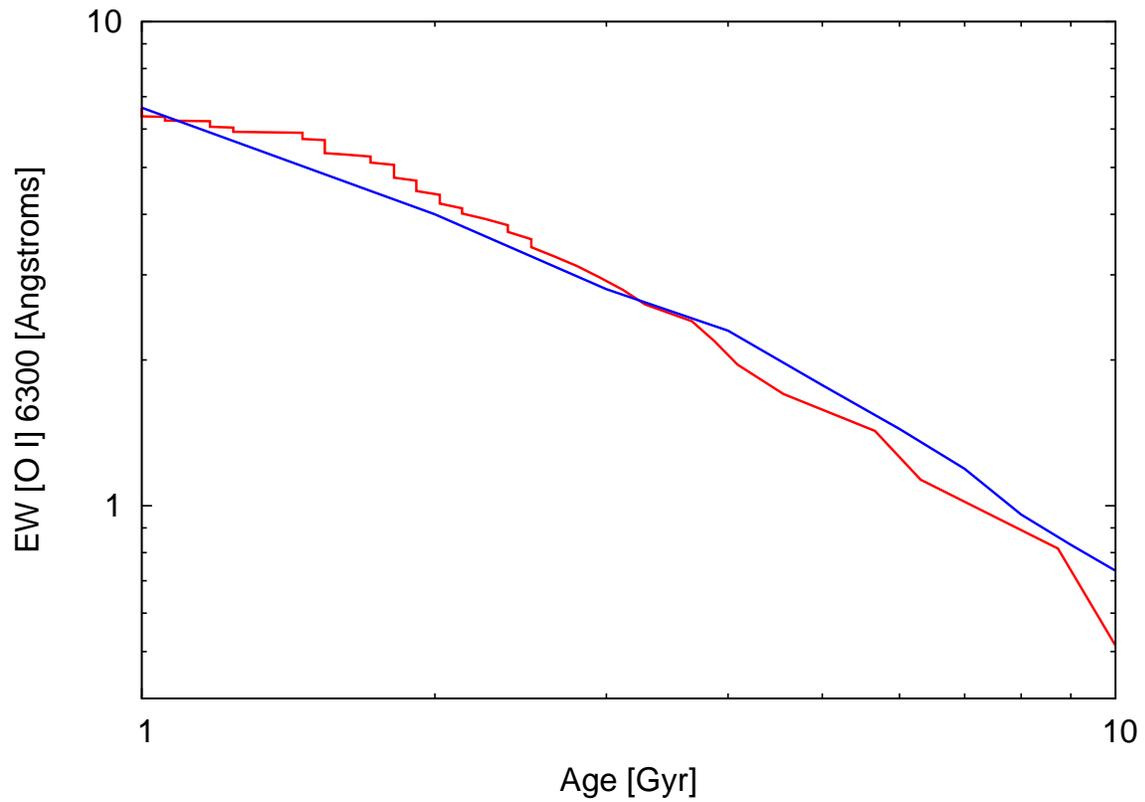
Figure 3.13: Equivalent width of the [O I] 6300Å emission line as a function of time for single-age SSPs (blue), and for composite populations (1Gyr and 10Gyr, in red) as a function of their "measured" age (Johansson et al, in prep).

early-type galaxies which host significant neutral and weakly ionized ISM, forbidden lines of [O I], [N I], and [CII] can be enhanced by up to ~ 50 times in the presence of a significant $(\dot{N}_{\rm Ia}({\rm SD}) \approx \dot{N}_{\rm Ia}({\rm total}))$, very hot $(T_{\rm eff} \gtrsim 5 \cdot 10^5 K)$ population of accreting, nuclear-burning WDs consistent with the SD progenitor scenario. In particular, past and presently ongoing optical spectroscopic surveys should already be able to either detect evidence of the SD channel or constrain its contribution to the SN Ia rate down to a few per cent of the observed total for inferred delay-times $1\ {\rm Gyr} \lesssim {\rm t} \lesssim 4\ {\rm Gyr}$. Future observations with the planned WSO (the World Space Observatory Shustov et al., 2011) should also be capable of making similar progress with observations of the [C II] 1335Å (and He II 1640Å) lines.

The possible contribution of the SD channel at the earliest delay-times ($\lesssim 1$ Gyr) can also be remarkably well-constrained with measurements of the specific (per unit stellar mass) luminosities of the "classical" strong emission lines, such as H_α, [O II] 3727 Å, [N II] 6583Å. For a 500 Myr-old stellar population, the Hα recombination line luminosity is predicted to be enhanced over the SSP-only case by up to $\sim$ two orders of magnitude for SD progenitor temperatures $T \lesssim 2 \cdot 10^5 K$. A similar enhancement is expected for the [O II] 3727Å line luminosity for SD temperatures spanning the $10^5 - 10^6$ K range, suggesting calorimetry of post-starburst galaxies may be able to constrain the SD contribution to less than $\sim 1\%$. Alternatively, observations of emission-line nebulae consistent with ionization by the old SSP alone may be interpreted as a constraint on the total mass accreted in the steady nuclear-burning regime. Assuming a hypothetical SD scenario accounted for all SNe Ia, this would restrict the mass accreted at the $10^5 - 10^6$ K range of photospheric temperatures to $\lesssim 10^{-2} - 10^{-3} M_\odot/{\rm yr}$.

Finally, if the SD scenario did indeed account for a significant fraction of the SN Ia rate, than one might expect the resulting enhancement in the luminosities of emission-lines Hα, [O II] 3727Å, and [C II] 157μm to introduce an age-dependent offset in their calibration as indicators of the SFR in galaxies. At the same time, one would expect nuclear-burning WDs to provide a vital ingredient in calculating the ionization budget in low-ionization emission line regions, necessitating a careful understanding of the evolution of accreting WD populations.

Acknowledgements

Bibliography

Anders E., Grevesse N., 1989, Geochimica et Cosmochimica Acta, 53, 197

Annibali, F., Bressan, A., Rampazzo, R., Zeilinger, W. W., & Danese, L. 2007, A&A, 463, 455

Annibali, F., Bressan, A., Rampazzo, R., et al. 2010, A&A, 519, A40

Athey, A. E., & Bregman, J. N. 2009, ApJ, 696, 681

Binette, L., Magris, C. G., Stasińska, G., & Bruzual, A. G. 1994, A&A, 292, 13

Brown T. M., Smith E., Ferguson H. C., Sweigart A. V., Kimble R. A., Bowers C. W., 2008, The Astrophysical Journal, 682, 319

Bruzual, G., & Charlot, S. 2003, MNRAS, 344, 1000

Cid Fernandes R., Stasińska G., Mateus A., Vale Asari N., 2011, Monthly Notices of the Royal Astronomical Society, 413, 1687

Dalgarno, A., & McCray, R. A. 1972, ARA&A, 10, 375

Di Stefano, R. 2010, ApJ, 712, 728

Eracleous, M., Hwang, J. A., & Flohic, H. M. L. G. 2010, ApJ, 711, 796

Gallego, J., García-Dabó, C. E., Zamorano, J., Aragón-Salamanca, A., & Rego, M. 2002, ApJ, 570, L1

Gilfanov, M., & Bogdán, Á. 2010, Nature, 463, 924

Groves, B. A., Dopita, M. A., & Sutherland, R. S. 2004, ApJS, 153, 9

Hachisu, I., Kato, M., & Nomoto, K. 1999, ApJ, 522, 487

Johansson, J., Thomas, D., & Maraston, C. 2012, MNRAS, 421, 1908

Kehrig, C., Monreal-Ibero, A., Papaderos, P., et al. 2012, A&A, 540, A11

Kennicutt, R. C., Jr. 1998, ARA&A, 36, 189

Levesque, E. M., & Richardson, M. L. A. 2013, arXiv:1309.0513

de Looze, I., Baes, M., Bendo, G. J., Cortese, L., & Fritz, J. 2011, MNRAS, 416, 2712

Meijerink, R., & Spaans, M. 2005, A&A, 436, 397

Meijerink, R., Spaans, M., & Israel, F. P. 2007, A&A, 461, 793

Osterbrock, D. E., & Ferland, G. J. 2006, Astrophysics of gaseous nebulae and active galactic nuclei, 2nd. ed. by D.E. Osterbrock and G.J. Ferland. Sausalito, CA: University Science Books, 2006,

Papaderos, P., Gomes, J. M., Vílchez, J. M., et al. 2013, A&A, 555, L1

Rappaport, S., Chiang, E., Kallman, T., & Malina, R. 1994, ApJ, 431, 237

Rauch T., 2003, Astronomy and Astrophysics, 403, 709

Rauch, T., & Werner, K. 2010, Astronomische Nachrichten, 331, 146

Sarzi, M., Falcón-Barroso, J., Davies, R. L., et al. 2006, Monthly Notices of the Royal Astronomical Society, 366, 1151

Sarzi M., Shields J. C., Schawinski K. e. a., 2010, Monthly Notices of the Royal Astronomical Society, 402, 2187

Sánchez S. F. et al., 2012, Astronomy and Astrophysics, 538, A8

Serra, P., Oosterloo, T., Morganti, R., et al. 2012, MNRAS, 422, 1835

Shull, J. M., & van Steenberg, M. E. 1985, ApJ, 298, 268

Shustov, B., Sachkov, M., Gómez de Castro, A. I., et al. 2011, Ap&SS, 335, 273

Singh, R., van de Ven, G., Jahnke, K., et al. 2013, A&A, 558, A43

Totani T., Morokuma T., Oda T., Doi M., Yasuda N., 2008, Publications of the Astronomical Society of Japan, 60, 1327

van den Heuvel, E. P. J., Bhattacharya, D., Nomoto, K., & Rappaport, S. A. 1992, A&A, 262, 97

Webbink, R. F. 1984, ApJ, 277, 355

Whelan, J., & Iben, I., Jr. 1973, ApJ, 186, 1007

Woods, T. E., & Gilfanov, M. 2013, MNRAS, 432, 1640

Worthey, G., Faber, S. M., Gonzalez, J. J., & Burstein, D. 1994, ApJS, 94, 687

Yan, R., & Blanton, M. R. 2012, ApJ, 747, 61

Chapter 4

Results from early-type emission-line galaxies in the Sloan Digital Sky Survey

4.1 Abstract

In this chapter, we discuss the author's role in several observational and theoretical works which make use of the diagnostic tools presented in chapters 2 & 3. In particular, we present the results of Johansson et al. (2014), who produce the first detection of the He II 4686Å recombination line in the extended emission-line regions of passively-evolving galaxies (LIERs, recall Chapter 1). We then demonstrate how, using our He II 4686Å/Hβ diagnostic from Woods & Gilfanov (2013), this can constrain the role of any "hot-mode" ($1.2–7\times10^5 K$) single-degenerate channel to $\lesssim$3–10% of the observed SN Ia rate at delay times of $1 \leq t_{\text{gal}}/\text{Gyr} \leq 4$. We then extend this emission-line constraint to T$\approx 10^6$K using our [O I] 6300Å/Hα diagnostic from Woods & Gilfanov (2014), to be submitted to *Monthly Notices of the Royal Astronomical Society* later this year[1]. Finally, using our results from our hybrid population synthesis code (Chen et al., 2014), we demonstrate that our diagnostics (and the observed He II 4686Å emission in passively-evolving galaxies) pose a considerable challenge to the presently accepted model of the evolution of accreting white dwarf binaries (Chen et al., 2015). We conclude by discussing some possible resolutions to this discrepancy, which we will explore in a future work.

---

[1]Note that there will be significant text overlap between the author's contribution to this forthcoming paper and the body of this chapter.

4.2   Introduction

The nature of the ionizing sources powering the emission-line regions observed in early-type galaxies remains uncertain. As discussed in chapter 1, post-AGB stars are the favoured candidate ionizing source population on a variety of grounds (Binette et al., 1994; Stasińska et al., 2008; Sarzi et al., 2010; Yan & Blanton, 2012; Papaderos et al., 2013; Singh et al., 2013), however other ionizing sources should exist as well within the old, evolved stellar population. In particular, accreting, steadily nuclear-burning white dwarfs (white dwarfs) are expected to number in the hundreds to thousands within a typical elliptical galaxy (e.g. Chen et al., 2014). With photospheric temperatures on the order of $\approx$1.5–10$\times 10^5 K$ and spectra well-approximated by blackbodies (in particular, without any sharp cutoff at the H I or He II ionization edges, see chapter 1 and references therein), accreting white dwarfs could in principle constitute an important part of the ionizing background in early-type galaxies. As demonstrated in the previous two chapters, if the single-degenerate channel accounted for the majority of SNe Ia at late ($>$1Gyr) delay-times, accreting nuclear-burning white dwarfs would be the **dominant** source of ionizing radiation in passively-evolving galaxies.

In order to evaluate the true role of accreting white dwarfs in providing the ionizing background in early-type galaxies, we can use the method outlined in the previous chapters to compare any measurement of any sensitive line ratio to our predictions for differing ionizing source population luminosities at varying temperatures. Plugging in the appropriate values into eq. 2.6, we have

$$L_{Ia} = 4.7 \times 10^{31} \left(\frac{\Delta m}{0.3 M_\odot} \right) \left(\frac{t}{1 Gyr} \right)^{-1.11} erg/s/L_{K,\odot} \tag{4.1}$$

where we have used the delay-time distribution of Totani et al. (2008). The stellar mass to K-band light ratio for an old ($t \gtrsim$ 1 Gyr) is of order 1 – a few $M_\odot/L_{K,\odot}$. Given an estimate of the ionizing background supplied by post-AGB stars (L_{pAGB}, from Bruzual & Charlot, 2003), the ratio of L_{Ia} (or indeed, the luminosity of any additional ionizing source population) to L_{pAGB} can then be constrained from our photoionization models above.

From the above considerations, and using the He II and [O I] diagnostics discussed in chapters 2 & 3 (Woods & Gilfanov, 2013, 2014), we can interpret any measurement (or upper limit) on the flux of He II 4686Å and [O I] 6300Å (or their ratios to Hβ and Hα, respectively). Given that these lines (in particular, He II 4686Å) are intrinsically weak (even with the putative enhancement expected in the single-degenerate scenario), we must turn to stacking analysis (as discussed in chapter 2) in order to make a robust detection. This forms the basis of Johansson et al. (2014), whose assumptions and selection criteria we discuss in §4.3, before using their emission-line measurements to constrain the role of any "hot-mode" single-degenerate scenario in §4.4. In §4.5, we then apply our constraint on the luminosity of any heretofore unidentified high-temperature source population to model accreting white dwarf populations, found using a modernized population synthesis code which we have developed (Chen et al., 2014).

4.3 Stacking analysis of passively-evolving early-type galaxies

In order to produce a robust detection of He II 4686Å in passively-evolving galaxies, Johansson et al. (2014) turned to stacking analysis using the largest sample of galaxy spectra available, that of the Sloan Digital Sky Survey (http://www.sdss.org/). In particlar, spectra were compiled from the SDSS-II Data Release 7 (Abazajian et al., 2009). From an initial sample of more than 930,000 galaxies, a number of selection criteria were then applied in order to produce a final sample of exclusively passively-evolving emission-line galaxies. We restricted our attention to galaxies in which both Hα and [N II] 6584Å emission are detected with an amplitude-to-noise ratio A/N > 3. This ensures that we only co-add galaxies with actually detectable emission-line regions. The S/N of all spectra in the SDSS sample decays quickly at distances greater than that corresponding to a redshift of z $\approx$ 0.1. Therefore, we exclude all galaxies at z > 0.1 from our sample. It is also important that we sample emission-line regions beyond the innermost nuclear regions of galaxies, where contamination from a central accreting source is most possible. To do so, we employ a minimum cut at a redshift of z = 0.04; all galaxy spectra are measured using a multi-object spectrograph fed from fibres with a diameter of 3 arc seconds, which at our minimum redshift corresponds to a diameter of $\sim$2.5kpc.

Following the WHAN diagnostic diagram (recall fig. 1.8), we employ a slightly more strict upper bound for the equivalent width of the Hα emission line, requiring an $\mathrm{EW}_{\mathrm{H}\alpha}$ < 2Å. This ensures the exclusion of not only nebulae ionized by low-luminosity AGN, but also emission-line regions powered by strong shocks, which are known to contaminate the spectra of some nearby passively-evolving early-type galaxies (Sarzi, Shields & Schawinski, 2010). For our analysis, it is extremely important that we also exclude any galaxies with significant ongoing star-formation. To this end, we employ the PCA analysis of Wild et al. (2007); Chen et al. (2012), which reproduces galaxy spectra using a set of orthogonal "principal components" which correspond to key diagnostic spectral features. These include the Balmer absorption lines and the 4000Å break, both of which are very sensitive measures of the age of stellar populations, and in particular the presence of young < 1Gyr-old) stars. Using this analysis, we exclude all galaxies for which $\gtrsim$1% of their total stellar mass is inferred to be younger than 1 Gyr. This provides us with a final sample of nearly 12000 passively-evolving emission-line galaxies.

As discussed in Johansson et al. (2014), the effectiveness of our age selection is corroborated with an alternative method, wherein we use the near-UV colours measured by the (now-defunct) Galaxy Evolution Explorer (GALEX) in order to search for and remove from our sample any galaxy with significant recent star formation. As demonstrated in Kaviraj et al. (2007), galaxies which have undergone star formation in the previous billion years are readily identified by their near-UV colour, with NUV-r < 5.5. This provides a smaller final sample of galaxies ($\approx$4000), but with largely consistent results for the measured emission-line fluxes (see discussion in Johansson et al., 2014). We therefore quote only those values recovered from the PCA-analysis-selected sample in our further discussion.

From our final sample, we can make a further classification based on the (luminosity-weighted) mean ages of the stellar populations. To measure this, we employ the standard Lick indices of (Worthey et al., 1994). With this, we find a broad distribution in (mean) ages which peaks at $\approx$5Gyrs (see Johansson et al., 2014, their figure 3). We then subdivide our sample into four bins of approximately equal S/N, with our youngest age bin (with 2740 galaxies) having ages in the range $1\mathrm{Gyr} < t_{\mathrm{gal}} < 4\mathrm{Gyr}$ (with a mean age of $\approx$3Gyrs). The results of Totani et al. (2008) and many others (Maoz et al., 2014) demonstrate clearly that the SN Ia supernova rate appears to evolve as the inverse of the age of the stellar population ($\dot{N}_{\mathrm{Ia}} \propto t^{-1.1}$, recall discussion in chapter 1). Therefore it is in this youngest age bin where the expected SN Ia rate is highest, and where we can make our strongest constraint. For this reason, we focus on the results for our youngest age bin in the rest of this chapter (for analysis of all of our stacking results, please refer to Johansson et al., 2014, 2015).

In order to identify and measure the total flux in our stacked spectra, we use the spectral fitting and analysis code GANDALF (Sarzi et al., 2006). Fitting the stacked spectrum of our youngest mean-stellar-age bin in the spectral range $3700\text{Å} - 6800\text{Å}^2$ we find the ratio He II $4686\text{Å}/\mathrm{H}\beta = 0.06 \pm 0.02$, and the ratio [O I] $6300\text{Å}/\mathrm{H}\alpha = 0.125 \pm 0.007$. We will use these measurements to constrain the role of any additional, heretofore unrecognized component of the ionizing background (such as accreting, nuclear-burning white dwarfs) in the following section.

4.4 Constraints on a hot-mode single degenerate scenario at late delay-times

In order to place constraints on any population of single-degenerate progenitors, we may then use the estimate given in eq. 4.1 of their luminosity, together with some reasonable assumption for their temperatures, in order to compare their combined spectra with that of pAGB stars. As discussed above, we can then compare predictions for optical emission line ratios with and without the inclusion of accreting white dwarfs to the ionizing background.

To do so, we use the detailed photoionization code MAPPINGS III (e.g. Groves et al., 2004), together with the procedure outlined in chapters 2 & 3. In brief, we model the ionizing emission from the "normally-evolving" stellar population (principally originating from post-AGBs) using the spectral synthesis models of Bruzual & Charlot (2003). We assume a plane parallel geometry with an ionization parameter (as defined in the previous chapters) $\log(U) = -3.5$ (as inferred from the observed O III/$\mathrm{H}\beta$ ratio in our stacked sample, see discussion in Johansson et al., 2014), with a warm ($T \approx 10^4 K$) gas phase density and metallicity of $n \approx 100 \mathrm{cm}^{-3}$ and $Z_{\mathrm{gas}} = Z_{\odot}$ respectively. In modelling the ionizing continuum from combinations of pAGB stars and SN Ia progenitor populations, Woods & Gilfanov

---

[2]Note that this differs from the slightly narrower spectral range ($3800\text{Å} - 6800\text{Å}$) fitted in Johansson et al. (2014). The larger range provides not only a slightly improved fit overall, but also a measurement of the [O II] $3726\text{Å}+3729\text{Å}$ doublet, as outlined in Johansson et al. (2015).

(2014) & Johansson et al. (2014) found that there was a negligible difference between using a single age stellar population (SSP) or a (more realistic) combination of old and young stellar populations with the same luminosity-weighted mean age. Therefore for simplicity we use a 3 Gyr-old SSP in modelling the ionizing continuum for our youngest age bin.

In (Johansson et al., 2014), we demonstrated that the observed He II 4686Å/Hβ ratio in our youngest stack excludes accreting white dwarfs with T $\approx 1.5 - 6 \times 10^5 K$ from contributing significantly to the SN Ia rate. We can extend those calculations to include our upper limits from the [O I] 6300Å/Hα ratio, as well as updating our He II constraint based on our new fit to the stellar continuum (see Johansson et al., 2015, as discussed above). These constraints are presented as a function of photospheric temperature in fig. 4.1. Note that our constraints are given for 90% confidence upper limits on both the He II4686Å/Hβ and [O I] 6300Å/Hα ratios; the observed values of both are consistent with ionization by pAGB stars alone.

As can be seen from fig. 4.1, the observed [O I] 6300Å/Hα ratio provides a stronger or equivalent constraint than the He II 4686Å/Hβ ratio across the entire range in expected temperatures for accreting, nuclear-burning white dwarfs. There are two reasons for this: first, the declining sensitivity of the He II diagnostic at high temperatures (see Woods & Gilfanov, 2013), and second, [O I] 6300Å is an intrinsically stronger line than He II 4686Å, as is Hα stronger than Hβ. Therefore the [O I] 6300Å/Hα diagnostic is built on two more robustly detected lines.

For both diagnostics, we have expressed our upper limit as a constraint on the total bolometric luminosity (per unit stellar mass) in excess of that provided by pAGB stars, as a function of the photospheric temperature of the sources. Note that the upper limit at each temperature is to the exclusion of an additional excess at any other temperature. To convert this upper limit on the luminosity to an average accreted mass per white dwarf, we may rearrange eq. 4.1 together with the stellar mass to K-band light ratio for a 3 Gyr-old stellar population from Bruzual & Charlot (2003) to find:

$$\Delta m_{ul}|_{3Gyr} = 0.005 \left(\frac{L_{Ia}/M_*}{10^{30} \text{erg/s/M}_\odot} \right) M_\odot \qquad (4.2)$$

From inspection of fig. 4.1, one sees that if all SN Ia are produced through some evolutionary channel consistent with the single-degenerate scenario, such a channel may only accrete $\approx 0.005 M_\odot$ in any "hot-mode." It is clear our constraint rules out any conventional accreting, nuclear-burning white dwarfs as the progenitors of SNe Ia in old stellar populations, unless they account for only a fraction of the total. As a conservative estimate, we may set $\Delta m_{Ia} = 0.3 M_\odot$ (recall our discussion of the maximum carbon-oxygen white dwarf mass in chapter 2). In this case, our upper limits constrain the contribution of the accreting, nuclear-burning white dwarfs to the total observed SN Ia rate to less than 10% (see fig. 4.1).
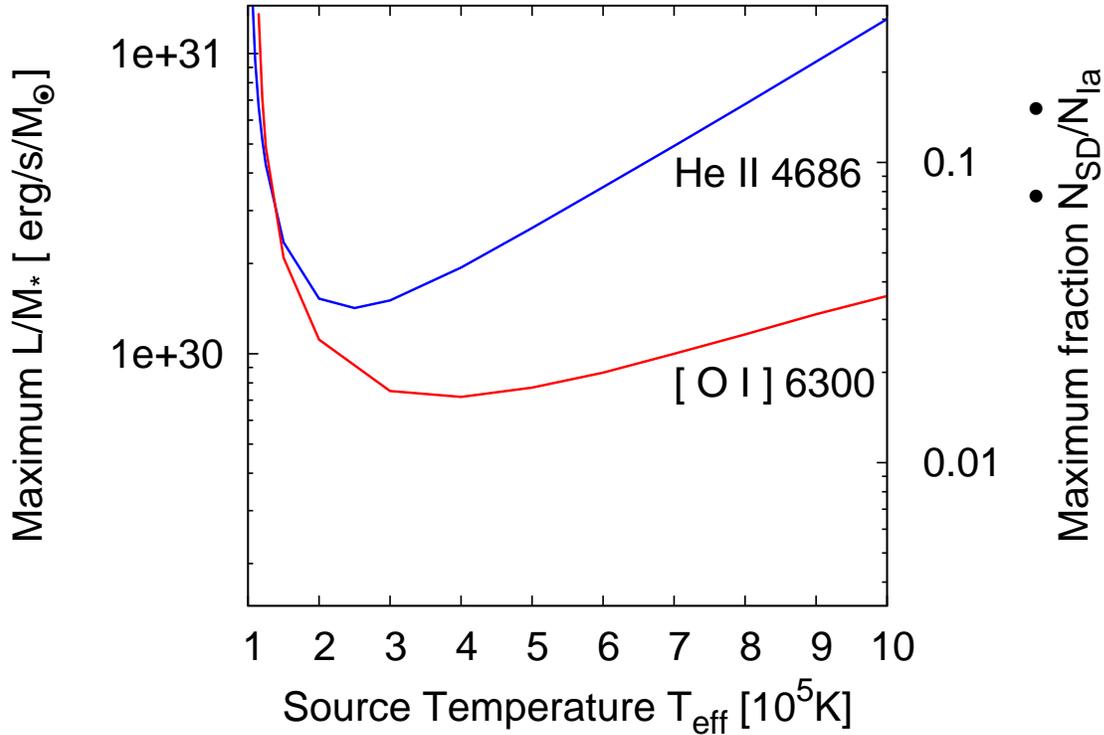
Figure 4.1: Upper limits (90% confidence) on the specific ionizing luminosity (left y-axis) and the (corresponding) possible contribution of accreting white dwarfs to the SN Ia rate (right y-axis) as a function of the photospheric temperature. Red denotes our upper limit using the [O I]/Hα diagnostic (Woods & Gilfanov, 2014), while blue gives the upper limit from He II 4686/Hβ (Woods & Gilfanov, 2013). For the contribution to the SN Ia rate, we assume a "minimal" average accreted mass per SN Ia of $\Delta M = 0.3 M_\odot$ (see text). Note that for each temperature, the upper limit is given excluding any emission at any other temperature, save for that from the ambient stellar population.

4.5   Confronting results from population synthesis

Our ionizing luminosity constraints are not only applicable to SN Ia progenitors. Recently, population synthesis studies have predicted a steep evolution with time for accreting white dwarfs regardless of the SN Ia rate (Chen et al., 2014), and for low-mass X-ray binaries (Fragos et al., 2013). In both cases, accreting compact objects are then expected to provide a strong contribution to the ionizing background in early-type galaxies of relatively young luminosity-weighted mean stellar age. With this in mind, we have updated and modernized a commonly-implemented population synthesis code in order to produce model accreting white dwarf populations. This has primarily been the work of a student at the Max Planck Institute for Astrophysics, Hai-Liang Chen, whom I have co-supervised since January, 2013.

In brief, the population synthesis method implemented in Chen et al. (2014) uses the now-standard binary population code BSE (Hurley, Pols & Tout, 2000; Hurley, Tout & Pols, 2002) in order to rapidly generate a population of white dwarf binaries in which the companion reaches the onset of Roche-lobe overflow (RLOF). The use of BSE is then terminated at this point, and the initial conditions for mass-transferring binaries are fed to the detailed binary stellar evolution code MESA (Paxton et al., 2013). This allows us to drastically improve the treatment of mass transfer, particular when driven by the thermal response of the donor star. Previous codes (including BSE, see Toonen et al., 2014, for a recent review and comparison of other popular codes) have used only simple prescriptions to treat mass transfer in interacting binaries, and assumed thermal equilibrium for the donor star throughout (even when the mass transfer is driven by the thermal disequilibrium of the donor!). This is shown to have a significant impact on the temporal evolution of accreting white dwarf binary populations (Chen et al., 2014). Assuming blackbody spectra, we can then compute the spectral evolution of an accreting white dwarf population as a whole as a function of time, as well as for useful spectral intervals (such as the soft X-ray band or the total ionizing flux).

If shown to be in conflict with our upper limits, these predictions would pose a strong challenge to our present understanding of binary stellar evolution (Chen et al., 2015). Therefore we turn now to a comparison of the expected ionizing background from a model accreting white dwarf population with our constraints presented above. The spectral synthesis output of Chen et al. (2014) and Chen et al. (2015) can be used as input for our MAPPINGS III calculations in much the same way as the calculations of Bruzual & Charlot (2003) for post-AGB stars, and the two combined to produce a possible ionizing background. This in turn can be used to produce predictions for diagnostic lines as done in chapters 2 & 3, including the He II 4686Å/Hβ ratio, which we can compare directly with our stacked spectra of observed passively-evolving galaxies discussed above.

Shown in fig.4.2 is a comparison of the He II 4686Å/Hβ ratio for differing input spectra in our MAPPINGS III calculations. In green, we have plotted the predicted He II 4686Å/Hβ ratio in the case of ionization by the single-stellar population alone (e.g. primarily the ionizing continuum supplied by post-AGB stars). Plotted in blue is the same ratio with the inclusion of our model accreting white dwarf population from Chen et al. (2014). We see that, while in this case we predict a considerably lower He II 4686Å/Hβ than in the
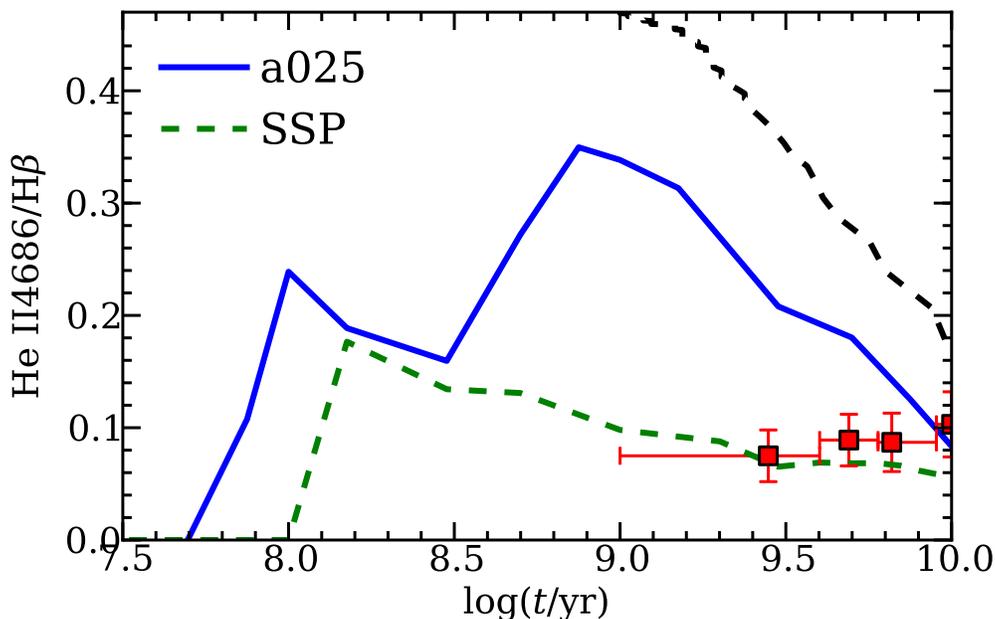
Figure 4.2: Comparison between the predicted values of He II $\lambda 4686/\mathrm{H}\beta$ in our starburst models and that which is observed in (stacks of) early-type galaxies, as a function of stellar age. The blue solid line shows the predicted values of He II $\lambda 4686/\mathrm{H}\beta$ for the combined populations of post-AGB stars and accreting white dwarfs (a025) and the green dashed line is for the single stellar population from (Bruzual & Charlot, 2003). The black dashed line shows the predicted values of He II $\lambda 4686/\mathrm{H}\beta$ for the model combining SNe Ia progenitors in SD-scenario and post-AGB stars (similar to the model in chapter 2). In the calculation of the emission of SNe Ia progenitors, we assumed the initial white dwarf mass $1.1 M_\odot$, white dwarf effective temperature $T_{\mathrm{eff}} = 2 \times 10^5 \mathrm{K}$ and the delay time distribution given by Totani et al. (2008). The observed values (red squares) are data from Johansson et al. (2014). Note that for these points the vertical bars denote the error in the observed value, but the horizontal bars simply indicate the width of each age bin. From Chen et al. (2015).

single-degenerate scenario (shown in black for the same sample calculation as in chapter 2), there is still considerable tension with the observed value, which not only falls far below that predicted with the inclusion of our model white dwarf population (at early delay-times) but also shows little-to-no evolution with time (after ≈ 1 Gyr). This is in stark contrast with our model predictions, which evolve roughly in parallel with that expected for single-degenerate progenitors (i.e. inversely with time).

What is the origin of this discrepancy? Having based our method on the BSE code, our underlying assumptions are consistent with the majority of modern population synthesis calculations. The use of MESA in treating RLOF shifts (somewhat) the time at which the accreting white dwarf population peaks, but does not considerably change the total luminosity or temporal evolution ($\propto t^{-1}$) of the number of accreting white dwarfs after $\approx$ 1 Gyr. As mentioned above, similar results have been found for low-mass X-ray binaries (Fragos et al., 2013), and are also found to be in tension with observations.

One sensible place to look for a solution is the treatment of common envelope evolution. This is understood to be highly uncertain (Ivanova et al., 2013), and would affect the formation rate of both accreting white dwarf and low-mass X-ray binary populations. Indeed, the conditions necessary for the onset of a common envelope are already understood to be poorly characterized by the standard prescription (Hjellming & Webbink, 1987). In fact, it is likely somewhat more difficult for many binaries to enter a common envelope phase than previously thought, with red giant donors much more stable against run-away mass loss than suggested by the conventional treatment (Woods& Ivanova, 2011). If fewer red giant donors undergoing RLOF enter a common envelope phase, the alternative is stable mass transfer, which would likely expand rather than significantly contract the orbital separation. This would scatter many binaries to a much wider orbit, potentially greatly reducing the number of X-ray binaries (especially at early delay-times) by rendering RLOF on the main sequence impossible for a greater number of systems. After identifying the discrepancy discussed here in Chen et al. (2015), we will explore this and other possible explanations in detail in a forthcoming paper.

4.6 Conclusions

In this chapter, we have reviewed the first, highly successful investigations to make use of the diagnostics we have developed in chapters 2 & 3. Stacking nearly 12000 spectra of galaxies from the SDSS sample, Johansson et al. (2014) made the first detection of He II 4686Å emission in passively-evolving stellar populations with extended low-ionized emission-line regions (LIERs). Using the measured ratio of He II 4686Å/Hβ in the youngest age bin in this sample ($1 \leq t_{\mathrm{gal}}/\mathrm{Gyr} \leq 4$, with a mean age of $\approx 3\mathrm{Gyr}$), we found that this constrains the role of any "hot mode" (≈ 1.5–$6 \times 10^5 \mathrm{K}$) single-degenerate progenitor channel to no more than 10% of the total observed SN Ia rate ($\lesssim 3\%$ for T $\approx 2 \times 10^5 \mathrm{K}$). Using the measured ratio of [O I] 6300Å/Hα (both considerably stronger, more robustly detected lines in our sample), we can extend this constraint to $\lesssim 3\%$ for T $\gtrsim 1.5 \times 10^5 \mathrm{K}$ (Johansson et al., 2015). Conversely, if the single-degenerate channel does indeed account for the observed

SN Ia rate, no more than $\approx 0.005 M_\odot$ may be accreted in any "hot mode" consistent with steady nuclear-burning at the surface of white dwarfs (as it is presently understood).

This upper limit may also be interpreted as a generic constraint on the luminosity of **any** additional, previously unaccounted-for high-temperature source population. With this in mind, we have produced model populations of accreting white dwarfs (Chen et al., 2014), using a modified population synthesis code which incorporates MESA to treat RLOF with white dwarf accretors. We find that, using the standard assumptions employed in the population synthesis code BSE to compute our model populations, we predict an accreting white dwarf population which conflicts significantly with our observed constraints on the ionizing continuum in aging, non-star-forming stellar populations. In particular, with the addition of our combined accreting white dwarf spectra, we find that the ionizing background is much too hard at relatively early delay-times (≈ 1 Gyr), evolving with the age of the stellar population as $\propto t^{-1}$. Conversely, our observations lie almost perfectly in line with the hardness of the ionizing continuum predicted from ionization by post-AGB stars alone (using the spectral templates of Bruzual & Charlot, 2003), as measured by the observed ratio of He II 4686Å/Hβ. We suggest that, given the similar discrepancy observed for low-mass X-ray binaries (Fragos et al., 2013), the origin of the problem may be in some prescription common to both predictions. The most immediately apparent candidate may be the treatment of common envelope evolution, which is critically important in modelling both populations, and also understood to be highly uncertain (Ivanova et al., 2013). We reserve a full consideration of this problem for a future paper.

Bibliography

Abazajian, K. N., Adelman-McCarthy, J. K., Agüeros, M. A., et al. 2009, ApJS, 182, 543

Binette, L., Magris, C. G., Stasińska, G., & Bruzual, A. G. 1994, A&A, 292, 13

Bruzual, G., & Charlot, S. 2003, MNRAS, 344, 1000

Chen, H.-L., Woods, T. E., Yungelson, L. R., Gilfanov, M., & Han, Z. 2014, MNRAS, 445, 1912

Chen, Y.-M., Kauffmann, G., Tremonti, C. A., et al. 2012, MNRAS, 421, 314

Chen, H.-L., Woods, T. E., Yungelson, L. R., Gilfanov, M., & Han, Z. 2015, *submitted to MNRAS*

Fragos, T., Lehmer, B., Tremmel, M., et al. 2013, ApJ, 764, 41

Gilfanov, M., & Bogdán, Á. 2010, Nature, 463, 924

Groves, B. A., Dopita, M. A., & Sutherland, R. S. 2004, ApJS, 153, 9

Hjellming, M. S., & Webbink, R. F. 1987, ApJ, 318, 794

Hurley J. R., Pols O. R., Tout C. A., 2000, MNRAS, 315, 543

Hurley J. R., Tout C. A., Pols O. R., 2002, MNRAS, 329, 897

Ivanova, N., Justham, S., Chen, X., et al. 2013, A&A Rev., 21, 59

Johansson, J., Woods, T. E., Gilfanov, M., et al. 2014, MNRAS, 442, 1079

Johansson, J., Woods, T. E., Gilfanov, M., et al. 2015, in prep.

Kaviraj, S., Schawinski, K., Devriendt, J. E. G., et al. 2007, ApJS, 173, 619

Papaderos, P., Gomes, J. M., Vílchez, J. M., et al. 2013, A&A, 555, L1

Paxton B. et al., 2013, ApJS, 208, 4

Rauch, T., & Werner, K. 2010, Astronomische Nachrichten, 331, 146

Sarzi, M., Falcón-Barroso, J., Davies, R. L., et al. 2006, MNRAS, 366, 1151

Sarzi, M., Shields, J. C., Schawinski, K., et al. 2010, MNRAS, 402, 2187

Singh, R., van de Ven, G., Jahnke, K., et al. 2013, A&A, 558, A43

Stasińska, G., Vale Asari, N., Cid Fernandes, R., et al. 2008, MNRAS, 391, L29

Toonen, S., Claeys, J. S. W., Mennekens, N., & Ruiter, A. J. 2014, A&A, 562, AA14

Totani, T., Morokuma, T., Oda, T., Doi, M., & Yasuda, N. 2008, PASJ, 60, 1327

Umeda, H., Nomoto, K., Yamaoka, H., & Wanajo, S. 1999, ApJ, 513, 861

Wild, V., Kauffmann, G., Heckman, T., et al. 2007, MNRAS, 381, 543

Woods, T. E., & Ivanova, N. 2011, ApJ, 739, LL48

Woods, T. E., & Gilfanov, M. 2013, MNRAS, 432, 1640

Woods, T. E., & Gilfanov, M. 2014, MNRAS, 439, 2351

Worthey, G., Faber, S. M., Gonzalez, J. J., & Burstein, D. 1994, ApJS, 94, 687

Yan, R., & Blanton, M. R. 2012, ApJ, 747, 61

Chapter 5

Why haven't we observed nebulae surrounding supersoft X-ray sources?

5.1   Abstract

Accreting, steadily nuclear-burning white dwarfs are associated with so-called supersoft X-ray sources (SSSs), observed to have temperatures of a few$\times 10^5$K and luminosities on the order 10^{38}erg/s. Such objects are expected to be capable of ionizing their surrounding interstellar medium; however, to date only one such nebula was detected in the Large Magellanic Cloud (for $\approx$10 known Magellanic sources), surrounding Cal 83. This has led to the conclusion that accreting white dwarfs cannot have been both luminous ($\gtrsim 10^{37}$erg/s) and hot ($\gtrsim$ few $\times 10^4$K) for the majority of their past accretion history, unless the density of the ISM surrounding most sources is much less than that inferred for the Cal 83 nebula (4–10cm^{-3}). Here we demonstrate that the latter is far more likely. In particular, past efforts to detect such nebulae have not accounted for the low density of the warm-neutral/warm-ionized & hot ISM in which the majority of these sources must be embedded. Cal 83 appears to lie in a region of ISM which is at least ten-fold overdense. We provide a revised model for the "typical" SSS nebula, and outline the requirements of a survey of the Magellanic clouds which could detect the majority of such objects. We then briefly discuss some of the possible implications, should there prove to be a large population of previously undiscovered ionizing sources. Sufficiently deep searches for nebular emission in the vicinity of SSSs may also serve as a new probe of the conditions in the warm-ionized medium of nearby galaxies.

5.2   Introduction

Supersoft X-ray sources (SSSs) comprise a unique and varied class of objects, first identified more than two decades ago by the Einstein observatory (HEAO-2). Close binary SSSs are characterized by significant emission in the 0.3–0.7 keV spectral band resembling the Wien tail of a blackbody, with $T_{\mathrm{eff}} \approx 2$–$10 \cdot 10^5 K$ and estimated $L_{\mathrm{bol}} \sim 10^{37-38}$ erg/s (Greiner, 2000). In the classic picture (van den Heuvel et al., 1992), these sources are white dwarfs (WDs) accreting hydrogen-rich matter from a main sequence or red giant companion, with steady nuclear burning of the accreted hydrogen at the WD's surface. This steady nuclear burning is only possible for mass transfer rates within a narrow range ($1 - \mathrm{few} \cdot 10^{-7} M_\odot/\mathrm{yr}$, e.g. Nomoto et al., 2007). For accretion rates less than this, nuclear-burning proceeds only in unsteady bursts, giving rise to novae. The upper bound is approximately given by the accretion rate at which a WD has the same nuclear-burning luminosity as an AGB star with the equivalent core mass. Above this threshold, the observational appearance is extremely uncertain. One possibility is that the photosphere of the WD will once more swell up to the thermal equilibrium radius of a giant (see e.g. Cassisi et al., 1998). However, dynamical processes, such as an optically-thick wind driven from within the photosphere, may modulate mass transfer before this can happen, with photospheric temperatures in the range 1–$2 \cdot 10^5 K$ (Hachisu, Kato & Nomoto, 1999) for $\dot{M} \lesssim 3 \times 10^{-6} \mathrm{M}_\odot/\mathrm{yr}$.

Apart from simply understanding their phenomenology, SSSs have come under particular scrutiny as candidates for the progenitors of thermonuclear (type Ia) supernovae (SNe Ia). In the so-called single degenerate channel (Whelan & Iben, 1973), a carbon-oxygen WD accretes hydrogen-rich material as described above until reaching the Chandrasekhar mass ($M_{\mathrm{Ch}} \approx 1.38 \mathrm{M}_\odot$), triggering a thermonuclear runaway (although both lower and higher explosion masses may be possible, see Maoz et al., 2014).

A considerable body of evidence has accumulated in the past several years demonstrating that such sources cannot be the progenitors of SNe Ia, or, should the SD scenario still hold, that accreting WD progenitors cannot manifest themselves as SSSs for the majority of their accretion phase (Gilfanov & Bogdán, 2010; Di Stefano, 2010). Such arguments were predicated on the notion that steadily nuclear-burning sources with radii typical of massive WDs should emit strongly in the soft X-ray band ($T_{\mathrm{eff}} \approx 5 \times 10^5$–$10^6 \mathrm{K}$), producing detectable emission where the intervening column density is low (e.g. along many lines of sight in the Magellanic Clouds, M31, and nearby early-type galaxies).

However, for lower WD masses ($M \lesssim 1 \mathrm{M}_\odot$, Wolf et al., 2013), or in case of considerable inflation of the photosphere above that expected from the WD mass – radius relation (Panei et al., 2000), the temperature may fall below $\sim 5 \times 10^5 \mathrm{K}$. This would shift the majority of the nuclear-burning luminosity to the extreme-UV, where it could not be directly detected. However, such objects should remain very strong sources of ionizing radiation (Rappaport et al., 1994), with no cut-off at the H I or He II ionization edges (Rauch & Werner, 2010). One can then demonstrate that, in the single degenerate scenario, accreting nuclear-burning WDs must produce an enormous combined ionizing luminosity, easily sufficient to dominate the ionizing background in many early-type galaxies (Woods & Gilfanov, 2013, 2014). Given that many early-type galaxies possess extended emission-line regions powered by the

continuum from their old stellar populations, we should then be able to detect emission lines characteristic of ionization by high-temperature sources, such as He II 4686Å and [O I] 6300Å. Following on this, Johansson et al. (2014) produced carefully-selected stacks of early-type galaxies with emission-lines in the SDSS, and found a He II 4686Å/Hβ ratio ($\approx$8%) consistent with $\lesssim 10\%$ contribution from any high-temperature (≈ 1.2–6×10^5K) sources for galaxies with luminosity-weighted mean stellar ages in the range 1Gyr < t < 4Gyr. Similar constraints from the [O I] 6300Å line extend this limit up to T $\approx 10^6$K SD progenitors (Johansson et al., in prep.). Note that at these high temperatures (exceeding $\sim 5 \times 10^6 K$), the contribution of accreting WDs is also very tightly constrained in soft X-rays ($\lesssim$1% Gilfanov & Bogdán, 2010).

In order to remain consistent with the observational constraints discussed above, the average mass accreted per WD in any "hot mode" (T$\gtrsim 1.5 \times 10^5$K) by SD progenitors is limited to 10^{-2}–10^{-3}M$_\odot$. However, accreting WDs **may** remain viable as the progenitors of at least some SNe Ia if they accrete principally at lower temperatures. Indeed, known SSSs are understood to undergo considerable variability, with many interchanging between optical-low/X-ray-on **(hot)** and optical-high/X-ray-off **(cold)** states. Searches for nebulae surrounding SSSs in the Magellanic clouds have detected only one, Cal 83 (Remillard et al., 1995), which itself has proven difficult to model (Gruyters et al., 2012). This implies that either the density of the ISM surrounding other SSSs is much less than that in the vicinity of Cal 83 (n ~ 4 – 10cm^{-3}, Remillard et al., 1995), or that these sources do not radiate at high temperatures for the majority of their accretion history, in keeping with the possibility that accreting, nuclear-burning WDs may still be a strong candidate for the progenitors of SNe Ia.

Here, we briefly review the physics of ionized nebulae surrounding high-temperature and variable sources in §5.3, before discussing the apparent absence of SSS nebulae in the Magellanic clouds in §5.4. We revisit the upper limits placed by Remillard et al. (1995), which do not constrain the temperature/luminosity of SSSs in low-density media (n$_{\mathrm{ISM}} \sim 0.1$ – 1cm^{-3}). We demonstrate however that such densities are typical of the warm-neutral/warm-ionized ISM, in which most SSSs are expected to be located. We then outline the requirements for a survey which can provide a more complete census of SSS nebulae in the Magellanic clouds in §5.5, and place this in the context of the only observed SSS nebula, as well as two candidate nebulae in M33. Before closing, we briefly discuss the plausibility and implications of a large, heretofore undiscovered ionizing source population for stellar feedback and the evolution of the ISM in §5.6.

5.3   Strömgren regions surrounding accreting WDs

5.3.1   The classical picture

The notion of emission-line nebulae ionized by SSSs was first explored by Rappaport et al. (1994). They identified several tell-tale signatures which would allow for the identification of such objects, namely pronounced [O III] 5007Å, [O I] 6300Å, and He II 4686Å emission,
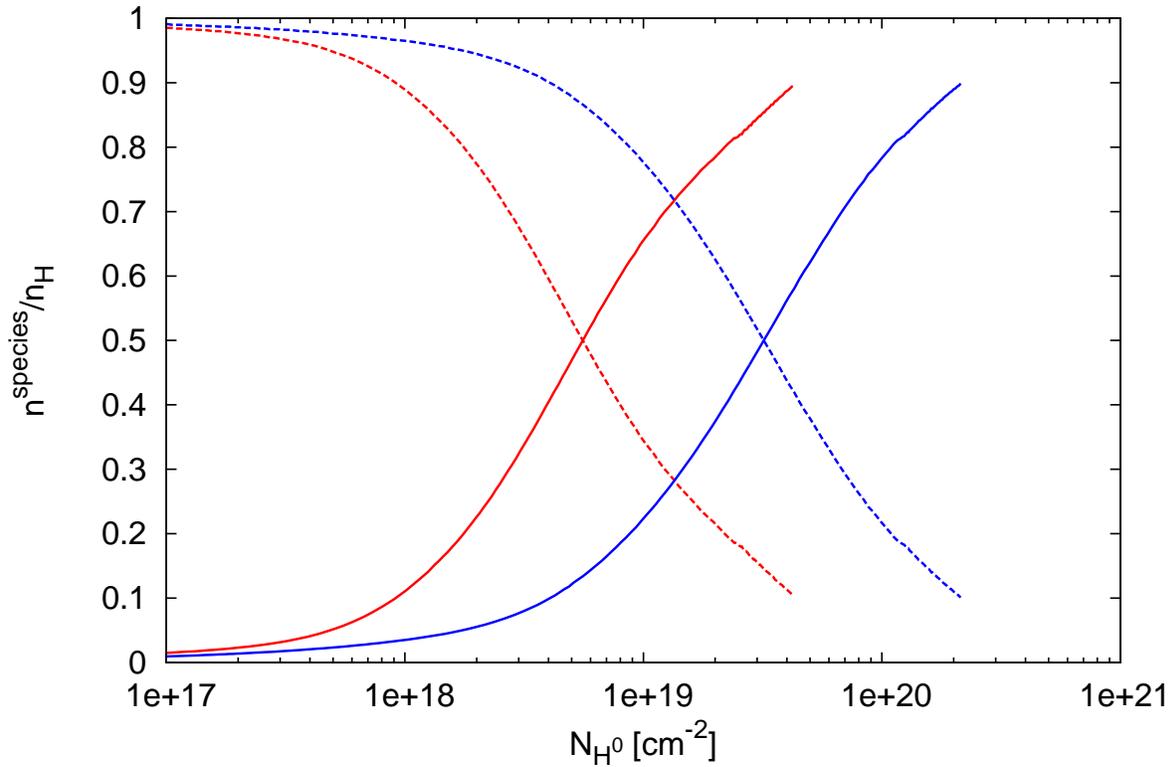
Figure 5.1: Ionized (dotted line) and neutral (solid line) fractions of the total hydrogen density, as a function of the total column density in neutral hydrogen (integrated outward from the central source). Blue and red lines denote constant ISM densities of 0.1 and 1 cm^{-3} respectively. In both cases, we assume ionization by a central blackbody source with temperature 5×10^5K and bolometric luminosity $10^{37.5}$erg/s. Note that we terminate our calculations when the temperature of the gas falls below 3000K.

similar to the most luminous planetary nebulae (PNe). However, contrary to PNe, these would be very extended objects, with typical Strömgren radii:

$$R_S \approx 35\text{pc} \left(\frac{\dot{N}_{ph}}{10^{48}\text{s}^{-1}} \right)^{\frac{1}{3}} \left(\frac{n_{ISM}}{1\text{cm}^{-3}} \right)^{-\frac{2}{3}} \tag{5.1}$$

where $\dot{N}_{ph}$ is the ionizing photon luminosity of the source, and n_{ISM} is the density of the surrounding ISM. In practice, nebulae ionized by high-temperature sources extend to somewhat larger radii than even this, as high energy photons penetrate deeper into the neutral ISM, yielding a broad interface at the Strömgren boundary (see e.g. Woods & Gilfanov, 2014, also fig. 5.1). Such nebulae may be resolved even by ground-based telescopes out to distances of a few Mpc.

Emission-line surveys represent an attractive alternative to searching for SSSs directly for a variety of reasons (Rappaport et al., 1994; Di Stefano et al., 1995). While soft-band ($\approx$ 0.3–0.7keV) X-ray sources may be completely obscured by relatively modest column densities ($\gtrsim$ few$\times 10^{21}$cm^{-2}), optical emission-line nebulae typically suffer only slight reddening. The most [O III] 5007Å- and He II 4686Å-luminous nebulae should also be those ionized by relatively low-temperature WDs ($\approx$1–5$\times 10^5$K), probing the SSS population in the temperature regime least sensitive to soft X-ray observations (Di Stefano et al., 1995).

Furthermore, if the progenitors of some SNe Ia do undergo a SSS phase, any nebula ionized by the accreting WD will remain for

$$\tau_{\mathrm{rec}} = 1/(\alpha_{\mathrm{B}} \mathrm{n}_{\mathrm{ISM}}) \approx 10^5 \left(\frac{\mathrm{n}_{\mathrm{ISM}}}{1\mathrm{cm}^{-3}} \right)^{-1} \text{years} \qquad (5.2)$$

after the end of this phase, potentially providing a test of the progenitors of young, nearby SN Ia remnants. Outside of the shell shocked by the supernova itself, such a "fossil nebula" (first discussed for O stars in Bisnovatyi-Kogan & Syunyaev, 1970) would remain largely unperturbed by the light of the supernova, as neither the initial shock breakout nor radiation due to ^{56}Ni decay will appreciably ionize the surrounding ISM (see discussion in Cumming et al., 1996), and the UV tail of SNe Ia spectra suffer from considerable line-blanketing, with little flux below $\approx$1000Å (for a comparison of NLTE atmospheres with observed spectra of supernovae, see e.g. Pauldrach et al., 1996).

5.3.2   Modeling simple SSS nebulae

In order to understand the observability of SSS nebulae, we must make an estimate of their typical surface brightnesses, which will depend not only on their time-averaged temperatures and luminosities, but also on the density of their surrounding ISM. In the following, we model nebulae ionized by high-temperature, luminous SSSs using the photoionization code Cloudy (v13.03, Ferland et al., 2013). For simplicity and ease of comparison with the results of Rappaport et al. (1994), we assume isochoric (constant density) ISM, solar gas phase abundances, and blackbody ionizing spectra throughout. The latter is well-justified, at least near the H I and He II ionization edges, by comparison with detailed NLTE calculations of SSS spectra (e.g. Rauch & Werner, 2010). At the outer boundary of our nebular models, we terminate our calculations when the gas temperature falls below 3000K (seen as the abrupt cutoff at an ionization fraction of $\approx$10% in fig. 5.1). This is easily sufficient to compute the total luminosity reprocessed in the most important diagnostic lines (particularly [O III] 5007Å, see fig. 5.2), and allows us to avoid making any assumption about the incident cosmic ray spectrum (which would become important in this part of the nebula).

This allows us to compute the volume emissivity $\epsilon(r)$ (assuming spherical symmetry) in any emission line as a function of radius, which we may then use to find the surface brightness in line i:
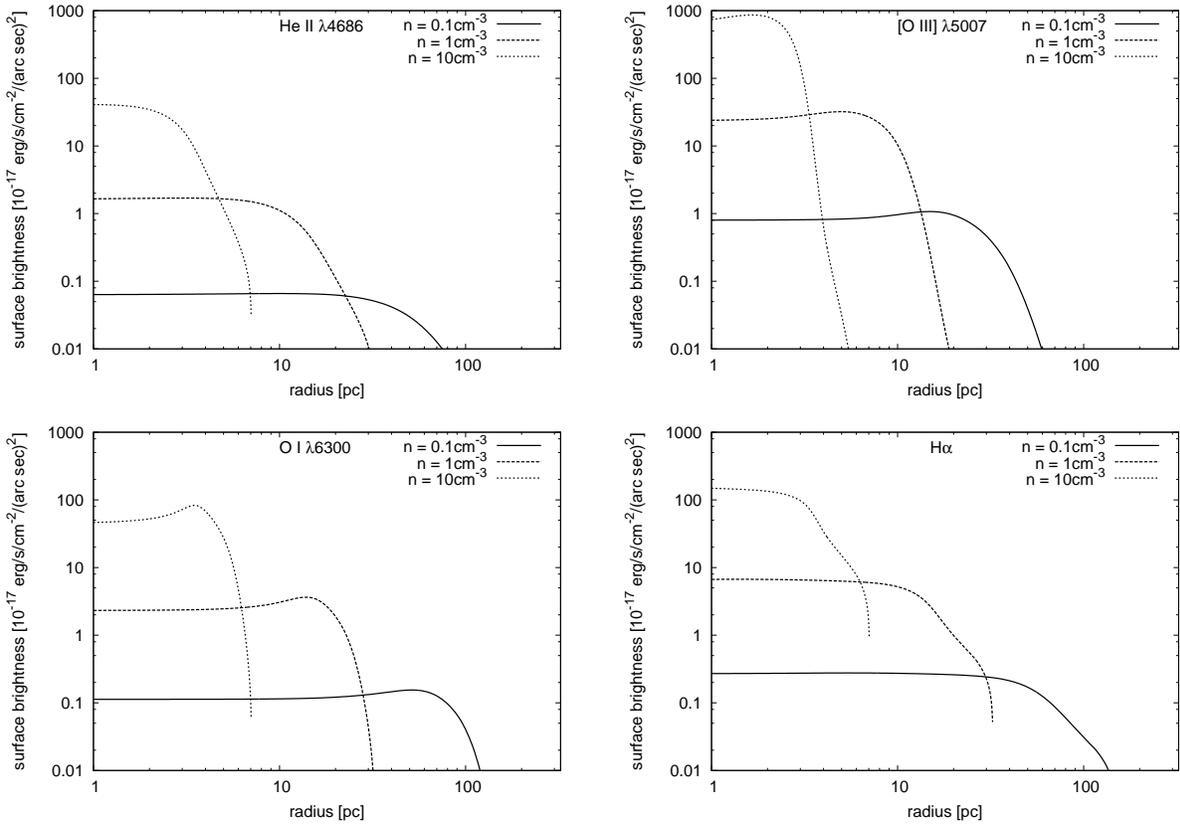
Figure 5.2: Surface brightness profiles for four optical emission lines assuming ionization by a central blackbody source in the LMC with temperature 5×10^5K and bolometric luminosity $10^{37.5}$erg/s. In each panel, the surface brightness is shown for a given emission line for differing constant ISM densities (0.1, 1, and 10 cm^{-3}).

Label	Name	L_{bol} 10^{37} erg/s	T_{eff} eV	N_H^X 10^{21}cm^{-2}	N_H^{MW} 10^{21}cm^{-2}	$N_H^{MC,tot}$ 10^{21}cm^{-2}	n_0 cm^{-3}
(1)	(2)	(3)	(4)	(5)	(6)	(7)	(8)
LMC							
A	RXJ0439.8-6809	10-14	20-30	$0.25 - 0.4$	0.45	0.28	0.22
B	RXJ0513.9-6951	0.1-6	30-40	$0.4 - 0.9$	0.84	0.70	0.55
C	RXJ0527.8-6954	1-10	18-45	$0.7 - 1.0$	0.62	0.78	0.61
D	RXJ0550.0-7151	-	25-40	2.0	0.89	1.04	0.81
E	CAL 83	<2	39-60	$0.7 - 0.95$	0.65	2.02	1.57
F	CAL 87	6-20	50-84	$0.7 - 2.1$	0.75	2.90	2.26
SMC							
G	1E 0035.4-7230	0.5–4	$30 - 50$	0.2-0.8	0.65	0.30	-
H	RXJ0058.6-7146	-	15-70	0.3-1.5	0.75	3.14	-

Table 5.1: Known SSSs in the Magellanic Clouds. Column 1 identifies each source with the corresponding label/location in fig. 5.3. Cols. 2 – 6 give the source name and measured values as tabulated by Greiner (2000): col 3 gives the estimate of the bolometric luminosity, col 4 the best-fit temperature, col 5 the H I column density from fitting the X-ray spectra, and col. 6 the galactic column density in the direction of the source. Note that no luminosities are given for those sources reported as being poorly fit or constantly declining in the Greiner catalog. Col. 7 provides the total H I column density associated with the MCs, as measured by integrating all H I 21cm emission (from McClure-Griffiths et al., 2009; Kalberla et al., 2010) with velocities >100 km/s along the line of sight of each source. Column 8 gives the inferred density in the midplane, assuming the H I in col 7 is distributed in an isothermal disk as discussed in the text. No value for n_0 is given for the two SMC sources, as the SMC is not a disk galaxy.

$$\mathrm{SB_i(r)} = \int_l \frac{\epsilon_i(\mathrm{r})}{4\pi} \mathrm{dl} \qquad (5.3)$$

where we have integrated along the line of sight l.

Shown in figure 5.2 are the surface brightness profiles in four lines (He II 4686Å, [O III] 5007Å, [O I] 6300Å, and Hα) for a nebula ionized by a SSS in the LMC as a function of radius, for varying ISM densities (0.1, 1, and 10cm^{-3}) and fixed source temperature and luminosity (5×10^5K and $10^{37.5}$erg/s). The most prominent signature is easily that of the [O III] 5007Å line (fig 5.2, top right), as expected (Rappaport et al., 1994).

5.3.3 Towards a more realistic model

Past efforts to search for nebulae surrounding SSSs have found only one, that of Cal 83 (Pakull & Motch, 1989; Remillard et al., 1995; Gruyters et al., 2012). The inferred density for the inner region of this nebula is $\approx$ 4–10cm^{-3}. For the 9 other Magellanic SSSs then known, Remillard et al. (1995) report an upper limit of $\lesssim 10^{34.6}$erg/s on the [O III] 5007Å luminosity for any associated nebula. Note however, that this upper limit was obtained specifically for an aperture with radius 7.5 pc, see the following section. In the context of the simple model presented above, this suggests that either the ambient gas density is much lower in the vicinity of most sources, or that perhaps most "SSSs" spend the majority of their accretion histories at much lower effective temperatures, implying some failure of our understanding of the radial response of WD photospheres to accretion. Indeed, many SSSs are observed to be variable to differing degrees (Greiner, 2000). In this case, the detection of surrounding emission lines may trace the time-averaged behaviour of the source, revealing the past accretion history (Chiang & Rappaport, 1996). Such variability is likely to explain in part the difficulty in fitting the Cal 83 nebula with any single-temperature model (Gruyters et al., 2012).

However, the simple picture presented above does not make mention of the density structure of the warm-neutral/warm-ionized ISM in star-forming galaxies. Furthermore, the photoionization calculations of Rappaport et al. (1994) and Remillard et al. (1995) make the standard assumption of an initially neutral medium. This is reasonable for classical H II regions powered by O stars, well-shielded as they are from any ambient radiation field by the dense clouds in which they are born. However, since SSSs are a much older population (with ages likely peaking around 1Gyr, e.g. Chen et al., 2014), there is no reason to assume they should typically be associated with dense H I clouds, but are rather immersed in the diffuse intercloud medium. A detailed treatment of the resulting nebulae requires modeling the 3D distribution of interstellar matter and ionizing sources, which we reserve for a future study. In the following section, we investigate the structure of the ISM in the Magellanic clouds in order to estimate the typical densities in the vicinity of SSSs, and compare this with the assumption made in Remillard et al. (1995).

5.4   SSS nebulae in the Magellanic clouds

5.4.1   A qualitative summary of ISM structure in the Magellanic clouds

Hα (Kennicutt et al., 1995) and H I 21cm maps (McClure-Griffiths et al., 2009; Kalberla et al., 2010, see fig. 5.3) of the Magellanic clouds reveal a complex, multiphase and multiscale ISM. Column densities in the LMC range from $\approx 4.5 \times 10^{21} \text{cm}^{-2}$ near the centre to $\approx 10^{20} \text{cm}^{-2}$ in the outer extremities (Brüns et al., 2005). The distribution of the neutral ISM with scale height above the disk may be estimated from the velocity dispersion of H I, which Kim et al. (1999) give as $\sigma \approx 7.3$ km/s. Assuming an isothermal disk for the LMC, they then find a scale height of $z_0 \approx 0.18$ kpc. From this, we can make an estimate of the *mean* density of the neutral ISM along any line of sight l from the relation:

$$\text{N}_{\text{HI}} = \int_{-\infty}^{\infty} \text{n}(l)\text{dl} = \frac{2}{\cos(\text{i})} \int_{0}^{\infty} \text{n}_0 \text{sech}^2 \left(\frac{\text{z}}{\text{z}_0} \right) \text{dz} \qquad (5.4)$$

where the factor $\cos(i)$ accounts for the fact that the disk is not face-on (the LMC is in fact inclined at $i \approx 30°$, e.g. Nikolaev et al., 2004). From the column densities typical of the LMC, we find a range in peak densities (i.e. in the midplane, n_0) of $\sim 0.1\text{–}4\text{cm}^{-3}$.

In practice, this provides only a crude picture of the interstellar medium in the Magellanic clouds, and in star-forming galaxies in general, for several reasons. First, the LMC disk appears to be flared at large radii, due to tidal interaction with the Milky Way (van der Marel, 2006). Second, we have assumed a smooth distribution, when in fact neutral gas in the Magellanic clouds displays a complex, fragmentary structure (e.g. Stanimirovic et al., 1999), with a significant fraction of H I being concentrated in dense cold clumps or filaments with a correspondingly low volume filling fraction (<5% in the Milky Way, Dickey & Lockman, 1990). The space between these filaments and clouds is filled with warm-ionized/warm-neutral ISM, with densities of order ~ 0.1 cm^{-3}, and hot supernova-heated ISM, with densities of order ~ 0.01 cm^{-3} (Cox, 2005). The rarefied hot interstellar medium occupies a significant fraction of the volume of the disk ($\approx$50% in the Milky Way, e.g. Cox, 2005), with warm-neutral/warm-ionized ISM occupying much of the remainder. From H I 21-cm emission alone, it is at best difficult to distinguish the contributions from warm and cold neutral gas. However, cold H I has been estimated to account for roughly 1/3 of the total H I mass in the LMC (Dickey et al., 1994), with much of this concentrated in the central region of the LMC associated with 30 Doradus.

5.4.2   Probability of the occurrence of a detectable SSS nebula – qualitative consideration

The much lower densities in the bulk of the volume discussed above provide a natural explanation for the difficulty in observing nebulae around most SSSs. Even for nebular densities of the order of the midplane densities ($\sim 0.1 - 4$ cm^{-3}), a typical accreting,
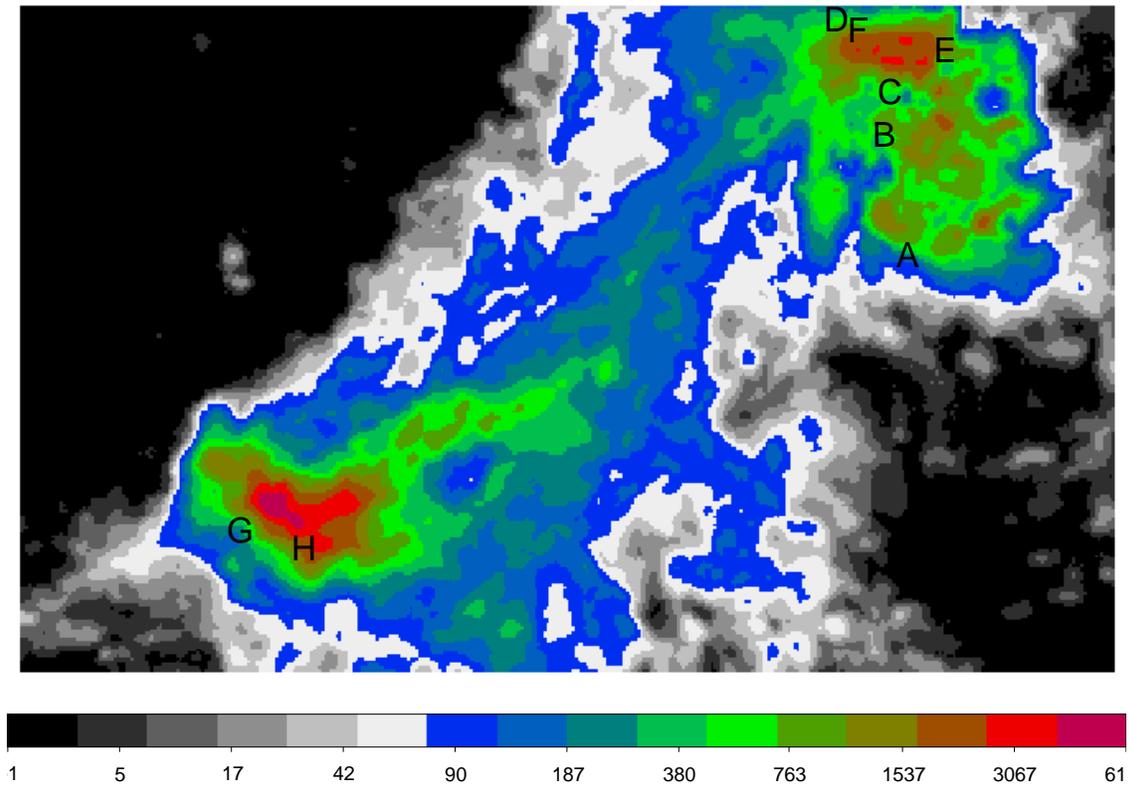
Figure 5.3: H I 21cm map of the Magellanic System (McClure-Griffiths et al., 2009; Kalberla et al., 2010). Units are in $K\frac{km}{s}$. In the optically thin case (valid for almost the entirety of the Magellanic Clouds) this gives the total column density with the simple scaling $1.82\times10^{18}cm^{-2}(K)^{-1}(km/s)^{-1}$. Labels denote locations of known SSSs, excluding PNe and symbiotics; letters correspond to sources in table 5.3.2.

nuclear-burning WD would have a Strömgren radius of $\approx$13pc–150pc ($\approx 50'' - 580''$ at the distance of the LMC), and correspondingly very low surface brightness (fig. 5.2). SSSs embedded in hot ISM would produce no nebulae at all in their immediate vicinity.

Remillard et al. (1995) do not detect [O III] 5007Å nebular emission surrounding any of the Magellanic SSSs other than Cal 83. Their quoted upper limit on the luminosity in this line of $10^{34.6}$erg/s is given for an aperture radius of 7.5 pc, corresponding to a limiting surface brightness at the distance to the LMC of $\approx 3 \times 10^{-17}$erg/s/cm^2/arcsec^2. However, as can be seen from fig. 5.2, this is not sufficient to exclude any nebula in the low-density ISM which must be typical of $\gtrsim$95% of the LMC's volume. This is further illustrated in fig. 5.4, where we plot the [O III] 5007Å luminosity enclosed in an aperture with a radius of 7.5 pc as a function of ISM density, computed using our Cloudy models as above for a "typical" SSS (T $= 5 \times 10^5$K) with differing luminosities (L$_{bol}$ between $10^{36.5}$ and 10^{38} erg/s). For comparison, we plot the upper limit given by Remillard et al. (1995). As one can see from the plot, for the spherically symmetric case, SSS bolometric luminosities L$_{bol} \lesssim 10^{37.5}$erg/s remain consistent with Remillard et al. (1995) upper limits for n$_{ISM} \lesssim 0.4$ cm^{-3}.

Furthermore, scale height of the intermediate and old stellar populations (as traced by the radial velocity dispersions of carbon stars and old variable stars, respectively, van der Marel, 2006) are larger than that of the neutral ISM (and roughly consistent with the warm ionized medium). If the peak delay-time for the production of SSSs is ~ 1 Gyr (Chen et al., 2014), then many are likely to lie off of the midplane, in the lowest density neutral and ionized interstellar medium. Given the very large Strömgren radii implied such densities, a considerable fraction of ionizing photons originating from SSSs may then escape the galaxy entirely. Estimates of the surface brightness, and the corresponding constraint on the [O III] 5007Å luminosity of known sources would then change accordingly.

The nebula associated with the SSS Cal 83, which has an inferred nebular density of $\approx$4–10cm^{-3} (Remillard et al., 1995; Gruyters et al., 2012), is overdense compared with that expected in the bulk ($\gtrsim 90\%$) of the volume of the LMC. Given that the total mass ionized by the central source is estimated at roughly 150M$_\odot$ (Remillard et al., 1995), this cannot simply be the result of an outflow from the inner binary. The natural conclusion, as discussed above, is that the unusually compact nebula surrounding Cal 83 may be the product of a chance encounter with a dense cloud or filament of cold neutral medium (hereafter CNM). This raises the question of how likely such an encounter would be. Estimates for the volume filling fraction of the CNM vary from $\approx$1–5% in spiral galaxies like the Milky Way (Dickey & Lockman, 1990; Cox, 2005). For six known SSSs in the LMC, simple application of the binomial distribution would then suggest a probability of $\approx$6–23% that precisely one SSS lies inside a cold neutral cloud ($\approx$ 97–99% for $\leq$1 SSS lying within the CNM), assuming SSSs and the CNM are distributed equally throughout the LMC.
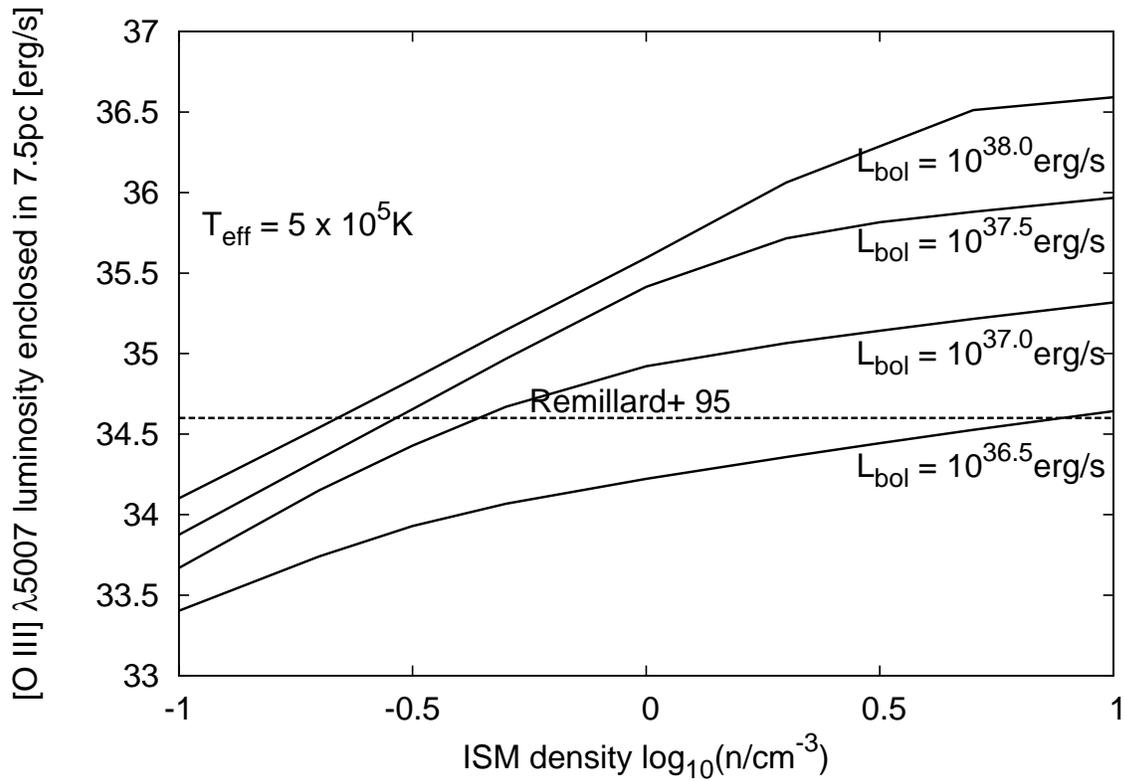
Figure 5.4: Total [O III] 5007Å luminosity enclosed within a 7.5pc radius as a function of (constant) surrounding ISM density. Different curves correspond to nebulae ionized by 5×10^5K blackbody sources with differing source luminosities. For comparison, the upper limit given by Remillard et al. (1995) is indicated by the dashed line.

5.4.3   A quantitative estimate of the proximity of cold neutral clouds

The analysis presented above only considers the likelihood that a SSS may lie *inside* a cold cloud. This does not account for the presence of dense ($n_{CNM} \sim 30\text{–}50 \mathrm{cm}^{-3}$) cold clumps of H I which may typically lie sufficiently *near* to SSSs so as to be ionized and produce an associated nebula. If the number density of small cold clouds is sufficiently high, then many SSSs may be near enough to high-density regions to produce a detectable nebula, rendering the above argument inaccurate. In practice, what we require then is the distribution of distances to the nearest cloud surface for a SSS located at any arbitrary position within the volume of a galaxy. In the following, we will derive this employing a probabilistic argument with a number of simplifying assumptions; a more realistic treatment will require a detailed simulation of the multiphase ISM populated with SSSs, which we leave for a future study. In particular, we will treat all CNM clouds as spherical condensations in line with the two-phase model of Field et al. (1969). In practice, the observed H I gas in the Magellanic clouds (and in our Galaxy) is now known to consist of many filaments, shells, and sheet-like structures, as well as clouds (Cox, 2005; Kim et al., 2007); however, this heuristic approach will allow us to make a first approximation.

We begin by considering the distribution of H I cloud sizes in the Magellanic system. Summing the total area of any contiguous H I structure connected in RA, DEC, and velocity in the LMC, and identifying the square root of this area as the appropriate length scale, Kim et al. (2007) find a distribution of H I cloud sizes which follows a roughly power-law distribution:

$$dN = Cl^{-\gamma}dl, \qquad\qquad 2.2 < \gamma < 3.0 \qquad\qquad (5.5)$$

from kpc scales down to the minimum resolution of their survey ($\approx 15 \mathrm{pc}$), and with larger values of γ for lower flux-limits. Similar results are found for the SMC (Stanimirovic et al., 1999), and observations in our own Galaxy as well as theoretical models of the formation and destruction of cold H I clouds suggest this distribution extends down to subparsec sizes (McKee & Ostriker, 1977; Dickey & Lockman, 1990, and references therein). In order to solve for the coefficient C, we assume spherical clouds and integrate over the volume of all spheres (for some reasonable choice of maximum and minimum cloud radii), and normalize this to the volume filling fraction of the CNM (per pc^3):

$$C = \frac{3(4-\gamma)}{4\pi} \frac{f_{\mathrm{fill}}}{l_{\mathrm{max}}^{4-\gamma} - l_{\mathrm{min}}^{4-\gamma}} \qquad\qquad (5.6)$$

As discussed above, H I 21cm surveys alone cannot distinguish between the warm and cold phases of the neutral ISM, therefore both are included in the distribution given in eq. 5.5. However, both in our Galaxy and the Magellanic clouds, the total mass in H I clouds is found to vary with their size as $\sim l^2$ (albeit with considerable scatter, Dickey & Lockman, 1990; Kim et al., 2007), suggesting that the characteristic gas density in clouds of size l should scale roughly as $\sim l^{-1}$. Observations in the solar neighbourhood suggest clouds

of size $\sim$0.5pc have densities $\approx 30 - 50\mathrm{cm}^{-3}$, therefore one may infer an upper bound of l$\approx$50pc (and typical corresponding densities $\approx 0.3 - 0.5\mathrm{cm}^{-3}$) for the transition from CNM to warm-neutral medium length scales. We set the lower bound for cloud radii at 0.4pc, the theoretical lower limit on the size of small clouds found by McKee & Ostriker (1977). Note however that very small ($\sim$10–100 AU) clouds have also been detected in the Milky Way along many sightlines, which may comprise up to 15% of the total H I column density in our galaxy (Frail et al., 1994). However, these structures are thought to be physically unrelated to the "standard" CNM, arising instead from shocks surrounding individual low-mass stars and other local phenomena (Stanimirovic et al., 1999).

We can normalize eq. 5.5 to the total number in order to obtain a probability distribution:

$$p_l(l) = (\gamma - 1)\frac{l^{-\gamma}}{l_{\max}^{1-\gamma} - l_{\min}^{1-\gamma}} \tag{5.7}$$

We would then like to find the distribution of distances from an arbitrary point to the nearest cloud surface. At first glance, this can be straightforwardly computed via convolution of eq. 5.7 with the distribution of distances to the nearest cloud centre:

$$p_D(D) = \int_{l_{\min}}^{l_{\max}} p_r(D + l)p_l(l)\theta(D + l)dl \tag{5.8}$$

with $D = r - l$ the distance to the nearest cloud surface and p_r being the standard inter-particle spacing distribution $p_r(r) = 4\pi r^2 n_{\mathrm{clouds}}e^{-\frac{4\pi}{3}n_{\mathrm{clouds}}r^3}$ (Chandrasekhar, 1943). However, this simple treatment is only accurate in the limit $f_{\mathrm{fill}} \to 0$, as it does not account for the overlapping of spheres (see e.g. Snyder, 1998, for a discussion of the analogous problem in the study of concrete porosity). In practice, it fails for values of the volume filling factor as small as a $\sim$few per cent[1]. For example, at $f_{\mathrm{fill}}= 0.05$, integration of eq. 5.8 gives a cumulative probability for D$<$0 (i.e. of a random point lying within a cloud) of only $\approx$1%, although the correct value is obviously equal to $f_{\mathrm{fill}}= 5\%$.

In order to improve on this, one must modify equation 5.5 in order to enforce the separation of clouds. This is a well-studied problem which arises often in materials science and chemistry; a more precise formulation is that of Torquato et al. (1990) (for mono-sized inclusions) and Lu & Torquato (1992) (for polydisperse clouds); its main results are summarized in Appendix A. The correct differential distribution of distances to the nearest cloud surface from Appendix A is plotted in fig. 5.5 for f_{fill}=0.05 and $l_{\min}$ and $l_{\max}$ as above. From eq. C.1, we find a probability of $\approx$86% that a CNM cloud surface lies within 7.5pc of any SSS (and thus within the aperture of Remillard et al., 1995). This is sensible: with a number density of $\approx 4\times10^{-4}$ cloud centres per cubic parsec, a spherical volume with radius 7.5pc should contain $\sim$1 cloud centre. However, from eq. 5.5 above, it is clear that the overwhelming majority of such clouds should be very small ($<$1pc). In order to estimate

---

[1]The reason is that two spheres overlap when the distance between their centres becomes smaller than $r_1 + r_2$. Therefore the effective filling factor in estimating the importance of overlapping is $2^3 \times f_{\mathrm{fill}}$, which equals 0.4 for $f_{\mathrm{fill}} = 0.05$.
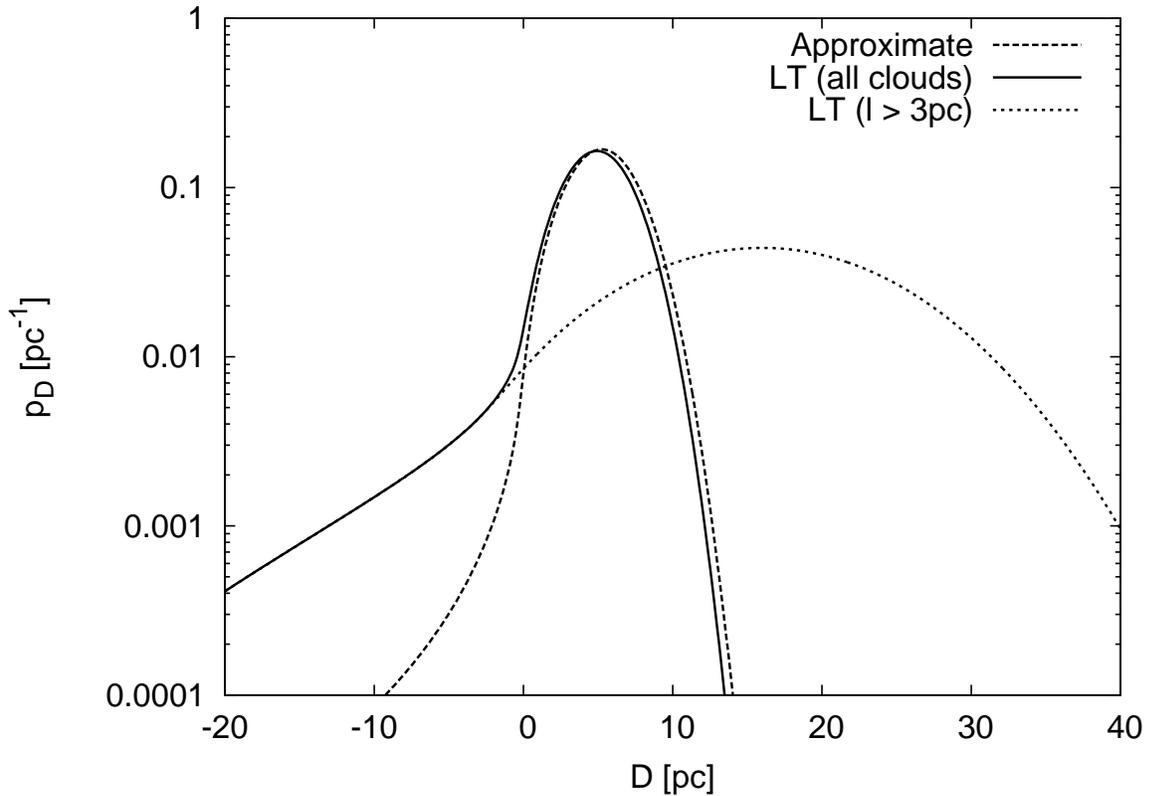
Figure 5.5: Nearest surface probability density distribution (p_D) for CNM clouds in the ISM. The three curves correspond to p_D as estimated from eq. 5.8 (dashed line), and using the "hard spheres" formulation from Lu & Torquato (1992) (solid line). Also shown is the nearest surface probability density distribution for only those CNM clouds with l > 3pc (dotted line). In all cases, we have assumed a *total* volume fraction $f_{\text{fill}} = 0.05$, with $\gamma = 3$, $l_{\text{min}} = 0.4$pc and $l_{\text{max}} = 50$pc.

the likelihood of a nebula such as that detected around Cal 83, we must then ask: what is the likelihood of a SSS being in close proximity to the surface of a cloud which is large enough to encompass a total mass of hydrogen which will be detectable when ionized?

For spherical clouds, the radius required to enclose a given mass for fixed density is simply:

$$l = 0.69\text{pc} \left(\frac{\text{n}}{30\text{cm}^{-3}}\right)^{-\frac{1}{3}} \left(\frac{\text{M}}{\text{M}_\odot}\right)^{\frac{1}{3}} \tag{5.9}$$

The total mass of the nebula surrounding Cal 83 has been estimated at $\approx 150 M_\odot$ (Remillard et al., 1995). A CNM cloud with an initial density of 30cm^{-3} (i.e. typical of the neutral gas, prior to being ionized) would need to be ≈ 3pc in size in order to supply the requisite material. Therefore, in fig. 5.5 we also plot the probability density function for the nearest

cloud surface for clouds with radii >3pc. Once ionized, the expansion timescale of the formerly cold cloud is roughly the length over the sound speed in the ionized cloud, or

$$\tau_{\text{expansion}} = \frac{l}{c_{\text{i}}} \approx 10^6 \left(\frac{l}{10\text{pc}} \right) \left(\frac{c_i}{10 \text{ km/s}} \right)^{-1} \text{years} \tag{5.10}$$

This is comparable to the lifetime of the SSS itself, so it is unsurprising if the observed ionized nebula is not in hydrostatic equilibrium with the surrounding warm ISM (see also Chiang & Rappaport, 1996).

These larger clouds occupy much of the volume (cf. eq, 5.5), therefore the cumulative probability of landing within a cloud (D < 0) with l < 3pc is only slightly reduced (P(D≤0) ≈ 0.0473). The probability of such a CNM cloud lying within 7.5pc is ≈18%. We may then conclude that out of six SSSs, only one having a detectable associated nebula appears entirely consistent with our crude model of the CNM; from the binomial distribution, the likelihood of 1 out of 6 known SSSs lying near a cloud is 40%. Therefore, on the basis of (presently very limited) published observations, one cannot make any statement of the long term time-averaged luminosities and temperatures of known SSSs without detected ionized nebulae.

5.5   Prospects for detecting SSS nebulae

5.5.1   Searching for previously undetected nebulae ionized by SSSs

The question then becomes whether deeper narrow-band observations could detect nebulae in lower density ISM, as well as possibly reveal an accreting, nuclear-burning WD population unseen in soft X-rays (see §5.6). As an initial check, we can estimate the exposure time needed to detect a nebula of constant density n surrounding an ionizing source of some fixed temperature and luminosity. For a line flux F_S which, for a given nebula, is spread over some solid angle with surface brightness I_S, the measured "signal" at a telescope on the Earth's surface (in electrons per second per pixel) is (see e.g. O'Connell, 2003):

$$C_{\text{S}} \approx \left(\frac{D_{\text{aperture}}}{4.86 \times 10^{-6} L} \right)^2 \frac{I_{\text{S}}}{h\nu} \mathcal{G} \langle \text{T} \rangle \text{d}_{\text{pix}}^2 \tag{5.11}$$

for a given telescope with an aperture diameter D_{aperture}, focal length L, physical pixel size d_{pix}, gain $\mathcal{G}$, line energy $h\nu$, and effective filter transmission $\langle T \rangle$. Note that we make the simplifying assumption here of a single effective mean transmission, independent of wavelength, and a single line energy.

In an observation this flux is integrated over an exposure time t and a total number of source pixels $N_{\text{pix,S}}$. The expected S/N of such a measurement may be estimated given some background flux (to be subtracted from the measured flux), as well as the read noise RN and the dark current DN, which characterize contributions to the uncertainty from the CCD detector itself. We adapt the standard formula (see e.g. Howell, 2000):

$$\frac{\mathrm{S}}{\mathrm{N}} = \frac{\sqrt{N_{\mathrm{pix,S}}}C_{\mathrm{S}}t}{\sqrt{C_{\mathrm{S}}t + (1 + \frac{N_{\mathrm{pix,bkg}}}{N_{\mathrm{pix,S}}})(C_{\mathrm{bkg}}\mathcal{G}\langle\mathrm{T}\rangle t + (\mathrm{DN})t + \mathrm{N}_{\mathrm{DIT}}(\mathrm{RN})^2)}} \qquad (5.12)$$

with N_{DIT} the total number of exposures (1 unless otherwise indicated), $N_{\mathrm{pix,bkg}}$ the number of pixels over which the background is measured, and C_{bkg} the background signal assuming some mean surface brightness I_{bkg} (where C_{bkg} is computed from I_{bkg} in a matter analogous to eq. 5.11). For the present estimates, we fix the ratio $\frac{N_{\mathrm{pix,bkg}}}{N_{\mathrm{pix,S}}} = 3$, although this may prove difficult for nebulae with the largest radii. Note that, in order to avoid the inclusion of any faint nebular emission in evaluating the background, it would be best to estimate the background far from the source, although care must be taken in selecting an appropriate region.

For the purposes of evaluating the detectability of SSS nebulae given modern capabilities, we shall assume narrow-band observations carried out with the FORS2[2] instrument of the VLT. We focus on the [O III] 5007Å line, as this is the strongest optical emission line in our calculations. Using the exposure time calculator provided by ESO[3], we find the effective filter transmission (reported combined with the gain) as $\mathcal{G}\langle T\rangle \approx 25\%$ for their "OIII+50" narrow-band filter, with $RN \approx 5\mathrm{e}^-$, and $DN = 6\mathrm{e}^-$ per pixel per hour. In order to estimate the surface brightness of a nebula, we compute the [O III] luminosities and nebular radii for varying SSS luminosities and ISM densities, assuming a photospheric temperature of $\mathrm{T} = 2\times10^5\mathrm{K}$. Note that we take a constant mean surface brightness as representative of the nebular emission, with the outer radius defined by the point at which the gas temperature falls below 3000K (recall §5.3.2). This will somewhat underestimate the surface brightness in the bulk of most nebulae, providing a conservative estimate of their detectability. The characteristic surface brightness of the background flux I_{bkg} is less certain, and is not generally well-approximated by a constant value in a star-forming galaxy. For our theoretical estimates presented here, we assume $I_{\mathrm{bkg}} = 5\times10^{-16}\mathrm{erg/s/cm}^2/\mathrm{arcsec}^2$, which Pellegrini et al. (2012) found to be a representative mean in their Hα images of the Magellanic Clouds. As the optical continua of irregular galaxies are fairly flat (Kennicutt, 1992) we take this as our estimate for the background continuum for all lines of interest discussed in §5.4. We ignore the sky background, as this is generally minimal for optical narrow-band observations. Note that the field of view of the E2V CCD mosaic is $6'.8\times6'.8$; a SSS nebula in a low density region of the ISM may easily encompass much of this. In our estimate of the S/N, we truncate the radius over which the signal is integrated at $3.9'$. Note that, for a real measurement, this may introduce difficulties in finding a suitable region to measure the background.

For a given source luminosity and temperature, we may then ask what surrounding ISM density would be required in order to produce a sufficiently compact nebula, such that it may be detected at a given S/N in a reasonable exposure time. Given that theoretical S/N estimates present only the best case scenario (with all sources of error accounted for),

---

[2]For reference, see the Period 94 manual at http://www.eso.org/sci/facilities/paranal/instruments/fors/doc.html
[3]http://www.eso.org/observing/etc/

here we define a "confident detection" as a measurement with S/N = 50, given a signal integrated over the entire nebula for any combination of parameters. Plotted in fig. 5.6 are the minimum surrounding ISM densities required for an [O III] nebula to be detected around a $T = 2 \times 10^5$K SSS of a given luminosity, for differing exposure times. Also shown for reference is the approximate limiting surface brightness inferred for the [O III] 5007Å and Hα upper limits given in Remillard et al. (1995). Note that the slope is somewhat steeper than may be expected from eq. 5.1 and with a fixed limiting surface brightness. This is because the total luminosity in [O III] 5007Å does not depend exclusively on the bolometric luminosity, but also (weakly) on the ambient ISM density. We see that given modern capabilities (i.e. the 8.2m VLT, as opposed to the 1.5m aperture available to Remillard et al., 1995), one could in a ≈ 1000s exposure detect any SSS nebula with $L_{\rm bol} \gtrsim 10^{37.3}$ erg/s down to ambient ISM densities $n \gtrsim 0.1$cm^{-3}.

5.5.2 Identifying "orphan" high-ionization regions as possible SSS nebulae

As an alternative strategy, one may also investigate known nebulae without identified ionizing sources which appear to have emission-line ratios and line fluxes consistent with ionization by a SSS. Although difficulties remain in modeling the observed optical emission-line ratios in the Cal 83 nebula, the basic properties (He II flux, its ratio to Hβ, and radial extent of the nebula, given the inferred density) appear consistent with ionization by a SSS near its centre. From an intuitive standpoint, and informed by our estimates above, it is unlikely this is the only object of its kind. Indeed, two extended He II nebulae have recently been identified in M33 (Kehrig et al., 2011) which have no observed optical or X-ray counterpart (a Wolf-Rayet star, high-mass X-ray binary, etc.). One of these, HBW 673, appears to have a He II Strömgren radius of ~ 20pc, with He II 4686Å/H$\beta = 0.55$ and a He II 4686Å line luminosity of $\gtrsim 10^{33}$erg/s. This is consistent with ionization by a $\approx 10^{37-37.5}$erg/s source with effective temperature 2–3$\times 10^5$K, embedded in a surrounding ISM with density ≈ 1cm^{-3}. Such a soft source could easily have evaded prior detection (Woods et al, in prep).

The other nebula, BCLMP 651, has a lower He II 4686Å/Hβ ratio of 0.11; if the ionizing source is indeed an accreting, nuclear-burning WD, then the photospheric temperature must either lie below $\approx 1.5 \times 10^5$K or above $\approx 6 \times 10^5$K (Rappaport et al., 1994; Woods & Gilfanov, 2013). The very low value of [O I]6300Å/Hα (≈ 0.01) and non-detection of any X-ray source favour the low-temperature case, however detailed photoionization modeling (and possibly X-ray and optical follow-up) are needed in order to resolve the nature of the sources ionizing both nebulae.

5.6 Implications for the ISM of star-forming galaxies

If there exists a large population of previously unaccounted-for ionizing sources, this may carry important consequences for our understanding of the ISM. In particular, the SD
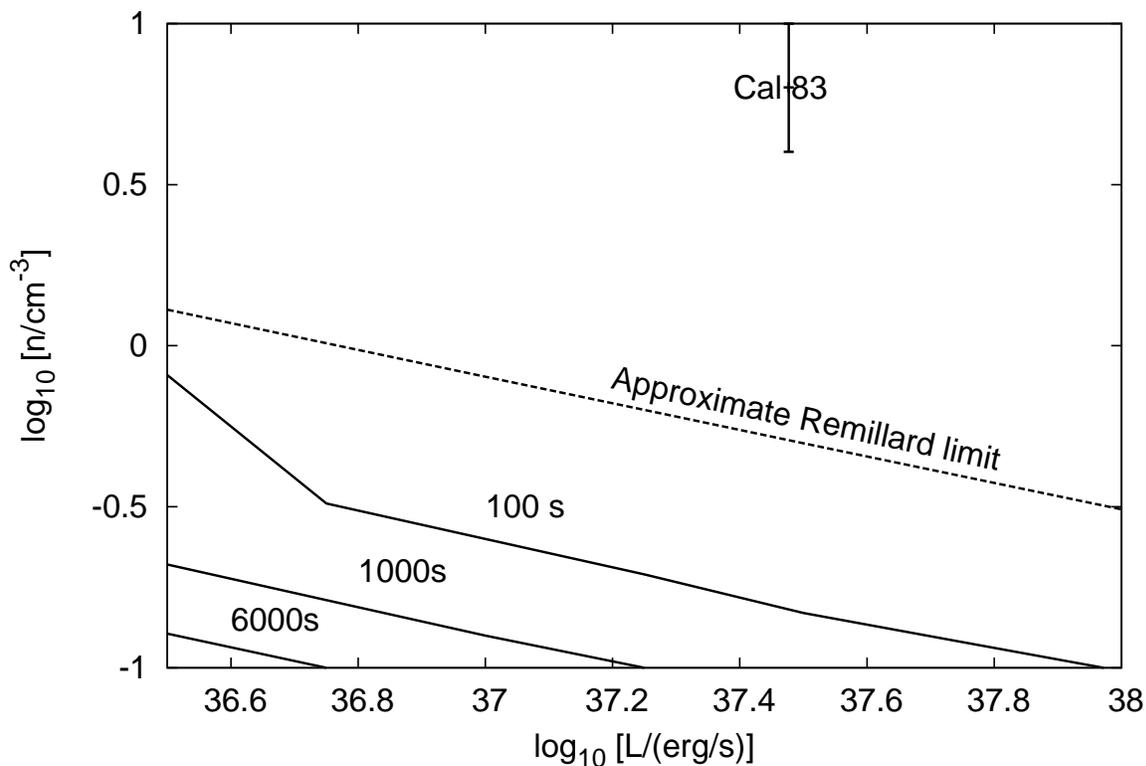
Figure 5.6: ISM density required to produce a detectable nebula ionizing by a 2×10^5K source with bolometric luminosity L. The three curves denote a signal to noise ratio of 50 for 100, 1000, and 6000 seconds total integration times on the VLT FORS2 instrument, respectively. For the latter, we assume the observation is carried out in 6 exposures (cf. eq 5.12). For reference, the inferred density and time-averaged luminosity of Cal 83 is also shown, as is the surface brightness limit inferred for the upper limits on the [O III] 5007Å line luminosity given in Remillard et al. (1995). Note that the "break" in the estimate for the 100s exposure is artificial; this comes about due to a transition from measuring the entire nebula to an aperture limited by the size of the FORS2 field of view (see text for details).

scenario predicts a minimum average total luminosity of the accreting, nuclear-burning WD population (Gilfanov & Bogdán, 2010):

$$L_{Ia} \approx 9 \times 10^{30} \left(\frac{\Delta M}{0.3 M_\odot} \right) \left(\frac{\dot{N}_{Ia}}{10^{-13} M_\odot^{-1} yr^{-1}} \right) \frac{erg}{M_\odot s} \tag{5.13}$$

neglecting those accreting WDs which do not explode as SNe Ia. The SN Ia rate has been measured in the Magellanic clouds from observations of expanding supernova remnants (Maoz & Badenes, 2010), and found to be roughly consistent with (and perhaps higher than) the rate in dwarf irregular galaxies, $\approx 8 \times 10^{-13}$SNe yr^{-1}M$_\odot^{-1}$ (Mannucci et al., 2005). The total stellar mass of the LMC is $\approx 2.7 \times 10^9$M$_\odot$ (van der Marel, 2006). Therefore, if SD progenitors accrete on average 0.3M$_\odot$ per WD at high photospheric temperatures ($\gtrsim 10^5$K), they would produce a total luminosity of 2×10^{41} erg/s. This would principally be in the extreme-UV, with blackbodies in this temperature range (2×10^5K $<$ T $< 10^6$K) producing 3–12$\times 10^9$ ionizing photons per erg. We can make an estimate of the total Hα luminosity this may produce (if no ionizing photons escape), assuming Case B recombination in the low-density limit, with a (typical) gas temperature of 10^4K (Osterbrock & Ferland, 2006). This gives us a predicted Hα luminosity of 1–3$\times 10^{39}$erg/s, roughly 10–30% of the total diffuse Hα luminosity of the LMC (i.e., excluding that immediately associated with resolved H II regions, Kennicutt et al., 1995). This fraction of the total non-H II region Hα emission is comparable to the "truly diffuse" Hα luminosity found by Kennicutt et al. (1995), which is not associated with either filamentary structures, or the diffuse flux within supergiant shells. Therefore, understanding the long-term variability of SSSs may be a question of vital importance to the study of the structure of the ISM in star-forming galaxies.

The few observed SSSs in the LMC have a combined luminosity that is less than 1% of the value suggested by eq. 5.13, even if we (very optimistically) sum only their maximum luminosities. The question arises: is it possible that a large number of accreting, nuclear-burning WDs could remain undetected in the LMC? Shown in fig. 5.7 is an estimate of the minimum bolometric luminosity for accreting nuclear-burning WDs of a given temperature required for it to be detected in soft X-rays, assuming differing column densities consistent with that observed in the MCs. To compute this, we make a simple estimate assuming blackbody spectra and a minimum detectable count rate of 10^{-3} counts per second, consistent with the faintest confidently detected SSSs in Sturm et al. (2013). In order to compute the observed count rate, we made use of the command-line PIMMS tool[4], using the thin filter for the EPIC-PN instrument of XMM-Newton. Also shown are results from the 1D steady-burning WD models of Wolf et al. (2013).

We see from fig. 5.7 that it is clear all high-mass ($\gtrsim 1.1$M$_\odot$) nuclear-burning WDs should now be detected in the MCs, unless during the majority of their accretion phase their photospheric radii deviate greatly from that expected in the 1D models of Wolf et al. (2013). Note that most population synthesis models do not predict a dominant SD channel in the production of SNe Ia (Nelemans et al., 2013; Chen et al., 2014), however, they

---

[4]http://heasarc.gsfc.nasa.gov/docs/software/tools/pimms.html

do predict a number of **low-mass** accreting, nuclear-burning WDs nonetheless. In star-forming galaxies, recent population synthesis calculations indicate the total luminosity of *all* accreting, nuclear-burning WDs could provide a significant source of ionizing radiation, although it is substantially below the estimate given above for the luminosity of a putative SD progenitor population (Chen et al., 2014, 2015). By far the majority of accreting nuclear-burning WDs should lie at lower masses ($0.6M_\odot$–$0.8M_\odot$), most of which should still remain undetected in the MCs (see fig. 5.7). Therefore, there may yet exist a considerable number of such low-mass, steadily nuclear-burning WDs which have not yet been detected.

The above considerations, together with the relatively low ionization state of Helium in the ISM, suggest nuclear-burning WDs likely play a very minor role in the overall ionization balance of diffuse interstellar gas (the "DIG"). However, if the typical ionization parameter (ionizing photons per unit gas density) is relatively low, most high-energy photons may be lost to maintaining the ionization state of Hydrogen (Woods & Gilfanov, 2013). Recall that the scale height of the old and intermediate age stellar populations in the Magellanic clouds is larger than that of the neutral gas. Even if SSSs are not a major component of the diffuse ionizing background in star-forming galaxies, they may play a role in the high [O III]/Hβ ratios seen in the low-density ($n\lesssim0.1\mathrm{cm}^{-3}$) ISM (Haffner et al., 2009). In particular, it appears that some heretofore unknown mechanism is needed to account for the additional heating ($\sim 10^{-26}$ erg/s/cm^{-3}) inferred in the diffuse ISM well above the midplane (Reynolds et al., 1999). Nuclear-burning WDs could naturally account for such a hardening of the ionizing continuum, should their numbers and distribution with scale height prove appropriate. This would require considerable further investigation before any definitive statement can be made. Given the high escape fraction, nuclear-burning WDs may also contribute to the heating balance of the hot coronal gas (S. Cantalupo, private communication). In particular, ionization of He II (an important coolant in the hot ISM) by nuclear-burning WDs may keep the gas sufficiently hot so as to provide an additional component of stellar feedback. The feasibility of such an additional mechanism should be tested by inclusion in theoretical models (such as Cantalupo, 2010; Kannan et al., 2014), coupled with deep observations of the ISM in the MCs (as outlined in §5.5).

5.7 Conclusions

Two decades after the discovery of SSSs, the long-term behaviour of accreting, nuclear-burning WDs remains poorly understood. Past efforts to search for nebulae ionized by these objects detected only one such object, with the implication that either the SSS phase is extremely transient in real accreting WDs, or most SSSs lie in low-density ($n\lesssim 1\mathrm{cm}^{-3}$) media. Here we have demonstrated that the latter is the far more likely case: for the six known SSSs in the LMC, the likelihood that only one source lies sufficiently near to a dense cloud to produce a nebula which could have been previously detectable is $\approx 40\%$ ($\approx70\%$ for ≤1 detectable nebula). We then outlined the prospects for a future survey which may be able to reveal all bright SSSs in the Magellanic clouds. The outcome of such a study carries important consequences regardless of the outcome. If no enhancement
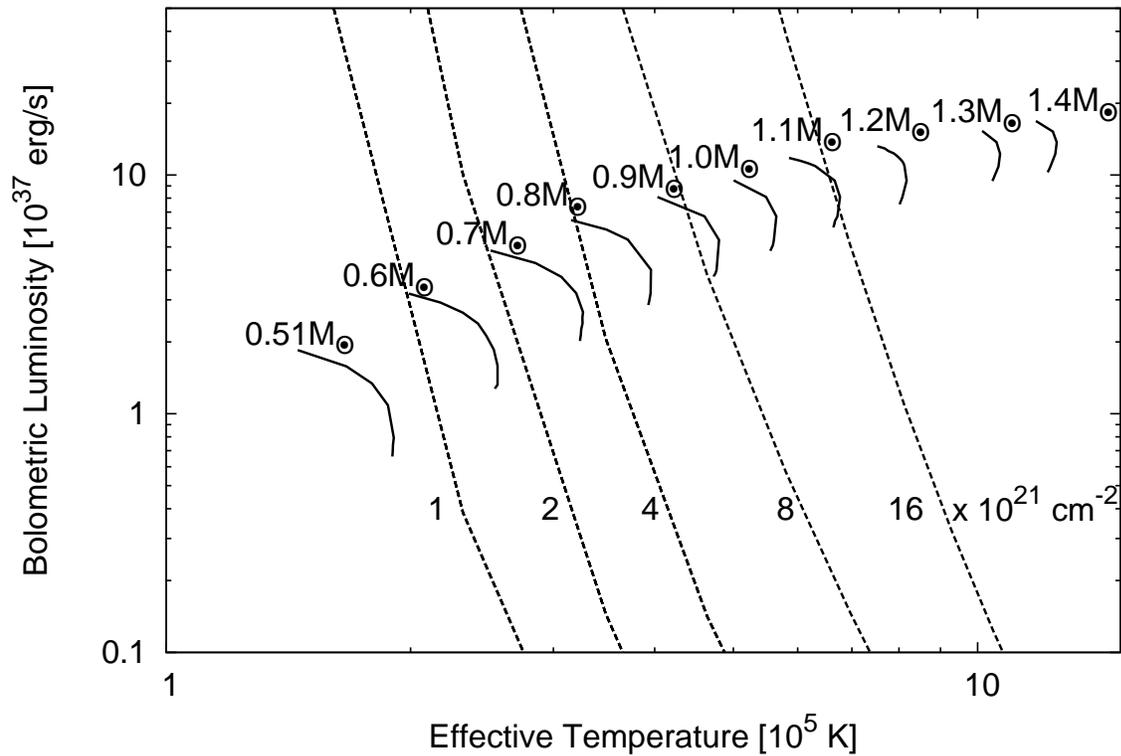
Figure 5.7: Estimate of the minimum bolometric luminosity needed for an accreting, nuclear-burning WD of a given temperature to be detected as a SSS by XMM-Newton. Dashed lines correspond to different fixed column densities, consistent with values observed in the MCs (from left to right, 10^{21}, 2×10^{21}, 4×10^{21}, 8×10^{21}, and 1.6×10^{22}cm^{-2}. Also shown are the temperatures and luminosities of the steady-burning models computed by Wolf et al. (2013) for accreting WDs of different masses (solid lines).

in [O III] 5007Å emission is seen in the vicinity of known SSSs, with limiting surface brightnesses of $\lesssim 10^{-17}$erg/s/cm^2/arcsec^2, then these objects are not well-described by our present understanding of accretion onto nuclear-burning WDs. Alternatively, the discovery of a large population of previously undetected ionizing sources, distributed throughout the warm-ionized ISM, may have profound implications for our understanding of the evolution of the ISM in star-forming galaxies.

Acknowledgements

Bibliography

Bisnovatyi-Kogan, G. S., & Syunyaev, R. A. 1970, Soviet Ast., 14, 351

Brüns, C., Kerp, J., Staveley-Smith, L., et al. 200 A&A, 432, 45

Cantalupo, S. 2010, MNRAS, 403, L16

Cassisi, S., Iben, I., Jr., & Tornambè, A. 1998, ApJ, 496, 376

Chandrasekhar, S. 1943, Reviews of Modern Physics, 15, 1

Chen, H.-L., Woods, T. E., Yungelson, L. R., Gilfanov, M., & Han, Z. 2014, MNRAS, 445, 1912

Chiang, E., & Rappaport, S. 1996, ApJ, 469, 255

Cox, D. P. 2005, ARA&A, 43, 337

Cumming, R. J., Lundqvist, P., Smith, L. J., Pettini, M., & King, D. L. 1996, MNRAS, 283, 1355

Di Stefano, R., & Rappaport, S. 1994, ApJ, 437, 733

Di Stefano, R., Paerels, F., & Rappaport, S. 1995, ApJ, 450, 705

Di Stefano, R. 2010, ApJ, 712, 728

Dickey, J. M., Mebold, U., Marx, M., et al. 1994, A&A, 289, 357

Dickey, J. M., & Lockman, F. J. 1990, ARA&A, 28, 215

Ferland, G. J., Porter, R. L., van Hoof, P. A. M., et al. 2013, Rev. Mexicana Astron. Astrofis., 49, 137

Field, G. B., Goldsmith, D. W., & Habing, H. J. 1969, ApJ, 155, L149

Frail, D. A., Weisberg, J. M., Cordes, J. M., & Mathers, C. 1994, ApJ, 436, 144

Gilfanov, M., & Bogdán, Á. 2010, Nature, 463, 924

Greiner, J. 2000, New A, 5, 137

Gruyters, P., Exter, K., Roberts, T. P., & Rappaport, S. 2012, A&A, 544, A86

Hachisu I., Kato M., Nomoto K., 1999, The Astrophysical Journal, 522, 487

Haffner, L. M., Dettmar, R.-J., Beckman, J. E., et al. 2009, Reviews of Modern Physics, 81, 969

Howell, S. B. 2000, Handbook of CCD astronomy / Steve B. Howell. Cambridge, U.K. ; New York : Cambridge University Press, c2000. (Cambridge observing handbooks for research astronomers ; 2),

Johansson, J., Woods, T. E., Gilfanov, M., et al. 2014, MNRAS, 442, 1079

Kalberla, P. M. W., McClure-Griffiths, N. M., Pisano, D. J., et al. 2010, A&A, 521, A17

Kannan, R., Stinson, G. S., Macciò, A. V., et al. 2014, MNRAS, 437, 2882

Kehrig, C., Oey, M. S., Crowther, P. A., et al. 2011, A&A, 526, A128

Kim, S., Dopita, M. A., Staveley-Smith, L., & Bessell, M. S. 1999, AJ, 118, 2797

Kim, S., Rosolowsky, E., Lee, Y., et al. 2007, ApJS, 171, 419

Kennicutt, R. C., Jr. 1992, ApJS, 79, 255

Kennicutt, R. C., Jr., Bresolin, F., Bomans, D. J., Bothun, G. D., & Thompson, I. B. 1995, AJ, 109, 594

Lu, B., & Torquato, S. 1992, Phys. Rev. A, 45, 5530

Mannucci, F., Della Valle, M., Panagia, N., et al. 2005, A&A, 433, 807

Maoz, D., & Badenes, C. 2010, MNRAS, 407, 1314

Maoz, D., Mannucci, F., & Nelemans, G. 2014, ARA&A, 52, 107

McClure-Griffiths, N. M., Pisano, D. J., Calabretta, M. R., et al. 2009, ApJS, 181, 398

McKee, C. F., & Ostriker, J. P. 1977, ApJ, 218, 148

Nelemans, G., Toonen, S., & Bours, M. 2013, IAU Symposium, 281, 225

Nikolaev, S., Drake, A. J., Keller, S. C., et al. 2004, ApJ, 601, 260

Nomoto, K., Saio, H., Kato, M., & Hachisu, I. 2007, ApJ, 663, 1269

O'Connell R. W., 2003, Astronomy 511: Observational techniques. University Lecture

Osterbrock, D. E., & Ferland, G. J. 2006, Astrophysics of gaseous nebulae and active galactic nuclei, 2nd. ed. by D.E. Osterbrock and G.J. Ferland. Sausalito, CA: University Science Books, 2006,

Pakull, M. W., & Motch, C. 1989, European Southern Observatory Conference and Workshop Proceedings, 32, 285

Panei, J. A., Althaus, L. G., & Benvenuto, O. G. 2000, A&A, 353, 970

Pauldrach, A. W. A., Duschinger, M., Mazzali, P. A., et al. 1996, A&A, 312, 525

Pellegrini, E. W., Oey, M. S., Winkler, P. F., et al. 2012, ApJ, 755, 40

Rappaport, S., Chiang, E., Kallman, T., & Malina, R. 1994, ApJ, 431, 237

Rauch T., Werner K., 2010, Astronomische Nachrichten, 331, 146

Remillard, R. A., Rappaport, S., & Macri, L. M. 1995, ApJ, 439

Smith, R. C., & MCELS Team 1998, PASA, 15, 163

Smith, R. C., Points, S. D., Chu, Y.-H., et al. 2005, Bulletin of the American Astronomical Society, 37, 1200

Snyder, K. A. 1998, Advanced Cement Based Materials, 8, 28

Stanimirovic, S., Staveley-Smith, L., Dickey, J. M., Sault, R. J., & Snowden, S. L. 1999, MNRAS, 302, 417

Sturm, R., Haberl, F., Pietsch, W., et al. 2013, A&A, 558, AA3

Stanimirovic, S., Staveley-Smith, L., Dickey, J. M., Sault, R. J., & Snowden, S. L. 1999, MNRAS, 302, 417

Torquato, S., Lu, B., & Rubinstein, J. 1990, Phys. Rev. A, 41, 2059

van den Heuvel, E. P. J., Bhattacharya, D., Nomoto, K., & Rappaport, S. A. 1992, A&A, 262, 97

van der Marel, R. P. 2006, The Local Group as an Astrophysical Laboratory, 47

Whelan J., Iben, Jr. I., 1973, The Astrophysical Journal, 186, 1007

Wolf, W. M., Bildsten, L., Brooks, J. and Paxton, B. 2013, ApJ, 777, 136

Woods, T. E., & Gilfanov, M. 2013, MNRAS, 432, 1640

Woods, T. E., & Gilfanov, M. 2014, MNRAS, 439, 2351

Chapter 6

Did the progenitor of the type Ia supernova SN2014J ionize its surrounding ISM?

6.1   Abstract

We report upper limits on the Hα + [N II] 6548Å+6583Å luminosity in the vicinity of the recent type Ia supernova SN2014J prior to its explosion. This is done using the continuum-subtracted Hα map available in the ancillary data provided by the Spitzer Infrared Nearby Galaxy Survey (SINGS, Kennicutt et al 2003). For a range in assumed densities of the surrounding ISM (n $\gtrsim$ 1cm^{-3}), we constrain the total luminosity of any putative source at the location of SN2014J for effective temperatures $8 \times 10^4 K \lesssim$ T $\lesssim 10^6 K$. This complements previous constraints in the soft X-ray band from Chandra pre-explosion images, which cannot meaningfully constrain the progenitor luminosity for temperatures below $\approx$ $5 \times 10^5 K$. For an unresolved nebula (n$\approx$ 10cm^{-3}) surrounding a T = $2 \times 10^5 K$ source, we exclude at 1σ (3σ) confidence a L$_{bol} \approx 5 \times 10^{37}$ erg/s ($\sim 1 \times 10^{38}$erg/s) source at the site of SN2014J within the last $\sim 10^4$ years. We exclude a maximally-accreting Chandrasekhar mass white dwarf at $\approx$4σ confidence. Progenitors which are either higher-temperature (though $<$8$\times10^5 K$) or embedded in low density ISM (n $\lesssim$ 4cm^{-3}) remain permitted by our results. However, given that any putative nebula should extend to radii of 5–50 pc, and be visible for 10^4–10^5 years after the turn-off of the ionizing source, follow-up spectroscopic study of the immediate vicinity of SN2014J will allow a resolution to this ambiguity. This will be accomplished shortly after the publication of this thesis, using Hα and [O III] 5007Å narrow-band observations from the Russian-Turkish 1.5m telescope on Mt. Bakyrlytepe in southern Turkey. This is the first constraint made on the ionizing luminosity of the progenitor of an individual type Ia supernova from measurements of the surrounding Hα emission.

6.2   Introduction

Thus far, efforts to constrain the luminosity of the progenitors of SNe Ia (as presented in this thesis) have focused primarily on detecting or placing constraints upon entire populations, fixing our attention on stellar populations with uniquely useful properties (Gilfanov & Bogdán, 2010; Woods & Gilfanov, 2013, 2014). In particular, we have relied on the lack of any other significant ionizing subpopulation (other than post-AGB stars) in passively-evolving galaxies to strongly constrain the role of any hot mode single-degenerate channel at delay times $\gtrsim$1Gyr (recall chapters 2, 3, & 4). However, other means exist for assessing the viability of differing SN Ia progenitor channels. One approach is to search for pre-supernova images of nearby, very recent SNe Ia. Such studies have already been carried out in the X-ray (e.g. Nielsen et al., 2012), making use of the great sensitivity of the Chandra X-ray telescope and the availability of more than a decade of its archival data. A great wealth of pre-explosion images in several wavebands are available of the immediate vicinity of SN2011fe, which exploded in M101 on August 24th, 2011 (Nugent et al., 2011). Together with observations made during the hours and days immediately following the explosion, this allowed unprecedented constraints on the progenitor of this event (Li et al., 2011; Nugent et al., 2011; Bloom et al., 2012; Chomiuk et al., 2012).

As demonstrated in the previous chapter, detecting nebulae ionized by individual accreting, steadily-nuclear burning white dwarfs (SSSs) is possible, albeit more difficult than previous thought. This presents a new opportunity to constrain the progenitors of individual, nearby events: one may search for nebulae in the vicinity of individual SNe Ia. Recently, Graur et al. (2014) have provided a constraint on the He II-ionizing luminosity of the progenitor of SN 2011fe from pre-explosion HST narrow-band images, placing an upper limit on any putative He II 4686Å nebula ionized by the progenitor (following on theoretical predictions from Rappaport et al., 1994, and Woods & Gilfanov (2013)). As identified in Bisnovatyi-Kogan & Syunyaev (1970) as well as the previous chapter, the advantage of this technique is that it may be followed-up on *after* the explosion, as any surrounding "fossil" nebula will require 10^4–10^5 years in order to recombine.

SN2011fe was the nearest SN Ia in nearly 40 years prior to the explosion of SN2014J in M82 (at a distance of only $\approx$3.5Mpc, Dalcanton et al., 2009). SN2014J (previously PSN_J09554214+6940260) was discovered by S. J. Fossey on 22 January 2014 (Cao et al., 2014), with pre-discovery images later identifying the time of first light to be ~ 14 January, 2014 (Zheng et al., 2014). Given its close proximity, this presents a remarkable opportunity for constraining the nature of the progenitor. So far, upper limits on the soft X-ray emission (Nielsen et al., 2014) have already ruled out an accreting Chandrasekhar mass white dwarf (WD) unless the photosphere is inflated, and infrared through near-UV photometry have ruled out a highly luminous giant companion (Kelly et al., 2014). Here, we extend this effort to include upper limits on the Hα+[N II] 6548Å+6584Å flux in the vicinity of SN2014J prior to the explosion. This allows us to make an independent test of the plausibility of the progenitor of SN2014J having been a hot, luminous WD, by placing upper limits on the luminosity reprocessed by any ionized nebula which would have surrounded the source.

We begin by outlining some theoretical considerations in §6.3, in particular reviewing some of the discussion from previous chapters most relevant to the present work. § 6.3 primarily serves to allow this chapter to stand on its own, and may be read quickly by the diligent reader of this thesis. We then analyze the Hα+[N II] map of M82 available from the Spitzer Infrared Nearby Galaxies Survey (SINGS, Kennicutt et al., 2003), as well as our additional data reduction and analysis, in §6.4. In §6.5, we describe our photoionization modeling of any putative (unresolved) ionized nebula in the vicinity of SN2014J, and present our constraints on the ionizing luminosity of its progenitor. Finally, in §6.6 we discuss our results in a broader context, and outline prospects for future constraints on SN2014J and other nearby SNe Ia. In particular, a follow-up campaign (presently in progress) will allow us to constrain the luminosity of the progenitor in the case of lower-density ISM (i.e. for extended nebulae).

6.3   Fossil strömgren regions

6.3.1   Steady nuclear-burning sources

In the canonical picture of the single-degenerate channel, a carbon-oxygen WD explodes after accreting sufficient matter from some Hydrogen-rich companion to reach $M \approx M_{Ch}$. This is most efficient in the so-called "stable nuclear-burning regime," a narrow range in accretion rates ($\approx 1 - $ few $\times 10^{-7} M_{\odot}/$yr, Nomoto et al., 2007) for which approximately all of the Hydrogen accreted by the WD is expected to be processed steadily in a narrow layer on its surface. As discussed previously (recall chapter 1), these objects are associated with observed supersoft X-ray sources, with approximately blackbody spectra, and temperatures on the order of 10^5–10^6K (van den Heuvel et al., 1992). Accreting WDs such as these are very strong sources of ionizing emission (Rappaport et al., 1994; Woods & Gilfanov, 2013), and would ionize any surrounding ISM.

Therefore, we can look for the presence, past or present, of stable nuclear-burning WDs by looking for their surrounding emission-line nebulae. This is particularly useful in the search for the progenitors of nearby SNe Ia. Any detection (or upper limits) on line emission in pre-supernova images of the vicinity of a SN Ia can constrain the progenitor's luminosity and temperature for the past 10^4–10^5 years (i.e. the recombination timescale of the gas, c.f. eq. 5.2). If the SN Ia under consideration is sufficiently nearby so as to allow a putative surrounding nebula to be resolved, then it becomes possible to constrain the nature of the progenitor of the explosion long **after** the event, with the use of long-slit or IFU spectroscopy (and the exclusion of the expanding supernova shell).

In the following, we will make use of a pre-supernova Hα+[N II] map of the galaxy Messier 82. Therefore, here we focus on considerations relevant to the expected Hα emission, as well as the nearby [N II] 6548Å+6584Å doublet.

The total luminosity reprocessed into Hα within a radius r_1 of the source is:

$$L_{H\alpha} = \frac{4\pi}{3} h\nu_{H\alpha} \int_0^{r_1} n_{H^+} n_e \alpha_{3\to 2}(T_{gas}, n_e) dr \qquad (6.1)$$

where n_{H+} is the density of the surrounding ionized Hydrogen, and $\alpha_{3\to2}(T_{gas}, n_e)$ is the effective recombination coefficient of the Hα transition.

However, the filter used by the SINGS survey in observing M82 also includes both wavelengths of the [N II] doublet 6548Å+6584Å. These lines carry a much more complex dependence on the incident ionizing flux and conditions in the ISM, with the ratio

$$\xi = \xi(T_{ISM}, n_{ISM}, Z_{ISM}) = \frac{L_{[NII]}}{L_{H_\alpha}} \tag{6.2}$$

typically lying in the range $0.5 \lesssim \xi \lesssim 2$. Assuming Case B recombination (Osterbrock & Ferland, 2006), in the low-density limit this gives us a total line emission of

$$L_{H\alpha+[NII]} \approx 3.5 \times 10^{31} \left(\frac{r}{pc}\right)^3 (1+\xi) \left(\frac{n_{H+}}{cm^{-3}}\right)^2 \frac{erg}{s} \tag{6.3}$$

where we have taken $n_{H+} n_e \approx 1.1 n_H$ for ionized, solar-metallicity gas.

In order to predict the total narrow-band flux observable in Hα + [N II], should the progenitor of SN2014J have been a hot and luminous WD, we make use of the photoionization code Cloudy v13.03 (Ferland et al., 2013). Here we model the ISM surrounding the site of SN2014J assuming a solar metallicity gas (following the gas phase metallicity found in M82 by McLeod et al., 1993) with varying densities, each model being isochoric. The surrounding ISM is assumed to be neutral in the absence of any ionizing source at the site of SN2014J. Note that, due to the uncertain nature of the grain composition and morphology in the immediate vicinity of SN2014J, we do not include grains in our calculations. From trial computations using Cloudy, we have determined that this has only a minor effect on our final result.

The only remaining input that we require is the emission from the putative ionizing source. A number of models exist for the observational characteristics of an accreting, nuclear-burning WD (Maoz et al., 2013). However, as discussed above (c.f. chapters 1 – 3), emission from a sufficiently hot, luminous WD is reasonably well-approximated in the extreme UV by a blackbody spectrum, neglecting numerous absorption lines (one may compare with the NLTE models of Rauch & Werner, 2010). In particular, there is no sharp cut-off at the H I and He II absorption edges. This is expected to hold even in the case of very inflated photospheres supported by an optically-thick wind (recall chapter 2, and particularly appendix A), such as that proposed by Hachisu, Kato & Nomoto (1999). Predicted temperatures range from $10^6 K$, typical of supersoft sources (SSSs), down to temperatures as low as ≈ 1–$2\times10^5 K$ or less (seen in some SSSs, and characteristic of greatly inflated photospheres). For generality, here we assume blackbody emission with temperatures in the range $8 \times 10^4 K - 10^6 K$. The luminosity expected for a stable nuclear-burning Chandrasekhar-mass WD is roughly ≈ 0.8–2×10^{38}erg/s.

6.3.2 The "accretion-wind" regime

In the so-called "stable-burning" regime, the luminosity of an accreting WD is proportional to the mass transfer rate from the donor star. However, for accretion rates of order $\dot{M}_{RG} \sim$

$10^{-6} M_\odot/\text{yr}$, the WD luminosity reaches that expected from the core-mass – luminosity relation for a typical AGB star. While it is understood that the WD mass cannot grow faster than this limit (Nomoto et al., 2007), the fate of the WD (and any excess matter) at such high accretion rates remains unclear. Should the WD photosphere swell to giant-like dimensions, its spectral emission would peak in the near-IR. However, such a configuration is ruled out at the time of explosion by existing constraints on the ambient density of the circumstellar matter (see discussion in §6.5), and is in any case unlikely to produce a Chandrasekhar mass WD (Cassisi et al., 1998).

Alternatively, it has been proposed that for $\dot{M} > \dot{M}_{\text{RG}}$, any excess material will be expelled in the form of an optically-thick wind, driven by the peak in the iron opacity at $T \sim 10^{5.2} K$. This would inflate the photospheric radius by an order of magnitude, correspondingly shifting the photospheric temperature of the WD to $\approx 1\text{–}2\times10^5 K$ (Hachisu, Kato & Nomoto, 1999). However, in this case the WD would remain a strong source of ionizing radiation (Woods & Gilfanov, 2013).

With a velocity of order $\approx$1000km/s, any such wind would easily excavate a cavity in the surrounding ISM. Such a region would have an inner particle density of only $\approx 10^{-3}\text{cm}^{-3}$, with a shock interface at the boundary ($r_{\text{inner}} \approx 1\text{–}40\text{pc}$) with typical densities of $n \approx 10$ – 100 cm^{-3} (Badenes et al., 2007). Such a boundary layer would be photoionized by the central source, with line emission detectable for τ_{rec} after the source turns off (c.f. eq. 5.2).

6.4   Data reduction

6.4.1   The SINGS survey Hα+[N II] map of M82

The updated coordinates for SN2014J are given as RA = 09:55:42.121, DEC = +69:40:25.88 in J2000 coordinates (ATel #5821, Smith et al, on behalf of STSci). In order to search for Hα+[N II] emission from any putative ionized nebula in the vicinity of the progenitor of SN2014J, we make use of the fifth data release of SINGS (Kennicutt et al., 2003). Included in its ancillary data are narrow-band Hα+[N II] images of the majority of the galaxies in their study[1]. As part of this survey, M82 was observed using the Kitt Peak 2.1m telescope on 2002-03-06T08:02:35 using the KP1563 filter (with central wavelength $\lambda_{\text{CW}} = 6573$Å, FWHM = 67Å). This band encloses the Hα line as well as both wavelengths of the [N II] 6548Å+6584Å doublet. The image of M82 consists of a single pointing 200 second exposure, carried out under photometric conditions. The Kitt Peak 2.1m telescope has a field of view of $\approx 10'$, with a pixel scale of $\approx 0.''305$. At the distance of M82 ($\approx$3.5Mpc), this corresponds to a physical distance of $\approx$5.2pc ($1'' \approx 17$pc). The image is calibrated from observations made of standard stars; the flux conversion is given as[2]

---

[1]SINGS   Spitzer   and   ancillary   data   are   available   for   download   from: http://sings.stsci.edu/proposal/CoreScience.htm

[2]From   the   SINGS   fifth   data   delivery   user's   guide,   available   at http://irsa.ipac.caltech.edu/data/SPITZER/SINGS/
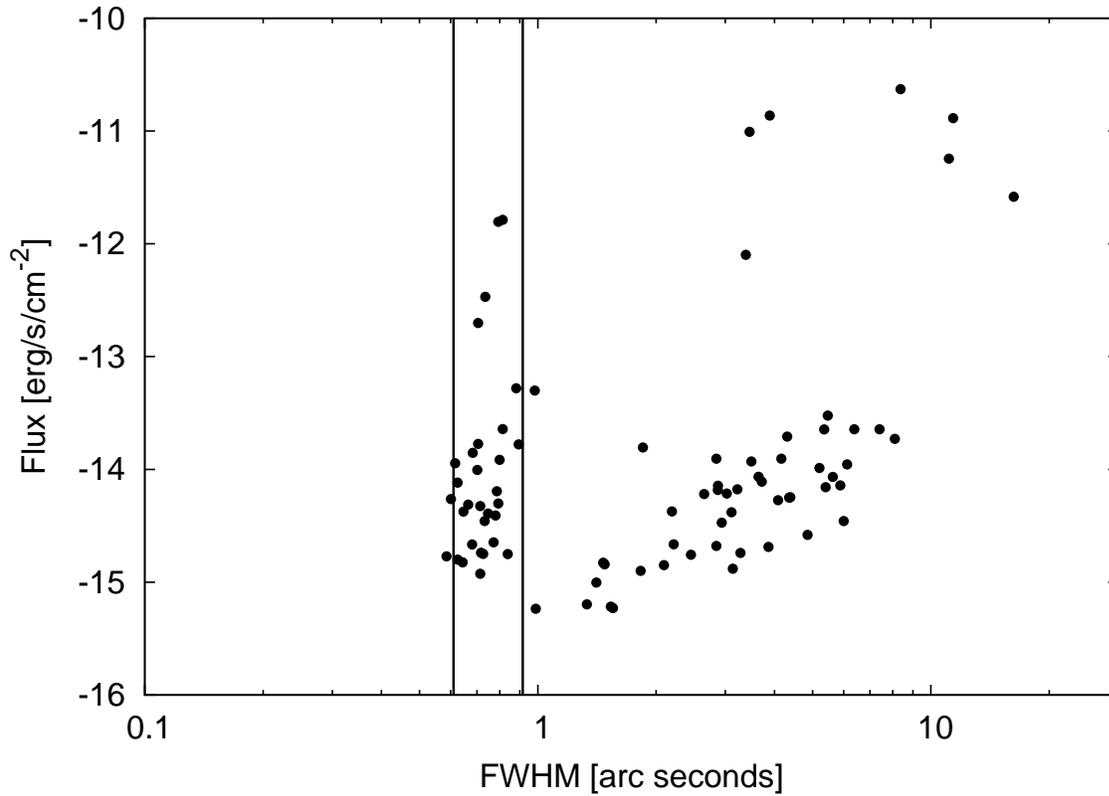
Figure 6.1: FWHM assuming a Gaussian profile and fluxes as measured for all sources identified by SExtractor in the SINGS Hα+[N II] image of M82. The two vertical lines denote the angular sizes corresponding to 2 and 3 pixels on the Kitt Peak CCD, respectively. All objects with FWHM <1" are identified as point sources, providing a measure of the seeing.

$$F(\text{erg cm}^{-2}\text{s}^{-1}) = 6 \times 10^{-10}\text{C}_\text{S} \times \text{FWHM}/\lambda_{\text{CW}}^2 \tag{6.4}$$

or $\approx 9.3 \times 10^{-16}\text{erg/cm}^{-2}$/count, with C_S the measured counts per second.

Prior to the delivery of all optical data, all images were bias subtracted, flat-fielded, and suspected cosmic rays removed by the SINGS Legacy Project. The continuum-subtracted Hα+[N II] image which we use in this study was similarly made available by SINGS, produced by scaling and subtracting the associated R-band image. However, no prior background subtraction was carried out. We reserve discussion of our background subtraction for the following subsection.

In order to estimate the seeing, we perform a search for all sources in the SINGS Hα+[N II] image of M82 using the publicly available[3] software SExtractor (Bertin & Arnouts, 1996). We perform a scan for all sources in which a minimum of 6 pixels are found with fluxes exceeding 5σ above the measured background level. The latter is found iteratively by averaging over a 64 pixel mesh, computing the mean and standard deviation, and rejecting the greatest outlying pixel, until all remaining pixels are within $\pm 3\sigma$ of the mean value. Prior to measuring the background, each region is first smoothed using a 4 pixel background filter. Approximating each source with a gaussian profile, the FWHM derived for all 85 sources thus detected are plotted in fig. 6.1, as well as their respective fluxes. Note that our estimate of the seeing is robust for a range of background and detection criteria; varying these only significantly changes our results for those "objects" found in the crowded central starburst of M82.

The objects detected by SExtractor here fall into three broad categories. In the lower right of fig. 6.1, a number of extended sources are found with FWHM ranging from $\approx 1''$ – $10''$ and fluxes $\approx 10^{-15}$–10^{-14} erg/cm^2/s. This includes a number of background galaxies, as well as several nebular regions on the outskirts of the central starburst of M82. In the upper right of fig. 6.1, we see that SExtractor identifies a number of extended, very bright "objects" which are produced in trying to fit multiple sources in the central starburst of M82, as well as two over-exposed objects in the south-east of the SINGS image. Finally, another family of sources, with measured fluxes spanning 4 orders of magnitude, have FWHM which in almost all cases lie between $\approx 0.61''$ and $0.92''$ (the horizontal lines in fig. 6.1), with none exceeding $\approx 1''$. This corresponds to ≈ 2–3 pixels on the Kitt Peak CCD. All are clearly point sources, providing a measure of the seeing on the night of the observation. Taking the mean of their FWHM, we estimate the seeing as $\approx 0.74''$. Note that no source is detected in the vicinity of the progenitor of SN2014J using our automated procedure, although we have chosen a somewhat high threshold for detection.

6.4.2   The warm ionized ISM of M82 in the vicinity of SN2014J

The location of SN2014J lies along the line of sight of an extended faint excess of Hα emission (see fig. 6.2). In order to evaluate the significance of any detection or upper limit, we require an estimate of the noise in the vicinity of the progenitor of SN2014J. Estimating

---

[3]http://www.astromatic.net/software/sextractor
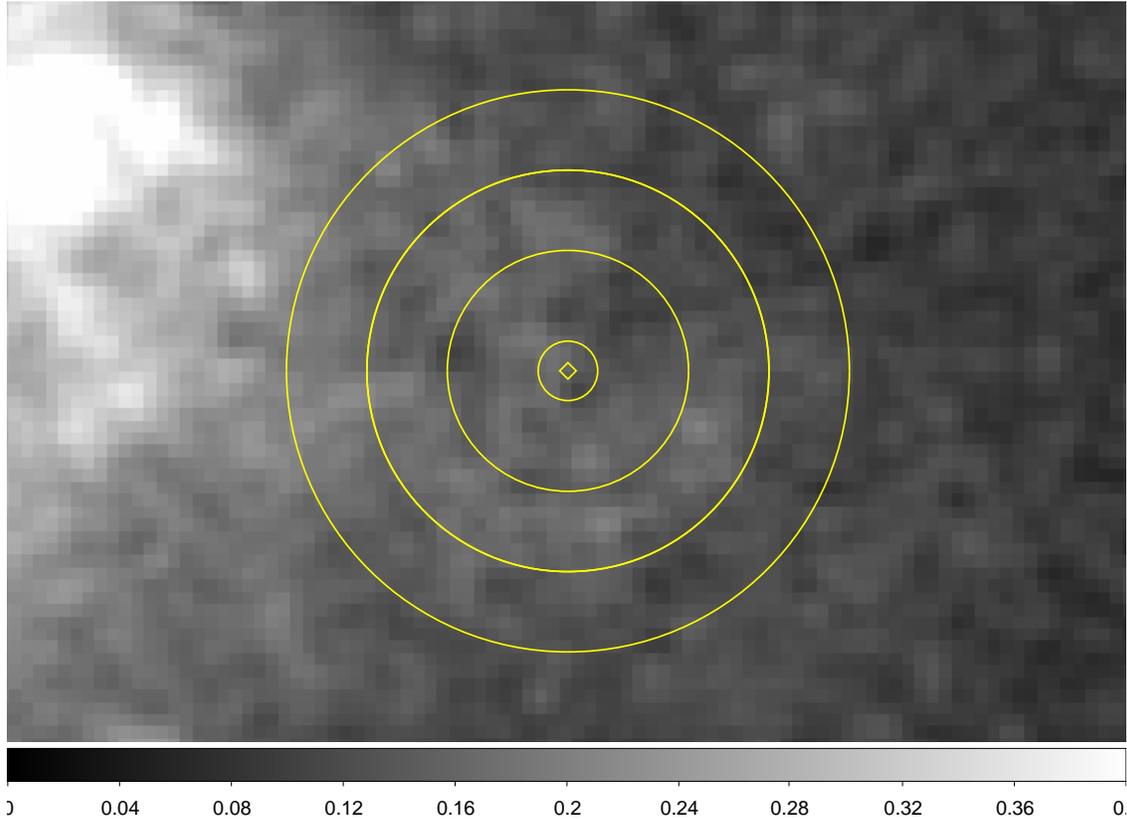
Figure 6.2: Pre-supernova Hα+[N II] image of M82 in the vicinity of SN2014J ($\approx 30''\times 20''$, progenitor location marked with an '$\diamond$'). The innermost circular aperture has a radius of $0.74''$, while the outermost annulus has inner and outer radii of $5''$ and $7''$, respectively, with the inner radius corresponding to the maximum radius used in comparison with our predictions in §4. This is the region we use in our local background subtraction. The inner annulus, with inner and outer radii of $3''$ and $5''$ respectively corresponds to a modest excess seen in most prominently in the lower-right. This will be investigated in a future work (see discussion). Units are counts/s. Note that in producing the above image, we have smoothed the SINGS data for display purposes using a Gaussian with FWHM of 2 pixels.

the noise from line projections in the vicinity of the site of SN2014J, we find a (per-pixel) variance of $\sigma^2 \approx 0.0017$ counts^2/s^2. This appears to be roughly consistent with the noise N per pixel expected from simple poissonian noise together with read noise from the CCD, as estimated from:

$$\sigma|_{\mathrm{expected}} \approx \sqrt{\overline{C}_{\mathrm{S,pix}} \mathcal{G} \mathrm{t}_{\mathrm{exp}} + (\mathrm{RN})^2} \qquad (6.5)$$

where $\overline{C}_{\mathrm{S,pix}} \approx 0.144$ counts/s is the mean flux per pixel in the source aperture (including the background), $\mathrm{t}_{\mathrm{exp}}$ is the exposure time, and the read noise RN = 4e$^-$ and gain ($\mathcal{G} = 3.6$e$^-$) are taken from the observation documentation. Note that we have neglected other instrumental contributions to the total noise, such as the dark current.

SN2014J also roughly coincides with the center of an observed soft X-ray excess associated with a possible superbubble in Nielsen et al. (2014). In order to measure the Hα+[N II] flux which may be associated with the progenitor of SN2014J alone, we require an estimate of the background flux, including any Hα emission within or surrounding this bubble.

In order to make an estimate of the background Hα+[N II] flux in the vicinity of SN2014J, we take the average (per pixel) count rate in an annulus with inner and outer radii of 5″ and 7″, respectively. This excludes the bright feature 7.5″ to the north-west, as well as the ring and any other flux from a possible nebula ionized by the progenitor. We take this as our estimate of the background ($\mathrm{C}_{\mathrm{bkg}} \approx 0.138$ counts/s/pixel, measured over $\mathrm{N}_{\mathrm{bkg,pix}}$=818 pixels) in the vicinity of SN2014J.

6.4.3 Upper limits on the Hα+[N II] line flux in the vicinity of SN2014J

In order to constrain the ionizing luminosity of the progenitor of SN2014J, we first require an appropriate estimate for the plausible extent of any putative photoionized nebula centered at the location of the explosion. Unfortunately, this depends on the as-yet uncertain density of the local ISM (though see discussion in § 6.5.2), as well as the temperature and luminosity of the progenitor (both of which we hope to constrain). We begin by measuring the flux under the assumption that any putative nebula is unresolved. For a simple Gaussian point-spread function, the aperture which maximizes the S/N of a point source has radius ≈2/3 that of the FWHM. However, this is only the optimum S/N for a "true" point source, such as a star, and not a nebula of some finite, but not quite resolved, extent. In practice the S/N only varies slowly up to at least r ≈ FWHM, even for a true Gaussian point source. Therefore, we take as our minimum aperture radius r = 0.74″. Within such an aperture, centered on the location of SN2014J, we measure a total flux of ≈2.7 counts/sec. Note that, here and throughout, we use circular (or annular) regions as found in SAO ds9[4] to measure count rates.

---

[4]http://ds9.si.edu/site/Home.html

After subtracting the appropriate background, we find an excess of ≈ 0.1 counts/sec within $0.74''$ of the eventual site of SN2014J (a total of $N_{\mathrm{pix,S}} = 19$ pixels). Adding the error on the source measurement and the background subtraction in quadrature, we arrive at an effective 1σ error of:

$$\sigma_{\mathrm{eff}} = \sqrt{\sigma^2 N_{\mathrm{pix,S}} + \sigma^2 \frac{N_{\mathrm{pix,S}}^2}{N_{\mathrm{pix,bkg}}}} = 0.19 \mathrm{counts/s} \tag{6.6}$$

From eq. 6.4, this corresponds to a flux of $(1 \pm 2) \times 10^{-16}$erg/cm^2/s within our minimum aperture. However, over the same range in temperatures and luminosities, we can expect much more extended nebulae for lower mean ISM densities. We address this in the following section.

SN2014J has been observed to suffer significant reddening, with E(B-V) $\gtrsim 1$ as inferred from the Na I D equivalent width (Cox et al., 2014), although Kotak (2014) found the light curve to be consistent with E(B-V) < 1. Goobar et al. (2014) found a best fit reddening model following that of Cardelli et al. (1989) with a remarkably low $R_V = 1.4 \pm 0.15$ and E(B-V) $= 1.22 \pm 0.05$ mag. In addition to this, we must also correct for absorption within the Milky Way along the line of sight. In the direction of SN2014J, Schlafly & Finkbeiner (2011) find a visual extinction of $A_V \approx 0.43$ assuming A_V/E(B - V) $= 3.1$. For $\lambda = 6563$Å, the combined Milky Way and M82 reddening amounts to a total correction of $F_{\mathrm{obs}}/F_{\mathrm{int}} \approx 0.22$.

6.5   Constraints on any nebula surrounding the progenitor of SN2014J

6.5.1   Unresolved nebulae

Eq. 5.1 indicates that for densities $n_{\mathrm{ISM}} \gtrsim 4$cm^{-3}, we should expect any putative nebula ionized by the progenitor of SN2014J to be unresolved (i.e. $R_S \lesssim 12.6$pc $= 0.74$" (recall discussion in § 5.3). However for nebulae ionized by very high temperature sources (T $\gtrsim 5 \times 10^5 K$), the Strömgren boundary region can be significantly broadened (see Rappaport et al., 1994; Woods & Gilfanov, 2014). Using the photoionization code Cloudy, we find that $R_S \lesssim 12.6$pc for ISM densities $n \approx 4$–10 cm^{-3}, source temperatures $8 \times 10^4 K$–$10^6 K$, and bolometric source luminosities $\lesssim 10^{38.25}$erg/s. The latter two span temperatures and luminosities characteristic of accreting, nuclear-burning white dwarfs near the Chandrasekhar mass. Therefore, the physical extent of such nebulae would be within the minimum resolution of the image of M82 provided by the SINGS survey.

For a range of temperatures, we then find the source bolometric luminosities corresponding to our upper limit on the narrow-band emission derived in § 6.4.3. Shown in fig. 6.3 are our 1, 2, & 3σ upper limits assuming $n = 10$cm^{-3}. For comparison, we also plot the 3σ upper limits on the bolometric luminosity of the progenitor from soft X-ray constraints (Nielsen et al., 2014).
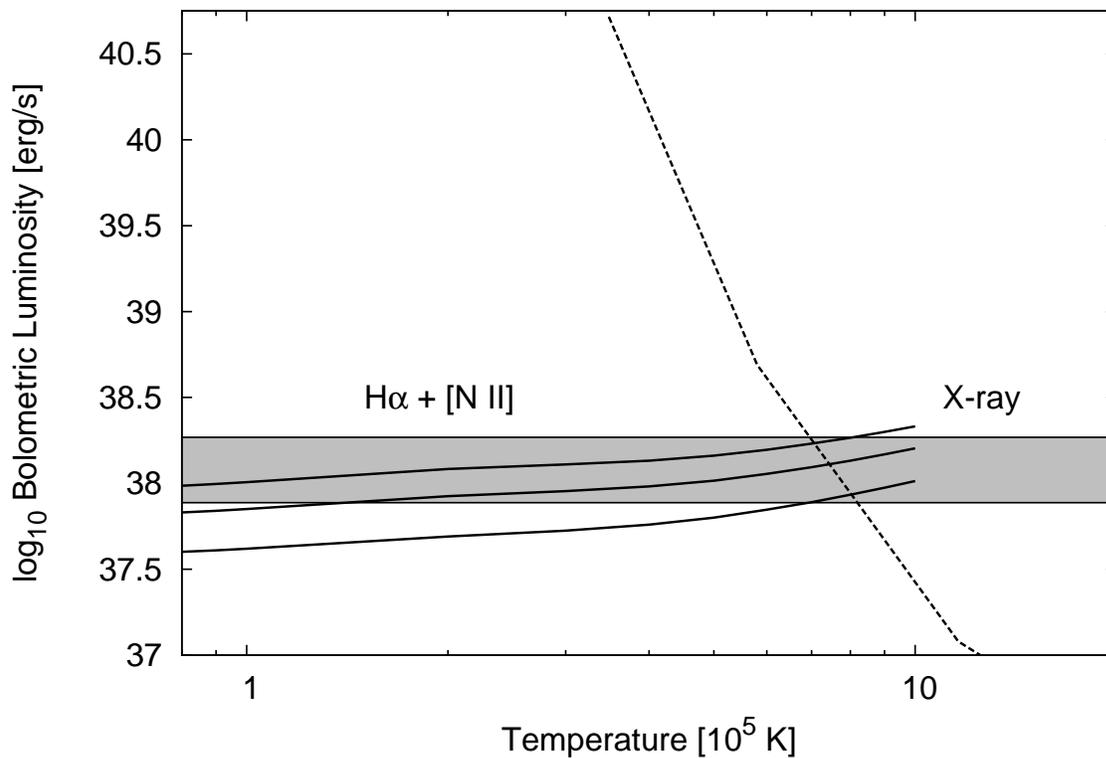
Figure 6.3: Upper limits on the bolometric luminosity of the progenitor of SN2014J as a function of the progenitor's possible temperature (solid lines, lower: 1σ middle: 2σ upper: 3σ), from limits on the pre-supernova Hα+[N II] flux from a 0.74" ($\approx$13pc) radius surrounding the site of the later explosion. Here we have assumed a constant density in the surrounding ISM of $10\mathrm{cm}^{-3}$ and blackbody emission from the source. The gray-shaded region denotes the expected range in bolometric luminosities of an accreting Chandrasekhar-mass WD in the stable nuclear-burning regime.

From our photoionization calculations, this places an upper limit at 1σ (3σ) confidence on the bolometric luminosity of a $2\times10^5 K$ progenitor to be $\approx 5\times10^{37}$ erg/s ($\approx 10^{38}$ erg/s), for unresolved nebulae (corresponding to densities $n_{ISM} \approx 10$cm^{-3}). Note the region denoted by the gray lines in fig. 6.3; this marks the minimum and maximum luminosities of a Chandrasekhar mass ($M_{Ch} \approx 1.4M_\odot$) WD in the stable burning regime, following the calculations of Nomoto et al. (2007). Therefore, our results do not entirely exclude a stably nuclear-burning WD with a photospheric temperature $\gtrsim 2 \times 10^5$K having been present at the site of the explosion of SN2014J within the last $\approx 10^4$–10^5 years (i.e. the recombination timescale in the local ISM).

6.5.2   Limits on extended sources?

If the progenitor of SN2014J was a sufficiently hot, luminous source embedded in a lower density environment ($n_{ISM} \lesssim 4$cm^{-3}, $L_{bol} \gtrsim 10^{38}$erg/s, $T_{eff} \gtrsim 10^5 K$), its surrounding emission-line region would be visible as a resolved, extended source in the Kitt Peak observation. This complicates our effort to relate the observed Hα+[N II] flux in the vicinity of SN2014J to an upper limit on the progenitor's ionizing luminosity, as the Strömgren radius of the nebulae (and thus the relevant aperture for our analysis) varies with the ionizing luminosity itself (recall eq. 5.1). At greater aperture radii, we may include an ever greater volume of the ambient warm-ionized ISM typical of star-forming galaxies, considerably contaminating our Hα measurements. For this reason, other diagnostic lines become much more useful in the search for extended nebulae, such as [O III] 5007Å, which is not particularly luminous in normal warm-ionized ISM but is highly luminous in SSS nebulae (recall the discussion in chapter 5). Fortunately, low-density nebulae will extend well beyond the shock radius of the expanding supernova remnant, allowing us to observe any extended nebula well after the explosion. To this end, we have initiated deep narrow-band observations of the vicinity of SN 2014J using the Russian-Turkish 1.5m telescope. These results will be analyzed after the publication of this thesis.

Until then, the actual density of the ISM surrounding the site of SN2014J unfortunately remains uncertain. If the progenitor of SN2014J was indeed located within the tentative superbubble identified in Nielsen et al. (2014), then pressure equilibrium with the hot ISM would require densities of order ~ 100cm^{-3}. On the other hand, this does not hold in the solar neighbourhood, where typical warm ISM densities are of order ~ 1cm^{-3}. From their non-detection of X-ray emission at the site of SN2014J at $\delta t \sim 20$ days after the explosion, Margutti et al. (2014) place an upper limit on the density of the surrounding circumstellar matter (CSM) of $n_{CSM} < 3.5$cm^{-3} within $\approx 10^{16}$cm of the progenitor. Accounting for uncertainties in the bolometric luminosity of SN2014J itself, as well as the column density toward SN2014J associated with M82, Margutti et al. (2014) quote an upper bound which may lie in the range $n_{CSM} \approx (1.5 - 8.0)$cm^{-3}. In the radio, the non-detection of any interaction between the expanding supernova shell and the circumstellar medium by Perez-Torres et al. (2014) limits the CSM density to $n_{CSM} \lesssim 1$cm^{-3}. Again, however, this constraint applies only to the inner $\approx 10^{16}$cm; the surrounding ISM density remains unknown. We note that in the discussion above, we have begun our photoionization calculations at an inner

radius of 10^{17}cm. Certainly, there is gas traced by dust in the environment surrounding SN2014J (e.g. Foley et al., 2014). The total absorbing column density measured along the line of sight toward SN2014J is $N_H \approx 4.2 \times 10^{21}$cm^{-3} (Goobar et al., 2014); nowhere in our calculations do we imply a column density exceeding this.

6.5.3   Wind-blown bubbles

The low upper limits on the density inferred for the CSM surrounding SN2014J exclude a WD undergoing a rapidly-accreting phase at the time of the explosion. However, at the same time such a result would not be surprising if a fast wind was driven from the progenitor WD long before the explosion, excavating a cavity within the ISM in the vicinity of SN2014J. This would leave a surrounding shell of swept-up material which would be ionized by the progenitor. For a Chandrasekhar-mass WD, the luminosity in such a regime would be fixed by the maximum burning rate (Nomoto et al., 2007), at $\approx 1.8 \times 10^{38}$erg/s, with a photospheric temperature on the order of $\approx (1 - 2) \times 10^5 K$ (Hachisu, Kato & Nomoto, 1999).

An assessment of the detectability of any ionized shell surrounding such a source depends on the inner radius of the shell, and the density of the gas swept up by it. For unresolved inner cavities ($r_{inner} \lesssim 13$pc) and sufficiently high shell densities ($n \gtrsim 4$cm^{-3}), the situation is entirely analogous to that of the "classical" unresolved SSS nebulae discussed above, except with a fixed source luminosity. In this case, we rule out a maximally accreting, $T = 2 \times 10^5 K$ WD with $M = M_{Ch}$ at $\approx 4\sigma$ confidence. For resolved (larger) shells, the situation is analogous to that discussed in the previous subsection for extended sources. Therefore, we leave any constraint on such progenitors to our forthcoming study.

6.6   Discussion

For modest ISM densities ($n \sim 10$cm^{-3}), our upper limit for the bolometric luminosity of an accreting white dwarf with a strongly inflated photosphere ($T \approx 2 \times 10^5 K$, assuming a blackbody spectrum) excludes (with $\approx 2\sigma$ confidence, cf. fig. 6.3) almost the entire range in luminosities consistent with stable nuclear-burning on the surface of a Chandrasekhar mass WD. Unlike X-ray constraints, this holds not only at the time of observation ($\lesssim 12$ years prior to the explosion of SN2014J), but for the past $t_{recombination} \approx 10^4$ years (assuming somewhat high ISM densities consistent with an unresolved source). Our results allow for a higher temperature ($T \gtrsim 5 \times 10^5 K$) Chandrasekhar mass white dwarf accreting in the stable nuclear-burning regime of Nomoto et al. (2007), but this is partly ruled out by X-ray constraints (Nielsen et al., 2014).

Note however that if the inflated photosphere was supported by optically-thick winds, one would expect the ISM surrounding the site of SN2014J to be swept up in a wind-blown bubble. This would not significantly effect the luminosity predicted to be reprocessed as Hα+[N II] emission for any given source, although this would obviously change the morphology and therefore the appropriate aperture. For SN2014J, we exclude many of

the models for the shell structure explored in Badenes et al. (2007), assuming a source temperature of $2 \times 10^5 K$ typical of WDs in the accretion-wind regime (Hachisu, Kato & Nomoto, 1999). In particular, we exclude an unresolved shell ($r_{inner} \lesssim 12$pc, $n_{boundary} \gtrsim 5$cm^{-3}) at $> 4\sigma$.

Follow-up observations of the surrounding medium, excluding the shock emission from the expanding supernova shell, will be able to greatly improve upon the constraints presented here. In particular, the forbidden transition at [O III] 5007Å is relatively weak in diffuse, warm-ionized ISM, but should be very strong (i.e. relative to Hβ) in nebulae ionized by high-temperature sources. Also useful would be deep observations in search of [O I] 6300Å and [N I] 5200Å, two lines whose peak emission should lie at the Strömgren radius (recall discussion in chapter 5). This would provide strong constraints in precisely the temperature range which remains allowed by both Hα+[N II] and X-ray constraints ($3 \times 10^5 K \lesssim$ T $\lesssim 5 \times 10^5 K$). To this end, shortly after the publication of this thesis we will analyse [O III] 5007Å and Hα narrow-band observations made by the Russian-Turkish 1.5m telescope after the explosion of SN2014J. The [O III] 5007Å observations in particular will allow us to resolve any ambiguity in interpreting the extended emission in the vicinity ($\approx$5" radius) of SN2014J.

Acknowledgements

Bibliography

Badenes, C., Hughes, J. P., Bravo, E., & Langer, N. 2007, ApJ, 662, 472

Bertin, E., & Arnouts, S. 1996, A&AS, 117, 393

Bisnovatyi-Kogan, G. S., & Syunyaev, R. A. 1970, Soviet Ast., 14, 351

Bloom, J. S., Kasen, D., Shen, K. J., et al. 2012, ApJ, 744, L17

Cardelli, J. A., Clayton, G. C., & Mathis, J. S. 1989, ApJ, 345, 245

Cassisi, S., Iben, I., Jr., & Tornambè, A. 1998, ApJ, 496, 376

Cao, Y., Kasliwal, M. M., McKay, A., & Bradley, A. 2014, The Astronomer's Telegram, 5786, 1

Chomiuk, L., Soderberg, A. M., Moe, M., et al. 2012, ApJ, 750, 164

Cox, N. L. J., Davis, P., Patat, F., & Van Winckel, H. 2014, The Astronomer's Telegram, 5797, 1

Cumming, R. J., Lundqvist, P., Smith, L. J., Pettini, M., & King, D. L. 1996, MNRAS, 283, 1355

Dalcanton, J. J., Williams, B. F., Seth, A. C., et al. 2009, ApJS, 183, 67

Di Stefano R., 2010, Astrophysical Journal, 712, 728

Ferland, G. J., Porter, R. L., van Hoof, P. A. M., et al. 2013, Rev. Mexicana Astron. Astrofis., 49, 137

Foley, R. J., Fox, O., McCully, C., et al. 2014, arXiv:1405.3677

Gilfanov M., Bogdán Á., 2010, Nature, 463, 924

Goobar, A., Johansson, J., Amanullah, R., et al. 2014, arXiv:1402.0849

Graur, O., Maoz, D., & Shara, M. M. 2014, arXiv:1403.1878

Greiner, J. 2000, New A, 5, 137

Hachisu I., Kato M., Nomoto K., 1999, The Astrophysical Journal, 522, 487

Haffner, L. M., Dettmar, R.-J., Beckman, J. E., et al. 2009, Reviews of Modern Physics, 81, 969

Hillebrandt, W., Kromer, M., Röpke, F. K., & Ruiter, A. J. 2013, Frontiers of Physics, 8, 116

Iben, Jr. I., Tutukov A. V., 1984, The Astrophysical Journals, 54, 335

Johansson, J., Woods, T. E., Gilfanov, M., et al. 2014, arXiv:1401.1344

Katz, B., & Dong, S. 2012, arXiv:1211.4584

Kelly, P. L., Fox, O. D., Filippenko, A. V., et al. 2014, arXiv:1403.4250

Kennicutt, R. C., Jr., Armus, L., Bendo, G., et al. 2003, PASP, 115, 928

Kotak, R. 2014, The Astronomer's Telegram, 5816, 1

Li, W., Bloom, J. S., Podsiadlowski, P., et al. 2011, Nature, 480, 348

Maoz, D., Mannucci, F., & Nelemans, G. 2013, arXiv:1312.0628

Margutti, R., Parrent, J., Kamble, A., et al. 2014, arXiv:1405.1488

McLeod, K. K., Rieke, G. H., Rieke, M. J., & Kelly, D. M. 1993, ApJ, 412, 111

Nielsen, M. T. B., Voss, R., & Nelemans, G. 2012, MNRAS, 426, 2668

Nielsen, M. T. B., Gilfanov, M., Bogdan, A., Woods, T. E., & Nelemans, G. 2014, arXiv:1402.2896

Nomoto K., Saio H., Kato M., Hachisu I., 2007, The Astrophysical Journal, 663, 1269

Nugent, P., Sullivan, M., Bersier, D., et al. 2011, The Astronomer's Telegram, 3581, 1

Nugent, P. E., Sullivan, M., Cenko, S. B., et al. 2011, Nature, 480, 34

Osterbrock, D. E., & Ferland, G. J. 2006, Astrophysics of gaseous nebulae and active galactic nuclei, 2nd. ed. by D.E. Osterbrock and G.J. Ferland. Sausalito, CA: University Science Books, 2006,

Perez-Torres, M. A., Lundqvist, P., Beswick, R., et al. 2014, arXiv:1405.4702

Perlmutter S. et al., 1999, The Astrophysical Journal, 517, 565

Rappaport, S., Chiang, E., Kallman, T., & Malina, R. 1994, ApJ, 431, 237

Rauch, T., & Werner, K. 2010, Astronomische Nachrichten, 331, 146

Riess A. G. et al., 1998, The Astronomical Journal, 116, 1009

Schlafly, E. F., & Finkbeiner, D. P. 2011, ApJ, 737, 103

Soraisam, M., & Gilfanov, M. 2014, arXiv:1401.6148

van den Heuvel E. P. J., Bhattacharya D., Nomoto K., Rappaport S. A., 1992, Astronomy and Astrophysics, 262, 97

Webbink R. F., 1984, Astrophysical Journal, 277, 355

Whelan J., Iben, Jr. I., 1973, The Astrophysical Journal, 186, 1007

Woods, T. E., & Gilfanov, M. 2013, MNRAS, 432, 1640

Woods, T. E., & Gilfanov, M. 2014, MNRAS, 350

Zheng, W., Shivvers, I., Filippenko, A. V., et al. 2014, arXiv:1401.7968

Chapter 7

Conclusions

In this dissertation, we have introduced an entirely new means to search for and, as has been the case so far, strongly constrain the nature of the progenitors of SNe Ia. In the classical form of the long-favoured single-degenerate scenario, a white dwarf composed of carbon and oxygen (with a maximum initial mass of $\approx 1.07 M_\odot$) reaches the Chandrasekhar mass after accreting sufficient mass from some companion, having grown through nuclear-burning of this material at its surface prior to explosion. This implies that any single-degenerate progenitor population should be extraordinarily luminous. Such sources should also be remarkably hot, with typical massive white dwarf radii implying photospheric temperatures of $\approx 10^6$K. For this reason, past efforts to detect any signature of such a large implied population of accreting, nuclear-burning white dwarfs have focused on searching for these objects in the soft X-ray (0.3–0.7keV) band (either on an individual basis, or their cumulative luminosity in the integrated emission of galaxies).

However, while straightforward, this approach does not account for any one of the several ways (outlined in chapter 1) in which the typical photospheric temperatures of accreting white dwarfs may differ from that predicted assuming typical radii for massive (M> $1M_\odot$) white dwarfs. In particular, if growth through steady nuclear-burning occurs primarily for less massive white dwarfs (as expected in recent, popular sub-Chandrasekhar mass explosion models), or if a fast wind inflates the photosphere by up to an order of magnitude (both frequently suggested solutions), then the typical photospheric temperatures of single-degenerate progenitors would lie $\lesssim 5 \times 10^5$K, with most or all of their emission at somewhat lower energies (peaking in the extreme UV). A more unlikely, but still plausible possibility, is that some process in the prior evolution of single-degenerate progenitor systems may leave sufficient ejected stellar material in the immediate circumstellar medium so as to enshroud the binary, absorbing much of the high-energy emission of any accreting white dwarf photosphere. These considerations necessitated the development of an alternative means to constrain the total luminosity of a possible high-temperature progenitor channel for SNe Ia.

In this thesis, we demonstrated such a method, in which we identify any putative single-degenerate accreting white dwarf binary population as a powerful contribution to the total ionizing radiation of many galaxies. In chapter 2, we showed that in the single-

degenerate scenario, accreting, nuclear-burning white dwarfs should easily dominate the ionizing background in early-type galaxies without an accreting, compact central source or significant ongoing star formation (so-called "passively-evolving" stellar populations). This should be particularly true for relatively young galaxies with low mean stellar ages, where star formation only recently stopped (within the last 1-5 Gyrs). Accreting, nuclear-burning white dwarfs have a much harder spectrum than any other, more conventional source of ionizing radiation in old stellar populations (such as post-AGB stars), and should reveal themselves in the extended nebulae of these galaxies from the detection of emission lines characteristic of ionization by the highest-temperature sources.

In this work, we have identified diagnostic emission-line ratios to test for this, including He II 4686Å/Hβ (chapter 2), [O I] 6300Å/Hα, and [N I] 5200Å/Hβ (chapter 3). Our He II diagnostic is shown to be most effective for temperatures $1.5 < T_{\rm eff}/10^5{\rm K} < 6$, where He II is ionized most efficiently. Meanwhile, our [O I] and [N I] diagnostics are most effective for higher temperatures, where these forbidden lines of neutral Oxygen and Nitrogen (with valence electron ionization energies close to that of Hydrogen) trace the volume of the Strömgren boundary, which grows considerably for ionization by the highest temperature sources ($T_{\rm eff} > 5 \times 10^5{\rm K}$). This is simply because high-energy photons penetrate deeper into the neutral gas, broadening the interface between ionized and neutral media in any nebula.

We then summarize in chapter 4 several collaborative works which successfully make use of our diagnostics. In particular, using a measurement of the He II 4686Å/Hβ ratio from the stacked spectra of thousands of passively-evolving early-type galaxies, we constrain the role of any "hot mode" single-degenerate channel with $1.5 < T_{\rm eff}/10^5{\rm K} < 6$ to less than 3–10% of the observed SN Ia rate for delay-times $1 < t_{\rm gal}/{\rm Gyr} < 4$. Using our [O I] 6300Å/Hα diagnostic from chapter 3, we extend this constraint to accreting white dwarf populations with photospheric temperatures up to $\approx 10^6{\rm K}$. Conversely, if SNe Ia do originate primarily through the single-degenerate channel, our constraints limit the role of any "hot mode" phase to accreting $\lesssim 0.005 M_\odot$ prior to explosion. Taking this as a generic constraint on the luminosity of **any** accreting white dwarf population (not necessarily single-degenerate progenitors), we then demonstrate that the standard assumptions employed in modern population synthesis studies of accreting white dwarfs produce model populations which grossly violate our constraints at relatively early delay-times (≈ 1 to a few Gyrs).

Finally, in chapters 5 & 6 we consider nebulae ionized by individual accreting, steadily nuclear-burning white dwarfs (rather than the extended, galaxy-spanning emission line regions of previous chapters). In chapter 5, we revisit the standard model for such emission-line regions, and revise previous overestimates of the typical ISM densities in which accreting white dwarfs are likely to be immersed. We then demonstrate that, due to the rather low ISM densities expected, it is unsurprising that only one confidently detected SSS nebula has been reported in the literature to date. This includes a rigorous treatment of the distribution of distances from an arbitrary point in a galaxy to the nearest surface of any dense cloud of cold neutral ISM. We then outline prospects for a search which can detect many more such objects, and justify such an investigation further by demonstrating the possible importance of accreting, nuclear-burning white dwarfs in providing an additional

contribution to the heating of warm interstellar matter. We then close with a constraint on the ionizing luminosity of the progenitor of the recent, very nearby SN Ia (in the galaxy M 82), SN 2014J, using a pre-supernova narrow-band Hα+[N II] image. For our present discussion, we confine our attention in this case to compact, unresolved nebulae (i.e. for relatively high ISM densities), in which case we rule out a maximally-accreting nuclear burning white dwarf as the progenitor at $\approx 4\sigma$ confidence. Our restriction to unresolved nebulae is purely due to the limitations of the available pre-supernova image. Thankfully, the existence of any extended nebula ionized by the progenitor of SN2014J can be assessed a posteriori using deep narrow-band images centered on strong cooling lines, such as [O III] 5007Å. Such a follow-up campaign has already begun at the Russian Turkish 1.5m telescope, and will be completed after the publication of this thesis.

Given the strong constraints placed by the work presented here (as well as past efforts cited within), we may conclude that no "classical," hot-mode single-degenerate channel plays a significant role in producing SNe Ia at delay-times greater than ≈ 1 Gyr. We have proposed means for extending this to earlier delay-times, as well as placing constraints on individual objects, with a demonstration of the latter for the recent, very nearby SN 2014J. This would appear to leave the double-degenerate scenario (or perhaps some very unusual single-degenerate model) as the only remaining possibilities, however this is far from a proof. Although there has been significant recent observational and theoretical progress in demonstrating the viability of the double-degenerate model, a rigorous proof of its role as the primary channel for the production of SNe Ia must await a well-observed SN Ia in our galaxy, or perhaps gravitational-wave observations using proposed space-based laser interferometers such as eLISA.

Appendix A

Do We Expect H/He II Absorption Edges in the Emergent Spectra of Rapidly Accreting WDs?

An accurate treatment of the radiative transfer physics is necessary in order to build a template of the spectral output of rapidly-accreting WDs, should they undergo an accretion-wind phase (Hachisu, Kato & Nomoto, 1999). However, for the purpose of this paper, we are principally concerned with whether or not there is a strong He II ionization edge in the emergent spectrum. As a simple check, we can estimate the number of photons needed to wholly ionize H and He above the photospheric radius of the wind and compare this with the expected ionizing photon luminosity produced by the nuclear-burning WD.

The total rate of hydrogen recombinations above the wind photosphere is:

$$Q_{\mathrm{R}} = \int n_e n_H \alpha_{\mathrm{A}}(T, H^0) \, dV = \tag{A.1}$$

$$\frac{x_e}{4\pi} \left(\frac{\dot{M}}{\xi \mathrm{m_H v}} \right)^2 \int_{R_{\mathrm{phot}}}^{\infty} \frac{\alpha_{\mathrm{A}}(T, H^0)}{r^2} \, dV$$

assuming spherical symmetry. Here $\xi = M_{\mathrm{wind}}/M_{\mathrm{H}} \approx 1.44$ for solar abundance, $x_e = n_e/n_H \approx 1.2$ for a fully ionized gas of solar composition, m_{H} is the mass of hydrogen, $\alpha_{\mathrm{A}}(T, H^0)$ is the Case A recombination rate for hydrogen, R_{phot} is the radius of the wind's photosphere ($\sim 0.1 - 1 \ R_{\odot}$ in the accretion wind phase), $\dot{M}$ is the wind mass loss rate, and v is the wind speed (v ≈ 1000km/s). Such an approach is similar to that taken by Cumming et al. (1996), with the wind originating at the WD surface rather than a red giant companion. As the wind density is always $\lesssim$ a few 10^{14}cm^{-3}, the coronal/nebular approximation is justified.

As a photoionized gas, the wind temperature at infinity can be expected to approach $\sim 10^4 K$ so long as there is a flux of ionizing photons. For an *extremely conservative* estimate of the photon flux needed to ionize the wind, we may assume simply that $T_{\mathrm{gas}} = 10^4 K$ for $R_{\mathrm{phot}} \lesssim$ r $< \infty$. In a more careful treatment, the gas temperature falls quickly from that
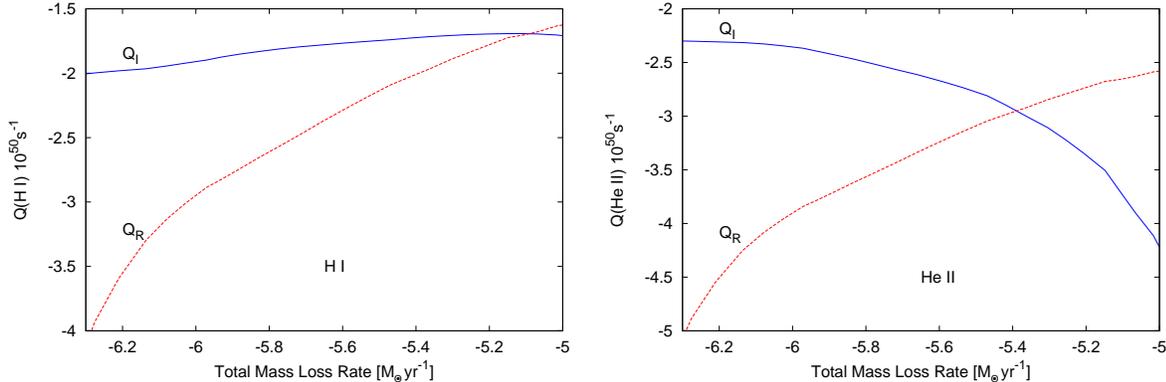
Figure A.1: Ionizing photon luminosity (solid line, blue in the color version of the plot) and an upper limit on the recombination rate (red dashed line) for hydrogen (*Top*) and He II (*Bottom*) in a wind-supported extended photosphere of a WD.

at the photosphere before leveling off at $T_{\mathrm{gas}} \approx 10^4 K$. This only lowers the recombination rate α_A, thereby raising the ionization fraction, where the density is highest.

Taking the model of Hachisu, Kato & Nomoto (1999), any quantity of interest in the wind can then be determined from the WD's mass and the mass loss rate of the envelope ($\dot{M} = \dot{M}_{\mathrm{wind}} + \dot{M}_{\mathrm{nuc}}$). From their Fig. 3, we take their result for the photospheric temperature as a function of $\dot{M}$ for a 1 $M_\odot$ WD, and set $L_{\mathrm{nuc}} = \epsilon_H \chi \dot{M}_{\mathrm{RG}}$. From the latter two quantities we can compute the ionizing photon flux at the photospheric radius. In fig. A.1, we plot the H-ionizing photon luminosity and the total recombination rate in the envelope versus $\dot{M}$. We find that the accreting WD's photosphere easily maintains H-ionization in the wind for $\log(\dot{M}) \lesssim -5.3$ [$M_\odot$/yr].

Given full ionization of hydrogen, a similar equation applies for He II.[1] In the lower panel of fig. A.1, we compare the expected recombination rate of He II in the accretion-wind atmosphere with the expected He II–ionizing photon luminosity from the wind's photosphere. Similar to hydrogen, we find that for $\log(\dot{M}) \lesssim -5.5$, the ionizing photon rate exceeds that necessary to maintain full He II ionization. Therefore, no significant break should be present at 54.4 eV in the emergent spectra of such WDs.

Such a mass transfer rate is well within the range relevant to the case of SN Ia progenitors in ellipticals. Indeed, as the mass transfer rate approaches $10^{-5} M_\odot$/yr, accretion becomes increasingly inefficient, and required donor masses exceed that available in old populations (Gilfanov & Bogdán, 2010). For example, $\dot{M}_{nuc}/\dot{M} \lesssim 0.1$ for $\dot{M} \gtrsim 10^{-5}$ $M_\odot$/yr (Hachisu, Kato & Nomoto, 1999), therefore a donor star more massive that $\sim 3-5$

---

[1] *Note that we ignore He I in this check. However, this should not significantly effect the ionization balance, as the He number density is roughly 1/10 that of H, and in the high-density limit more than $\sim$ 1/2 of all He I recombinations produce H-ionizing photons (see Osterbrock & Ferland, 2006).*

M$_\odot$ is needed in order to provide $\Delta M_{nuc} \sim 0.3 - 0.5$ M$_\odot$. Such donors are unavailable in the stellar population older that 1(3) Gyrs, where the main sequence turn-off mass is ~ 2.5 (~ 1.6) M$_\odot$.

In practice, the wind is not expected to be spherically symmetric, increasing the likelihood that much of the radiation escapes. Note also that, were the ionizing radiation absorbed near the source, one should expect strong emission lines similar to WR stars (Lepo & van Kerkwijk, 2013).

Appendix B

He II recombination lines in low ionization nebulae

Under the circumstances typically encountered in photoionized nebulae, the flux in any recombination line of X^{i} can be computed easily from the incident flux of X^{i}-ionizing photons, and the ratio of the relevant transition's recombination rate to the total rate of recombinations (Osterbrock & Ferland, 2006). For the He II 4686Å line, this gives us:

$$L_{4686,\mathrm{max}} = h\nu_{4686}\frac{\alpha_{\mathrm{HeII4\to3}}^{\mathrm{eff}}(\mathrm{T_{gas}})}{\alpha_{\mathrm{B}}(\mathrm{T_{gas}})}\int_{\nu_{54.4eV}}^{\infty}\frac{L_\nu}{h\nu}\mathrm{d}\nu \tag{B.1}$$

However, this assumes that hydrogen is completely ionized, and therefore no He II–ionizing photons are lost in maintaining the ionization of Hydrogen. As pointed out by Stasińska & Tylenda (1986) (see also Raiter, Schaerer & Fosbury, 2010; Maggi, 2011), this is no longer valid for high T_{source} and low U, in which case He II-ionizing photons are lost in ionizing H I.

In ionization equilibrium, we require that the number of recombinations at any point be equal to the photoionization rate. Ignoring for the moment elements other than hydrogen, we can express the different densities in terms of the particle density using the ionization fraction $x(r) = n_{\mathrm{e}}(r)/n(r)$ at a depth r within a nebula. We can then find a quadratic expression for $x(r)$:

$$\frac{x^2(r)}{1-x(r)} = \int_{\nu_0}^{\infty}\frac{\mathrm{a}_\nu}{\alpha(\mathrm{T})}\left(\frac{\dot{Q}_{ph,\nu}}{4\pi r^2 n_{\mathrm{H}}}\right)d\nu \tag{B.2}$$

where a_ν is the ionization cross-section, and n_{H} is the density of hydrogen. The final bracketed term may be recognized as proportional to the ionization parameter U (when the integration over ν is carried out). For an incident 54.4 eV photon, the H cross-section is $\sim 1/10$ that of He$^+$, however $n_{\mathrm{H}} \sim 10n_{\mathrm{He}}$. Therefore, for relatively low-ionization nebulae, high-energy photons capable of ionizing He II are lost in maintaining the ionization of H I (and He I), greatly diminishing the expected flux of any He II recombination line.
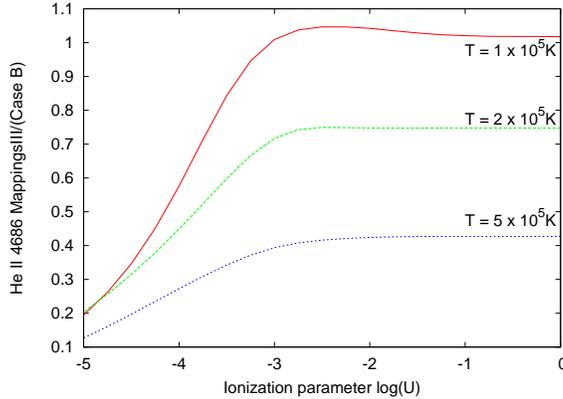
Figure B.1: The discrepancy between the predicted He II 4686Å flux computed analytically assuming Case B recombination for $T_{\mathrm{gas}} = 10^4 K$ (Osterbrock & Ferland, 2006), and the result of an accurate consideration of the ionization structure of the gas using MAPPINGS III (with gas temperature computed self-consistently, assuming n = 100 cm^{-3}). Curves are labeled by temperature of the ionizing source.

From the above, we expect the efficiency in producing He II 4686Å emission to fall off dramatically at low U. It is clear from eq. B.2 that at low ionization fraction $x(r) \sim \sqrt{U}$. As He II-ionizing photons are lost to ionizing Hydrogen, the luminosity of any He II line should fall accordingly (therefore at sufficiently low U, $L_{4686} \sim U^{0.5}$). Inspecting the results for varying U in Fig. B.1, we see that this holds for $\log(U) \lesssim$ -4, above which it levels off and saturates. For high source temperatures, we see that the line luminosity falls short of that predicted by eq. B.1, even for $\log(U) \approx 0$. This deficiency grows roughly linearly with increasing $\dot{Q}_{>54.4\mathrm{eV}}/\dot{Q}_{>13.6\mathrm{eV}}$. This is precisely the effect found by Stasińska & Tylenda (1986), in its original context. As the ratio $\dot{Q}_{>54.4\mathrm{eV}}/\dot{Q}_{>13.6\mathrm{eV}}$ grows with source temperature, an increasing fraction of photons are lost in maintaining H-ionization. Note that at the same time, the equilibrium temperature for the gas rises, slightly decreasing $\alpha_{\mathrm{HeII4\to3}}^{\mathrm{eff}}(\mathrm{T_{gas}})/\alpha_{\mathrm{B}}(\mathrm{HeII, T_{gas}})$, while increasing $\alpha_{\mathrm{B}}(\mathrm{HeII, T_{gas}})/\alpha_{\mathrm{B}}(\mathrm{HI, T_{gas}})$ (~ 6 at 10^4K).

The competition between H- and He-ionization makes it rather difficult to constrain the emission from very high temperature sources, or where the ionization parameter is quite low. At such temperatures there should be a significant enhancement in lines characteristic of ionization by very hard spectra, such as [O I] 6300Å and [N I] 5200Å (see e.g. Rappaport et al., 1994), both of which trace the width of the Strömgren boundary. The ability to make a robust statement based on such diagnostics would however be far more susceptible to the uncertainties in our knowledge of the warm gas in ellipticals, such as the metallicity and ionization state. As discussed above, measurements of the soft X-ray emission have already placed strong limits in this temperature range, therefore we focus our attention on sources with $T \lesssim 6 \cdot 10^5 K$; this includes the USSs and most SSSs.

Appendix C

Lu & Torquato treatment of the distribution of nearest surfaces

In order to find the probability distribution of distances to the nearest surface for an arbitrary system, Lu & Torquato developed an approximation using n-point correlation functions and obtaining exact expansions for mono-sized spheres of arbitrary dimension (Torquato et al., 1990). This was then extended to the case of "polydisperse" sphere radii (Lu & Torquato, 1992). For hard (impenetrable) spheres (i.e. with an interaction potential which is infinite within any given sphere and zero elsewhere), Lu & Torquato (1992) give the cumulative distribution function for distances to the nearest "particle" (cloud) surface $p_D(D) = -de_V(D)/dD$, where $e_V(D)$ is given by:

$$e_V(D) = \begin{cases} 1 - \frac{4\pi}{3}n\langle(D+l)^3\theta(D+l)\rangle & D < 0 \\ \\ (1 - f_{\text{fill}})\exp[-\pi n(aD + bD^2 + cD^3)] & D > 0 \end{cases} \tag{C.1}$$

where:

$$\langle(D+l)^3\theta(D+l)\rangle = \int_{l_{\min}}^{l_{\max}} (D+l)^3\theta(D+l)p_l dl \tag{C.2}$$

and the coefficients a,b, and c defined as:

$$a = \frac{4\langle l^2\rangle}{1 - f_{\text{fill}}} \tag{C.3}$$

$$b = \frac{4\langle l\rangle}{1 - f_{\text{fill}}} + \frac{12\xi_2}{(1 - \xi_2)^2}\langle l^2\rangle \tag{C.4}$$

$$c = \frac{4}{3(1 - f_{\text{fill}})} + \frac{8\xi_2}{(1 - f_{\text{fill}})^2}\langle l\rangle \tag{C.5}$$

with

$$\xi_k = \frac{\pi}{3} n 2^{k-1} \langle l^k \rangle \tag{C.6}$$

where $\langle l^k \rangle$ is the expectation value of l^k:

$$\langle l^k \rangle = \int_{l_{\min}}^{l_{\max}} l^k p_l(l) dl \tag{C.7}$$

with p_l given by eqs. 5.5 & 5.6.

Bibliography

Cumming R. J., Lundqvist P., Smith L. J., Pettini M., King D. L., 1996, Monthly Notices of the Royal Astronomical Society, 283, 1355

Gilfanov M., Bogdán Á., 2010, Nature, 463, 924

Hachisu I., Kato M., Nomoto K., 1999, The Astrophysical Journal, 522, 487

Lepo, K., & van Kerkwijk, M. 2013, ApJ, 771, 13

Lu, B., & Torquato, S. 1992, Phys. Rev. A, 45, 5530

Maggi P., 2011, Master's thesis, Université de Strasbourg, Observatoire Astronomique, 11, rue de l'Université, 67000 Strasbourg

Osterbrock, D. E., & Ferland, G. J. 2006, Astrophysics of gaseous nebulae and active galactic nuclei, 2nd. ed. by D.E. Osterbrock and G.J. Ferland. Sausalito, CA: University Science Books, 2006,

Raiter A., Schaerer D., Fosbury R. A. E., 2010, Astronomy and Astrophysics, 523, A64

Rappaport S., Chiang E., Kallman T., Malina R., 1994, The Astrophysical Journal, 431, 237

Stasińska G., Tylenda R., 1986, Astronomy and Astrophysics, 155, 137

Torquato, S., Lu, B., & Rubinstein, J. 1990, Phys. Rev. A, 41, 2059

Acknowledgements

I would like to thank Rashid Sunyaev for kindly supporting me as a member of the High Energy group, and for his helpful advice in the course of my time at the MPA. I would also like to express my gratitude to Marat Gilfanov for his guidance, insight, and great patience over the past years, and without whom this thesis would not have been possible.

I also thank the many other people with whom I've collaborated while at the MPA, including Jonas Johansson, Marc Sarzi, Lev Yungelson, Mikkel Nielsen, Akos Bogdan, and Hai-liang Chen, who has likely taught me as much as I've taught him. I would also like to thank Filippos Koliopanos, for help with the formatting of this thesis, and assorted hijinks, Pierre Maggi, for the many scientific discussions (and occasional diligent picking over of drafts), which helped flesh out my first ideas, and all the friends I've met who have brightened my time here. Perhaps most pertinent to this thesis, I would like to thank Thomas Ertl, as well as Janina von Groote, Stefan Heigl, and Alexander Summa, for their help in writing a good abstract in German!

I also would like to thank my parents, Jerry and Michelle Woods, and my siblings Ezra, Gia, Seamus, and Callum for their love and support throughout my life. Finally, I would like to give my greatest thanks to my wife, Cheryl Woynarski, who travelled halfway around the world and learned a language so I could pursue a dream, whose love and support have sustained me in moments good and bad, and whom I dearly love.

Curriculum Vitae

Name: Tyrone Woods

Nationality: Canadian
Birthdate: January 8th, 1987
Place of Birth: Edmonton, Alberta, Canada

09.2011 – 04.2015	PhD Physics, Ludwig Maximilian University of Munich
	Dissertation title: Emission-line diagnostics of the progenitors of type Ia supernovae Advisors: Marat Gilfanov & Rashid Sunyaev
09.2009 – 09.2011	MSc Physics, University of Alberta Thesis title: Selected topics in the evolution of binary stars Advisor: Natalia Ivanova
09.2005 – 04.2009	BSc Honours Astrophysics, University of Alberta
09.2002 – 06.2005	International Baccalaureate Diploma (honours), Harry Ainlay High School